COMPUTATIONAL CIVIL ENGINEERING

2013

Editura Societății Academice "MATEI -TEIU BOTEZ"

Proceedings of the 11th International Symposium

"Computational Civil Engineering"
Iasi, Romania - May 24th, 2013

Scientific publication
ISSN 2285-2735, ISSN-L 2285-2735
Director, prof.dr.ing. Constantin Ionescu
Editor in Chief, dr. Rodian Scînteie

Table of Contents

1. Razvan Mircea Chirila, Vasile Musat, Daniela Grigore
Shear strength mobilization of soil behind the systems which support deep excavations 5-16

2. Paul Ciobanu, Nicolae Țăranu, Sergiu Nicolae Popoaei, Sebastian George Maxineasa
Analysis of reinforced concrete beams subjected to flexure using ANSYS nonlinear concrete model 17-25

3. Vitalie Florea
Computer modelling of a footbridge between two neighbour buildings with roof and sides made of thick glass 26-33

4. Vasile Iacob
High performance methods and techniques for demolition 34-44

5. Vasile Iacob
Aspects regarding the post-use construction stage 45-50

6. Mohammad Mehdi Khabiri, Mohammad Saberian
Effect of embankment height on the pavement and road culverts reactions 51-57

7. Septimiu-George LUCA, Cristian PASTIA
Numerical Simulations of a Frame Structure with a Single Passive or Semi-Active Tuned Mass Damper 58-64

8. Mihaita Mihai
A Bayesian approach to seismically induced fragility 65-74

9. Daniela Oanea (Fediuc), Mihai Budescu, Vasile-Mircea Venghiac, Alexandrina-Elena Pandelea
Observations on the design of elastomeric bearings used in base isolation 75-82

10. Cerasela P. Olariu, Mihaela Movilă
Push-over analysis of a reinforced concrete structure considering soil-structure interaction 83-90

11. Raluca Pleșu, George Țăranu, Mihai Budescu
FEM analyses of a 1:2 scale historical unreinforced masonry building 91-101

12. Claudiu Romila
CFD analysis of free convection characteristics inside cavity walls 102-109

13. Octavian Victor Roşca
Some Considerations Regarding Renumbering Techniques for Sparse FEM Matrices 110-119

14. Mario A. Salgado, Daniela Zuloaga, Gabriel A. Bernal, Miguel G. Mora, Omar D. Cardona
Probabilistic seismic risk assessment of the building stock in Medellín, Colombia 120-135

15. Jerzy Szołomicki, Piotr Berkowski, Jacek Barański
Numerical analysis of FRP reinforced masonry cross vaults 136-145

16. George Taranu, Mihai Budescu, Raluca Plesu, Ionut Ovidiu Toma
FE modeling of a glass fiber reinforced mineral composite structure 146-154

17. César Velásquez, Omar Cardona, Luis Yamin, Miguel Mora, Liliana Carreño, Alex H. Barbat
Hybrid loss exceedance curve (HLEC) for risk assessment 155-174

18. Mihai Vrabie, Sergiu Baetu
Comparative analysis of the bending theories for isotropic plates 175-188

19. Mihai Vrabie, Vasile-Mircea Venghiac
Considerations regarding the bending of sandwich plates 189-198

THE 11th INTERNATIONAL SYMPOSIUM
"COMPUTATIONAL CIVIL ENGINEERING 2012"

ORGANIZERS

Faculty of Civil Engineering and Installations
Academic Society "Matei - Teiu Botez"
Spanish Association of Seismic Engineering

Co-ordination committee

Prof.Dr.Eng. Mihai Budescu
Prof.Dr.Eng. Alex. Horia Barbat
Prof.Dr.Eng. Constantin Ionescu

Scientific commission

Prof.Dr.Eng. Doina Ştefan
Prof.Dr.Eng. Elena Axinte
Dr. Eng. Rodian Scînteie
Dr. Eng. Gabriela Covatariu
Dr. Eng. Mihai Petru

Organizing commission

Eng. Nicoleta Paşehonov

Shear strength mobilization of soil behind the systems which support deep excavations

Razvan Mircea Chirila, Vasile Musat, Daniela Grigore
Faculty of Civil Engineering and Building Services, Technical University "Gheorghe Asachi" to Iasi, Code 70050, Romania,

Summary

The increasing density of urban areas, leading to the need to build high buildings with deep basements, thus being necessary supporting wall papers. For geotechnical engineers is a continuous challenge to design the walls to support deep excavations but also to keep in safe the neighboring buildings. This paper presents a case study regarding the design of a support wall on a deep excavation in an urban area of the Iasi city, Romania, achieved of reinforced concrete piles disposed at spacing of 1.00 m and stiffened at the top with a concrete beam.. It was used a computer program based on the finite element method (FEM) to shape complex behavior of soil-structure interaction. The results provide information about the earth pressure, stress occurring in the soil and structure, for each stage of execution. Depending on the maximum deformation occurring in the field behind the support wall is revealed the degree of mobilization of shear resistance of the soil in the area of influence.

KEYWORDS: excavations, finite element method, soil-structure interaction, mobilization of shear resistance, piles,

1. INTRODUCTION

Urbanisation made cost of land high and it necessitated to go deeper into the ground and also towering vertically towards the sky. A deep excavation into the ground is indispensible to create additional floor space to meet increasing space requirements for parking for multi-storey buildings at the town centres. Numbers of deep excavation pits in city centers are increasing every year. Structures in the immediate vicinity of excavations, dense traffic scenario, presence of underground obstructions and utilities have made excavations a difficult task to execute [1]. In this context, analysis and design of proper deep excavations and their supporting systems are essential. Even in complicated urban settings, deep retaining systems have been deployed successfully by overcoming construction challenges.

An Excavation is basic phase in the construction of foundations orbasements of high rise buildings, underground oil tanks, subway stations etc [2]. The process of an excavation may encounter different kinds of soils underneath the same excavation site-from soft clay to hard rocks. During excavation, some soil types pose greater problems than others. Sandy soil is always considered dangerous even when it isallowed to stand for a period of time after a vertical cut. Vibration from blasting, traffic and heavy machinery movement, and material loads near the cut can also cause earth to collapse in sandy soil.

The instability can be caused by moisture changes in the surrounding air or changes in the water table. Clayey soils in general, present less risk than sand; however, softclay can prove to be very treacherous. Silty soils are also unreliable and require the sameprecautions and support provision as sand.

To engineer an excavation, the basic steps which should be carried out by design engineer are: site characterisation; selecting dimensions ofexcavation; surveying adjacent structures; establishing permissible movements; selecting earth retaining system; selecting supporting and construction scheme; predicting movements; compare predicted with permissible movements; alter supporting (bracing) and construction scheme; if needed; monitor instrumentation, alter as needed; compare monitored results with predicted and permissible values; alter bracing and construction scheme, if needed [3]. Site characterisation is the first major step to betaken by a geotechnical engineer.

Most common practices tend to greatly simplify soil profile and to select appropriatedesign parameters like strength, and compressibility as the basis of simple laboratory tests. Since deep excavation is a total technique, proper coordination and integration of design and construction are of utmost important.

In this study, details of various deep excavation supporting systems are furnished and comprehensive design philosophy of an excavation supporting systems is presented. This paper also contains details of a case study on the analysis and design of a contiguous pile wall for supporting deep excavation at a town centre.

2. GEOLOGICAL AND GEOTECHNICAL CONDITIONS

The process of an excavation may encounter different kinds of soils underneath the same excavation site from soft clay to hard rocks. The closer the construction site to a hillside, the more complicated the geological condition. The geological condition determines the type and construction of retaining walls and greatly influences the excavation behavior as well. In addition to the geological condition, the distribution of groundwater also contributes to the excavation behavior.

For example, it may fall below the hydrostatic water pressure in an urban area because of the long-term overuse of groundwater. On hill sides, there might exist an artesian aquifer, which has a rather high pressure. In seaside areas, seawater may permeate into the soils and tides will make the water level fluctuate daily. To sum up, the geological investigation of an excavation project aims at the soil conditions underneath the construction site and the distribution of groundwater.

To sum up, the geological investigation of an excavation project aims at the soil conditions underneath the construction site and the distribution of groundwater.

There are many soil tests for deep excavations. These include tests of basic soil behavior, such as unit weight, specific weight, water content, Atterberg limit, etc., and tests of mechan¬ical behavior, such as consolidation and strength, etc. According to the information from the soil tests, engineers can judge whether the soil is a drained or an undrained material. Since the strength differs significantly between drained and undrained materials, the choice of analysis methods and retaining walls varies accordingly. The more precise the results of soil tests, the more reasonable are the analysis results and the more economical are the retaining and excavation systems. However, the merits of soil tests can not be seen directly and therefore are often neglected.

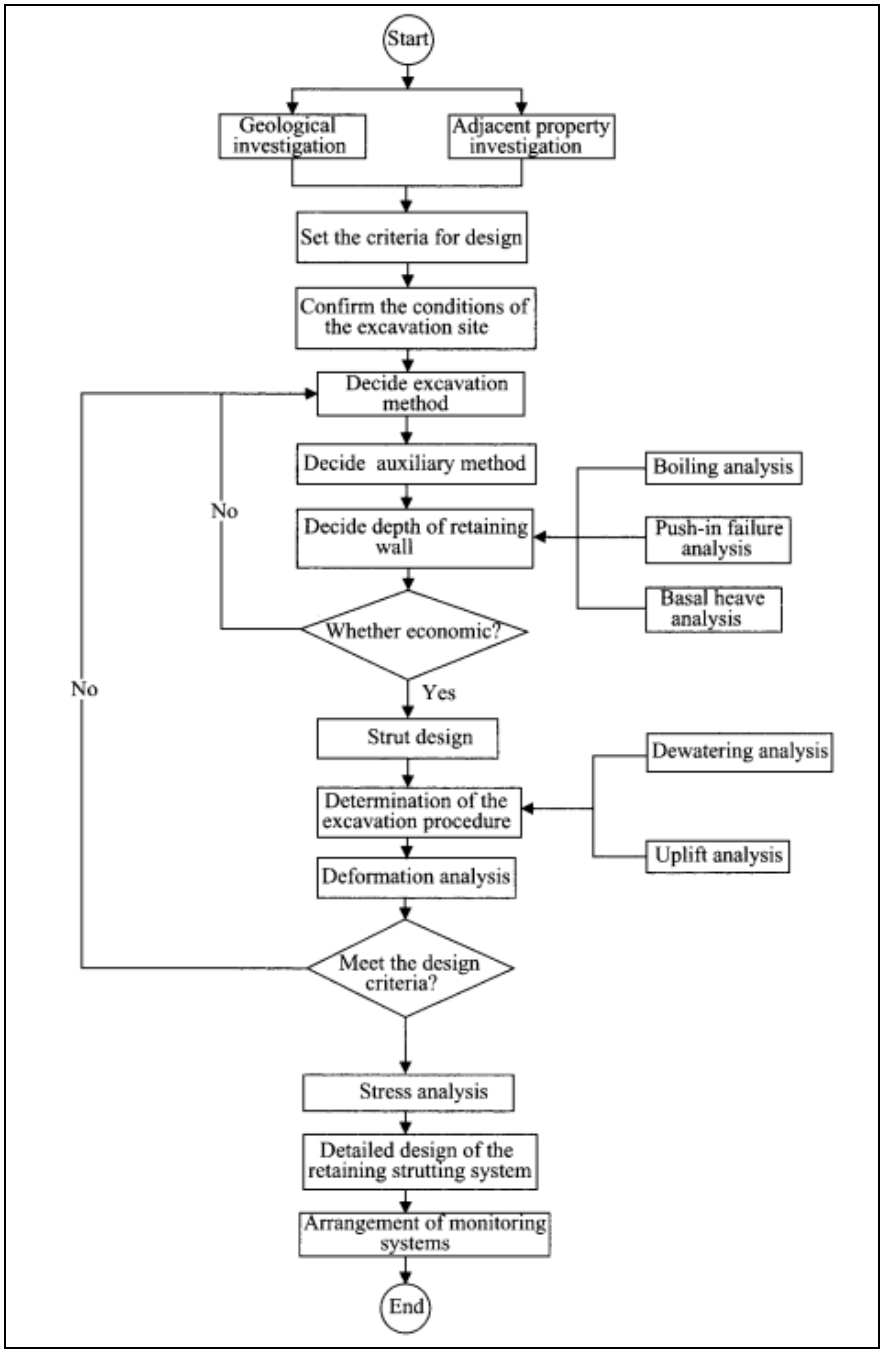

Fig. 1 Flow chart for analysis and design of an excavation [2]

3. INFLUENCE ON NEIGHBORING BUILDINGS

From the perspective of mechanics, deep excavation necessarily gives rise to movement of the soils near the excavation site. However, if the movement or settlement is too large, it will damage neighboring buildings or public facilities. Some buildings or facilities are especially sensitive to settlement, a little of which may bring about cracks in beams or columns, while others can stand more settlement. The allowable settlement of a building or a facility is highly correlated to its foundation type, construction material, structural type, and age. Therefore, investigation of the condition of adjacent properties and public facilities before designing an excavation project is required to determine the allowable settlement, which in turn determines the type of retaining and strutting systems and the selection of auxiliary methods. [2]

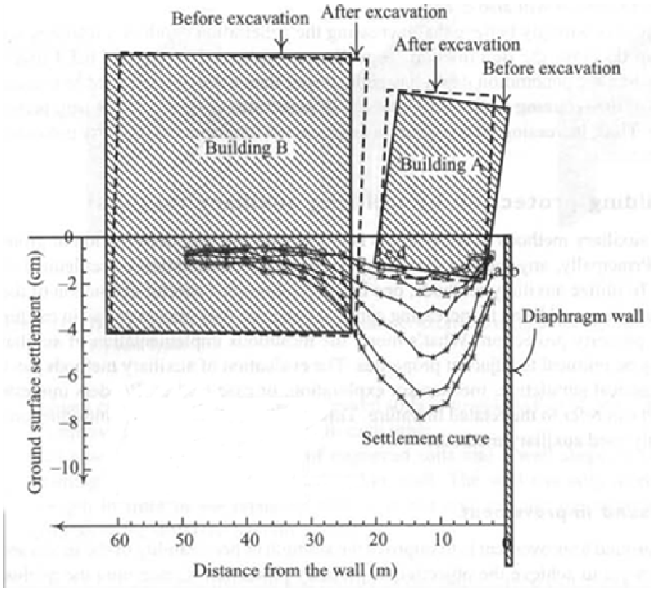

Figure 2. Influence area after excavation

4. DESIGN CRITERIA OF DEEP EXCAVATIONS

Whether an excavation is successful is significant to the lives and properties of many people. Thus, an appropriate design criterion must be selected before design.

A deep excavation design criterion should include, at least, the method of stability analysis, the methods of simplified and advanced deformation and stress analyses, a dewatering scheme, the design of structural components, property protection, etc.

4.1.Design criteria related to the nearby structure

The design criteria are established to minimize the risk of damage (structural damage, appearance) to the adjacent structures. Potential causes of damage are often related to differential settlements of the structure affected by the deep excavation or dewatering [5]

The vast problem of selection of the parameter values for displacement controlled design is widely recognized. The ground investigation and laboratory tests should be relevant for the intended construction method and calculation models; test results should be compared with published data and local experience. Main factors when analysing the results of ground investigation and selecting parameter values for the prediction of ground movements due to excavation or dewatering are:

The heterogeneity of the subsoil under the nearby structure as well as the variations of parameter values should be identified and quantified, as the occurrence of damage is by far more governed by differential displacements than by the absolute magnitude of a mean deformation. It should be noted in this respect that the ground under the existing structures is quite impossible to explore The influence of initial stress conditions including the previously experienced effective stresses prior to commencement of excavation or dewatering is often underestimated. The errors involved by this can be at the side of safety as well as at the opposite site.

Parameters for time dependent effects are difficult to obtain and to translate to reliable design parameters

4.2. Constitutive models of soil behaviour

In recent years, numerical methods have become standard tools in the analysis of geotechnical problems. This use is principally owed to the availability of sufficient computer capability to solving 2D and 3D analyses, as well as to the continuous achievements being made in the development of the constitutive soil models. Although a large number of constitutive models have been developed, the majority are predominantly used for research oriented proposes. Schweiger (2009) grouped practical oriented constitutive models into five categories:

- Linear or non-linear elastic models
- Elastic-perfectly plastic models
- Isotropic hardening single surface plasticity models
- Isotropic hardening double surface plasticity models
- Kinematic hardening multi-surface plasticity models

In the first category, the elastic model, soil behaviour is said to be elastic, with one stiffness parameter used. In most cases, the results from the elastic model are unrealistic and, therefore, should not be adopted in practice. The second category, elastic-perfectly plastic (Mohr-Coulomb) model, is relatively simple, and is considered the most widely used model among practising engineers. The elasticperfectly plastic model seems to be sufficient for some areas of geotechnical

problems, especially when being used by experienced engineers. For example, the deformation of the diaphragm wall, induced by excavation, can be actually predicted when used in conjunction with a total stress analysis and a back analysed stiffness parameter [6].

The isotropic hardening single surface plasticity model category (the third category) is the first step to modelling real soil behaviour. The principal soil model of this category is the Modified Cam-Clay (MCC) Model [7]. The MCC Model introduced an elliptic yield surface which separates the elastic behavior from the plastic behaviour. The application of this mode has been widely accepted, especially for cases of embankments on soft clay modelling. Where there is an unloading problem, such as an excavation, the soil stress path remains generally inside the yield surface. Thus, the predicted deformations are governed by the elastic behaviour. The forth category is the isotropic hardening double surface plasticity model. The predominant model in this category is the Hardening Soil Model which was developed from the double hardening model, introduced by Vermeer (1978). It is believed that this type of model will replace the standard Mohr Coulomb. The last category contains the kinematic hardening multi-surface plasticity models.

These models are generally able to capture more complex soil behaviour, including softening, small strain, anisotropy, and structured soils. Examples of soil models in this category are the Kinematic Hardening Model or Bubble Model and the Three-Surface Kinematic Hardening (3-SKH) Model . Such models have been developed from the Cam-Clay Model and, therefore, share the basic assumptions of linear behavior within the elastic (recoverable) state, while the associated flow rule at the yield surface is applied.

5. EXAMPLE

To execute a building with two basements and four floors, it is necessary to execute a cut to a depth of 6.50 m Excavation will be supported by a support structure made of reinforced concrete piles disposed at spacing of 1.00 m and stiffened at the top with a concrete beam. Piles of reinforced concrete has a total length of 15.00 m and the support structure has a total length of 80.00 m Due to the complexity of the problem for a more accurate approach to the calculation adopted by numerical solutions based on Finite Element Method (FEM) using computer programs.

5.1. Geotechnical conditions

Tabel 1. Geotechnical characteristics of the ground

Layer	Layer depth	γ [kN/m^3]	c [kPa]	Φ [^{o}]	Sr [%]	E [kPa	R_{int}
Stuffing of earth	4.00	18.13	10	5	0.70	6000	0.67
Loamy dust	1.00	17.14	7	16	0.60	16000	0.67
Yellow clay	15.00	19.17	27	6	0.87	22000	0.67

5.1. Characteristics of materials

Tabel 2. Characteristics of materials

Name of the object	EA [kN/m]	γ [kN/m^3]	EI [kNm^2/m]	ν
Piles	1.2*10^7	25.00	1.6*10^6	0.2

5.2. Modelling by finite element method

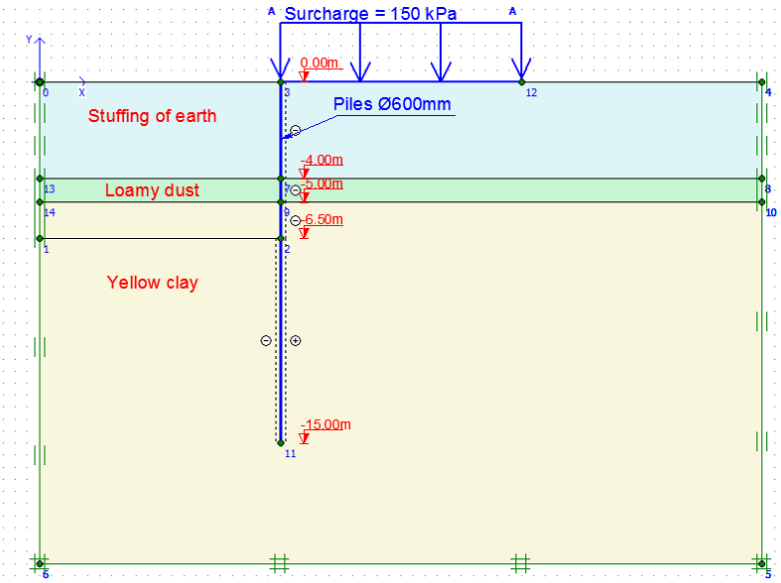

Figure 3. The geometry of the model

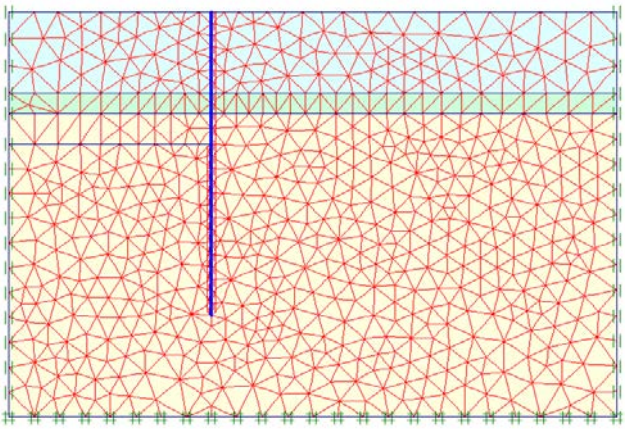

Figure 4. Meshing in finite element of the model

5.3. Results

In practice, the construction of an excavation is a process that can consist of several phases.
Have been considered three stages of construction:
1. Implementation of the piles and consider of existing construction loads - determining the initial efforts;
2. Execution of the excavation up to quota provided in the project;
3. Determination of the safety factor by the criteria of shear strength parameters are reduced to overcome resistance to shear.

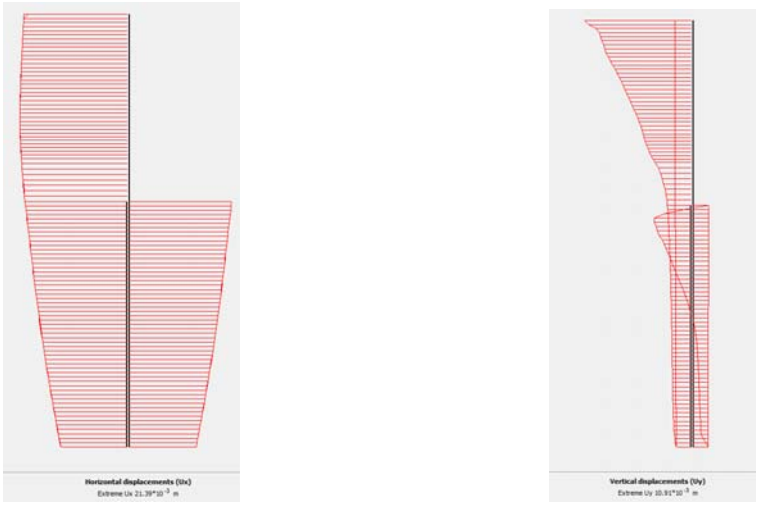

a) Horizontal displacement b) Vertical displacement

Figure 5. Displacements of piles

Horizontal displacement: 22 mm
Vertical displacement: 11 mm

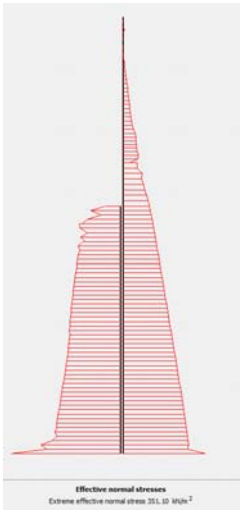

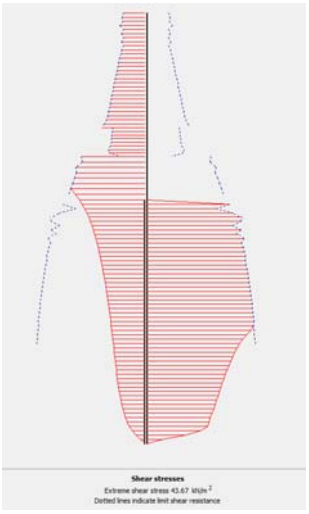

a) Effective normal stresses b) Shear stresses

Figure 6. Stresses

Effective normal stresses: 351.10 kPa
Shear stresses: 43.67 kPa

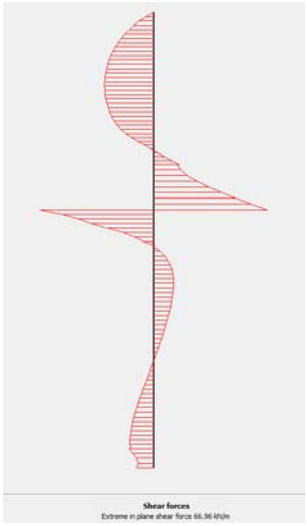

a) Shear forces b) Bending moments

Figure 6. Forces

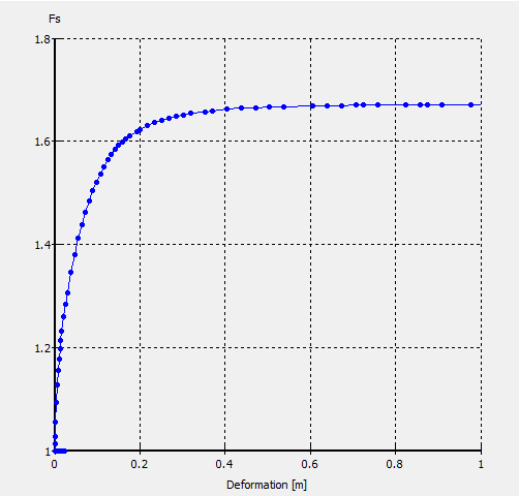

Figure 7. Safety factor

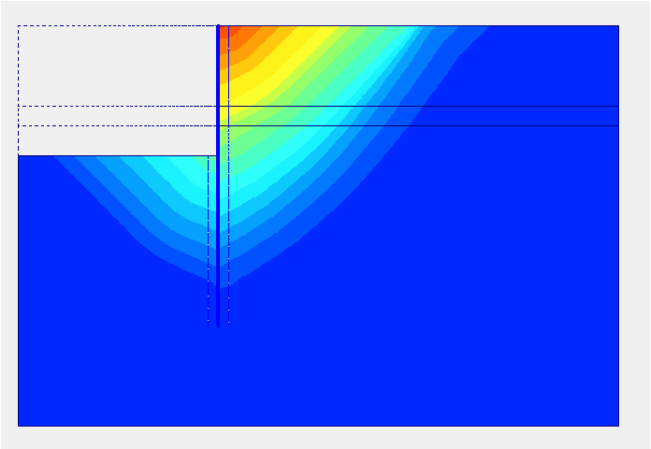

Figure 8. The influence area of excavation

6. CONCLUSIONS

As shown in the above diagrams, calculation results by finite element point out the efforts of ground displacements, strains, active pressure and passive resistance of the earth. It can be seen that the maximum horizontal deformations of the upper level piles are approximately 22 mm. These results are theoretical and are obtained after introducing geotechnical characteristics in the computer program. After

monitoring other similar works was found that the deformations are within 50-60% of those calculated.

From the safety factor chart can be seen that the support structure ensure the stability of neighboring buildings and maintains safely inside the excavation

Figure 8 highlights the mobilization earth resistance and the influence area due to deformation of the support structure.

References

1. Manish Kumar, Deep support systems using diaphragm walls and contiguous piles, National Seminar on Deep Excavation in Urban Environment, Mumbai, 2008, p. 1-18.
2. Chang-Yu Ou, Deep Excavation: Theory and Practice, Taylor and Francis Group, London, UK, 2006
3. Puller, M., Deep Excavations: A practical Manual, Thomas Telford, London, UK, 1998
4. Das B.M., Principles of Geotechnical Engineering, Cengage Learning, CT, USA, 2010
5. Boscardin, M.D. & Cording, E.J. 1989. Building response to excavation induced settlement. Jn. Geotech. Eng.> ASCE, 115(1): 1-21.
6. Phienwej, N., Ground movement in station excavation of Bankok first MRT. In: Proceeding of the 6 th International Symposium (IS-Shanghai 2008), Shanghai, China, 181 – 186
7. Rsocoe, K. H., Burland, J.B. On the generalized stress-strain behavior of wet clay, Engineering Plasticity, Cambridge University Press, New York, 1968, 535-609

Analysis of reinforced concrete beams subjected to flexure using ANSYS nonlinear concrete model

Paul Ciobanu, Nicolae Țăranu, Sergiu Nicolae Popoaei, and Sebastian George Maxineasa

Department of Civil and Industrial Buildings, "Gheorghe Asachi Technical University, Ia i, 700050, Romania

Summary

This paper presents the basic concept of using the finite element method of analysis, for the study of reinforced concrete beams subjected to flexure. The numerical modelling is carried out using ANSYS software. Element types, real constants and material properties chosen to represent the concrete, steel reinforcement and rigid steel supports are discussed. The purpose of this paper is to elaborate a numerical model with an ultimate aim of developing a quick way of studying reinforced concrete beams in the full range of loading.

KEYWORDS: finite element method (FEM); reinforced concrete (RC)

1. INTRODUCTION

In recent years, extensive research has been carried out in order to simulate the flexural response of RC beams subjected to flexure, using ANSYS finite element software.

The program is based on finite element method, which can solve problems ranging from relatively simpler linear analyses to the most challenging non-linear simulations. The analysis of a structural element in ANSYS is performed in three stages: pre-processing (defining the FE model); analysis solver (solution of FE model) and post-processing of results [7].

The main difficulty in FE analysis of RC structures is the characterization of nonlinear material models. The concrete nonlinearity appears due to three major causes: cracking of the concrete in the tensile zones; nonlinearity of the concrete in compression and plasticity of the steel reinforcement [1].

The objective of this paper is to elaborate a numerical model that can precisely predict the structural response of RC beams subjected to flexure in the full range of loading.

ISSN 2285-2735, Pages 17 - 25

2. FINITE ELEMENT ANALYSYS

2.1. Geometry of the RC beam

A simply supported reinforced concrete beam subjected to a monotonically increasing four point bending (two points loading) up to failure of the specimen is analyzed (Figure 1). The beam has a total length of 3000 mm and of rectangular cross-section having a width and height of 200 mm and 300 mm, respectively.

The longitudinal steel reinforcement consists of three 8 mm-diameter bars in the tension zone (bottom reinforcement) and two 8 mm-diameter bars in the compression zone (top reinforcement). In addition shear reinforcement, designed to induce the flexural failure, consists of steel stirrups of 8 mm nominal diameter spaced at 100/150 mm. The thickness of the concrete cover is 25 mm on the lateral and upper faces of the beam and 35 mm on the bottom one.

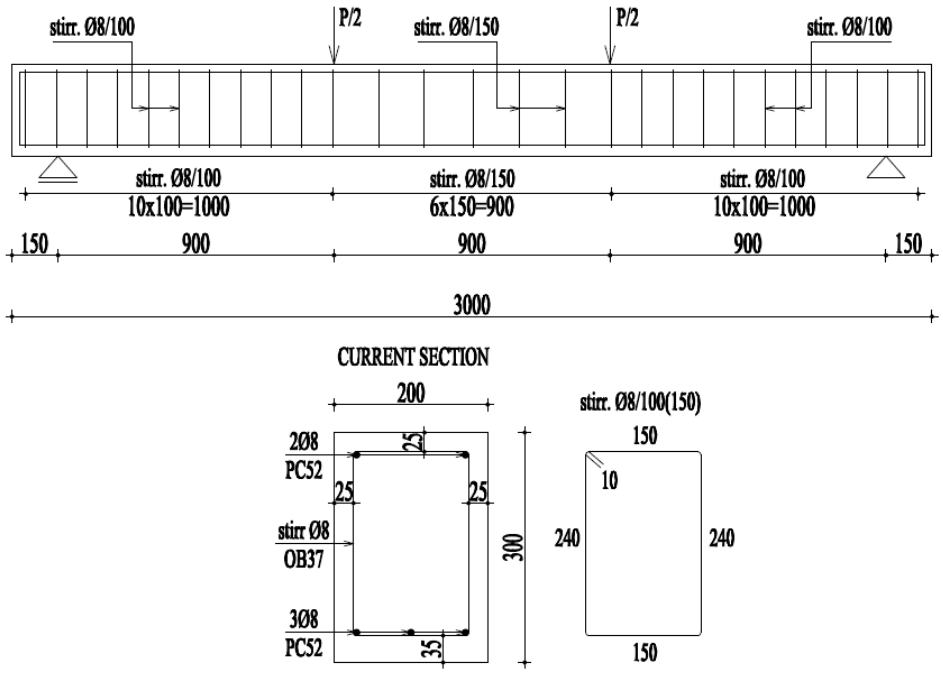

Figure 1. Loading and geometry of the analyzed beam

2.2. Element description

The concrete is simulated using a solid structural element (SOLID65) that is defined by eight nodes with three degrees of freedom at each node. The element is suitable for modeling the nonlinear behavior of the concrete due to its capability in cracking in tension and crushing in compression (Figure 2).

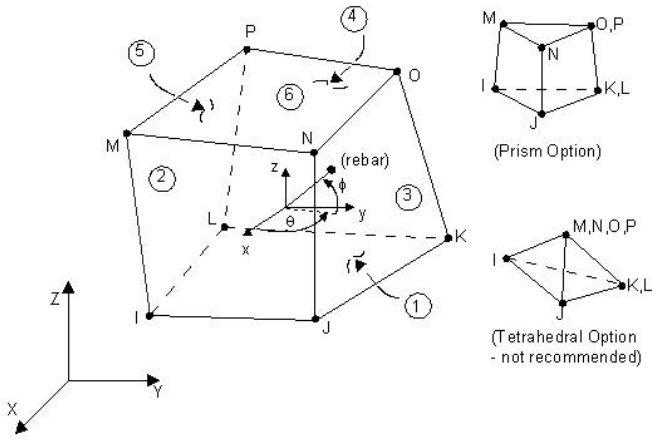

Figure 2. SOLID65 element [7]

The steel reinforcement is modeled using a 3D 2-node structural bar element (LINK8) defined by two nodes along the length of the element, with three degrees of freedom at each node. The three-dimensional spar element is a uni-axial tension-compression element capable of representing the plastic deformation (Figure 3).

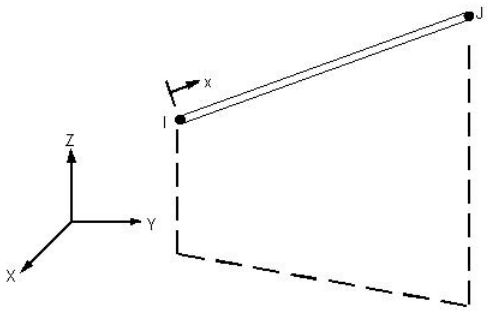

Figure 3. LINK8 element [7]

The rigid steel supports are simulated using a 3D 8-node structural element (Solid45) which is defined by eight nodes having three degrees of freedom at each node (Figure 4).

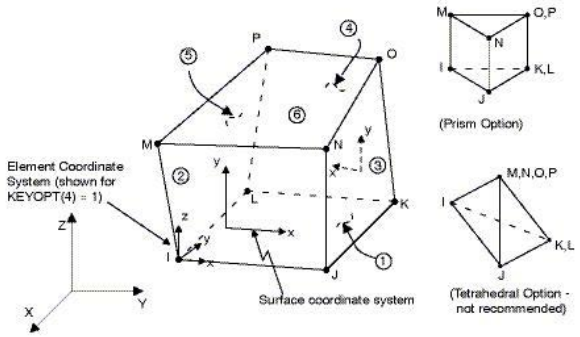

Figure 4. SOLID45 element [7]

2.2. Material properties

In this study, the mechanical properties of the concrete including compressive strength (f'_c) of 69 MPa, tensile strength (f_t) of 5.1 MPa and the instantaneous elastic modulus (E_c) of 39200 MPa, are used to define the nonlinear material behavior along with a Poisson's ratio of 0.2. William and Warnke model along with Von-Misses failure criteria are used to define the constitutive material models for the concrete [8]. The compressive uniaxial stress-strain curve for the concrete [9] are incorporated in the FE model with the Multi-linear Isotropic Hardening (MISO) option (Figure 5).

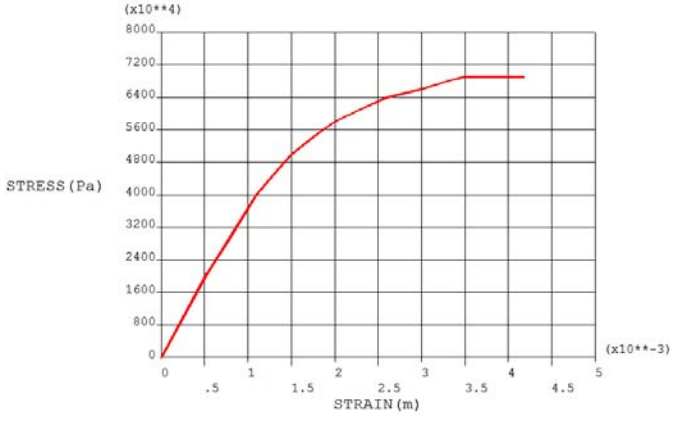

Figure 5. Uniaxial stress-strain curve for concrete

The nonlinear response of the steel reinforcement bars is assumed to be linear elastic-perfectly plastic [2]. A Poisson’s ratio of 0.3 is specified and the elastic modulus and yield strength of steel reinforcement are taken as 200 GPa and 310 MPa, respectively (Figure 6).

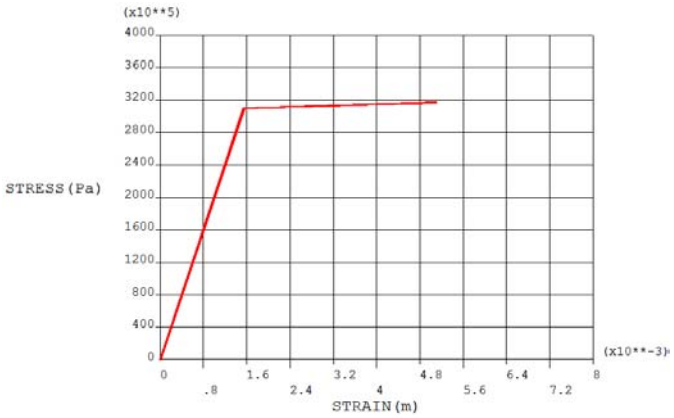

Figure 6. Uniaxial stress-strain curve for steel reinforcement

To avoid stress concentration problems, steel plates (60 mm width, 30 mm thick and 200 mm length) are added at the support and loading locations in the FE models. The rigid supports are simulated with elastic steel material properties, having a modulus of elasticity of 200 GPa and a Poisson’s ratio of 0.3.

2.3. Geometry of the developed FE model

Due to the symmetry of the geometry, loadings and boundary conditions, only one-quarter of the beam is modeled using symmetry boundary conditions in two planes. The advantage of such a decision is the reduction of the total number of elements which leads to a less computational time. Symmetry is simulated by restraining the displacement in the plane perpendicular to the plane of symmetry [3,4].

SOLID65 and SOLID45 elements are meshed using rectangular elements of 30x30x30 mm in order to obtain satisfactory results [2].

The reinforcement bars are included in the finite element model as a discrete model [6].

The bond between concrete and reinforcement is assumed to be perfect.

For the LINK 8 element no mesh is needed because individual elements are created thru the nodes created by the mesh of the concrete volume.

The overall meshes of the specimen beam are shown in Figure 7.

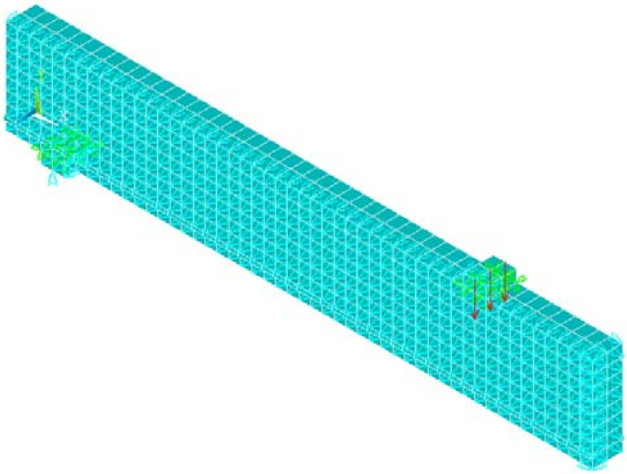

Figure 7. Meshed FE model

2.4. Nonlinear solution and convergence criteria

The nonlinear response of the RC beam requires dividing the applied monotonic load into a series of sub-steps. The nonlinear change in the structural stiffness is simulated by adjusting the stiffness matrix at the end of each sub-step using Newton-Raphson equilibrium iterations. The convergence tolerance limits are 0.5% for the force checking and 5% for displacement checking. The predicted ultimate load capacity of the beam is defined when the solution for a 10 N load increment does not converge [7].

2.5. Results

The predicted load-deflection curve (Figure 8) for the specimen beam can be divided into three parts consisting of (a) precracked, (b) working load and (c) post yielding regions [5].

At the initial stages of loading, concrete resists both compression and tension forces. It is clear from the predicted results that the response of the beam is linear up to first crack which appears at 14.62 kN. Once the tension zone of the concrete cracks, its tensile force resistance becomes negligible and the external load is primarily carried by the steel reinforcement.

The post cracking region starts after the first crack and terminates when the reinforcement starts to yield.

Once the steel starts to yield, deflection increases rapidly with every little increase in load (moment). The specimen beam fails by crushing of concrete at a ultimate of 48.17 kN.

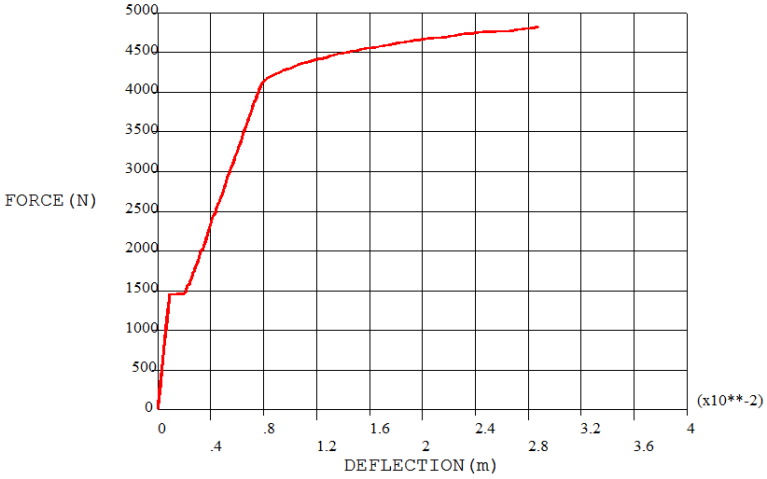

Figure 8. Load-deflection curve for the specimen beam

The predicted maximum midspan deflection of the specimen beam at ultimate load is 28.7 mm (Figure 9).

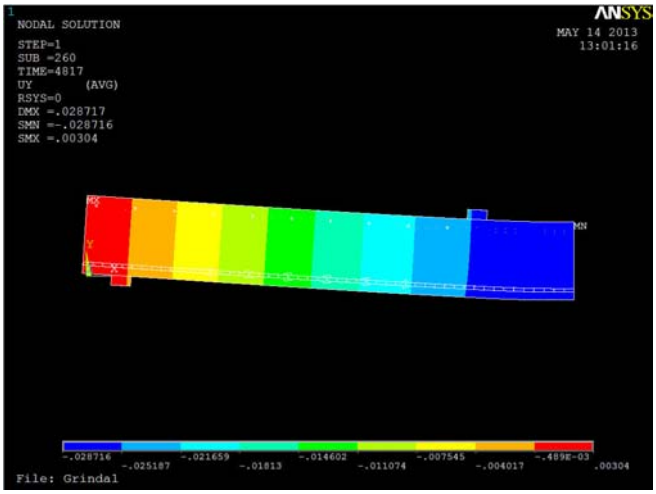

Figure 9. Defection at ultimate load

The initial cracking of the beam in the FE model corresponds to a load of 14.62 kN and can be seen in Figure 10.

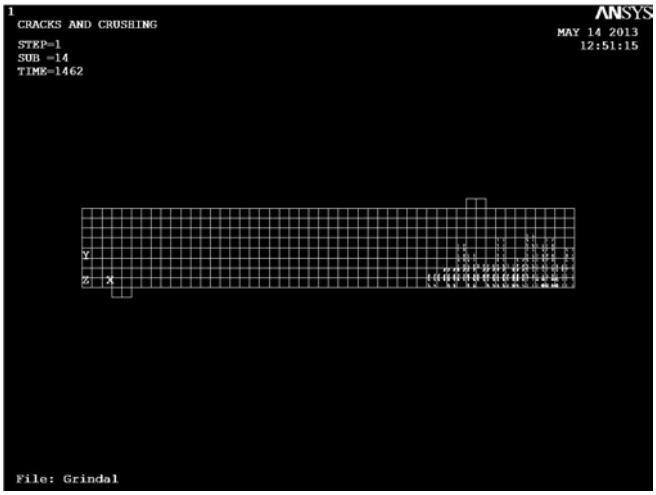

Figure 10. Crack patterns at load 14.62 kN

Figure 11 shows successive cracking of the concrete after yielding of the steel reinforcement occurs.

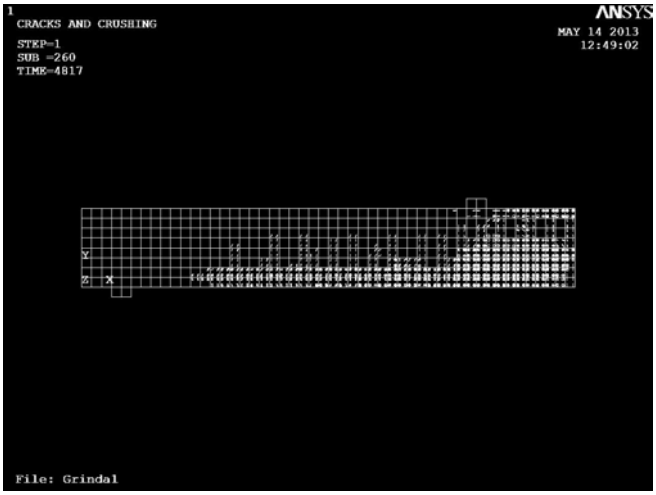

Figure 11. Crack patterns at ultimate load

3. CONCLUSIONS

This study intended to investigate the possibilities of performing a static nonlinear FE analysis of RC beams using ANSYS software. To ensure that the FE model can produce a satisfactory prediction of the response of RC beams subjected to flexure, any model should be calibrated with good experimental data.

References

1. Hawileh, R.A., Nonlinear finite element modeling of RC beams strengthened with NSM FRP rods, *Construction and Building Materials*, vol. 27, 2012
2. Omran, H.Y., El-Hacha, R., Nonlinear 3D finite element modeling of RC beams strengthened with prestressed NSM-CFRP strips, *Construction and Building Materials*, vol. 31, 2012
3. Hawileh, R.A., Naser, M.Z., Abdalla, J.A., Finite element simulation of reinforced concrete beams externally strengthened with short-length CFRP plates, *Composites: part B*, vol. 45, 2013
4. Zhou, Y., Gou, M., Zhang, F., Zhang, S., Wang, D., Reinforced concrete beams strengthened with carbon reinforced polymer by friction hybrid bond technique: Experimental investigation, *Material and Design*, vol. 50, 2013
5. Balaguru, P., Nanni, A., Giancaspro, J., *FRP composites for reinforced and prestressed concrete structures*, Taylor&Francis, New York, 2009
6. Wolanski, A.J., *Flexural behavior of reinforced and prestressed concrete beams using finite element analysis*, Milwaukee, 2004
7. ANSYS – release version 11. A finite element computer software theory and user manual for nonlinear structural analysis, ANSYS 2007, Inc. Canonsburg, PA
8. William, K., Warnke, E.D., Constitutive model for triaxial behavior of concrete, *Proceedings, international association for bridge and structural*, vol. 19, 1975
9. Hognestad, E., Hanson, N.W., McHenry, D., Concrete stress distribution in ultimate strength design, *ACI J Proc*, vol. 52, 1955

Computer modelling of a footbridge between two neighbour buildings with roof and sides made of thick glass

Vitalie Florea
Department of structural mechanics "Gheorghe Asachi" Technical University, Jassy, Romania

Summary

This work briefly describes the computer modelling of a footbridge between two neighbour buildings with a total length of 2280 cm and a height – 300 cm, the project – Neurocampus, University of Bordeaux Segalen, France. The footbridge has a width of 155 cm, the roof and sides are made of thick glass. For presented footbridge finding a solution for sustaining the glass structure was imposed, so that the footbridge should be supported only at the ends and to comply with the conditions of resistance and maximum permissible deformation (L/500). Due to architectural restrictions, the footbridge deck's height was limited to 75 cm so that the total height of the footbridge does not exceed 300 cm.

KEYWORDS: footbridge, thick plates, loads, glass, snow, wind.

1. INTRODUCTION

The footbridge analyzed in the paper is part of the project – hospital Neurocampus, University Bordeaux Segalen, France (contest stage), [6]. One of the issues approached in this project assumed to make a footbridge between two wings of neighbour buildings having the roof and the side walls made of thick glass.

Due to the architectural and functional restrictions, the footbridge sizes should have fit between the following limits:

- width – 155 cm;
- height – 300 cm (215 cm – the height of the glass structure);
- length – 2280 cm;
- bridge floor (support) height – 75 cm (75 cm – bridge floor + 5 cm concrete slab);

Considering that the bridge floor followed to support a thick glass structure, the vertical drifts of the footbridge were limited at L/500 (opening/500). The steel that was used for calculation is S235 – min. tensile yield stress fy=230 N/mm^2.

ISSN 2285-2735, Pages 26 - 33

2. CALCULATION AND DESIGN OF STRUCTURE

2.1. Details about the structure, loads

The beneficiary commanded the footbridge calculation in two versions:

- version I – 1 cm - thick glass structure;
- version II – 2 cm - thick glass structure.

In the automatic calculation, only the footbridge floor was patterned and submitted to the following loads:

- weight of the 5 cm concrete slab (C) – 1.25 KN/m^2;
- useful load (U) – 4.00 KN/m^2;
- snow (S) – 0.40 KN/m^2;
- wind (W)– 1.00 KN/m^2;
- weight of the glass structure – 8 KN/ml (version I – 1 cm thickness), 16 KN/ml (version II – 2 cm thickness).

The weight of the glass structure + own weight (G_1=8 KN/ml (16 KN/ml - double thickness glass)), as well as the snow loads (S=0.31 KN/ml) and wind loads (W-wind) were patterned in the calculation under the form of linear and evenly distributed loads on the bridge floor along the side glass walls. To appropriately pattern the wind action, the calculation considered the force couple W=2.10 KN/ml (the moment generated by the wind action on the glass walls) and W_1=4.00 KN/ml – the horizontal force applied to the top of the bridge floor, Figure 1. On the final footbridge floor, a 5 cm - thick concrete slab followed to be executed and fastened with connectors.

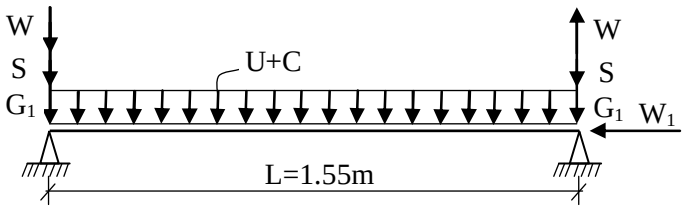

Figure 1. Charging scheme

Only the static calculation was conducted, for the seismic calculation was not necessary, the footbridge being located in an area of low seismic activity. The pattern analysis used 4 combinations of loads. The first 2 combinations match the ultimate limit state ULS (resistance), the next two – service limit state SLS (allowable flexure). The combinations of loads are made based on the equation 1 and the "k" coefficients of the Table 1.

$$\mathbf{k(D+C+G_1)+kU+k(W+W_1)+kS_g} \quad (1)$$

Table 1. Load combinations, value of coefficient "k"

ID Number	Dead	C	G_1	U	$W+W_1$	S	Type
1	1.35	1.35	1.35	1.50	2.625	-	ULS
2	1.35	1.35	1.35	1.50	-	2.625	ULS
3	1	1	1	1	1.75	-	SLS
4	1	1	1	1	-	1.75	SLS

The footbridge under study, is supported at one end on two rectangular columns having the cross - section of TUBO 400x200x14.2, and at the other end on a reinforced concrete beam girder having the cross-section of 50 cm x 100 cm, Figure 2. The 4.20 m long columns are embedded in the base, and, on the higher side, these columns do not take bending moment in any of both directions (longitudinal, transversal). At the opposite end, the supports of the footbridge on the reinforced concrete beam girder were shaped as to take over only loads in the transversal and vertical directions (simple supports), in the longitudinal direction being able to move freely.

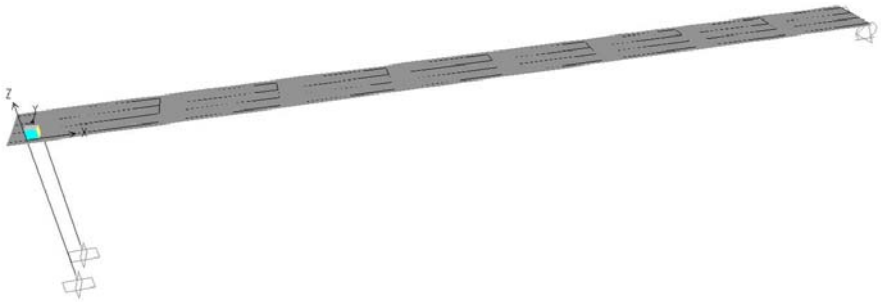

Figure 2. Static scheme

2.2. Patterns analyzed

2.2.1. Pattern made of 4 longitudinal beam girders HEB 700 (version I)

The first pattern under study was made of 4 longitudinal beam girders – laminated profiles HEB 700, arranged at equal distances on the width of 155 cm, Figure 3. These beam girders were stiffened in transversal direction with plates having the section of 1.5 cm x 70 cm – h = 63 cm, that were vertically arranged at equal distances of 280 cm, and one plate – with the section of 2 cm x 155 cm, horizontally disposed in the higher side of the beam girders HEB 700.

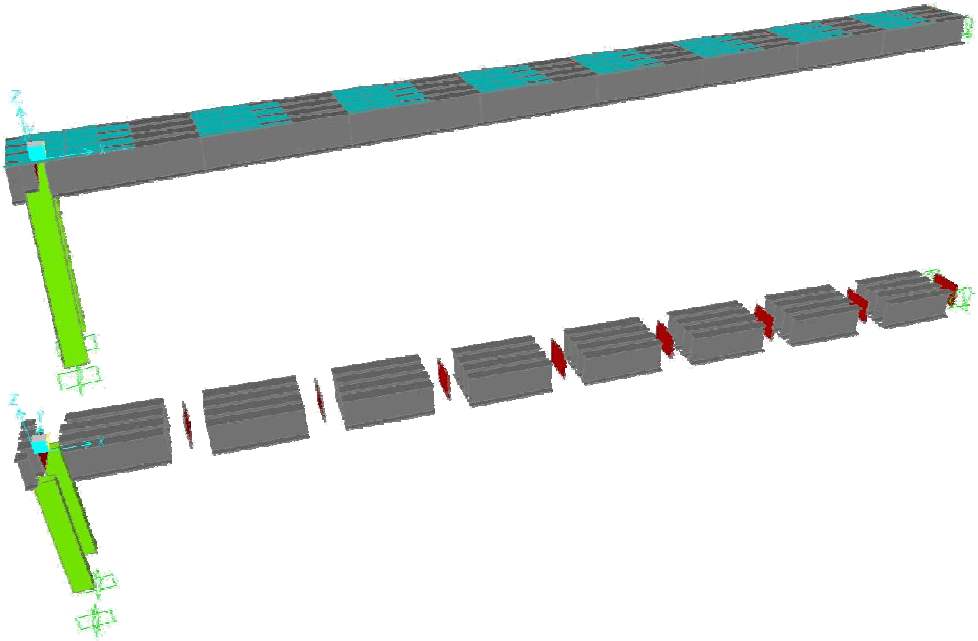

Figure 3. Analyzed model with 4 longitudinal beams HEB700

Following the analysis of the bridge floor in the “version I” it was established that it can be executed in this solution (total steel weight - 29.50 tons), exceeding the max. limit flexure requirements - Δ = 4.79 cm > 4.48 cm – the combination 4 (L/500=22.40/500), Figure 4, the resistance requirements being met more than the necessary.

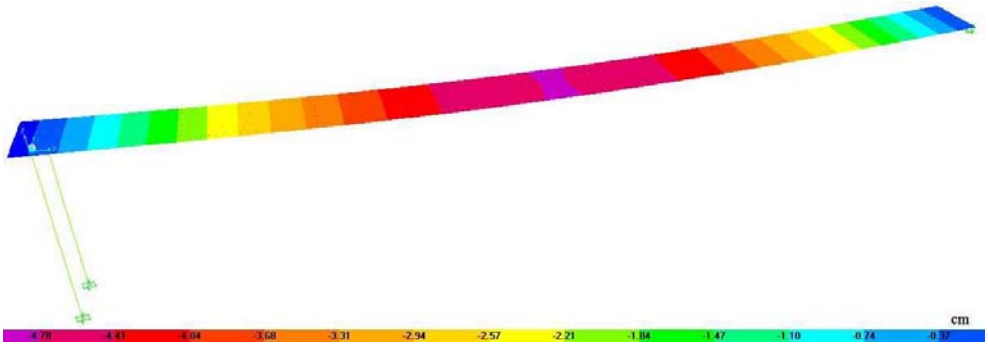

Figure 4. Deformed bridge floor (combination 4)

Due to in the “version II” the footbridge floor could no longer be executed in this solution (no higher cross-section profile could be taken into calculation), and due

to the fact that the height and width of the bridge floor were limited at max. 75 cm and 155 cm, this pattern was abandoned.

Further on, it was preceded at the execution of a pattern that is completely made of thick plates, keeping the same support solutions and the same loads.

2.2.2. Pattern completely made of thick plates (version I, version II

In the second stage, a pattern completely made of thick plates having the height of 75 cm and the width of 155 cm, Fig. 5 was designed.

The bridge floor was designed with three longitudinal vertical walls having the sizes 1.2 cm x 2280 cm – h = 75 cm and two horizontal plates of variable thickness, marked by "a....c". Along the bridge floor, two bracings – plates of 1.2 cm x 2280 cm – h = 20 cm were located at the higher base, and eight plates having the section of 1.2 cm x 155cm – h = 75 cm were positioned crosswise for stiffening at the distances of 320 cm.

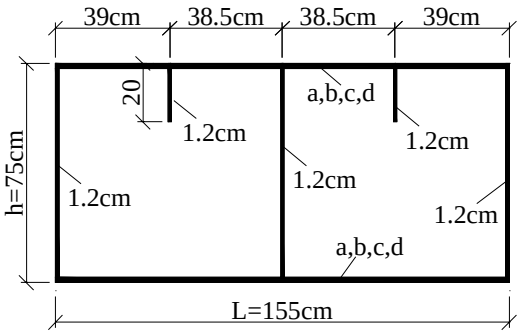

Figure 5. Bridge floor - cross section.

Following the calculations it was established that the resistance requirements were met without any issue for both versions (versions I, II). However, to meet also the max. allowed flexure requirements, it was necessary that for both patterns, on the central part of 3 x 320 cm = 960 cm, between the four cross-section bracings, the bases are thickened against the ends at 2.8 cm (b) instead of 1.8 cm (a) – Fig. 6, and, respectively, 5.0 cm (d) instead of 2.8 cm (c) Fig. 8.

As a result of the study conducted for the version I, it resulted a max. flexure Δ = 4.52 cm $\cong$ 4.48 cm (Figure 7) – the combination 4 (L/500=22.40/500), (total steel weight - 19.90 tons).

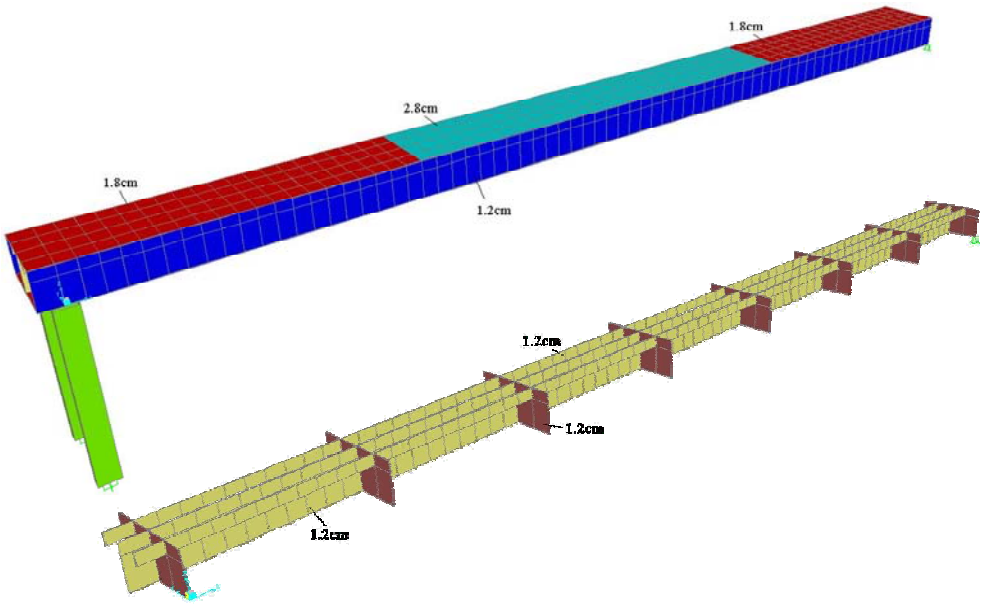

Figure 6. Analyzed model made of thick plates – Version I

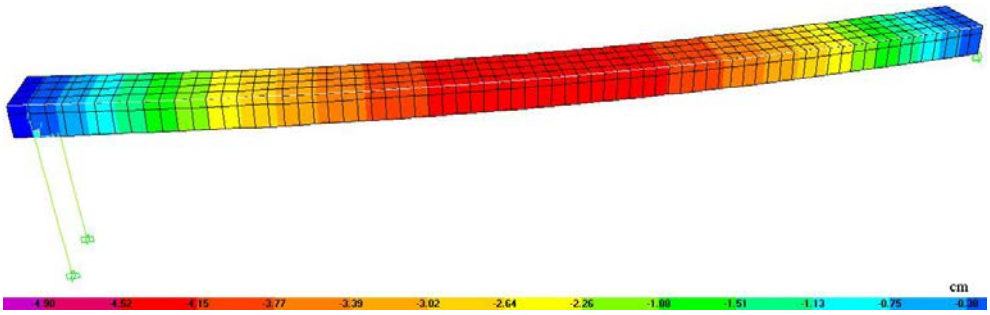

Figure 7. Deformed bridge floor (combination 4) - Version I

For the version II (double thickness glass - fig. 8), following the calculations a max. flexure Δ = 4.65 cm $\cong$ 4.48 cm (Fig. 9) resulted – combination 4 (L/500=22.40/500), (total steel weight - 28.40 tons).

In the version II, it was not necessary to change the other characteristics, except for the base thicknesses.

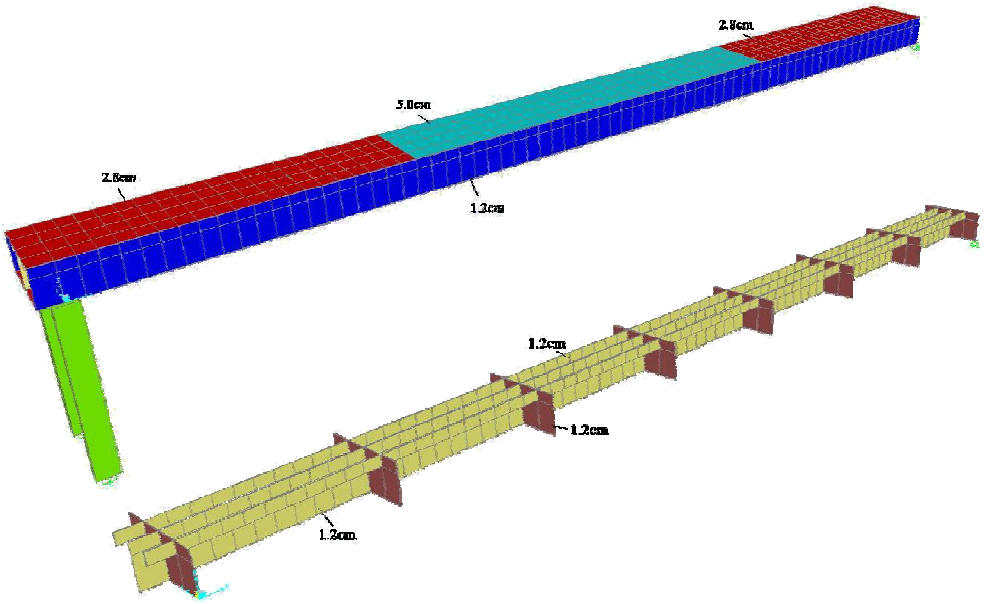

Figure 8. Analyzed model made of thick plates – Version II

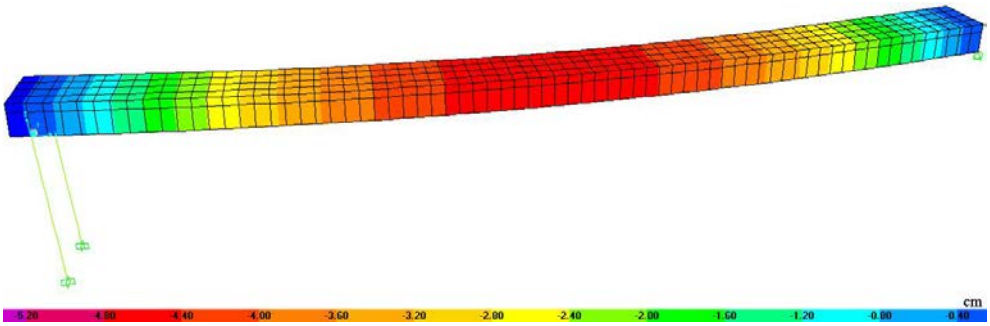

Figure 9. Deformed bridge floor (combination 4) - Version II

3. CONCLUSIONS

Based on the studies conducted, the following conclusions may be drawn: when there are architectural restrictions, in terms of drifts, big openings, etc., the most advantageous solution is to use the thick plates instead of laminated profiles. In turn, this solution assumes more work to execute the structure but, in the end, it leads to a substantial saving of materials.

In this case, the material consumption reduced from 29.50 tons for the version with laminated profiles, down to 19.90 tons for the version with thick plates. In order to find the optimum solution, the engineer has to analyze many times more than one possible solution, this significantly increasing the work load. The solution adopted in the end highly depends on the technical means that the engineer has available, on the acquired knowledge and, not lastly, on the engineer's expertise in design.

References

1. *** Eurocode 1: Actions on structures, Part 1-1: General actions – Densities, self-weight, imposed loads for buildings , EN 1991-1-1.
2. *** Eurocode 1: Actions on structures, Part 1-3: General actions – Snow loads, EN 1991-1-3.
3. *** Eurocode 1: Actions on structures, Part 1-4: General actions – Wind actions, EN 1991-1-4.
4. *** Eurocode 3: Design of steel structures, Part 1-1: General rules and rules for buildings, EN 1993-1-1.
5. *** Eurocode 3: Design of steel structures, Part 1-6: Strength and Stability of Shell Structures, EN 1993-1-6
6. Neurocampus, Bordeaux University Segalen, France., SC Construct Concept Gepa SRL, Iaşi, 2012.

Modelarea pe calculator a unei pasarele între două clădiri vecine cu acoperisul si părțile laterale realizate din sticlă groasă.

Introducere

Această lucrare descrie pe scurt modelarea pe calculator a unei pasarele între două clădiri învecinate cu o lungime totala de 2280cm şi o înălțime – 300cm, proiectul - Neurocampus, Bordeaux Universitatea Segalen, Franța. Pasarela are o lățime de 155cm, acoperişul şi părțile laterale sunt realizate din sticlă groasă. Pentru pasarela prezentată s-a impus gasirea unei soluții de rezemare a structurii din sticlă, astfel încăt pasarela să fie rezemată numai la capete şi să respecte condițiile de rezistență şi de săgeată maximă admisă (L/500). Datorită restricțiilor arhitecturale înălțimea tablierului a fost limitată la 75cm astfel încăt înălțimea totală a pasarelei să nu depăşească 300cm .

High performance methods and techniques for demolition

Vasile Iacob
[1] *Faculty of Civil Engineering and Building Services, "Gheorghe Asachi" Technical University, Iasi, 700050, Romania*

Summary

In the case of demolition, the efforts are naturally headed to some high performance methods and techniques for demolition choice that can assure the objectives achievement in the most economical and the safest way.
Choosing the demolition conditions and methods depends on the conditions that are imposed by the project, the construction emplacement, neighborhoods and the available equipment.
Most of the methods are applicable for all the structures type which has to be demolished, but there are some special methods that applies to a certain kind of structures that have some particularities. Based on the type and the composition of the demolition structure, a set of demolition procedures will be applied.
In this work, the author presents a series of demolition techniques and methods, and it's making a comparison between these.

KEYWORDS: methods, techniques for demolition, building demolition.

1. INTRODUCTION

During the execution of a demolition process, a very important role has the choosing of the methods and techniques for demolition which can provide achieving the goal initially established in a safe and economical way.

These methods can be established only after an extensive analysis of the project, setting the demolition target or targets, their form and structure, the materials of which they are made of and also the aspects regarding the location and neighborhoods. According to this information one may use a series of methods of demolition shown in figure 1.

ISSN 2285-2735, Pages 34 - 44

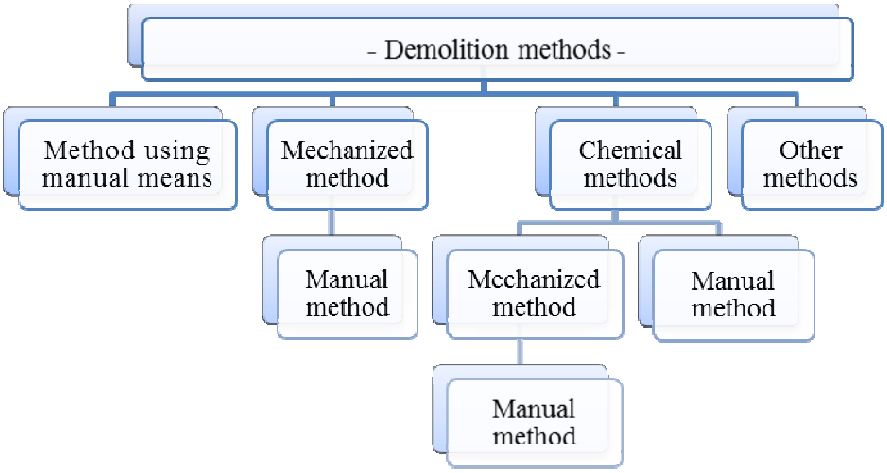

Figure 1. The ranking of the methods of demolition

As one can see in Figure 1, the role of the method using manual means is the most important during the process of demolition of a construction. It is the easiest method and it is also part of the other methods. The mechanized method is a newer method which man has been replaced by machines or tools but not entirely, so that after the machines demolish, the human force interferes by applying manual demolition processes.

The same can be said about the demolition using chemical methods. Once the construction is tilted or knocked down, the machinery cuts it into smaller pieces and shatters it. At the same time the human labor interferes for collecting manual the remaining armature from the broken concrete. So we can say that these methods are not independent but they complement each other in order to have a good achievement of the demolition process, to maintain the necessary time assigned for the process, to decrease the risk of accidents and to respect the legislation on labor protection.

2. THE METHOD OF MANUAL DEMOLITION

This is a traditional method which uses the human workforce for the main processes of demolition. The valuations of the risks have shown that using manual demolition processes leads to frequent accidents in construction sites.

The structures that are demolished using this method are usually buildings made of rock or brick, they have 2-3 levels and they do not require other special protection works. The working area of this method is low, that is why in order to decrease the time assigned for this process, the number of employees must be increased,

sometimes this method becoming uneconomic. The order of stages using the mechanical method will always be opposite to the order in which is was built, also taking into account the type of construction that is demolished. For constructions made of armored concrete, hammers can be used to break the concrete. The oxyacetylene flame is used for cutting the armatures. The structural elements are knocked down in a certain order using alternative methods. The armatures must not be loosened until the concrete blocks are pillared or sustained by other elements.

The balconies and the exterior walls are important elements in the demolition of a construction. In tight spots the fall of these elements can lead to accidents and that is why their demolition is done taking extreme safety precautions. When using ropes and cables to anchor these elements, their capacity must be at least 4 times bigger than the weight of the elements that are going to be sustained. The workers that are loosening the elements of the building must be anchored with ropes or cables which are checked at least twice a day.

If it is necessary to work at height and this thing cannot be done taking safety precautions, work platforms are assembled. These platforms must be adapted according to the need and the duration of the work undertaken.

The order of the demolition processes is determined by the conditions, the restrictions and the composition of the structures which are about to be demolished:

- the demolition will begin with the exterior walls, the balconies, the overhangs and other elements that are not aligned to the facades or to the walls of the structure;
- when demolishing the roofs, the elements will be loosen from the outside to the inside;
- the floors will be demolished starting from the middle to the end while they are pillared on beams (figure 2);
- the beams must be demolished in the following order:
    - the cantilever beams;
    - the secondary beams;
    - the main beams.
- if the beam stability is affected, they will be pillared to prevent their breaking before the original proposed order.

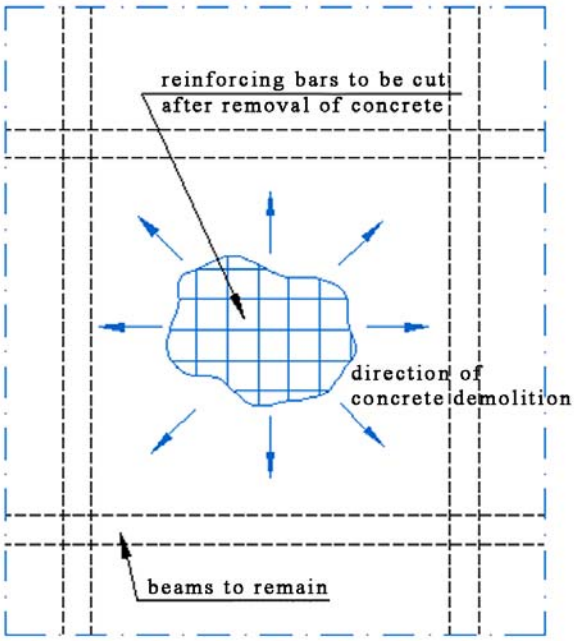

Figure 2. The breaking of the floor’s direction

- the bulkheads that do not carry any weight will be demolished before the resistant walls;
- the pillars and the main walls will be demolished only after they do not pillar any other elements.

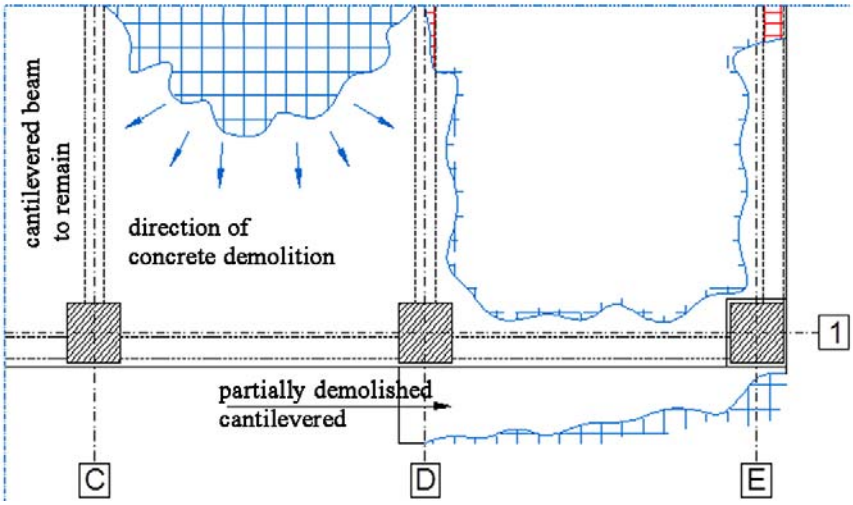

Figure 3. Slab demolition and cantilevered demolition

- the exterior walls, beams and pillars:
  - to avoid the falling of the bricks from a building's wall, they will be demolished or pushed inside the building before the armature of the following below plaque to be cut;
  - the concrete frames will be put down loosening each element one from another.
- exterior beams:
  - exterior beams can be gradually demolished by breaking the concrete or tearing the entire section.
- exterior column (figure 4):
  - the top of the pillars must be ensured by binding or attaching other elements which will be demolished later;
  - the concrete will be broken from the bottom of the pillar in a sense to direct the bending and the fall of the item in the originally wanted spot.

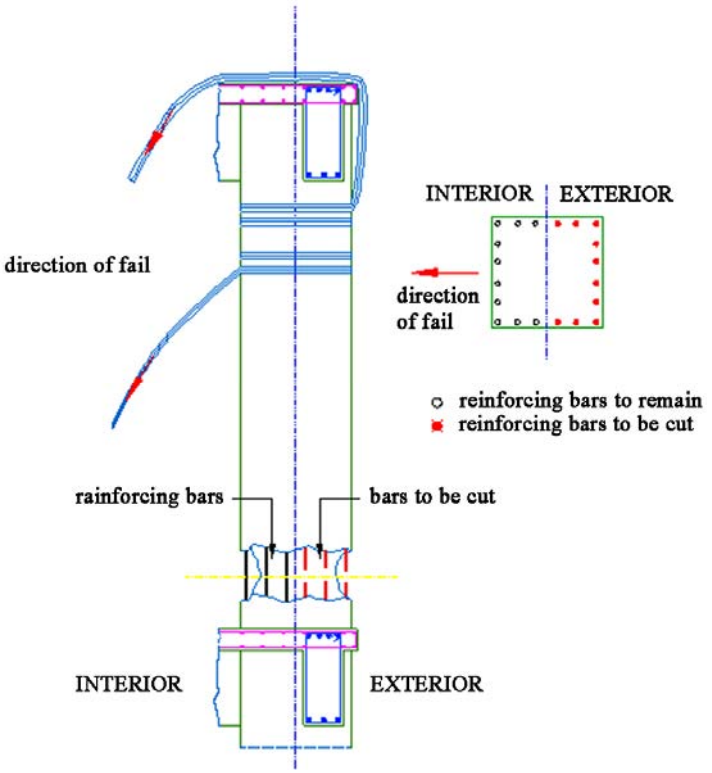

Figure 4. Pre-weakening and dismantling of column (manual method)

- exterior reinforced concrete frame:
  - the exterior reinforced concrete frame may be demolished in sections;

- for manual demolition, the optimum section of the frame to be demolished shall be a bay between the two adjacent columns but shall not be wider than 3 m;
- the frame section shall be secured to other structural members with wire and winch before disconnecting the framing from the remaining structure;
- pre-weakening shall be performed at the bottom of the two columns.

- reinforced Concrete Wall:
  - reinforced concrete walls may be demolished by cutting down the wall into manageable sections;
  - the width of the wall shall not be wider than 2 m.

When demolishing just a part of the building, the stability and integrity of the building in the area that work is not executed will be checked and monitored at fixed time intervals.

3. METHODS OF DEMOLITION WITH MECHANICAL MEANS

With the development of human society and technology, the human labor was replaced with the mechanized one. In the construction industry this phenomenon has resulted in the emergence of machineries and tools classified according to the processes for which they were designed.

According to the method chosen, the demolition method by machinery may include:

- mechanical demolition ‘‘top-down’’, with compact equipment used in lifting;
- mechanical demolition by pushing or pulling;
- mechanical demolition using the demolition ball;
- mechanical demolition by cutting with scissors or pneumatic hammer.

Replacing human labor with machines did not entirely removed the risk of accidents, so that according to each machinery and the work done by it, some safety measures for preventing accidents must be taken. All machinery, equipment and their accessories must be used, inspected and maintained in accordance with the manufacturer’s recommendations (figure 5).

Figure 5. Hydraulic scissors arm of 21 m damaged

Before using the devices for cutting, breaking and lifting, they must be carefully examined. The persons handling them must be qualified to handle that equipment and they must have some experience in demolition work in order to ensure that the working range of the machine is not exceeded because that can cause the instability of the machine.
At any time the driver of the machine must be aware of the progress of the demolition target. This can be done by appropriate means such as:

- a direct view over the object for demolishing;
- the use of a surveillance system;
- a direct informing by a signalman.

There will be determined the exact criteria by which the demolishing will be done, there will be a organization of the work for seeing the space used by the action of the equipment, to ensure access to the objective of demolishing and also the space used for retreat in case of danger. It will be decided the places where the machinery can move the torn pieces of the building, so that they do not constitute a danger to others around and also in order to facilitate an easy access for the machines used for loading and transporting (figure 6).

Figure 6. Arranging ramp access to the objective to be demolished

3.1. The mechanical demolition ‘‘top-down’’

The mechanical demolition ‘‘top-down’’ is a complex method and may be applied to multi-level buildings. The demolition begins by the machine’s lifting on the top of the building. Before this operation there will be a technical expertise to see if the stability and the resilience of the building is not affected by placing the excavator on the building. If it is considered that the weight of the excavator is greater than the ability to support the floor on which it runs, linings will be assembled on the lower floor.

3.2. Mechanical methods using machines for working at greater heights

This method involves using mechanical means of great productivity. It cannot be applied to constructions with a large development on horizontal and higher than 30m. In this type of tools may be part: hydraulic shears for concrete and iron, concrete sprays, hydraulic hammers or breaking balls – which provide a high efficiency for the demolition and safe conditions for the targets that are near the constructions which are being demolished.
With this kind of equipment one can demolish buildings made of brick, stone, armored concrete, metal having different forms or structural types: buildings and industrial buildings, chimneys, bridges, silos, trestles, foundations. In principle, the demolition of buildings with mechanical methods for working at great heights lies in cutting from top to the bottoms of the floors, the main and secondary beams and finally the pillars, paying particular attention to the fall direction of the structures which are at height.

4. DEMOLITION BY CHEMICAL TECHNIQUES

The chemical techniques for demolition are relatively new and they may be applied to a certain area of demolition objectives, apart from the controlled explosion method which has a very diversified application area.
The methods are the following:

- demolition by controlled explosions;
- demolition using chemical agents for breakage and rupture;
- demolition using the hot cutting;
- demolition using water jets.

Those that use these methods need more qualifications because the these methods are more complex by increasing the risk of accidents that can happen because of not paying attention or not knowing some factors that interfere while applying them.

4.1. The demolition using controlled explosion

Each demolition project represents a special and unique case, the account of shooting parameters adapting to the situation. A set of shooting parameters are counted on the basis of the constructive element targeted for fragmentation and of the explosive used taking into account the precautions of the environmental protection. A simple modification of one of these types of input data leads to the changing of the values of the shooting set resulted.
The method for calculating the shooting parameters is based on the calculation of the explosive charges based on the geometrical size of the elements and the desired effect.

Nowadays, we use two controlled methods of the demolition of buildings, namely:

- the demolition with vertical collapse, without a large scattering of the resulting fragments. In this way there are the demolitions with a development between collapse and the vertically fall by scattering the building fragments on a small area;
- The demolition with lateral collapse (by tipping). This collapse represents the fall on a part of the construction by destabilizing a part of the base of the construction.

Since in most cases the demolition of buildings takes place near other targets which must remain intact, it is necessary to assess the effect of the explosion on the neighboring buildings because they can be affected by the slide of the materials, by the air wave and by the seismic wave.

4.2. The demolition using non-explosive demolition agent (NEDA)

NEDA are static demolition agents. They are used for demolition in restrictive environments where the noise and the vibrations are less tolerated, at breaking the foundations, the pillars and also for blasting. It is a compound comprising a mixture of chemicals and water, forming a paste which if it is poured into drilled holes, it will expand and so it will result the breaking of the elements made of concrete.

NEDA' s breaking effect is relatively small compared to that of blast and ancillary works for loosening and removing the remained scraps are necessary.

4.3. The demolition using methods of hot cutting

The demolition using hot cutting techniques involves hot temperatures up to 2000-4000◦ C. These conditions also require some special precautions and accident prevention measures.

The using of these methods will not be used unless:

- a project has demonstrated that there is no alternative to demolition;
- special measures were taken to prevent fire, it's spreading and also to isolate the operation;
- there were taken adequate safe measures to prevent the injury of the personal involved;
- in the working environment ventilation measures were taken and the persons with direct contact with the fire have protection equipment.

5. CONCLUSIONS

One may say that the choice of the demolition methods depends on the project condition, the equipment available, the amount and the type of materials which

result from the demolition, the location of the building to be demolished (urban or industrial area), and it's surroundings.
We must also consider the level of protection to be provided, the number of technical means and the personnel allocated to work, the quantity of material to be discharged and the distance to the place of storage.
Most methods are applicable to all types of structures to be demolished, but there are special methods that apply to certain types of structure.
Within the pale of the execution of a demolition project, you will be never able to use just a demolition method, although there will always be a main method. Starting from that, a certain comparison can be made the main methods to see which one of them will suit better for a project.
So, in the next table are presented some similarities and differences between the main demolition methods.

Table 1. Preliminary comparison between different types of demolition methods

Parameters	Demolition method		
	Manual	Mechanized	Controlled explosions
Material	Brickwork, stone, ground construction	Any material, but harder for metal and concrete constructions	Any kind of material
Maximum height	Maximum 2,3 levels constructions	Until 20 m height construction	No limitation
Work area	Small, it's growing in the same time with the no. of employees, but it's getting uneconomical	Large, depending on the number of the outfits used	For the execution speed, the explosion is made sectorial, not depending on the area
Noise level	Medium, persistent	High, long time	High, but instantaneously
Seismic vibration	It's not the case	It's not the case	Directed, controlled
Cracks	It's not the case	Medium	Controlled by explosion
Dust releases	Local, medium	Local, large	Very large, but for a short time
The demolition effects	It's not the case	Are not being watched as usual	Indicated by the following tools.
Security of performers	Poor	Poor	Maximum, for keeping the technology
Affected time	Very high	High	Small
Costs (depending of mechanized method)	Medium, 60%	100 %	Small, as usual under 40%

References

1. Iacob, V., erbănoiu, I., *Managementul demolării construc iilor i valorificarea materialelor rezultate*, Ed. Societă ii Academice "METEI – TEIU BOTEZ" , Ia i, 2011.
2. Iacob, V., Teză de doctorat - *Managementul dezafectării construc iilor i valorificării materialelor rezultate*, Universitatea Tehnică "Gheorghe Asachi" din Ia i, Ia i, 2011.
3. Buildings Department, Code of practice for demolition of buildings, New York, 2004.
4. BSI, Code of practice for demolition, London.

Aspects regarding the post-use construction stage

Vasile Iacob
Faculty of Civil Engineering and Building Services, "Gheorghe Asachi" Technical University, Iasi, 700050, Romania

Summary

After the lifetime ending of a construction, this is entering into the post-use stage. This new phase represents a component of the quality system of the construction, being pre-established and organized in such a way that it can be developed in more phases, in order to solve the problems that come with the constructions and the improvements from the construction site, after their use and exploitation it's totally finished.

In this work, the author describes this stage, presenting detailed the main phases that need to be made in the last part of a construction lifetime.

KEY WORDS*:* construction lifetime, post-use stage, building demolition.

1. INTRODUCTION

The life cycle of a building represents the period of time from its ''conception'' until its ''death'', in which a built space satisfies the requirements of its users.
The life of a building – a fixed space subject to usage – is difficult to predict due to the physical and moral usage of that occurs throughout the life of the buildings. The physical life of a building can be defined as the time between the moment it was built and the moment when it no longer satisfies the strength and stability requirements.

2. POST-USE CONSTRUCTIONS STAGE

The life cycle of a building comprises the period in which a series of stages follow one another, namely:

- the conception and design stage;
- the execution of the project stage;
- the utilization stage (exploitation / utilization / prosecution);
- the post-use stage.

ISSN 2285-2735, Pages 45 - 50

After the end of the life of a building, it enters the post-use stage. This new stage is a part of the quality system in construction, being pre-established and organized to take place in several stages in order to solve the problems raised by the buildings and their design from the built environment, after the complete ceasing of their exploitation and use.
Before the post-use stage, there can be established two main directions (based on a technical expertise):

- the physical demolition of the building;
- the restoration of the building which aims to restore the existing building into a new state of functionality. This can mean:
  - the structural restoration – restoring or increasing the carrying capacity of some structural elements;
  - the functional restoration – establishing a new stage of functionality in order to satisfy new requirements, such as: environmental requirement, ambient requirements, technical and constructive requirements, ecologic ones etc.

In the post-use stage (figure 1), one can go through the following stages:

- the decommissioning of the building;
- the dismantling and demolition of the components of the building;
- the refurbishment, the recycling and the reuse of the materials resulted from the dismantling ant the demolition;
- the reintegration in nature of the non-recyclable waste.

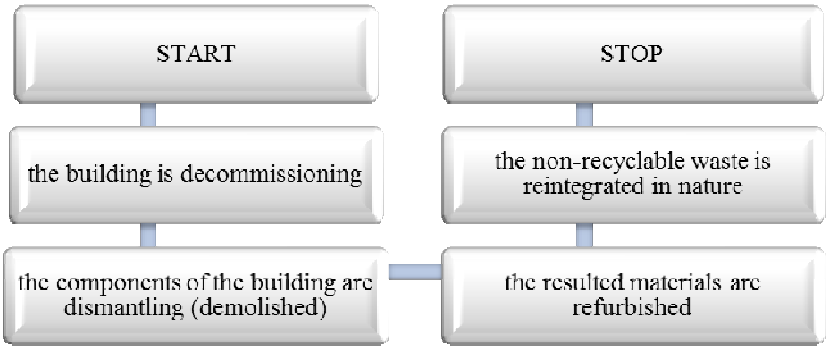

Figure 1. The post-use stage

It should be noted that after the utilization stage of a building, its beneficiary can decide its restoration and not its decommissioning. In this way, after the restoration, the building starts a new stage of usage, with other words – a new life cycle which, according to some authors, it should submit the following structure (figure 2).

Stage	Stage content
	START
1	A feasibility study on the restoration of the building is drawn up
2	Is the restoration feasible?
3	A technical expertise is drawn up
4	Can the building be restored?
5	The building is demolished
6	STOP
7	The technical documentation for the approval of the restoration is established
8	The technical documents for the execution is made by the designer
9	The publicity for announcing the executors interested in the restoration of the building is organized
10	The bidding documents is made by the designer
11	The tender documents are made by the interested executors
12	After the analysis of the executors' tenders, the winner of the auction is chosen
13	The restoration work is performed
14	The operating cycle of the building is resumed
15	Once the operating cycle of a building is finished, is a new restoration of the building possible?

Diagram

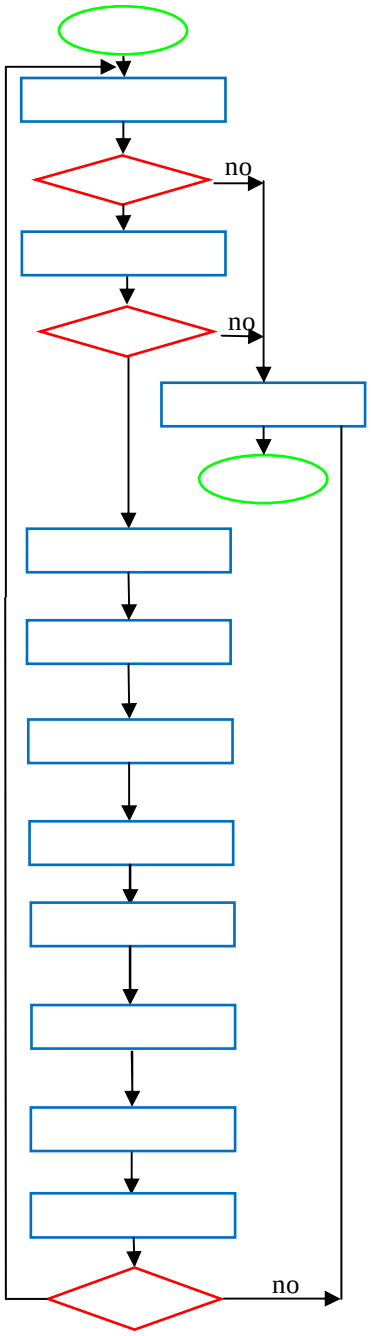

Figure 2. The decision stage to restore the building or to demolish it

The entire route of the post-use stage can be seen in the diagram in figure 3, where we can see the main tasks that the builder and the beneficiary of a demolition project have.

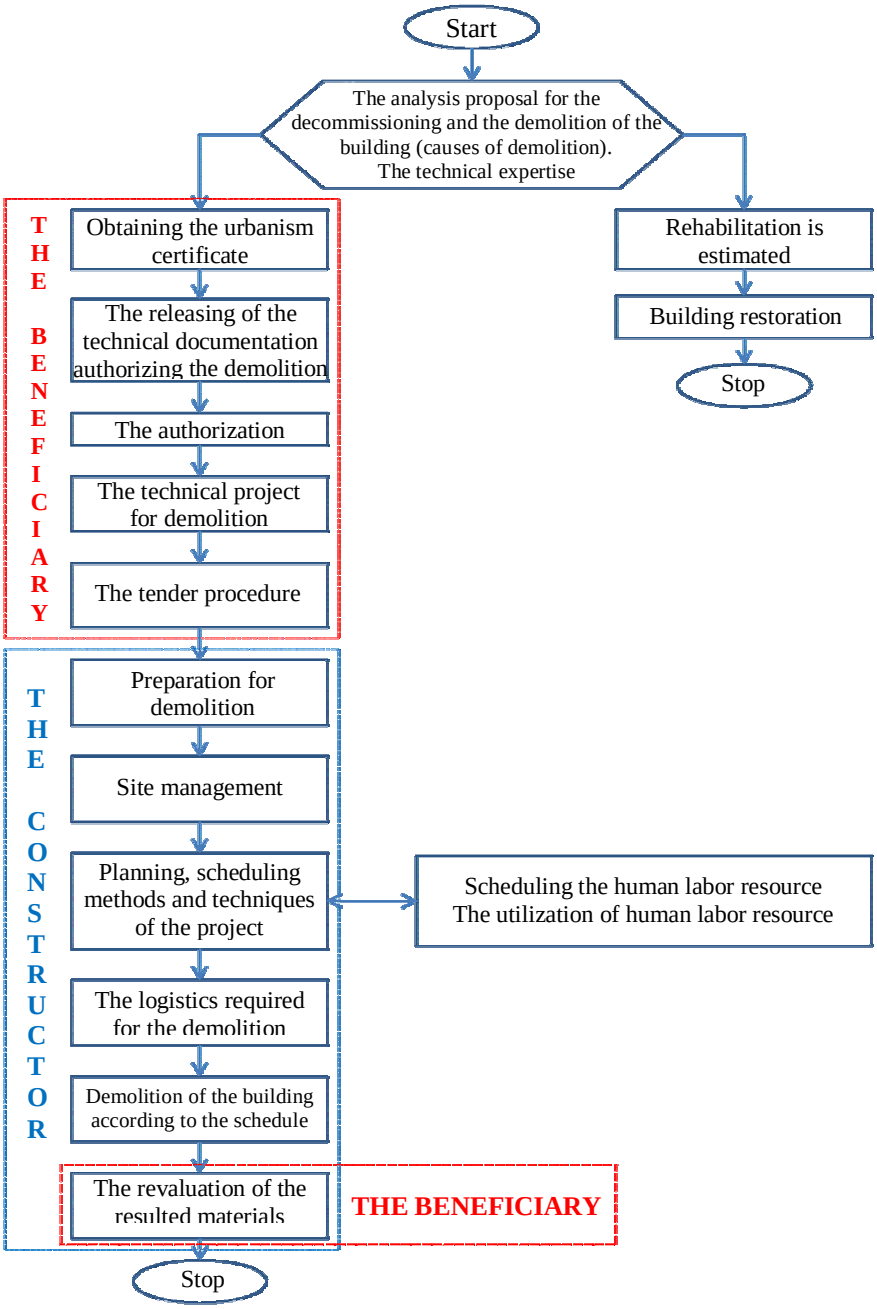

Figure 3. Tasks of the beneficiary and the constructor regarding the demolition project

The post-use is a decision stage, the beneficiary having the power to decide the restoration or the demolition of the building, this thing being possible only when the causes for which the possibility of demolition is studied are normal, resulting from:

- limited lifetime of the component parts of the building;
- the materials form which the elements of the building are made of;
- the operating conditions of which the buildings are subject to;
- the environmental conditions provided for the buildings;
- the action of the external agents, temperature variation (freezing-thawing), wind,

or the moral utilization which occurs due to the development of the requirements of users regarding the building's functionality, the utility consumption, comfort etc.

When there is an accidental attrition, which occurs due to earthquakes, uncontrolled explosions, storms, blizzards, long-term rainfalls, subsidence of the land, mostly we cannot speak about the restoration of the damaged buildings, but more about their demolition. The only study that can decide between the restoration and the demolition is the technical expertise, which establishes the exact stage of degradation of the affected building.

Once the beneficiary has decided to demolish the building, he will have to make a file which follows a series of steps to authorize the demolition, starting with the obtaining of a town planning certificate until the election by auction or direct commitment of the project to a builder who will precede the demolition.

The builder will schedule the work for the execution of the demolition project, according to the contract settled with the beneficiary. Also according to all the terms of the contract originally set, the beneficiary and the builder will evaluate the materials resulted from the demolition of the building.

3. CONCLUSIONS

The concept – the projection, the achievement and the utilization are important stages in the life cycle of a building. Equally important is it post-use. Of late years, the construction market has greatly expanded, new and advanced materials have appeared, the execution time has decreased. In this way has appeared the need to demolish the buildings that no longer satisfy the current requirements or that have exceeded their lifetime. And this thing is not very easy because decades ago when they were built, there was not today's problem with the ecological and fast demolition.
The researchers, the executors need to come up with a set of measures to make the decommissioning and the demolition of buildings much easier. The urban

agglomeration does not allow anymore demolition sites that have a large area or a long period of activity. Thereby, there must be designed materials and types of constructions that can be removed easily, removed in a short time period and mounted elsewhere. Currently, there are special types of constructions suitable for these requirements. They are especially industrial buildings made of prefabricated metal or concrete.

References

1. Iacob, V., Şerbănoiu, I., *Managementul demolării construcţiilor şi valorificarea materialelor rezultate*, Ed. Societăţii Academice ”METEI – TEIU BOTEZ” , Iaşi, 2011.
2. Iacob, V., Teză de doctorat - *Managementul dezafectării construcţiilor şi valorificării materialelor rezultate*, Universitatea Tehnică ”Gheorghe Asachi” din Iaşi, Iaşi, 2011.
3. Iliescu, C. R., *Managementul reabilitării blocurilor de locuinţe pe baza costului global*, Ed. Societăţii Academice ”METEI – TEIU BOTEZ” , Iaşi, 2010.
4. Cozmescu, C., Teză de doctorat - *Contribuţii privind evaluarea riscului financiar în execuţia construcţiilor*, Universitatea Tehnică ”Gheorghe Asachi” din Iaşi, Iaşi, 2009.

Effect of embankment height on the pavement and road culverts reactions

Mohammad Mehdi Khabiri, Mohammad Saberian
Civil Engineering Department, Yazd University, Yazd, 8 9 19 574 1, Iran

Summary

The soil is poured onto the bridge deck in various thicknesses to provide adequate pavement Height and highway appropriate slope. This layer reduces the reflection cracks and other Failure from concrete slab deck to the pavement surface also provides soft bed and Comfort for wheel vehicles. Also has a positive effect on the height of the bridge section bending moment, bottom Stress intensity is reduced and hence extended Cracks and damage growing slower. The finite element software has been used in the research process. Concrete bridge, aggregate material and the asphalt top layer has been modeled by elastic systems on it. Span bridges culverts lengths and aggregate base material thickness are variables in research. Abaqus modeling software and Two-dimensional elastic model has been. Increased by an average of 2 0% of the layer thickness reduces the stress intensity, as well as the life of the pavement and bridge structure increases. So if the road culvert is adequate for water flowing, should be added to the height of the embankment.

KEYWORDS: embankment height, pavement Reactions, road culverts.

1. INTRODUCTION

Occurrence of all type of pavement failures leads to reduction of its surface quality and longevity. Bridge is usually used for traffic intersection and culverts are usually used for road drainage and passing of surface water due to raining are made along the way. Done researches show that all failures are occurring in pavement and bridge structures.Figure1 represents the occurred failure in one of Fasa bridges. The occurred longitudinal and transverse cracking on this bridge is due to weakness of subgrade. The height of backfilling on bridges and culvert are usually depending on:

1-Providing the height of road balance line.

2-providing the minimum backfilling height on bridge slab.

ISSN 2285-2735, Pages 51 - 57

High height of backfill on bridge deck and culverts can decrease the stress of loading of vehicle wheels. But high height of backfill not only has economical restrictions, but also it has executive restrictions for example for providing the suitable higher for backfill shouldn't decrease the height of culvert span. In present study, it's examined the effect of various backfill heights on bridge deck over maximum stress and strain, that they are the reasons for failures and occurrence of cracks on bridge and pavement structures, by use of finite element in 2D coordination

Figure1. Pavement distress on bridge situation (Fasa Bridge)

2. LITTERER REVIEW

One of methods for analyzing the effect of soil structure interaction is using from software finite element which has the program 2-D ANSYS for calculating the soil pressure and structural deformation. One of the results indicates increasing the backfill modulus of elasticity results in decrease in soil-structure interaction and when the poison's ratio of soil decrease, it has a positive effect on compressive stress of arched steel bridge [1].

Most of researches are about the effect of backfilling behind bridge retaining wall. One of them has examined the behavior of integral bridges with full weight abutments against cyclic (seasonally-daily) due to temperature variations. The research method was experimentally and was used for six different modals [2].

The specifications of Caltrans state that the minimum thickness soil filling coverage or embankment depth should be Span/25 or 1m minimum. Figure 2 shows the desired thickness by this specification.

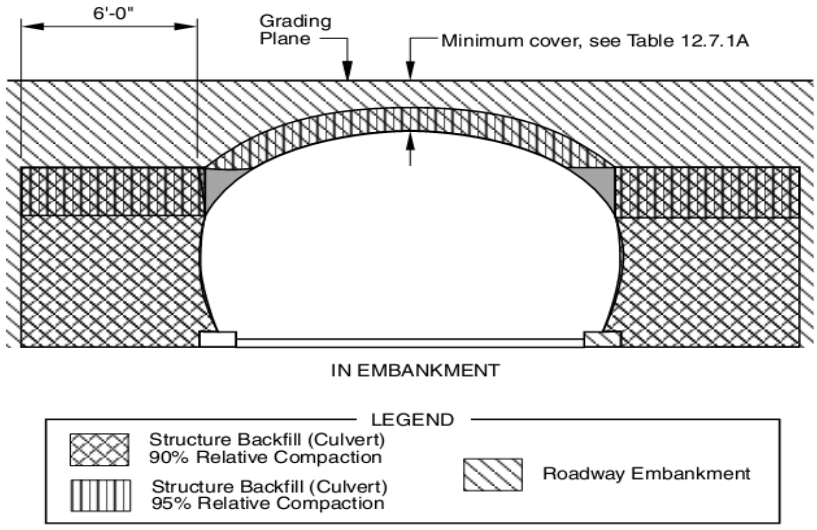

Figure2. Soil coverage for the metal ring culvert [3]

In a previous investigation, the full-scale performance testing of cast in place concrete box culvert is proposed. Strain distributed through the rigid pavement on top of slab culvert discussed and combining experimental work on the design is presented [4].

By another researcher to study factors affecting on the rate of culvert deformation, were chosen 16 culverts that have settlement in forest road. Table 1 shows the some of these studies results, deformation decreases with height [5].

Table1. Effect of culvert depth on culvert settlement in forest road [5]

Culvert depth (M)	Culvert settlement (Cm)
0.5-0.9	31.2
0.9-1.2	16.4
1.2-1.5	14.2

In other research result indicates, that, a variety of types of structural damage to RC culverts happen during service age. Numerical simulation and field tests is performed to examine the effect of soil characterizes on the structural reliability of RC culverts under high backfill [6].

3. ANALYSIS AND RESULTS

Pavement modeling in agreement with figure3 is done by software ABAQUS in 2-D forms. Modulus of elasticity, materials of concrete slab, backfill on deck slab and asphalt layer are considered invariable in all models. Loading on pavement and bridge has been done by single wheel load of a truck standard axle 4.1 tons that this amount of load is placed widely and uniformly in center of the bridge span.

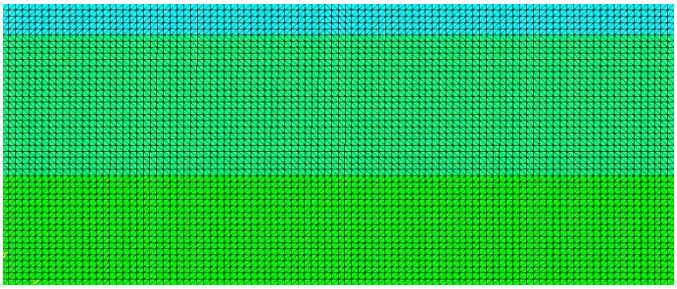

Figure3. Geometric modal and meshing of pavement layer on bridge

To analyses the effect of height changes on reaction of pavement and bridge deck, the following different forms are considered in analysis and software performance:

1-Changes of bridge or culvert spans, 1.5, 2.0 and 2.5 m

2-Thickness changes of backfilling on bridge; 30, 45; 60; 75 and 90 centimeters

3-The reaction of pavement were measured in some areas containing stress and strain, such as: under wheel, on slab (under backfill) and slab support.

For controlling the accuracy of modeling by software ,figure 4, shows the pavement reaction towards loading, that in this figure can see the reactions are symmetrical because geometrical and strength of bridge and pavement components is symmetry.

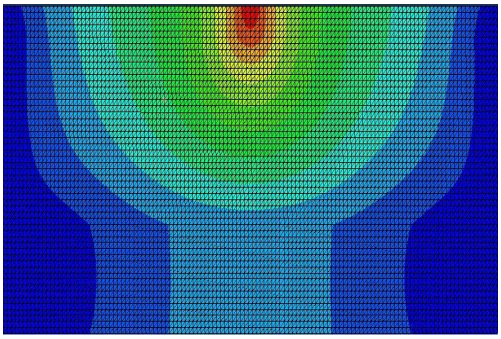

Figure 4. Model pavement response to central loading

In continue the manner of strain and stress changes in different areas of pavement are examined as follows:

A) The effect of backfill height on stress under wheel

In a bridge with width 1.5 m, the amount of stress on pavement surface will be decreased by increasing the backfill height on bridge slab. Figure 5, shows these change. The bridge with span 2m and 2.5 have been compared in this figure, too. The stresses on pavement in its failure are defined as pavement rutting.

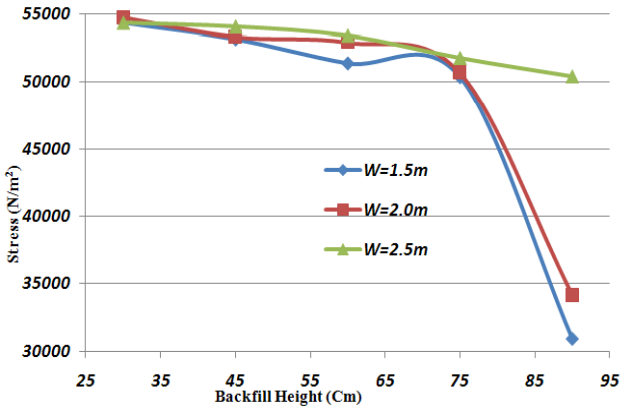

Figure5. Stress change on pavement due to increase in backfill height

B) Strain changes under subgrade

Strain under subgrade, which is the starting point in tension crack, increase as a result of changes of backfill height on concrete slab. Figure 6, represent that this form is examined for spans 2 and 2.5 m.

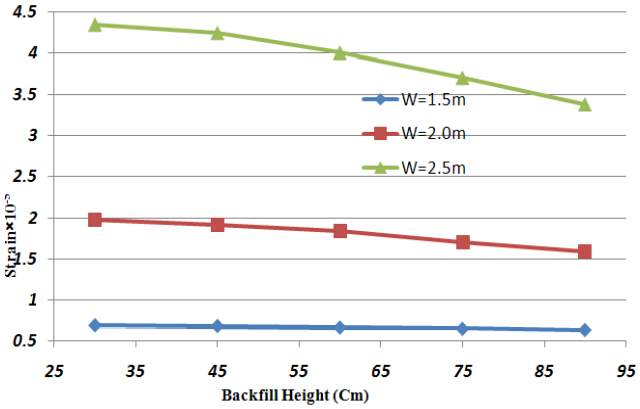

Figure6. Strain change on slab (under subgrade) due to increase in backfill height

C) Effect of bridge span on pavement performance and reaction of bridge deck

In these studies, three different forms of bridge span 1.5,2 and 2.5m are considered. The diagram of strain changes on pavement in three different heights: low (30 cm), average (60 cm) and high (90cm), are drown in figure 7 to examine the effect of changes of bridge span on pavement operation. Figure 7, shows the accrued stress changes in support for different spans and thickness of backfill.

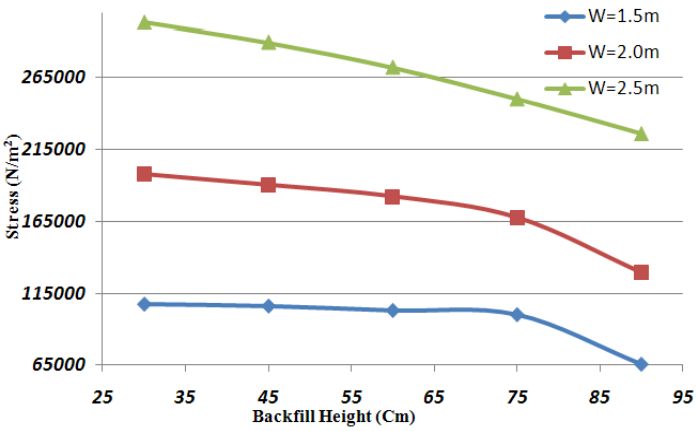

Figure7. Stress change on support for different spans and thickness of backfill

4. CONCLUSIONS

By considering the changes and diagram slops in figures 5 to 7 it can be understood the flowing:

1-The effect of backfill height in strain changes will be lower by increasing the bridge span. It means the height of backfill doesn't have any significant role in decrease of failures in high spans.

2- The effect of double broken pavement i.e. strain on pavement and strain under subgreade increase due to the effect of backfill height with different rates. As increase of strain failure on pavement will be more due to decrease of backfill.

3-The change of bridge and culvert span have no significant in height changes of backfill in bridge.

In another examination, it can be used from 3-D analysis and also loading modeling and pavement reaction can be used from dynamic mode. Moreover, by experimental tests in laboratories can examine the validity of this study results.

Acknowledgements

This analysis was done by M.Saberian, Master of science Student in Yazd University.

References

1. Liu B., Zhang M. ,Li P. and Feng Z., *Effect of parameters on soil structure interactive of a buried corrugated steel arch bridge*, The Open Civil Engineering Joutnalvol.5,Pp154-162,2011.
2. Tsang N., England G. and Dunstan T., *Soil/ structure interaction of integral bridge with full height abutments*, 15th ASCE Engineering Mechanics Conference, EM2002, June 2-5, Columbia University, Newyork, 2002.
3. Caltrans, *Bridge design specification*, Section 11, April, Pp10-12, 2002.
4. Abdel-Karim, A M,Tadros, M K and Benak, J V, *L ive load distribution on concrete box culverts*, Transportation Research Record No. 1288, Geotechnical Engineering, p. 136-151, 1990.
5. Nasiri M., *Investigation of culvert settlement in hyrcanian forest roads*, *International* Journal of Civil and Structural Engineering, Volume 2, No 2, pp532-543, 2011.
6. Chen B. and Sun L., *The impact of soil properties on the structural integrity of high-fill reinforced concrete culverts*, Computers and Geotechnics, Volume 52, July 2013, Pages 46–53. *http:/ / dx.doi.org/ 10.1016 / j.compgeo.2 013 .03 .006*

Numerical Simulations of a Frame Structure with a Single Passive or Semi-Active Tuned Mass Damper

Septimiu-George LUCA, Cristian PASTIA
Departament of Structural Mechanics, „Gh. Asachi" Technical University of Iaşi, Romania

Summary

A three-storey structure coupled with passive or semi-active tuned mass damper is described and analytical models are obtained. Uncertainties in dynamic characteristics of a structure as well as the frequency content and intensity of the excitation may cause a deterioration of the performance of the passive tuned mass damper (TMD). For these reason a semi-active tuned mass damper (STMD) with variable damping is studied. Semi-active clipping strategy is performed in order to optimize the performance of the STMD. The models are analyzed from numerical simulations point of view for harmonic and seismic excitations. Comparison of the results demonstrates the efficiency of a STMD is better than that of a passive TMD.

KEYWORDS: structural control, vibrations control, semi-active damping, passive control.

1. INTRODUCTION

Passive tuned mass damper (TMD) is widely used to control structural vibration under wind load but its effectiveness to reduce earthquake induced vibrations. The first structure in which a TMD was installed appears to be Certerpoint Tower in Sydney, Australia. Also, the first major buildings using a TMD, in the USA were the John Hancock Tower in Boston, completed in 1975 and the Citicorp Center in New York, completed in 1976. In Japan, the first TMD was installed in the Chiba Port Tower, followed by other installations [4].

Generally, inertial mass is attached near the top, through a spring and a viscous damping mechanism (e.g. fluid damper or viscoelastic damper) in order to absorb energy inputted into the structure and can be very effective if it's tuned to a natural frequency of the structure. The effective region of the TMD is limited to a narrow frequency band centring its tuned frequency. The damping characteristic is present in order to limit the device displacements. The very narrow band of suppression frequency and the sensitivity problem due to detuning are the inherent limitations

ISSN 2285-2735, Pages 58 - 64

of the passive TMD [1]. A TMD, by definition, do not require external power for its operation.

Active structural control require considerable amount of power for enhancing structural functionality and safety against natural hazards such as strong earthquakes and high winds. An active control device consists in an actuator able to generate a request force [5]. This can be calculated with a great variety of control law (optimal control, acceleration feedback control, integral force feedback control, H_2 control, H_∞ control, PID etc.) based on acceleration, speed, displacement or force measurement [8]. Energy cannot only be taken away with active control, but can also be inserted into the structure. Active tuned mass damper (ATMD) systems can provide significant reduction in building displacement and acceleration than that of passive TMD. Although the ATMD demonstrates superior performance, the active systems have the disadvantage of power failure during vibrations and great costs to implement such technologies.

Semi-active control systems are a class of active control systems for which the external energy requirements are smaller amounts than those of typical active control. A battery power, for instance, is sufficient to make them operative [9]. Semi-active devices cannot add or remove energy to the structural system, but can control in real time parameters of the structure such as spring stiffness or coefficient of viscous damping. These control devices are often viewed as controllable passive devices.

As an extension of semi-active damping concept that has been successfully applied to a broad class of vehicle vibration isolation problems, a STMD with variable damping has been proposed for structural vibration control [5]. Hovrat et al. [3] investigated a STMD in order to control wind-induced vibrations in tall buildings. Simulations studies showed the proposed system is superior to conventional passively controlled and comparable to actively controlled system. Pinkaew and Fujino [7] demonstrated the effectiveness of a STMD with variable damping under harmonic excitation using an optimal control law, which minimizes the quadratic performance index for the STMD.

The purpose of this paper is to investigate the control characteristics of the STMD for vibration mitigation in harmonic and seismic excited frame structure. Employing numerical simulations, comparison among displacement responses of a frame structure coupled with a TMD, a STMD and an ATMD are discussed.

2. DESCRIPTION OF THE FRAME STRUCTURE

The frame structure constructed inside the ELSA laboratory has three storeys. It consists of a steel frame with floors constituted by sheet metal and concrete

properly connected. The inter-storey high is 2 meters because the scale was considered 2/3 of a real structure. The structure has been tested with dynamic and pseudodynamic techniques. Without entering into details, the mass, stiffness and damping matrices that will be used in the analytical model are as follow:

$$\mathbf{M} = \begin{bmatrix} 5000 & 0 & 0 \\ 0 & 5000 & 0 \\ 0 & 0 & 5000 \end{bmatrix} \quad \text{(Kg)},$$

$$\mathbf{K} = \begin{bmatrix} 45774000 & -25936000 & 647000 \\ -25936000 & 36260000 & -17555000 \\ 647000 & -17555000 & 12600000 \end{bmatrix} \quad \text{(N/m)},$$

$$\mathbf{C} = \begin{bmatrix} 5854 & -3547 & 1347 \\ -3547 & 5073 & -1571 \\ 1347 & -1571 & 2273 \end{bmatrix} \quad \text{(Ns/m)}.$$

With the above matrices, the identified natural frequencies and the damping ratios are reported in the following table:

Table 1: Frequencies and damping ratios

Frequencies	f_1	f_2	f_3
	3.018 (Hz)	10.29 (Hz)	19.09 (Hz)
Damping ratios	ξ_1	ξ_2	ξ_3
	0.8 %	0.32 %	0.8 %

These low values of the damping ratio are normally for a steel structure. The modal matrix of the structure is the following:

$$\mathbf{\Phi} = \begin{bmatrix} 0.2756 & 1 & -1 \\ 0.7168 & 0.7550 & 0.9138 \\ 1 & -0.8169 & 0.3794 \end{bmatrix}$$

3. EQUATIONS OF MOTION

The equations of motion of lumped mass structure at which it's considered a STMD with variable damping, installed at its top may be written as

$$\begin{cases} \mathbf{M}\ddot{X} + \mathbf{C}\dot{X} + \mathbf{K}X = \begin{bmatrix} 0 \\ 0 \\ c_{sa}\dot{x}_{tmd} + k_{tmd}x_{tmd} \end{bmatrix} + \begin{bmatrix} -m_1\ddot{x}_g + P_1 \\ -m_2\ddot{x}_g + P_2 \\ -m_3\ddot{x}_g + P_3 \end{bmatrix} \\ m_{tmd}\ddot{x}_g + c_{sa}\dot{x}_{tmd} + k_{tmd}x_{tmd} = -m_{tmd}(\ddot{x}_g + \ddot{x}_3) \end{cases} \quad (1)$$

where $\ddot{x}_g$ represents the horizontal components of a recorded ground acceleration and $\{P\}$ is a vector containing the horizontal harmonic forces.

4. DESIGN OF THE TMD AND THE STMD

TMD can be very effective if it's precisely tuned on the resonance frequency, which we want to reduce it. The structural mode of vibration to be controlled with TMD is the first because the other two modes give a negligible contribution to the total response. The ratio μ between the mass of the TMD and of the system should be chosen typically around 1/100. Considering $\mu = 0.0105$, the following dynamic characteristics of the optimal TMD were assumed:

Table 2: Dynamic characteristics of the optimal TMD

m_{tmd}=157.2(Kg)	k_{tmd}=53950(N/m)	ξ_{opt}= 6.1%

where, the damping ratio ξ_{opt} of TMD is obtained by Den Hartog as function of mass ratio μ as

$$\xi_{opt} = \frac{1}{2}\sqrt{\frac{3\mu/2}{1+3\mu}} \quad (2)$$

In case of semi-active tuned mass damper it's consider a variable orifice device in order to control the damping coefficient of the TMD. The variable damping devices compromise a hydraulic cylinder with a controllable by-pass valve and can be fashioned from a conventional damper with provision for fast modulation of the damping coefficient. The damping characteristics of a variable orifice can be controlled between two damping values (low damping when the valve is completely opened and high damping when the valve is completely closed) by varying the amount of flow passing through the by-pass pipe from one chamber of the piston in the other. If the valve is open, the damping can be virtually reduced to zero if the by-pass is large enough. In the intermediate position the device produces a specific damping dissipation. The adjustment of the valve can be made usually electromechanically (e.g., servo valve or solenoid valve). It can be assumed that the

cylinder of semi-active device is attached by to the building mass, and the piston is connected to the TMD, which acts as a dynamic absorber.

For the passive mode of operation, the valve is stationary and partial open, which corresponds to the standard passive scheme. During semi-active mode of operation electrical signals from a control computer initiate the control valve action. Thus, different damping levels are produced depending on the valve position.

The adjustment of the time-depending damping coefficient *c(t)* can be produced by the semi-active damping law [6,7] as:

$$c_{sa} = \frac{f_c}{\dot{x}_{tmd}}, \text{ for } x_{tmd} \neq 0 \tag{3}$$

where f_c is desired control force computed by an active control strategy. The function $f_c / \dot{x}_{tmd}$ saturates between c_{min}=10 Ns/m and c_{max}=750 Ns/m. The variation of c_{sa} occurs only when the term $f_c / \dot{x}_{tmd}$ lies within a variable range. Otherwise is set to either the minimum or maximum value. For this reason the control law is similar to the continuous clipping control strategy. The control is accomplished by measuring the actual relative velocity of the STMD and the acceleration of the third storey of structure.

The required force is computed according to the Figure 1 and has the relationship as follow:

$$f_c = g m_{tmd} \ddot{x}_3 \tag{4}$$

where *g* is control gain. There is considered an actuator, which acts on the tuned mass damper. This actuator is not attached by the structure mass and for this reason the control system is called ideal active tuned mass damper (ATMD) in order to help us to design a semi-active control law. Dyke et al. [2] experimentally demonstrated efficiency to use a control strategy, which weights the acceleration of the structure in order to design an active tuned mass damper. In that case the actuator had interaction with the structure.

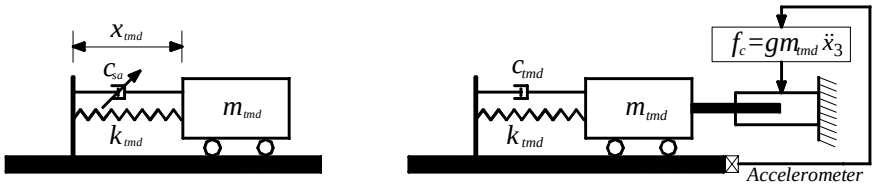

a) b)

Figure 1: a) Configuration of semi-active tuned mass damper (STMD);
b) Ideal active tuned mass damper (ATMD)

5. NUMERICAL RESULTS

The frame system has been modelled with Simulink and several simulations has been performed using as input El Centro earthquake acceleration and harmonic excitation. Figures 2 to 5 show the comparisons among the time history displacement responses of the structure in the uncontrolled case and controlled case with passive and semi-active TMD under El Centro simulated earthquake and harmonic excitation. The harmonic forces excitation is used at the frequency $\omega = 18.965$ rad/s (corresponding with the first natural frequency of the structure) and the force amplitude is F=1000 N. It's supposed that the force acts at the level of each floor in horizontal direction.

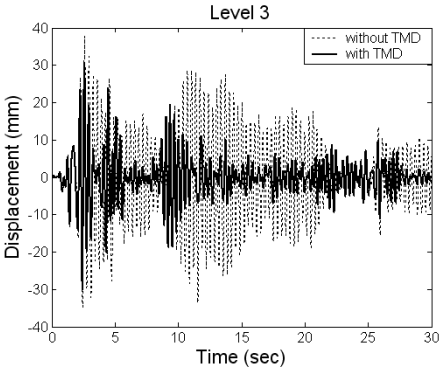

Figure 2: Comparison between displacement responses of the structure without and with TMD under El Centro earthquake

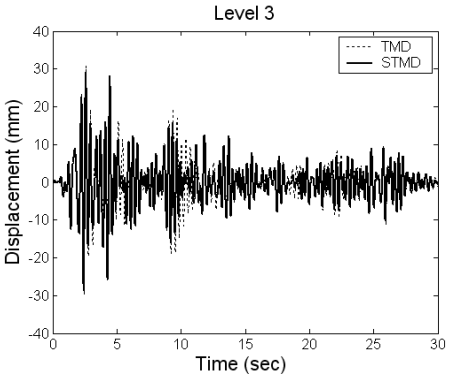

Figure 3: Comparison between displacement responses of the structure with TMD and STMD under El Centro earthquake

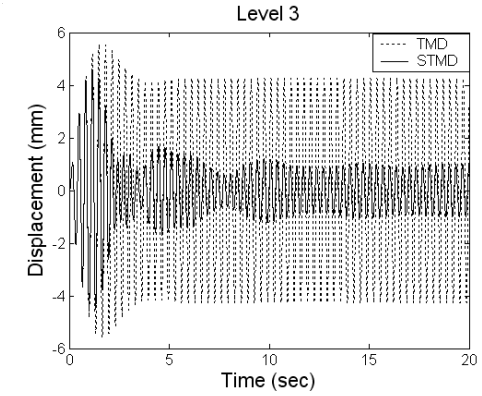

Figure 4: Comparison between displacement responses of the structure with optimal TMD and STMD under harmonic excitation.

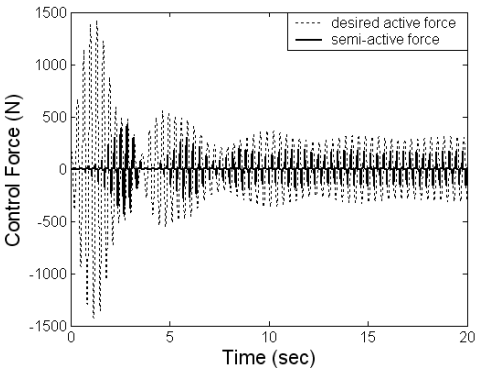

Figure 5: Comparison between desired active control force and actual semi-active control force.

The control gain is g = 4.8 for the active case. In the semi-active case the gain is g = 5.5 for achieving the desired active force that is used in order to optimize the damping coefficient c_{sa}. The curves show that significant displacement reduction can be achieved with STMD than with passive TMD under harmonic excitation. In steady state response, this reduction is approximately 70%. Figure 5 illustrates the time history of the semi-active damping force and the active force. It's seen that the semi-active force acts like a large impulse force. However, the STMD, which utilizes the modulation of damping to achieve the performance of an active system, cannot supply the energy into the system because the dashpot always dissipates the energy. Therefore, for the first 1.5 s, the damping of the STMD is set to minimum in order to maximize the energy transfer from structure.

6. CONCLUSIONS

The semi-active TMD performance has been compared with those of passive and active TMD systems. The results of numerical simulations indicate that the STMD can substantially improve the response of the structure around the tuning frequency over the passive TMD.

References

1. De Silva, C.W, Vibrations: Fundamental and Practices, Boca Raton, Florida, USA, CRC Press LCC, 2000.
2. Dyke, S.J., B.F. Spencer, P. Quast, D.C. Kaspari and M.K. Sain, Implementation of an AMD using Acceleration Feedback Control, *Microcomputers in Civil Engineering: Special Issue on Active and Hybrid Structural Control*, 1996.
3. Hrovat, D., P. Barak and M. Rabins, Semi-active versus passive or active tuned mass dampers for structural control. *ASCE Journal Eng. Mech.*, 691–705, 1983.
4. Housner, G.W, L.A Bergam, T.K Cauchy, A.G. Chassiakos, R.O Claus, S.M and R.E. Skelton, T.T. Soong, B.F. Spencer, and J.P.T. Yao, Structural control: Past, present and future control. In *Journal of engineering mechanics*, 897-971, 1997.
5. Marazzi, F., Semi-active Control of Civil Structures: Implementation Aspects. *Phd thesis*, University of Pavia, Structural Mechanics Department, 2002.
6. Pastia, C., Passive and Semi-Active Control Systems: Theoretical, Numerical and Experimental Aspects. *Final Report*, Special Publication I9040, European Commission JRC, Ispra (Italy), 2004.
7. Pinkaew, T. and Y. Fujino (). Effectiveness of Semi-Active Tuned Mass Dampers under Harmonic Excitation. Engineering Structures 23, 850-856, 2001.
8. Preumont, A., Vibration Control of Active Structures: An Introduction 2nd Edition, Kluwer Academic Publishers, 2002.
9. Soong, T.T. and B.F. Spencer , Supplementary Energy Dissipation: State-of-the-Art and State-of-the-Practice. In *Engineering Structures*, Vol. 24, pp. 243–259, 2002.

A Bayesian approach to seismically induced fragility

Mihaita Mihai
Department of Structural Mechanics, "Gh. Asachi" Technical University, Iasi, 700050, Romania

Summary

Seismic action is a major cause of structural damage that leads to significant reductions of the structure' s load-bearing capacity. Therefore, all works targeting the structural carrying capacity reassessment should include models specifically designed to account for damaging. This paper addresses a strength and safety theoretical analysis, based on probabilistic concepts, of reinforced concrete structures subjected to stochastic loads. Unlike the design of new structures, evaluation of existing buildings requires, most of the time, the presence of local damage that reduces element' s strength and stiffness. This aspect complicates computation and requires the use of appropriate behavioral models, able to accurately reproduce the degradation phenomena. Given the continuous processes of cracking and damage as a result of environment action the reinforced concrete structures are the appropriate candidates for such analysis. The paper tackles the problem of structural failure with the help of limit state function that depends on a set of parameters. Means of estimating element' s fragility and of constructing fragility curves, using a Bayesian approach, are presented. In the final part an example a of fragility curves, built according to FEMA/ HAZ US methodology, is also presented.

KEYWORDS: fragility, fragility curves, Bayesian analysis.

1. INTRODUCTION

In recent decades structural engineering experienced a fast progress which led to great advances in both the basic concepts of safety and design standards [1]. It became imperative to study the ductility exceeding risk of existing structures, designed and built according to old concepts and design rules. This is done in order to determine their insurance level in relation to current regulations and establish, on this basis, the response measures during extreme events as well as the building's life spam. Relevant examples of related researches are: Kazanti et. al. [2], Zahr et. al. [3], Senel and Kayhan [4], Bakhsh and Asadi [5].

Construction safety, an essential part of the design process, is based on evaluating the structure's behavior to loads represented in the computing flowchart as

ISSN 2285-2735, Pages 65 - 74

stochastic processes [6] and the analysis of load carrying capacity parameters. This goal can only be achieved if one takes into account all the factors that enter into this "equation", from the initial stage (conceptual approaches) until service phase.

In this context, the safety assessment of buildings under seismic actions is based on a comparison between the large number of plastic incursions cycles and an admissible value, taking into account only the maximum plastic strain cycle and neglecting other cycles [7]. In contrast, closely related to structural seismic risk assessment, is the structure fragility concept [8] which is a brittle structures characteristic, where the strength of this type of structure is given by the strength of the weakest element that composes it.

In respect to the above, a frequently used philosophy to achieve the objectives set out previously uses the deformation energy as a mean to quantify hysteretic degradation [9]. Thus, it is considered that failure occurs when a structure dissipates energy equal to, or exceeding a certain threshold value. Unlike strength of the material that uses failure criteria to account for different types of breaking modes in the case of seismic applications there is not a unique failure parameter that could exhaustively describe degradation. The aim is to design structures to meet the requirements of high ductile deformation. Such structures absorb the seismic energy is by transforming the kinetic energy into plastic strains.

All these ideas have led to a new modern approach of design, a method that is called "resilience design". The principles underlying this method are: stress limiting, establishment of energy dissipation areas, overload protection of brittle zones, behavior assessment of the load carrying frame. The strong point of this design strategy is that it provides the structure ductility reserves.

As an integrated component of the resilient design philosophy one will notice the seismic fragility concept, which is defined as the failure probability of a structural component or assembly. Most of the time, seismic motion intensity is expressed by a single variable, for example, the peak ground acceleration – PGA.

Over time fragility estimation was performed using an expert’s opinion [10], using the Monte Carlo simulation for specific structural systems [11], by Bayesian analysis of observed damage data of structural sub-system [12] or by combination of the above [13].

This paper proposes a stochastic estimation method of the reinforced concrete frames seismic damage, using fragility models. Fragility curves are determined statistically as well as by Bayesian updating. The main advantage of this new approach is that the fragility of these models can be transferred to other structural systems.

Finally the methodology of constructing fragility curves for reinforced concrete structures using FEMA/HAZUS methodology is presented. The model is applied to

the Romanian built stock, taking into account the technical regulations in force over time in our country.

II. FRAGILITY

II.1. Fragility of structural elements

A component structural fragility is defined as the conditional probability that the component reaches or exceeds a predetermined limit state, for a given set of boundary variables.

The function $g(x,\theta)$ will denote a mathematical model that describes the limit state for the targeted component, where **x** is a vector of measurable variables and θ is a vector of model parameters. The function $g(x,\theta)$ is defined so that the event

$$g(x,\theta) \le 0 \tag{1}$$

represents reaching or exceeding structural component's limit state.

Generally **x** can be partitioned as **x=(r, s)**, where **r** is a vector of variables that describes the capacity of the structural component, and **s** is a vector of variables that describes the structural component loading states by boundary forces or displacements.

The components of θ are non-measurable parameters that are introduced into the limit state model building process and. The structural component fragility is given by:

$$F(s) = P\left[g(r,s,\theta) \le 0 | s\right] \tag{2}$$

where $P[E|s]$ is the conditional probability of event E given the values of the variables (from the vector) **s**. The uncertainty of event $g(r,s,\theta) \le 0$ for a given **s** is due to: the inherent randomness of the capacity variables **r**, the inexact nature of the limit state model $g(r,s,\theta) \le 0$ and the inherent uncertainty of the θ model parameters.

For a given set of boundary variables **s** (i.e. loading) the component's fragility is given by:

$$F(s) = P\left[\bigcup_i \{g_i(r,s,\theta) \le 0\} | s\right] \tag{3}$$

where $g_i(r,s,\theta)$ is the limit state model for failure mode i.

The above approach has an important advantage given that the test results help build the components of fragility curves. Simultaneously the approach provides alternatives when using mathematical models describing the behavior of structural components based on the principles of Solid Mechanics. It also allows the use of an analysis covering all uncertainties significant to the fragility assessment process.

The following is based on the concept of Bayesian probability theory. It is important that the Bayesian approach contains all available information, including: mathematical models describing structures behavior, laboratory test data, field observations and engineering judgment. As previously, it also is important that the Bayesian approach takes into account all uncertainties, including those that are intrinsic in nature and purely theoretical. Therefore, the Bayesian concept is ideal for this purpose and these requirements.

II.2. Fragility estimation

If (θ,σ) is considered as the set of limit state model parameters and $f(\theta,\sigma)$ as the coupled posteriori probability density function obtained by a Bayesian analysis, for the given parameters one can define the conditional fragility function using the following relationship:

$$F(s,\theta,\sigma) = P\left[\hat{g}(r,s,\theta) + \gamma \le 0 \middle| s\right] \tag{4}$$

In this case, fragility estimation depends on the values of θ and σ, although these parameters are still unknown because of uncertainties given by the theoretical knowledge.

II.2 .1 Predictive fragility

Another way of addressing parameter's uncertainty when estimating fragility is to treat θ and σ as random variables and apply the same algorithm as in the case of θ and γ. Therefore, fragility estimation is defined as a predictive measure. It is obtained by integrating the function of conditional fragility when subjected to all possible values of the (θ,σ) vector, with the corresponding probability density of (θ,σ) as weighting function:

$$\tilde{F}(s) = P\left[\hat{g}(r,s,\theta) + \gamma \le 0 \middle| s\right] = \int F(s,\theta,\sigma) f(\theta,\sigma) d\theta d\sigma = E_{(\theta,\sigma)}\left[F(s,\theta,\sigma)\right] \tag{5}$$

In the above equality $E_{(\theta,\sigma)}[\ldots]$ is the average with respect to the random variables θ and σ, and one can immediately notice that the predictive fragility is the

conditional fragility average for all possible values of θ and σ, and that it accounts for the uncertainty of human knowledge.

II.2 .2 . Fragility boundaries

Assuming that $F(s,\theta,\sigma)$, for a given **s**, is a function of the random variables θ and σ, its probability the distribution is determined. In the next step, $F(s)_p$ will denote the fragility value corresponding to the cumulative probability p, which is equivalent to stating that there is probability p that $F(s,\theta,\sigma)$ is less than $F(s)_p$. Mathematically this is expressed by the following relationship:

$$p = P\left[F(s,\theta,\sigma) \le F(s)_p\right] \tag{6}$$

where the interval

$$\left[F(s)_p, F(s)_{1-p}\right] \tag{7}$$

is the confidence interval (1-2p) x100% of the fragility estimate for a given **s**. The interval range is a direct measure of fragility's epistemic uncertainty. From the above it is clear $F(s)_p$ computed according to relation (7) requires a probabilistic locally inverse analysis.

II.3. Fragility computing methods

The method to point wise estimate $\hat{F}(s)$ and $\tilde{F}(s)$ requires integration over the entire domains of possible values of the random variables **r** and γ for each given **s**. Computing the predictive fragility $\tilde{\tilde{F}}(s)$ additionally requires integration over the entire domain of θ and σ. Confidence intervals, a given by relations (6) and (7), require one to perform a probabilistic superimposed analysis.

III. FRAGILITY CURVES DEVELOPMENT

When estimating the failure probability of a structure all the elements that may cause must be considered. As a phenomenon, one has to account that all elements interact and the failure of one element can lead to failure of the entire structure. On this basis it is considered that the structure consists of a combination of elements. For a structure made of brittle materials, the structure's strength is given by the

strength of its weakest element. To analyze the structural safety the most widely used method is the one that leads to the development of fragility curves. Using these curves the probability that a structure's response exceed a threshold is expressed. The probability is determined taking into account the parameter that defines the seismic motion [14].

III.1. Fragility curves formulation

The data required for formulating probabilistic fragility curves (seismically induced fragility data) are usually very difficult to obtain, requiring testing and fine-tuned engineering judgment.

Fragility curve for any component and also its related uncertainty can be best expressed by an approximation of the average ground acceleration $\breve{A}$, multiplied by the product of two random variables. The ground acceleration corresponding to failure is given by the following relationship:

$$A = \breve{A}\varepsilon_R\varepsilon_U \tag{8}$$

where ε_R şi ε_U are random variables with unit mean.

The advantages resulting from the previous formulation are:

1. The fragility curve as well as its related uncertainty can be expressed by only three parameters: $\breve{A}$, ε_R and ε_U. Because of the limited data amount regarding the seismic fragility it is simpler to make estimates based only on the three parameters than based on the entire shape of the fragility curve of and itsuncertainty;

2. The formulation given by relation (8) when assuming lognormal distribution for the random variables leads to an easier solving.

III.2. Parameters influencing the fragility curves

To approximate the fragility curve parameters $\breve{A}$, ε_R and ε_U it is desirable, from the calculation time point of view, to operate with a random variable called safety factor – F.

Structural safety factor can be obtained from the composition of a capacity factor F_C and a conservative response factor F_{RS}, the relationship being expressed by the formula:

$$F=F_C \bullet F_{RS} \tag{9}$$

where $F_C= F_S \bullet F_\mu$, F_S – strength factor and F_μ – inelastic energy absorption factor.

The inelastic energy absorption factor F_μ highlights that structures and components are capable of absorbing large amounts of energy without losing stability.

The conservative response factor F_{RS}, shows that the structural response during design phase is computed using specific deterministic parameters.

III.3. Methods used in fragility curves development

Depending on the input data and the methods used to obtain the probabilities associated with each damage state, the methods used to develop fragility curves are: methods based on observed data, experimental methods, methods based on the results of surveys, analytic methods. The above listed methods relate to a lognormal distribution function for the obtained results. The lognormal distribution function is used to determine the probability of exceeding a certain level of damage D_{si}. The damage level is computed for a given value of the seismic intensity.

IV. CASE STUDY - Fragility curves development for reinforced concrete structures, using the fema/hazus methodology

The following case study presents the results of an analysis performed on concrete and masonry structures. The input data includes seismic characteristics of Romania's territory and built stock. The HAZUS methodology, developed by The Federal Emergency Management Agency (FEMA), was used to estimate the potential losses from disasters. The most common types of concrete and masonry structures in contemporary Romania have been classified, using the FEMA / HAZUS methodology, and are presented in Table 1.

Table 1. Classification of concrete and masonry structures in Romania [15]

HAZUS Code		Structure type	HAZUS height	
			Name	Floors
17	CIM	Reinforced concrete frames	Mid-rise	4÷7
18	CIH		High-rise	8÷
20	C2M	Reinforced concrete shear walls	Mid-rise	4÷7
21	C2H		High-rise	8÷
23	C3M	Reinforced concrete frames with unconfined	Mid-rise	4÷7
24	C3H	masonry	High-rise	8÷
34	URML	Unconfined masonry	Low-rise	1 – 2
35	URMM		Mid-rise	3+

The FEMA/HAZUS methodology defines four stages of building damage or degrees of damage (slight, moderate, extensive and complete). Table 3 provides

guidance for vulnerability assessment of buildings in Romania being based on buildings' age and seismic zonation maps that were available during building construction. The percentages of damaged buildings, belonging to the four damage scenario, were computed and are presented in Table 2.

Table 2. Percentage of buildings different damage states, to MGA = 0.2 g and 0.4 g [15]

HAZUS Code		Damage type	% of buildings with different damage levels for MGA=0.2g			% of buildings with different damage levels for MGA=0.4g		
			Pre-code	Low-code	Moderate-code	Pre-code	Low-code	Moderate-code
18	C1H	Damage≤S.		14	18		2	2
		S.≤Damage<M.		19	25		4	9
		M.≤Damage<E.		35	44		21	41
		E.≤Damage<C.		21	11		29	31
		Damage ≥C.		11	2		44	17
20	C2M	Damage≤S.		21	33		3	6
		S.≤Damage<M.		26	33		9	19
		M.≤Damage<E.		37	28		35	44
		E.≤Damage<C.		12	5.5		29	24
		Damage≥C		4	0.5		24	7
21	H	Damage≤S.		18	22		2*	3
		S.≤Damage<M.		29	37		10	16
		M.≤Damage<E.		37	36		35	52
		E.≤Damage<C.		13	4.6		31	23
		Damage≥C.		3	0.4		22	6
34	URML	Damage≤S.	25	19	Not	4	5	Not
		S.≤Damage<M.	15	21	allowed	5	9	allowed
		M.≤Damage<E.	26	27	by	16	22	by
		E.≤Damage<C.	17	13	HAZUS	20	23	HAZUS
		Damage≥C.	17	10		55	41	

In Table 2 the following abbreviations have been made: S – slight, M – moderate, E – extensive, C – complete.

Table 3. Guidelines for choosing the damage function for buildings in Romania [15]

MKS intensity as given by the seismic zonation map	Building erection period				
	Before 1940	1941-1963	1964-1977	1978-1990	After 1990
VI	Pre-code		Low-code		
VII				Moderate code	High Code
VIII					
IX					

Table 4. The relationship between the percentage of buildings damaged by MGA = 0.4 g and the buildings damaged by MGA = 0.2 g [15]

Damage type	Seismic design level		
	Pre-code	Low code	Superior code
Extended≤Damage<Complete	1.2	1.9	4.1
Damage≥ Complete	3.2	5.2	12.5

The vulnerability curves, computed using the lognormal model, for most of the buildings in Romania are presented in Figure 1. The example presented is in terms of equivalent PGA.

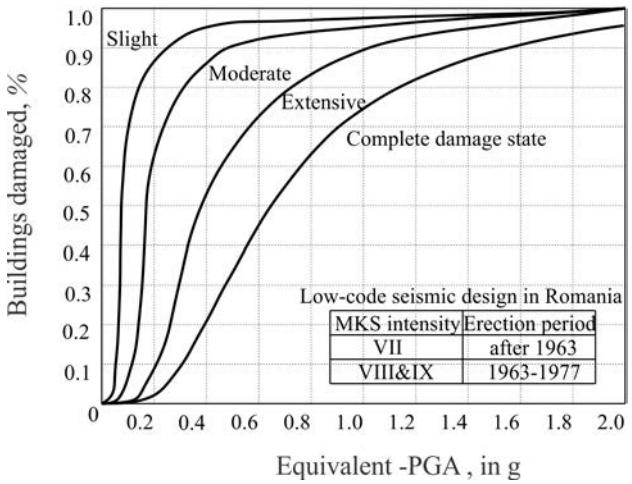

Figure 1. Fragility buildings for tall buildings with shear walls, according to FEMA/HAZUS

V. CONCLUDING REMARKS

The types of structural systems analyzed above exhibit a good agreement with results obtained using other analysis methods. For other types of systems the correlation with other methods could be poorer. In conclusion it can be said that HAZUS methodology (1977) is suitable for investigating seismically induced fragility.

Fragility analysis, as part of the extended area of vulnerability should enroll in the assessment and reduction of seismic losses in case of earthquakes. This type of work should be regarded as a collaborative effort between all factors involed, such as: goverment institutions, insurance industry and engineers.

References

1. Galambos, T. V., *Structural Design Codes: The Bridge Between Research And Practice*, available on-line at http://www.inti.gob.ar/cirsoc/pdf/puentes_hormigon/L03_References.pdf
2. Kazantzi, A.K., Righiniotis, T.D., Chryssanthopoulos, M.K., *The effect of joint ductility on the seismic fragility of a regular moment resisting steel frame designed to EC8 provisions*, Journal of Constructional Steel Research, Vol. 64, Issue 9, Pp. 987–996, 2008;
3. Zahr, M. J., Luco, N., Ryu, H. , *Mitigation of Seismic Risk pertaining to Non-Ductile Reinforced Concrete Buildings using Seismic Risk Maps*, Post-doctoral research report, Berkley, 2009, available on line at http://peer.berkeley.edu/education/files/2009-Paper_Final_Zahr.pdf
4. Senel, S. M., Kayhan, A. H., Fragility based damage assesment in existing precast industrial buildings: A case study for Turkey, Structural Engineering and Mechanics, Vol. 34, No. 1, Pp. 39-60, 2010;
5. Bakhsh, A., Asadi, P., Probabilistic evaluation of seismic design parameters of RC frames based on fragility curves, Scientia Iranica, 2012;
6. Paez, T. L., Lacy, S. L., Babuska, V., *Stochastic Process Models for L inear Structure Behavior*, American Control Conference, Baltimore, MD, USA, June 30-July 02, 2010 available on-line at https://www2.lirmm.fr/lirmm/interne/BIBLI/CDROM/ROB/2010/ACC_2010/data/papers/1642.pdf
7. Barroso, L. R., *Performance evaluation of vibration controlled steel structures under seismic loading*, Ph. D. Thesis submitted to Stanford University, 1999;
8. Jehel, P., Léger, P., Ibrahimbegovic, A., *Chapter 16 : Structural Seismic Fragility Analysis of RC Frames with a New Family of Rayleigh Damping Models*, Computational Methods in Stochastic Dynamics, Vol. 2, Springer Netherlands, 2013;
9. Kazantzi, A.K., Vamvatsikos, D., *A study on the correlation between dissipated hysteretic energy and seismic performance*, 15th World Conference on Earthquake Engineering, Lisbon, Portugal, 2012;
10. ATC-13, *Earthquake damage evaluation data for California*, Applied Technology Council Report ATC-13, Redwood City, CA, USA, 1985;
11. Hwang, H. H. M., Huo, J-R., *Generation of Hazard-Consistent Fragility Curves*, Soil Dynamics and Earthquake Engineering, Vol. 13,Pp. 345-354, 1994;
12. Shinghal, A., Kiremidjian, A.S., *Methods for Developing Motion Damage Relationship for Reinforced Concrete Frames*, Technical Report, NCEER-95-0008, National Center for Earthquake Engineering Research, 1995;
13. Casciati, F., Faravelli, L., *Fragility Analysis of Complex Structural Systems (Mechanical Engineering Research Studies: Engineering Design Series)*, John Wiley & Sons, 1991;
14. Kircher, C. A., Nassar, A. A., Kustu, O., Holmes, W. T., *Development of Building Damage Functions for Earthquake L oss Estimation* Earthquake Spectra, Vol. 13, No. 4, Pp. 663-682, 1997;
15. Lungu, D., Aldea, A., Arion, C., *ENGINEERING, STATE & INSURANCE EFFORTS FOR REDUCTION OF SEISMIC RISK IN ROMANIA*, 12th World Conference on Earthquake Engineering, Auckland, New Zealand, 2000.

Observations on the design of elastomeric bearings used in base isolation

Daniela Oanea (Fediuc), Mihai Budescu, Vasile-Mircea Venghiac, Alexandrina-Elena Pandelea
Department of Structural Mechanics, "Gheorghe Asachi" Technical University, Iasi, Zip code:700050, Romania

Summary

Currently, for the base isolation seismic protection systems, elastomeric and sliding bearings are predominantly used. Elastomeric bearings are used in new constructions as well as in the rehabilitation of existing constructions: civil and industrial buildings, including some with high risk such as nuclear and chemical plants, heritage buildings, bridges and viaducts.

This paper presents the design process of elastomeric bearings used in the seismic isolation systems for buildings. The parameters which influence the size and correct behaviour of elastomeric bearings are: the vertical stiffness, the horizontal stiffness and the load bearing capacity.

KEYWORDS: base isolation, elastomeric bearings, seismic design, vertical stiffness, horizontal stiffness.

1. INTRODUCTION

Base isolation consists of installing a system of mechanisms with the role of "bearing" which provides the separation of the structure from the ground. This system allows the structure to move freely from the foundation and is designed to reduce the seismic forces transmitted to the structure.

The base isolation can be performed on different types of "bearings" or supports. A bearing should ensure the horizontal displacement of the structure relative to the foundation and at the same time should have a high vertical stiffness to avoid possible swinging phenomena of the structure.

An analysis of the seismic isolated structures shows that, so far, the most used bearings are elastomeric bearings.

The elastomers are materials which have similar mechanical particularities with incompressible liquids, whose Poisson's ratio is 0.5. Normally, an elastomeric layer does not have compressive load-bearing capacity, for this reason these bearings are

ISSN 2285-2735, Pages 75 - 82

made by reinforcing with horizontal plates which prevent horizontal deformations of the material as shown in figure 1.

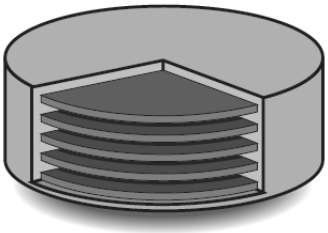

Figure 1. Elastomeric bearing (http://www.freyrom.ro/produse-aparate-razem-elastomer.php)

The idea to introduce thin steel plates in elastomeric bearings belongs to the French engineer Eugène Freyssinet. He affirmed that the vertical capacity of an elastomeric bearing is inversely proportional to its thickness, while the horizontal flexibility is directly proportional to it. In 1954 Freyssinet obtained a patent in which the constraint between the rubber sheets and the reinforcing steel plates was maintained by friction. Two years later, bonding of thin steel plates to rubber sheets during vulcanization was adopted to get a better behaviour of the bearing (Kelly, J.M., et al., 2011).

The elastomeric bearings used in the base isolation are made either of natural or synthetic rubber, such as neoprene, chloroprene, etc. Elastomeric bearings may have circular, square or rectangular shape. Circular bearings have the advantage of uniform stiffnesses on all directions.

2. CIRCULAR ELASTOMERIC BEARINGS DESIGN

Specific requirements on the elastomeric bearings are specified in a series of design codes: Romanian design code P100-1:2006 (Section 11), European codes SR EN 1998-1:2004 (Section 10), SR EN 1337-3:2005 (Section 3) and SR EN 15129:2010, American codes UBC 1997 and FEMA 356:2000 (Section 9), Italian code Ordinanza 3274:2003 (Section 10) etc.

The dimensions of elastomeric bearings are established depending on the vertical load capacity transmitted by the structure and the horizontal stiffness necessary for the system to obtain a high fundamental period, which is the key element in the implementation of seismic base isolation.

For the elastomeric bearing design it is necessary to analyse three properties: the vertical stiffness, the horizontal stiffness and the stability (Thomas, A.G., 1982).

2.1. The vertical stiffness

The vertical stiffness of an elastomeric layer with thickness *t* and area *A* is defined by:

$$K_V = E_c \cdot \frac{A}{t} \tag{1}$$

where E_c is the compression modulus of the elastomer, which depends on bearing dimensions, which is quantified by the shape factor *S* and the shear modulus *G*:

$$E_c = 6 \cdot S^2 \cdot G \tag{2}$$

This formula for E_c is considered for elastomeric bearings with moderate shape factors (Kelly, J.M., 1997). In the case of an elastomer layer with a diameter φ, the shape factor is $S = \varphi / (4 \cdot t)$.

For a bearing with n layers, the vertical stiffness is given by:

$$K_{V,n} = \frac{K_V}{n} = E_c \cdot \frac{A}{n \cdot t} \tag{3}$$

where $n \cdot t$ is the total thickness of elastomer.

The main parameter that influences the vertical stiffness of elastomeric bearings is the shape factor. The shape factor of elastomeric bearings is called secondary shape factor and is calculated with the relation: $S_2 = \varphi / (n \cdot t)$.

2.2. The horizontal stiffness

The horizontal stiffness of an elastomeric layer with the thickness *t* and area *A* is defined by:

$$K_H = G \cdot \frac{A}{t} \tag{4}$$

For a bearing with *n* layers, the horizontal stiffness becomes:

$$K_{H,n} = \frac{K_H}{n} = G \cdot \frac{A}{n \cdot t} \tag{5}$$

To reduce the swinging phenomenon of the structure on the bearings, the vertical stiffness is required to be much higher than the horizontal stiffness, the ratio value between stiffnesses is indicated to be 1/300.

Depending on the horizontal frequency of the bearing, the horizontal stiffness of an elastomeric bearing can be defined by the relation (Kelly, J.M., 1997):

$$K_{H,n} = \frac{W}{g} \cdot (2 \cdot \pi \cdot f_H)^2 \tag{6}$$

where:

W is the vertical force which acts on the bearing;

g – the gravitational acceleration.

Replacing the elastomeric bearing stiffness from equation (5) in (6), it results the elastomer shear modulus, which depends on the strain corresponding to the vertical load transmitted on bearing (*R*) and the horizontal frequency bearing.

$$\frac{G}{n \cdot t} = \frac{R}{g}(2 \cdot \pi \cdot f_H)^2 \Rightarrow G = \frac{n \cdot t \cdot R}{g}(2 \cdot \pi \cdot f_H)^2 \tag{7}$$

2.3. The bearing stability

After the geometry of elastomeric bearings is determined, it is necessary to verify if the stability requirements for both buckling and rollout are fulfilled.

The first notions for the buckling of anti-seismic bearings were made by Haringx (1947). In 1964 Gent applied Haringx's theory to study the stability of multilayer elastomeric bearings (Kelly, J.M., et al., 2011).

Figure 2 shows the deformed shape of an elastomeric bearing subjected to shear and compression, with the trend of buckling.

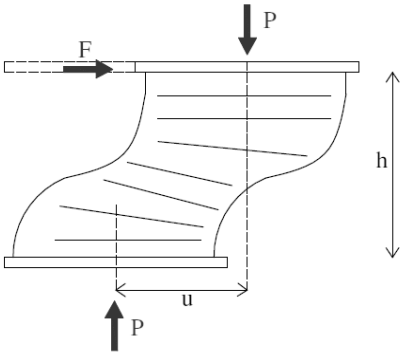

Figure 2. The deformed shape of an elastomeric bearing subjected to shear and compression (Cardone, D., et al., 2012)

Kelly (2011) defines the safety factor against buckling (s_f) by the formula:

$$s_f = \frac{P_{crit}}{W} \tag{8}$$

where P_{crit} is the critical load, which can be approximated in case of circular bearings, for a shape factor $S \geq 5$, by formula:

$$P_{crit} = \frac{\sqrt{2} \cdot \pi \cdot G \cdot A \cdot S \cdot r}{n \cdot t} \tag{9}$$

where r is the gyration radius of the bearing, $r = \varphi /4$.

2.4. The bearing design process

The design process for elastomeric bearings used in base isolation is based on the computing model proposed by Kelly (1997). Thus, a number of parameters are required: the vertical load (W), the horizontal (f_H) and vertical frequency (f_V) of the bearing, the permissible compression stress of the elastomer (R), horizontal displacement (D) and maximum permissible shear strain (γ). All of these are related to the elastomer modulus and obviously with its hardness.

The bearing area is defined by the following formula:

$$A = \frac{W}{R} \tag{10}$$

Thus, the elastomeric bearing diameter is:

$$\varphi = \frac{4A}{\pi} \tag{11}$$

The vertical stiffness of the bearings is defined by:

$$K_{V,n} = \frac{W}{g} \cdot (2 \cdot \pi \cdot f_V)^2 \tag{12}$$

The horizontal stiffness of the bearings is defined by:

$$K_{H,n} = \frac{W}{g} \cdot (2 \cdot \pi \cdot f_H)^2 \tag{13}$$

Knowing the stiffness of the bearing, the shape factor can be determined with the formula:

$$S = \sqrt{\frac{K_{V,n}}{6 \cdot K_{H,n}}} \tag{14}$$

Thus, the thickness of an elastomer layer can be determined with the relation:

$$t = \frac{\varphi}{4 \cdot S} \tag{15}$$

The total thickness of the elastomer should be higher or equal to the ratio between the displacement and the shear strain, so the number of layers is:

$$n = \frac{D}{\gamma \cdot t} \tag{16}$$

The shear modulus of the elastomer is defined:

$$G = \frac{K_{H,n}}{A} \cdot n \cdot t \tag{17}$$

The compression modulus of the elastomer is:

$$E_c = 6 \cdot G \cdot S^2 \tag{18}$$

After the design process it is necessary to verify the standard requirements, the design process being an iterative one.

Elastomer layer thicknesses for elastomeric bearings used in base isolation, are between 3 and 9 mm, and the thickness of the steel plates can have values between 2.5 and 4.5 mm. The usual diameters of elastomeric bearings are between 300 and 1200 mm. The shear modulus of the elastomers, used in these applications, is between 0.4 and 1.1 MPa. The elastomers are capable to take over compressive stresses up to 15 MPa.

The compression modulus and the shear modulus of the elastomer depend on the vertical frequency, respectively horizontal frequency of the bearing, which in turn depend on the vertical load transmitted on the bearing.

To avoid swinging and vertical oscillations of a seismic isolation system, the vertical stiffness of the bearing should be as high as possible. Thus, the specialty literature shows a good behaviour in conditions of vertical frequency between 8 and 12 Hz.

Figure 3 illustrates an example in which the vertical stiffness of elastomeric bearings can be chosen depending on the vertical load applied on the bearing and the vertical frequency. The example was given for elastomeric bearings with 5 layers and the chosen shear modulus is $G = 0.7$ MPa.

From the graph it can be noticed that for a certain value of the vertical force acting on the bearing, its vertical stiffness increases with increasing the vertical frequency.

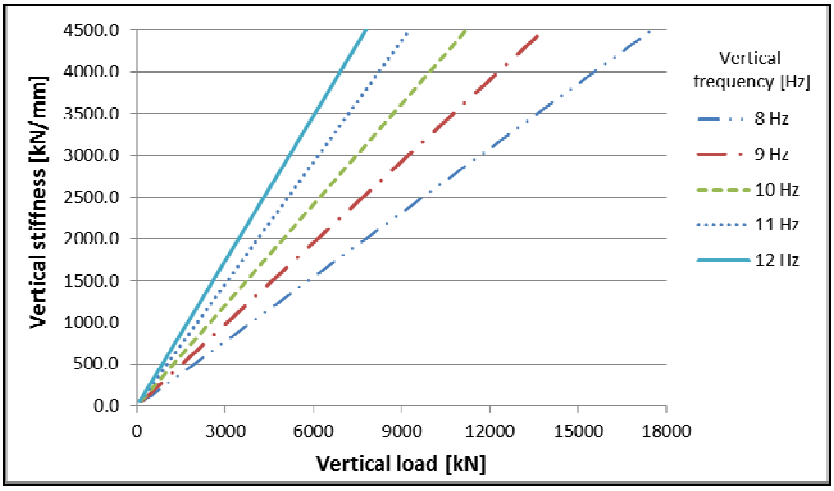

Figure 3. The variation of the vertical stiffness depending on the vertical frequency.

Once the vertical stiffness of the elastomeric bearing is chosen, its dimensions can be determined, respectively the diameter and the height, for different thicknesses of the elastomer layers (fig. 4).

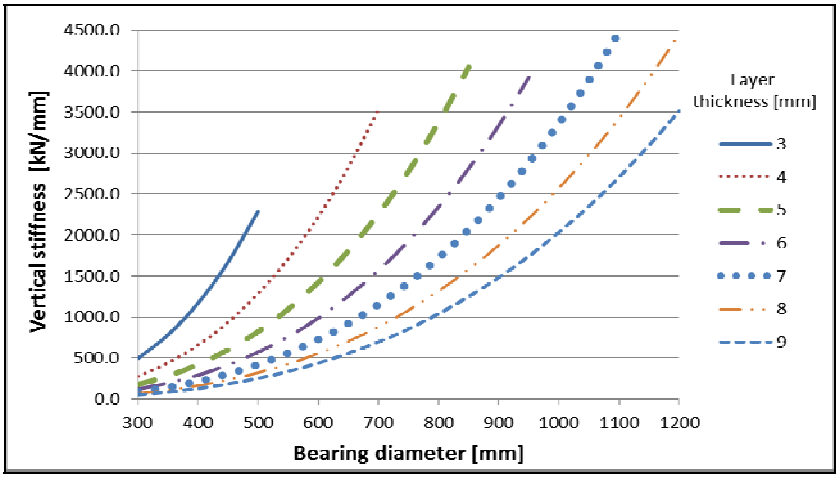

Figure 4. The bearing size selection depending on its vertical stiffness.

In the final phase the stability of the bearings will be tested, resulting in fact an iterative process in establishing bearings.

This procedure is quite complex, iterative and is a direct collaboration with the manufacturer of the bearings. For this reason, the designers prefer to address the problem by taking a type of bearing and checking the parameters performance of

the seismic isolation system. Most of the time, bearings with different stiffnesses are chosen to solve all the imposed criteria, which represents a major difficulty.

3. CONCLUSIONS

This paper makes a synthesis of the calculation method for the circular elastomeric bearings, presenting the conditions that must be fulfilled to avoid some dysfunctions in the base isolation approach to the seismic action.

Since the design process is complex, a number of parameters are required: the vertical load, the horizontal and vertical frequency of bearing, the strain which corresponds to the vertical load transmitted on the bearing, horizontal displacement and maximum permissible shear strain. After the design process it is necessary to verify the standard requirements, the design process being an iterative one.

The dimensions of elastomeric bearings are established depending on the vertical load capacity transmitted by the structure and the horizontal stiffness necessary to the system to obtain a high fundamental period, which is the key element in the implementation of seismic base isolation.

The compression modulus and the shear modulus of the elastomer depend on the vertical frequency, respectively horizontal frequency of the bearing.

To avoid dysfunctions related to the swinging and vertical oscillations of a seismic isolation system, the vertical stiffness of the bearing should be as high as possible. This can be achieved by using an iterative process for the bearing design, but difficult in terms of producers and current materials. All the requirements demanded by a seismic isolation system can be fulfilled by introducing the bearings with different stiffnesses in the limits imposed by manufacturers.

References

1. Cardone, D., Perrone, G., Critical load of slender elastomeric seismic isolators: An experimental perspective, *Engineering Structures*, vol. 40, 2012.
2. Kelly, J.M., *Earthquake-Resistant Design with Rubber*, Second Edition, Springer, London, 1997.
3. Kelly, J.M., Konstantinidis, D.A., *Mechanics of rubber bearings for seismic and vibration isolation*, Wiley, United Kingdom, 2011.
4. Kelly, T.E., Holmes Counsulting Group Ltd, *Base Isolation of Structures*, Design Guidelines, Wellington, New Zealand, 2001.
5. Thomas, A.G., The Design of Laminated Bearings I, *Proceedings of the International Conference on Natural Rubber for Earthquake Protection of Buildings and Vibration Isolation*, Direct Art Co, Malaysia, 1982.
6. SR EN 1337-3:2005, *Aparate de reazem pentru structuri, Partea 3: Aparate de reazem din elastomeri*, Asocia ia de Standardizare din România, Bucure ti, 2005. (in Romanian)
7. http://www.freyrom.ro/produse-aparate-razem-elastomer.php.

Push-over analysis of a reinforced concrete structure considering soil-structure interaction

Cerasela P. Olariu, Mihaela Movilă
Structural mechanics Department, Gheorghe Asachi Technical University, Iasi, Romania

Summary

The dynamic response of a structure subjected to seismic action is complex and it depends on a series of difficult to estimate parameters such as: the precise ground motions, the maximum deformation limit of a structure, the shape in which the entire structure is and also the soil-structure interaction effects.

Among the most important effects of considering the soil-structure interaction in a structural analysis are the decreasing of the overall structural stiffness and the increasing of the natural period of vibration. These aspects imply fewer requirements for the forces acting upon the structure and more requirements for displacements.

In order to determine the seismic response of structures considering soil-structure interaction a nonlinear static analysis can be used as to establish the possibilities and the location of the occurrence of plastic hinges.

This paper presents the results of a pushover analysis for a reinforced concrete structure having different types of foundations soils. The structure was considered to have a rigid base and a flexible base in order to compare the results in these two situations. The finite element analysis is performed in Sap 2 000 program and it aims to study the foundation soil influence upon the appearance of plastic hinges.

KEYWORDS: push-over analysis, modal analysis, plastic hinges, reinforced concrete structures, FE analysis, soil-structure interaction, seismic risk.

1. INTRODUCTION

The structural response of a building during an earthquake depends on the characteristics of the soil motion, the nature of the foundation soil and on the structural system particularities.

Structures are generally assumed to be fixed at the base in the analysis process. This assumption has a great influence on estimating the real behavior of the

ISSN 2285-2735, Pages 83 - 90

structure. It is known that taking into consideration the real soil conditions lead to more exact results (Dutta, 2002).

One of the main effects of considering soil – structure interaction during an analysis is a decrease in the overall stiffness and an elongation of the overall structural period, which in general decreases force demand and increases displacement demand on the structure (Olariu et al., 2011).

Usually, during earthquakes, support failures may appear which can significantly reduce the usability of structures even though it may not lead to collapse. Therefore, considering soil-structure interaction in seismic analysis can be essential in order to prevent the structure to reach critical states.

In most of the SSI analysis the foundation soil is considered linear elastic. Due to the complex nature of soils many uncertainties arise when various aspects of the foundation soils are defined and modeled in order to perform the analyses (Fillaurant, 2002).

Depending on the stiffness characteristics and on the propagation velocity of the seismic wave, foundation soils are the main pawns in performing a correct seismic design.

Soil-structure interaction effects are salient for foundation soils defined by seismic shear wave velocities smaller than 800 m/s, because they tend to increase or decrease the structural response compared to the fixed base support. Sometimes, for soils with seismic shear wave velocities greater than 800 m/s structures can be considered as fixed at the base (Johnson, 2003; FEMA 450).

There are various types of models for soil structure interaction, but the most frequently used are the lumped models and the finite element models. One of the most common assumptions considers the foundation soil stiffness applied as a set of elastic springs in one or more support points of the structure.

There are different formulas which define the foundation stiffness taking into account the geometry of the foundation-soil contact area, the properties of the soil beneath the foundation and the characteristics of the foundation motion. The paper uses the frequency independent foundation stiffness relations given by Newmark - Rosenblueth, these stiffnesses allow the estimation and the control of the foundation impedances, foundation soil damping and natural frequency of the structure (Victor Davidovici, 1999).

This paper studies the influence of soil conditions in plastic hinges development and on failure mechanism occurrence. Plastic hinges are dissipative areas for the seismic energy. The best way to identify and observe the soil-structure interaction effects is to compare the structure responses having a rigid base as well as a flexible one. Therefore, analyses considering both types of supports were performed. Also, provisions from FEMA 440 were used in order to highlight the

cinematic interaction and the foundation's damping effects for being applied on a design spectrum. Comparisons were performed for the capacity curves and for design spectra in order to observe the influence of soils conditions upon the seismic risk of a reinforced concrete structure.

2. CASE STUDY

2.1. Description of the structural system

In the present case study a nonlinear static analysis (pushover) is performed on a 3D reinforced concrete structure considering different types of soils. The pushover analysis is a nonlinear static analysis, which allows a simplified representation of the behavior of structures under the different loading scenarios that may occur during an earthquake. The incremental load increase allows the identification of sensitive structural elements and their failure modes. This analysis attempts to estimate the actual resistance of the structure. The analysis was performed in Sap 2000 program.

The considered structure is a 3D reinforced concrete frame designed according to the Romanian Seismic design code P100-1/2006. The frame has 6 levels each having a 3.6 m height and 3 bays with the following dimensions: 4.8x2.7x4.8 m on each direction. It is a symmetrical structure. The columns are constants along the height and they have a 0.5x0.5 m cross-section and a reinforcement ratio of 1.5%. The beams have a cross-section of 0.4x0.5 m with a reinforcement ratio of 0.9%. The total weight of the structure is 2675.733 KN and it was assumed a live load of 2 KN/m^2.

Table 1 presents the material properties used for the structure.

Table 1. Material properties used for the structure

Materials	E (MPa)	ν	f'c (MPa)	fy (MPa)	fu (MPa)
Concrete, C20/25	$30 \cdot 10^3$	0.2	20.5	-	-
Longitudinal reinforcement, PC 52	$210 \cdot 10^3$	0.3	-	355	570
Shear reinforcement, OB 38	$210 \cdot 10^3$	0.3	-	235	360

In order to model the elastic support, elastic springs were considered. The foundation is a rectangular surface mat, made from reinforced concrete having the following dimensions 12.9x12.9 m and a 0.6m depth. As for the foundation soils 4 different types of soil were considered characterized on the shear wave velocity

according to the site classification provided by SR EN 1998-1:2004. The properties of the chosen foundation soils are shown in table 2.

Table 3 presents the foundation stiffness for each type o foundation soil which was computed with the formulas given by Newmark - Rosenblueth using the properties presented in table 2.

Table 2. Properties of different foundation soils used in analysis

Soil Name	Shear wave velocities [m/s]	Soil type according to SR EN 1998-1:2004	Poisson's coefficient, ν	Unit weight, γ [KN/m^3]	Elastic Modulus, E [MPa]	Shear Modulus, G [MPa]
V150	150	D	0.45	19.62	4.804940	1.656876
V300	300	C	0.40	20.00	13.757818	4.913506
V600	600	B	0.35	22.00	23.534400	8.716444
V900	900	A	0.30	25.00	37.807740	14.541438

Table 3. Spring constants

Soil Name	k_h [KN/m]	k_v [KN/m]	k_θ [KNm/rad]	k_t [KNm/rad]
V150	61983.727	851061.8373	3233452.063	2578678.020
V300	140560.875	111978.811	34877960.140	5847683.800
V600	251982.808	183367.161	57113238.460	10483114.770
V900	423340.826	2486045.866	88474909.770	17612036.730

2.2. Results and discussions

Performing the modal analysis the frequencies and the natural period of the structure were obtained for each type of support considered. Table 4 consists in a synthesis of the results from the modal analysis highlighting the influence of soil conditions upon the overall results.

Table 4. Modal analysis results

Soil Name	Period [s]	Frequency [Hz]
V150	0.528	1.892
V300	0.416	2.399
V600	0.393	2.541
V900	0.348	2.870
Fixed	0.341	2.903

From the push over analysis results an essential difference in the behavior of the structure having different foundation soils was noticed in the failure mechanism.

Figure 1 presents three different failure mechanisms. Although in all cases the failures occur at the supports, the position and the number of the supports differs in accordance with the type of soil considered. Also, the number of plastic hinges is larger for the V600 and V900 foundation soil and is smaller for the fixed base assumption. The failure mechanisms for V150 and V300 are similar, respectively for V600 with V900 and with the fixed base.

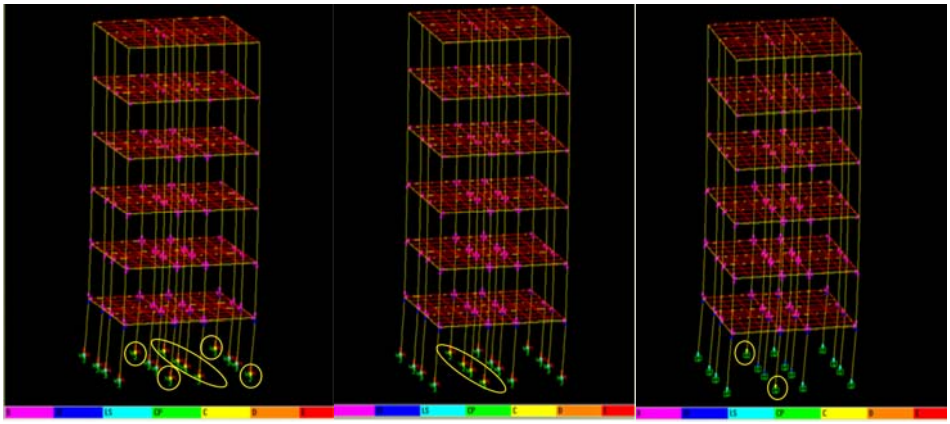

V 600 V900 Fixed support

Figure 1. Plastic hinges location

The structure capacity was evaluated in SAP 2000 assuming a fixed base and a flexible base. The nonlinear static analysis lead to capacity curves.

In figure 2 a comparison between the capacity curves is performed. It can be noticed that the foundation soil flexibility leads to more ductile structures but also to smaller bearing capacity.

The difference between the limit displacement at the top of the structure computed for the structure having a soil type V150 (soft soil) and the displacement for the fixed base situation is 45 mm. A comparison is performed by SAP2000 between the material strengths and structure tensions, the analysis ending when one of the strengths is overcome by an effort.

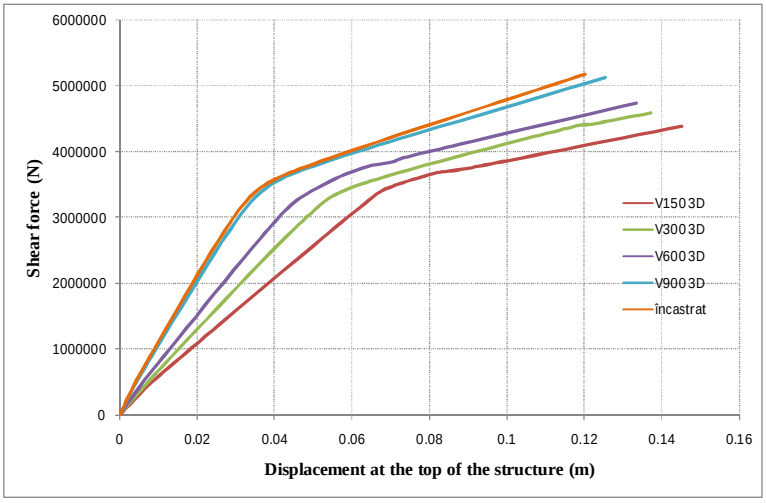

Figure 2. – Comparison between the capacity curves

Figure 3 presents the design spectra comparison provided by Sap 2000 program in order to assume soil structure interaction effects in push over analysis.

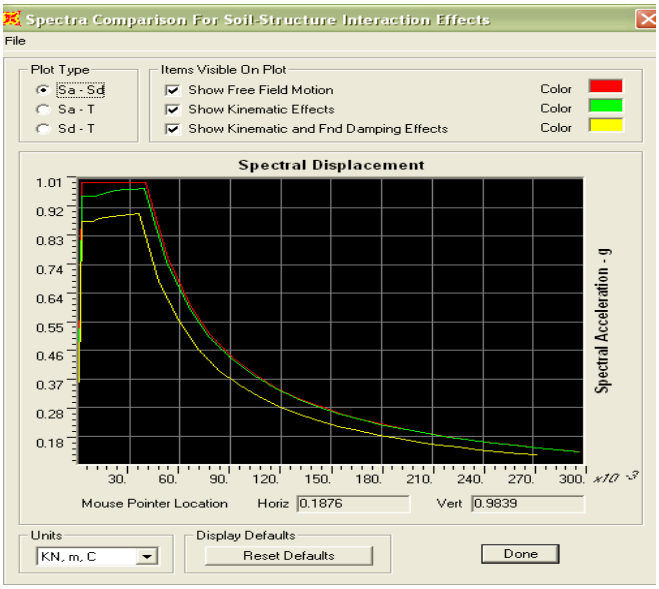

Figure 3. Spectra comparison for soil-structure interaction effects

Based on the spectra provided in figure 3 the graphs in figure 4 were created by intersecting the capacity curve from push over analyses with the spectra provided by the program. Based on these graphs performance points of the structure can be

obtained in order to evaluate its bearing capacity in accordance with the foundation soil.

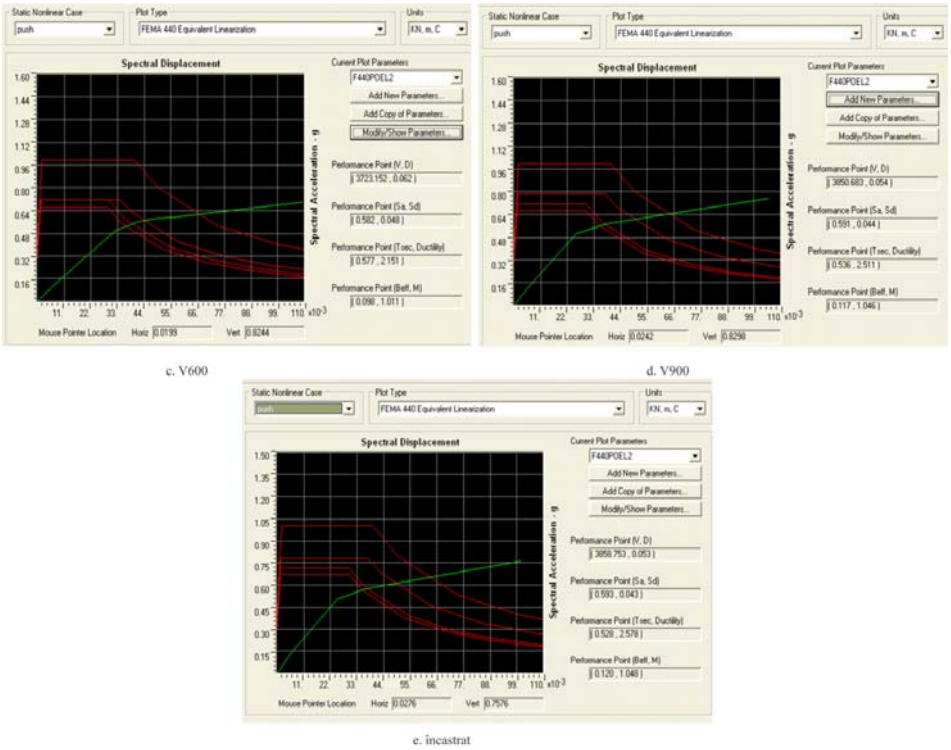

Figure 4. Capacity curves considering soil-structure interaction effects

Sap 2000 program provides the possibility of performing spectra comparison in which soil structure interaction effects can be included. Therefore, based on the theoretical background provided by FEMA 440 which deals with nonlinear analyses considering the effects of soil structure interaction there can be obtained free field motion spectra, free field motion reduced for kinematic effects spectra and free field motion for kinematic effects and foundation impedance spectra.

3. CONCLUSIONS

This study shows the importance of considering soil structure interaction effects in push over analyses in order to establish the failure perspective of a structure. From the modal analysis results it can be noticed the importance of considering soil

structure interaction as it affects the natural period of the structure and its frequencies.

Also by taking into account the foundation soil in seismic nonlinear analyses provides results closer to the real behavior of a structure but less covering as in the conservative assumption of the fixed base.

Special attention should be taken in choosing the right type of support because if the stiffness of the support soil is small it can lead to collapse or it can cause severely damage to the structure, influencing its exploitation ability.

Changes in the location of occurring of the plastic hinges in the structures depending on the foundation soil type were noticed according to the performed push over analyses for the fixed and flexible base situations.

Therefore, from this study it can be concluded that taking into consideration the real foundation soil conditions in seismic risk analyses leads to a better insight on the manner of plastic hinges development.

References

1. *** ATC-40 (1996). Seismic evaluation and retrofit of concrete buildings. Applied Technology Council, Redwood City, California.
2. *** Eurocod 8: Proiectarea structurilor pentru rezistența la cutremur, Partea 1, SR EN 1998-1-2004, 15 decembrie 2004
3. *** Fema 450 (2003). NEHRP recommended provisions for seismic regulations for new buildings and other structures, Part 1-15, Washington, D.C.
4. ***P 100-1/2006 „ Cod de proiectare seismică- Partea I- Prevederi de proiectare pentru clădiri”, Monitorul oficial al României
5. *** Fema 440 (2005). Improvement of nonlinear static seismic analysis procedures, prepared by the American Society of Civil Engineers for Federal Emergency Management Agency, Washington, D.C.
6. Davidovici, V., (1999) La construction en zone sismique, Le Moniteur, Collection : Référence technique, pp. 144-163
7. Computer & Structures Inc., SAP 2000 Software, v.14.2.3, CSI Berkeley, USA, 2010;
8. Olariu, C.P. - Influența deformabilității terenului de fundare asupra comportării unor structuri de rezistență, Universitatea Tehnica “Gheorghe Asachi” din Iasi Teză de doctorat, 2011
9. Olariu, C.P., Olteanu, I., Vargas, F.Y., Budescu, M. -Influence of soil conditions on building vulnerability, „The Bulletin of the Polytechnic Institute of Jassy, Construction. Architecture Section”, LVI (LX), 3, 2011,
10. Dutta, S.C., Roy, R. (2002) - A critical review on idealization and modeling for interaction among soil-foundation-structure system, Computers and structures 80
11. Filiatrault, A. (2002) - Elemets of earthquake engineering and Structural Dynamics, Second Edition, Foreword by Shel Cherry, Polytechnic International Press, Canada,
12. Johnson, J.J. (2003) - Soil structure interaction: Statement of the problem, Earthquake Engineering handbook, CRC Press, Chapter 10, pp. 10-1/10-29

FEM analyses of a 1:2 scale historical unreinforced masonry building

Raluca Pleşu, George Ţăranu, and Mihai Budescu
Department of Structural Mechanics, "Gheorghe Asachi" Technical University, Iaşi, Zip code:700050, Romania

Summary

Most of unreinforced masonry structures are well known for their high vulnerability to seismic actions, due to low flexibility respectively poor shear and bending resistance of masonry walls, which are considered as major load-resisting elements in most of masonry structures.

This paper presents the results of a preliminary FEM numerical analysis performed on a 1:2 scaled unreinforced masonry (URM) building. In order to provide the structural response of the masonry model to static and dynamic actions. For the relevance of the numerical analysis, experimental tests of the mechanical behavior of the materials are used.

The interpretation of these results consists in observing the vulnerable areas of masonry walls, where maximum stress concentration can occur and can lead to failure mechanisms. Moreover, the results provided by the numerical analysis are used for further experimental studies on shaking table and possibilities of strengthening solutions.

KEYWORDS: unreinforced masonry, numerical analysis, failure mechanism.

1. INTRODUCTION

Unreinforced masonry (URM) is the most common form of historical building construction used in Romania, like in most of the European countries. This lead to extensive studies performed in the last decades, by many researches, of the behavior of URM structures. Although the vulnerability of the URM to moderate seismic actions is well known and accentuated by their poor performance to the past earthquakes.

In this context, this paper presents an ongoing experimental program set to assess the ability of a reversible, reduced-cost, low weight, easy to apply strengthening system based on a fiber reinforced mineral matrix composite (FRMMC) overlay

ISSN 2285-2735, Pages 91 - 101

used to retrofit a URM structural model. The mineral matrix, which is the base material in the composition of the strengthening system consist in an ecological binding solution and a totally recyclable one, obtained exclusively from industrial waste (phosphogypsum, lacto gypsum, citrogypsum, gypsum desulphurization). The production process consists of a low temperature burning (below 750°C) of the waste, opposed to Portland cement, which does not imply CO_2 emissions, that lead us to the ever-growing demand for using sustainable, durable and eco-friendly solutions.[1]

For this purpose, a 1:2 scale building was constructed, using a single wythe clay brick masonry laid on a particular lime sand (specific from Jassy area) mortar with a conventional timber floor diaphragm and timber roof. This structural model is designed to simulate a particular type of masonry buildings, representative for 17th-19th century in the Moldavian region of Romania. In order to provide the structural response of the masonry model to static and dynamic actions a preliminary FEM numerical analysis is performed to the same 1:2 scale masonry construction in order to e the observe the vulnerable areas which correspond to the to the stress concentration that can lead to failure mechanisms.

2. DESIGN OF THE MODEL BUILDING

The testing building is a 1:2 scale model which intends to represent the typical URM buildings that was common in the last century in the Moldavian region particularly from Jassy. An URM building, using a single wythe clay brick laid on a lime sand mortar with a traditional timber floor flexible diaphragm and a timber roof. The layout of windows and door opening were sized and positioned in order to obtain a regular shape of the building. The model was constructed using a half-scale sized bricks, designed especially for this project by a specialized company in the production of bricks, S.C. CERAMICA S.A.

Due to the limitation in the geometry and capacities of the shaking table a length scale of 1:2 was decided in order to design and build the masonry structural model. This lead to the fallowing dimensions, presented in Figure.1, 1.975 m x 2.453 m the footprint of the model, which had 1.464 m high of the floor and 0.395m the gable wall, or the high of the roof. In respect of the thickness of the wall is equal to the dimensions of the length of the clay brick ~ 0.12 m.

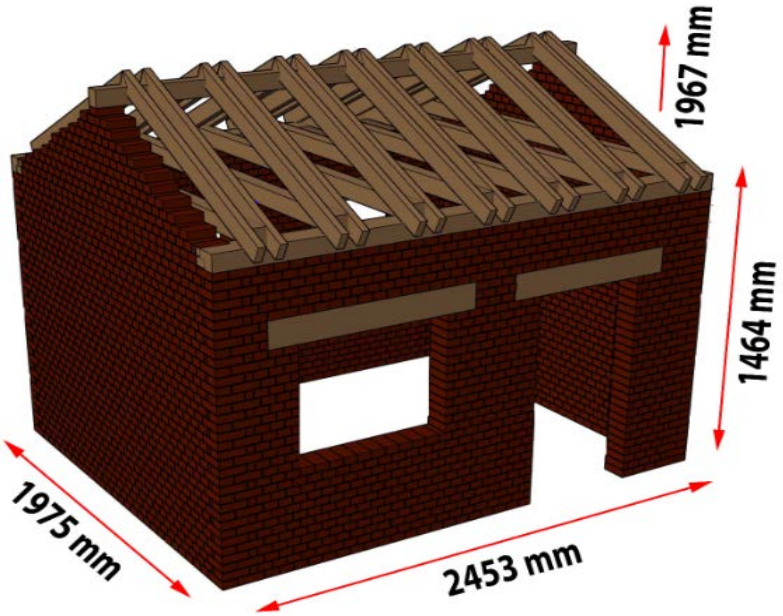

Figure 1. Axonometry of the model

2.1. Laws of similitude

Seismic behavior of a real URM structure is complex. In order to study it on a control environment, we should use a structural model. A structural model is defined as a physical representation of a prototype build usually to a reduced scale for which laws of similitude are applied. In order to achieve true dynamic similitude requirements, loads and the results must be designed and interpreted according the dimensional analysis and similitude theory, which is considered the major issue regarding reduced scaled models. [2-4]. To simulate a perfect true replica model it is necessary to obtain a true simulation of:

- The geometry;
- The stress-strain relationship of the materials;
- The mass and the gravity forces;
- The initial and boundary conditions.

In order to obtain a realistic modeling of a strongly non-linear dynamic response of a masonry structure Froude and Cauchy similitude laws must be respected, [5]. This lead to the following scale factors which are presented in Table 1.

Table 1 Cauchy-Froude scaling factors

Quantity	Scale factor	Quantity	Scale factor
Length, L	$Lp/Lm=\lambda$	Mass, m	$e\lambda^2$
Mass density, ρ	$\rho p/\rho m=e/\lambda$	Weight, w	$e\lambda^2$
Young's modulus, E	$Ep/Em=e$	Force, F	$e\lambda^2$
Area, A	λ^2	Moment, M	λ^3
Volume, V	λ^3	Stress, σ	e
Time, t	$\lambda^{1/2}$	Strain, ε	1
Frequency, f	$\lambda^{-1/2}$	Poisson's ratio, ν	1
Displacement, d	λ	Pressure, q	e
Velocity, v	$\lambda^{1/2}$	Energy	λ^3
Acceleration, a	1	Gravitational acceleration, g	1

2.2. Material properties

During the construction of the model building, comprehensive material test were conducted to track the mechanical proprieties of the materials.

The compressive strength and modulus of elasticity have been determinate by testing brick prism under uniaxial compression in accordance with the British Standard BS EN 1052-1:1999. Also masonry specimens were tested in order to evaluate the flexural strength under a four point loading in accordance with the BS EN 1052-2:1999. Average values of the mechanical properties measured from these tests are presented in Table 2. To ensure the accuracy and the relevance of the modeling, these results will be used as input data in the numerical analysis.

Table 2. Average material proprieties

Test type	Material	Parameter	Test results
Uniaxial compression	Brick	Compressive strength	19.37 N/mm^2
Uniaxial compression	Mortar	Compressive strength	2.18N/mm^2
Uniaxial compression	Masonry prism	Compressive strength	8.2N/mm^2
		Young's modulus E	385MPa

3 DESCRIPTION OF THE NUMERICAL MODEL

3.1 Theories and methods for modeling masonry

A finite element method is used to model and analyze very different geometrical shapes, complex loads or support conditions in order to solve structural problems of masonry.

The basic logic of finite element method is subdivision of the structure into small sized elements that are called finite elements. The connection points of the elements are called nodes. The stresses and displacements are calculated for each finite element and these results are transferred to the whole structure. In other words, the finite element converts the structural problem into finite degrees of freedom, [6].

The first step in the finite element analysis is the idealizations of structure in order to obtain the geometrical model, which can be done by using frame, shell or solid elements depending on the different degrees of complexity encountered in the studied problem. Another important step requires the idealization of material behavior. When dealing with masonry structures, the most common idealizations of material behavior are linear (elastic) behavior, plastic behavior and non-linear (inelastic) behavior.

In this study case in order to obtain the main modes of failure of the URM structural model, a preliminary numerical FEM linear analysis was performed. The main goal of this analyze was just to have a simple overview of the vulnerable areas of the masonry walls, were maximum stress concentration can occur and lead to severe damages or failure mechanisms.

3.2 Numerical modeling

As we have previously mentioned the first step in the FEM analysis is the geometrical idealization, square shell finite elements were used for the URM walls and wood gambles discretization. The composition of the model and the FE discretization are presented in Figure 2, 3. The model has 4589 planer finite elements, 81 bar finite elements, 4754 nodes and 28 080 static degrees of freedom.

The structure gravity center has the following coordinates:

- X = 1.158 *(m)*
- Y = 0.946 *(m)*
- Z = 0.825 *(m)*

Central moments of inertia of the structure:

- Ix = 1938.317 *(kg*m2)*

- Iy = 3011.660 *(kg*m2)*
- Iz = 3721.028 *(kg*m2)*
- Mass = 2515.661 *(kg)*

In order to provide the equivalent scale factor for the similitude laws considered, additional masses were added, obtaining the following coordinates and global mass. Coordinates of structure centroid with static global masses considered:

- X = 1.160 *(m)*
- Y = 0.940 *(m)*
- Z = 0.996 *(m)*

Central moments of inertia of a structure with static global masses considered:

- Ix = 2473.686 *(kg*m2)*
- Iy = 3685.761 *(kg*m2)*
- Iz = 4358.491 *(kg*m2)*
- Mass = 3387.213 *(kg)*

The considered loads were established for the specific Jassy area, taking in account beside self weight, equivalent roof weight, snow and the additional masses, according to the similitude laws.

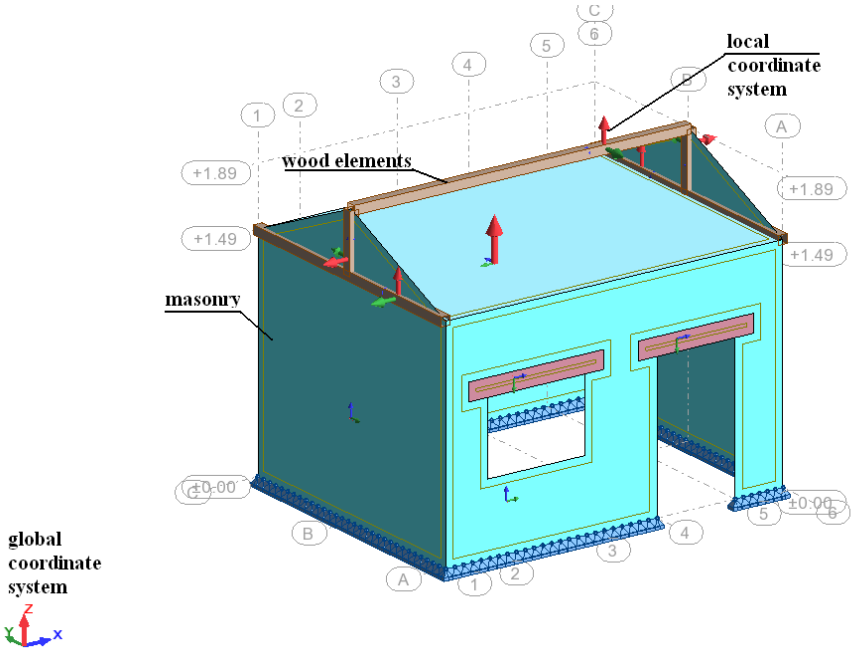

Figure 2 General overview of the structural model

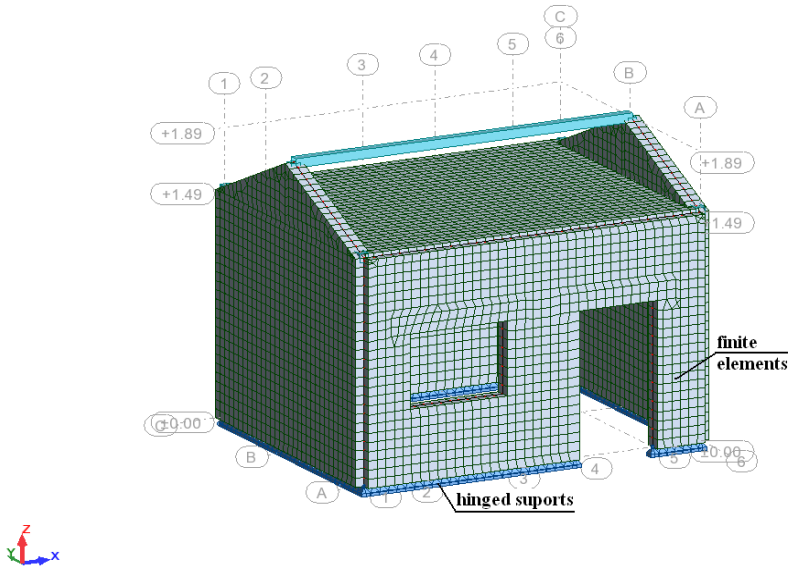

Figure 3 Mesh discretization with square shell elements and base support mode

4. ANALYSIS RESULTS AND DISCUSSION

One of the main goals of the numerical FEM was accomplished through the stress and deformations distribution maps. These are considered important in order to describe the vulnerable areas of the structural model that are able to anticipate the failure mechanism of the URM structural model. The modal analysis shows the deformed shape model and the vibration mode. The displacement map distribution in the global X direction and the natural frequency (10.99 Hz) of the structural model are presented in Figure 4. This value of the natural frequency was confirmed later by an experimental shaking table test. Also the stress maps presented in Figures 7, 8 showed the distribution of maximum and minimum principal stress which correspond to the propagation of the cracks in the walls around the corners of the windows and door openings. Beside these areas the transversal walls were subjected to the out-of-plan flexural bending which can be observed in the spectral dynamic analysis. The maximum vertical displacement obtained of the gravitational combination was 3 mm. In the case of the spectral dynamic analysis the maximum displacement was 12 mm.

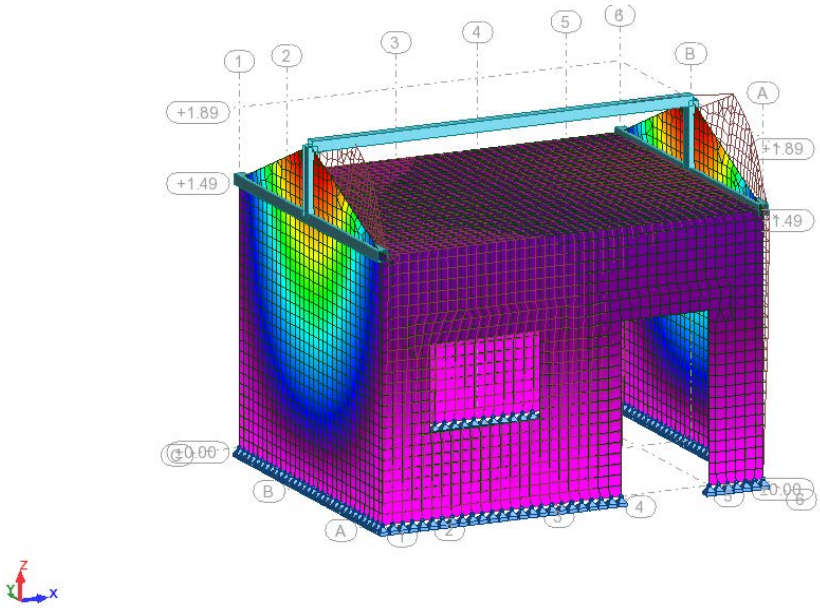

Figure 4 Model analysis first mode of vibration, displacements maps on global X direction, fundamental frequency 10.99 Hz

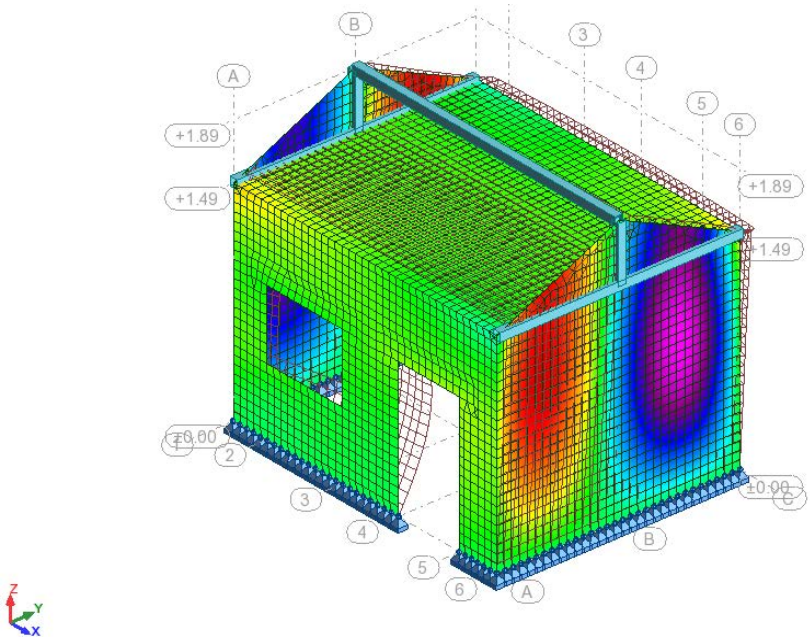

Figure 5 Model analysis third mode of vibration, displacements maps on global X direction

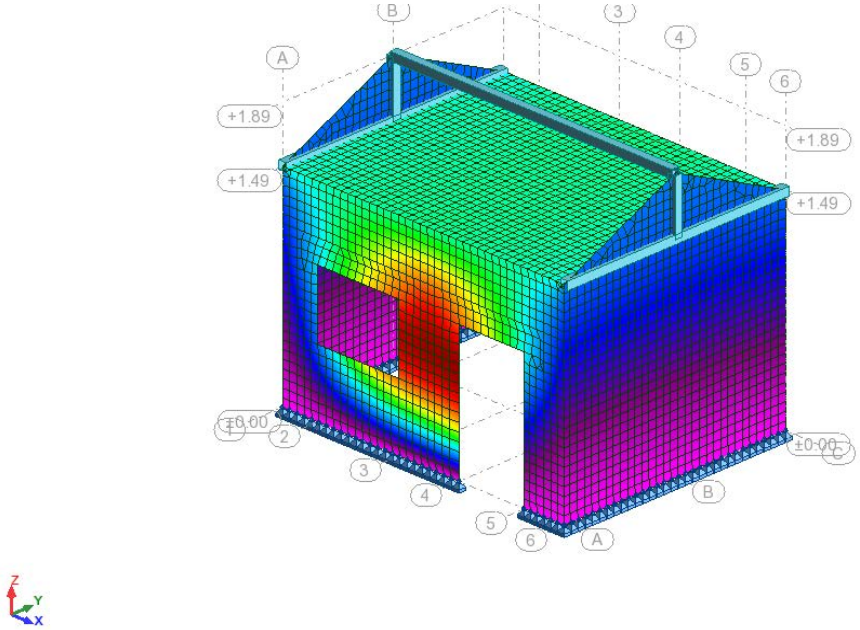

Figure 6 Model analysis third mode of vibration, displacements maps on global Y direction, fundamental frequencies 16.66 Hz

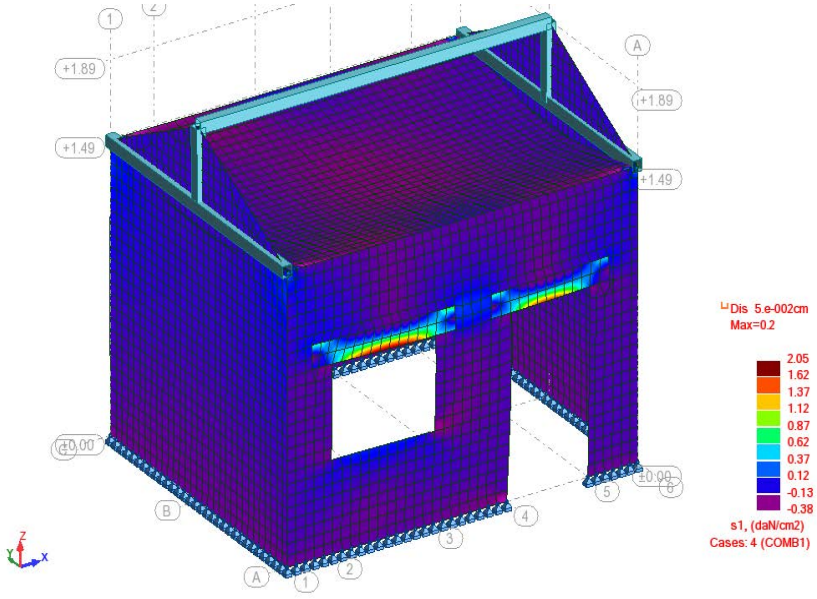

Figure 7 Maximum principal stress from the gravitational combination loads

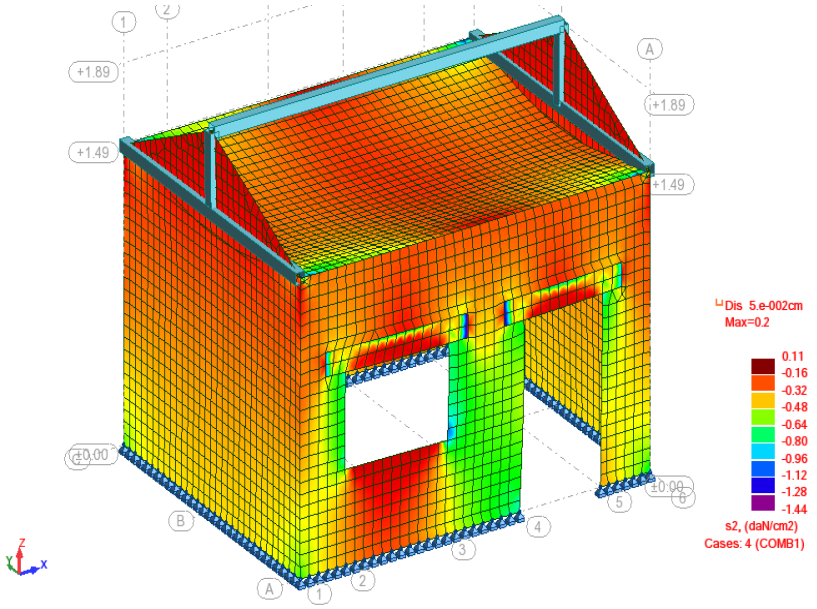

Figure 8 Minimum principal stress from the gravitational combination loads

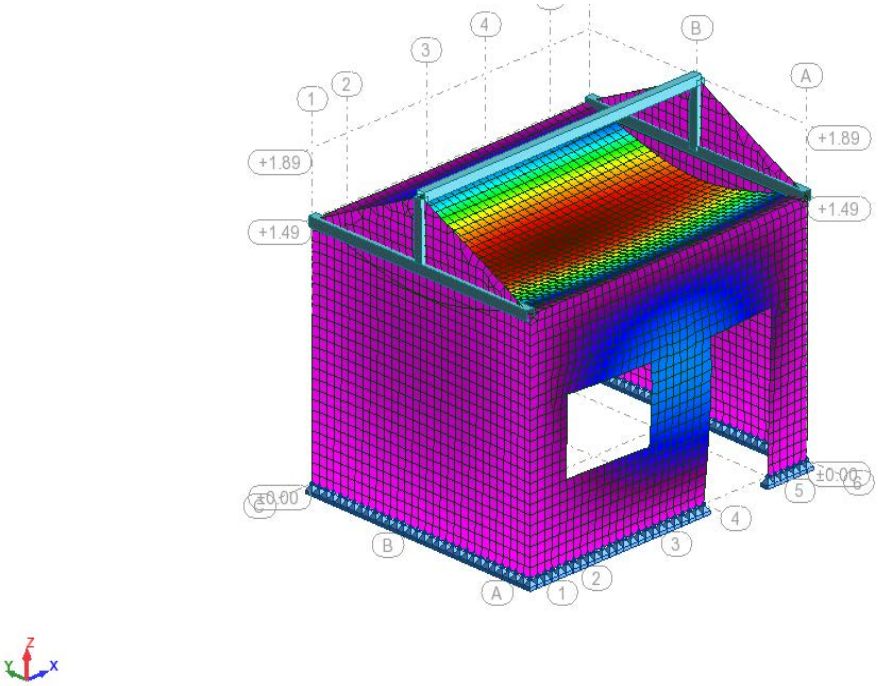

Figure 9 Total displacements map from gravitational combination loads

CONCLUSION

In this paper, a 1:2 scale URM structural model was analyzed with a linear FEM. For this analysis the model was loaded with gravitational actions uniform distributed load on the top of the walls. Static and dynamic analyses were performed observing the behavior of the structural masonry elements. Stress and deformations maps showed distribution of the maximum and minimum values. From the modal analysis the anticipated natural frequency in the first vibration mode and the deformed shape were obtained. These values were approximately confirmed by the experimental tests.

This FEM analysis was founded necessary as a preliminary step in the experimental program, which consisted in the evaluation of a new strengthening method.

Acknowledgements

This paper was realised with the support of POSDRU CUANTUMDOC “DOCTORAL STUDIES FOR EUROPEAN PERFORMANCES IN RESEARCH AND INOVATION” ID79407 project funded by the European Social Found and Romanian Government.

References

1. Țăranu, G., Budescu, M., Lungu, I., Țăranu, N., Pleşu, G., Susan, M., *Materiale compozite cu fibre sintetice, o soluție eficientă pentru lucrările de construcții*, Asociația Inginerilor Constructori Proiectanți de Structuri (AICPS), Edit. MorLink, Bucuresti, 2010.
2. Harris H.G., Sabnis G.M., *Structural Modeling and Experimental Techniques*, CRC Press, London, pp 56-60, 1999.
3. Kasparik, T., *Behaviour of Partially Grouted Nominally Reinforced Masonry Shear Walls under Dynamic Loading* (2009). Open Access Dissertations and Theses. Paper 4197.
4. Hughes, K. J ., "Behaviour of Reduced-Scale Reinforced Concrete Masonry Shear W alls and Components" (2010). Open Access Dissertations and Theses. Paper 4205
5. Yang, G., *Dynamic analyses of masonry building tested in a shaking Table*, Master’s Thesis in Advanced Masters in Structural Analysis of Monument and Historical Constructions, University of Minho, Portugal, 2010
6. Ozen, G.O., *Comparison of elastic and inelastic behavior of historic masonry structures at the low load levels*, Middel Est Tehnical University, pp 47-50, 2006

CFD analysis of free convection characteristics inside cavity walls

Claudiu Romila
Department of Civil and Industrial Engineering, "Gheorghe Asachi" Technical University of Iaşi, Iaşi, 700050, Romania

Summary

Ventilated systems are increasingly used in Europe for the rehabilitation of building envelope that does not comply with current thermal protection requirements. Ventilated façades, or cavity walls, are largely studied because the exterior wall is considered one of the most important elements of the building envelope due to large impact exerted in overall heat loss in virtue of its significant area.

These systems, if properly designed, can lead to important energy savings while the durability of the exterior walls is increased by the two stages tightening. The air flow, due to effect of buoyancy forces, decreases thermal load on the building in summer because heat is eliminated through the outlet openings. In winter, a decrease in heating energy demand can be obtained due to some thermal insulation effect of the air layer.

Nevertheless, thermal performance of the ventilated systems depends on several factors among which channel geometry, physical properties of the constitutive materials and climatic conditions which interaction is difficult to estimate by in situ observations or by laboratory measurements.

CFD analysis techniques have become an increasingly effective method to determine the characteristics of the air flow and consequently heat transfer inside the channel. This article presents some thermal characteristics of the airflow for a cavity wall made of an insulated masonry wall and an exterior wood cladding. Temperature and velocity profiles are analyzed function of the channel thickness.

KEYWORDS: ventilated façades, CFD, air flow, temperature, velocity.

1. INTRODUCTION

The study of air circulation and heat transfer inside ventilated façades by numerical methods is necessary when the validity of field measurements can be questioned due to the influence of climatic conditions. Laboratory measurements, although accurate, cannot take into account complex wind flow around the façade. Therefore, in many cases, fluid flow can be solved only with the help of computers assisted programs, using numerical methods of Computational Fluid Dynamics (CFD).

CFD analysis contains a group of computational techniques used to approximate the behavior of motion and heat transfer inside the fluid, using finite element method. This method allows that approximate solutions to differential equations with partial derivatives to be obtained. Thus, the partial differential equations of fluid movement can be solved using basic principles of thermodynamics and mechanics: energy conservation, mass conservation, momentum and angular momentum variation.

The wall system that is presented in this paper consists of a typical masonry wall, a layer of mineral wool and wood planks. Between the layers of mineral wool and wood lays an air gap with a variable thickness between 1 and 6 cm. It can be stated that this constructive system is specific to ventilated façades of masonry walls. The characteristic section is shown in Fig. 1.

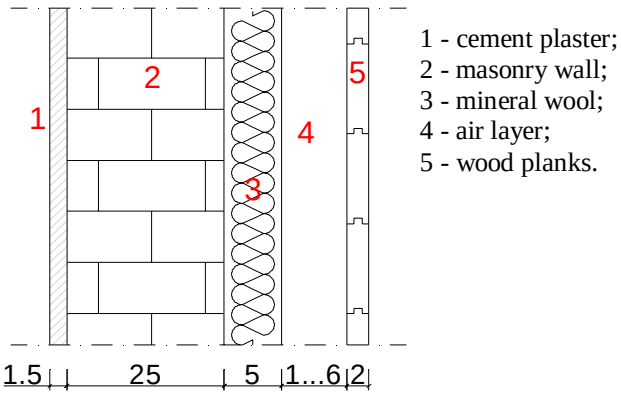

Fig.1. Current section of the analyzed wall

Physical properties of the constituent materials used in the calculation are presented in Table 1:

Table 1. Physical properties of the constituent materials

	Thickness (cm)	Density (kg/m^3)	Conductivity (W/m·K)
plaster	1.5	1800	0.93
hollow brick	25	1400	0.50
mineral wool	5	80	0.04
air layer	1…6	1.25	0.024
fir planks	2	550	0.17

For the chosen example, thermal resistance, without the effect of thermal bridges was 1.93 m^2K / W, slightly greater than the imposed value of 1.8 m^2K/W proposed by norm C107/2005 and amended by gouvernamental order 2513/2010. The mineral wool thickness was chosen only of 5 cm so the ventilation effects could be better observed.

Climate conditions (outdoor temperature for summer and winter) are those of the city of Jassy, with the following conventional air temperatures (Table 2):

Table 2. Bulk air temperatures for Jassy

	Outside (°C)	Inside (°C)
Summer	+28	+25
Winter	-18	+20

2. MODEL SET-UP

Generally, the resulting system of equations are solved respecting the following steps (González et al., 2008):

- define the computational domain;
- define the finite element mesh;
- define boundary conditions;
- define the turbulence and radiation models;
- iteration of the solutions.

2.1. Computational domain

The **computational domain** is represented by the geometry of the ventilated channel with the dimensions presented in Table 3. The fixing elements of the outer layer were not modeled in order to minimize model complexity and computing time. To compensate for this effect, some authors propose the increase of the surface roughness value of the boundering layers (Patania et al., 2010), but this solution can be applied only for turbulence models.

Table 3. Dimensions of the computational domain

	Value (cm)
height	300
thickness (δ)	1...6
height of the inlet/outlet	2
outer layer thickness	2
support wall thickness	31.5

2.2. Finite element mesh

Defining the **finite element mesh** represents an important element in solving fluid dynamics problems. A finer grid will produce a more accurate solution, but will require a longer processing time. The studied geometry does not require a very complex network, but special attention was given to refining it to inlet and outlet orifices. Finite elements used in this case had dimensions of 1 mm x 1 mm, which accounts for a fine mesh element (Fig. 2).

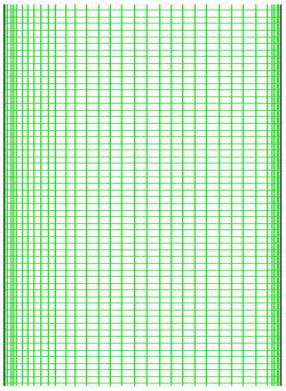

Fig. 2. Finite element mesh for a 3 cm thick air layer

Triangular finite elements have not been used due to large errors that can occur in the calculation of Reynolds stresses. Results for the 2D and 3D networks do not differ significantly, but the latter are time and resource intensive (Mesado et al., 2010); therefore a 2D network was preferred.

2.3. Boundary conditions

Boundary conditions are a number of assumptions and values considered by the user, necessary to describe the initial conditions of the flow. Air movement was considered laminar, as small *Re* numbers for the studied thickness suggests this type of flow. Its specific boundary conditions are given in Table 4.

Table 4. Boundary conditions for the laminar flow

	y = 0	y = h	x = 0	x = δ
p	$p = p_0$	$p = p_0+\rho gh$	-	-
T	$T = T_0$	-	$T = T_2$	$T = T_3$
ν	-	-	$\nu = 0$	$\nu = 0$
R	-	-	$R = R_2$	$R = R_3$

where: x - position in the transverse direction, y - position in the longitudinal direction, p - air pressure (Pa), p_0 - air pressure at the inlet level (Pa), ρ - air density (kg/m^3), g - acceleration gravity (m/s^2), h - height of channel (m), ν - kinematic viscosity of air (m^3/s), T - temperature (K), T_0 - temperature at the inlet (K), $T_{2,3}$ - channel boundary surface temperatures (K), $R_{2,3}$ - heat resistance of the outer and inner layer (m^2K/W).

2.4. Radiation model

The **radiation model** chosen to describe radiation heat transfer was the Discrete Ordinates model (DO). This model transforms the radiative heat transfer equations in a transport equation, solving a number of equations equal to the number of flow vectors associated with a number of discrete solid angles (Sanjuan et al., 2011). DO model considers air as a non-participatory environment.

3. RESULTS

Fluent 6.3 CFD software calculates and permits a detailed view of the velocity, temperature, pressure and turbulence fields inside the channel. Compared with experimental measurements, the results will not be altered by errors caused by the measuring equipment and data reading and interpretation.

Numerical simulations were performed for the ventilated system and climatic conditions proposed in the previous chapter. However, the effect of solar radiation on the outer surface was not considered. Temperature and air velocity distribution can be analyzed either on the entire section of the channel or on smaller areas, as shown in Fig. 3. In this figure it can also be observed that the outer layer temperature is higher than the temperature of the air inside the channel due to radiation heat transfer from the warmer wall. The fully developed flow inside the channel can also be observed, as velocity profile has a constant shape on the entire analyzed height.

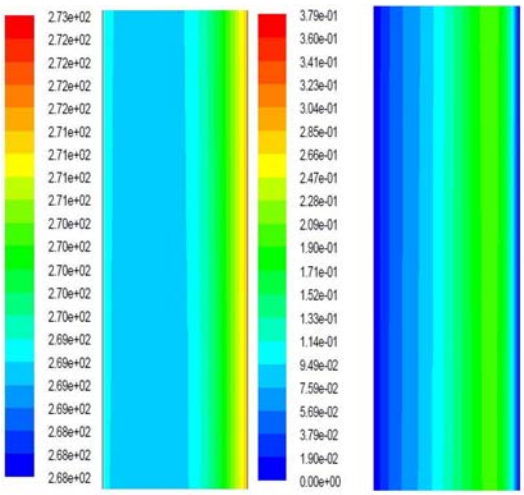

Fig. 3. a. Temperature and b. Velocity fields for a 5 cm thick channel, obtained at the middle of the channel for T_e = - 5 °C and T_i = + 20 °C

It is important to establish correlations between velocity and temperature fields in order to understand and analyze airflow in ventilated channels. For the proposed geometry, velocity and temperature distribution is presented in a dimensionless form, depending on the ratio x / δ; the value 0 corresponds to the cold surface, while the 1 for the hot wall.

Temperature and velocity profiles developed in cross section were compared for a temperature difference T_i - T_e equal to 15, 25 and 35 °C and for different channel thicknesses, ranging between 1 and 6 cm. The large temperature differences can be obtained in winter. The obtained values are shown in Fig. 4 - 6.

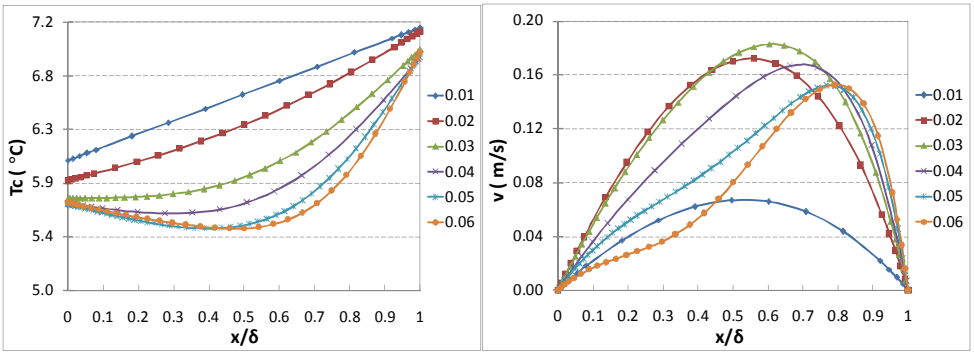

Fig. 4. a. Temperature and b. Velocity profiles in the ventilated channel for T_e = + 5 °C and T_i = + 20 °C

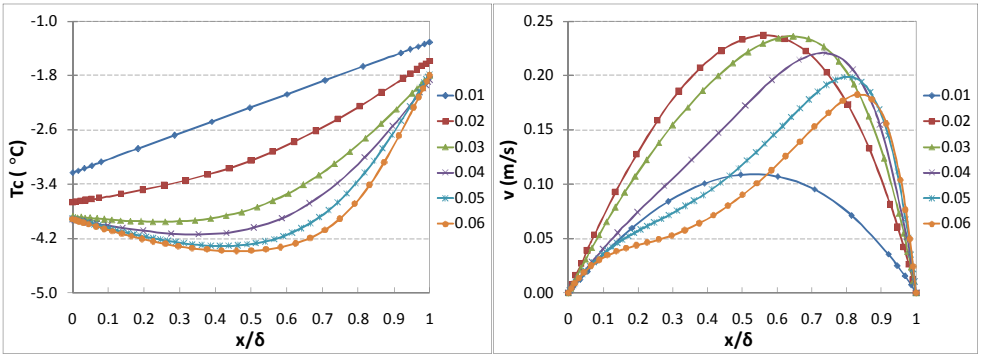

Fig. 5. a. Temperature and b. Velocity profiles in the ventilated channel for T_e = - 5 °C and T_i = + 20 °C

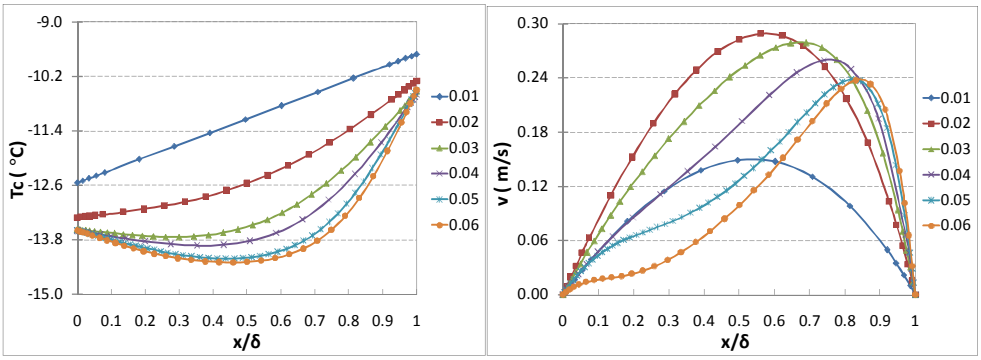

Fig. 6. a. Temperature and b. Velocity profiles in the ventilated channel for T_e = - 15 °C and T_i = + 20 °C

It can be observed that temperature and velocity profiles have a bigger variation with the channel thickness than with the temperature difference T_i - T_e. Temperature in the 1 and 2 cm thick channels decreases linearly from one face to the other, with a profile similar to that of unvented channels. For other thicknesses, the analyzed profile has a convex shaped curve. It is important to note that the minimum temperature is not formed in the mid section, but closer to the hot wall. Its lower values are obtained for larger thickness of the channel.

3. CONCLUSIONS

The tendency of the air flow to cleave to the warmer wall is greater for bigger temperature differences and for channel thicknesses that exceed 4 cm. It results that

increasing the channel thickness over this size does not necessarily lead to an increased airflow. The air will flow only near the warmer surface and will not occupy the entire section of the channel. Maximum values of velocity in cross section are obtained in channel 3 cm, while for higher temperature differences, maximum speeds are reached inside the 2 cm channel.

This study confirms some other experimental and analytical results (Romila et al., 2012), which have shown that the air flow that can be vented will not differ significantly with the increase of the channel thickness. This is explained by the fact that, when the thickness of the channel will increase, the average speed will decrease. Other calculations are needed to establish the correlation between intake and exhaust vents area and the channel thickness.

Numerical results confirm the difficulty of determining air velocity and temperature by experimental measurements because of large fluctuations in height, and the width of the channel. Experimental measurements provide rather a view on the order of magnitude, while an accurate value is difficult to obtain. Therefore, it can be asserted that CFD numerical simulation programs are the most appropriate analysis technique for describing air flow in ventilated channels.

References

1. González, M., Blanco, E., Rio, J.L., Pistono, J., San Juan, C., *Numerical study on thermal and fluid dynamic behaviour of an open-joint ventilated façade*, Proceedings of PLEA 2008 Conference on passive and low energy architecture, Dublin, Ireland, 2008.
2. Normativ C107-2005, *Normativ privind calculul termotehnic al elementelor de construcție al clădirilor*, 2005 (in Romanian).
3. Patania, F., Gagliano, A., Nocera, F., Ferlito, A., Galesi, A., *Thermofluid-dynamic analysis of ventilated façades*, Energy and Building 42, pp. 1148-1155, 2010.
4. Romila, C., Popovici, C., G., Cherecheş, N., C., *Reduction of building energy consumption using ventilated façades*, Environmental Engineering and Management Journal, vol 11, no. 4, april, ISSN: 1582-9596, pp. 806-811, 2012.
5. Sanjuan, C., Sánchez, M.N., Heras, M.R., Blanco, E., *Experimental analysis of natural convection in open jointed ventilated façades with 2D PIV*, Building and Environment 46, pp. 2314-2325, 2011.

Some Considerations Regarding Renumbering Techniques for Sparse FEM Matrices

Octavian Victor Roşca
Structural Mechanics Department, Technical University"Gh. Asachi", Iaşi, 700241, Romania

Summary

Most of the FEM models in structural analysis lead to very large matrices, with a sparse shape. Tenths of thousands or hundreds of thousands of degrees of freedom are usual. The first static analysis deals with the stiffness matrix then after some condensation procedures the modal analysis and/or transient solvers are required. All the solution and the time consumption are sensitive to the characteristics of the structural system matrices.

Therefore in the last decades important efforts have been made to study and control the automatic re- numbering algorithms in order to narrow the bandwidth of coefficient matrices.

This paper deals with the study of these algorithms and several case- studies are performed. In the end the conclusions of the analysis and the computational effort is depicted.

KEYWORDS: Structural Analysis, Sparse matrices, Renumbering Techniques, Structural Topology.

1. INTRODUCTION

Most of the FEM models in structural analysis lead to very large matrices, with a sparse shape. Tenths of thousands or hundreds of thousands of degrees of freedom are usual. The first static analysis deals with the stiffness matrix then after some condensation procedures the modal analysis and/or transient solvers are required. All the solution and the time consumption are sensitive to the characteristics of the structural system matrices.

In now days the FEM software contains algorithms to reorganize the structural topology (node renumbering/ element renumbering). The implementation of these routines leads to very important decrease of memory used and computational effort.

In this paper there are presented several algorithms that are widely used to decrease de bandwidth or the front width of the equation system. There are presented in comparison the performances of these and the domain for use. In one of the milestone works "The reduction of the sparse symmetric matrix bandwidth", E. Cuthill and J. Mckee [1] emphasize that "the displacement method and the finite element method lead to the solution of large algebraic equations" with characteristic matrices to be symmetric and sparse.

There is a direct correlation between the structure of the coefficient matrix, namely the stiffness matrix in this case and the space structure that defines the configuration of the finite elements. For the efficient solution of these systems it is desired to use an automatic numbering (or re- numbering) mesh scheme to ensure that the coefficient matrix shall have a narrow bandwidth.

In the paper [15] it is considered a matrix to be sparse if only a small percentage of the coefficients are nonzero. J.H. Wilkinson in his important paperwork "The Algebraic Eigen value Problem" defines a sparse matrix to be "one that has enough zero elements that is worthwhile to be taken into account" from the point of view of separating the operations. Thus, the large number of zero elements can be seen as an advantage. By eliminating the zero element operations the time consumption is reduced. Another important aspect is that the memory usage is diminished in the case of sparse matrices because only nonzero elements need to be stored. In [17] it is considered a workbench with an A matrix with 4096 x 4096 elements from which 20224 nonzero.

In the table No. 1 it is presented the memory usage and run time using a Sun SPARK – 1 workstation in two cases: A matrix in condensed format (only nonzero) and A matrix in complete format.

Table 1

	Condensed Format	A complete (4096 x 4096)
Memory	0.25 Mb	128 Mb
Vector product A * x	0.2 sec.	30 sec.
Linear Sys A x = B	10 sec.	~ 12 ore

The direct methods for the solution of the sparse systems depend directly of the shape of the characteristic matrix. There are specialized routines for the solution of several patterns (see figure no. 1):

- Tri diagonal matrices (in this case the run time is reduced from N3 to N operations and the memory – from N2 to N – fig. 1.a);
- band matrix, diagonal with band M or with half bandwidth denominated by NBW (fig. 1.a);
- triangular band matrix;
- diagonal matrix on blocks or tri diagonal matrix on blocks (fig. 1.b);
- cyclic band matrix (fig. 1.a);
- diagonal block matrix, simple or double borded (6.1.c, d – diagonal double borded, e) etc.

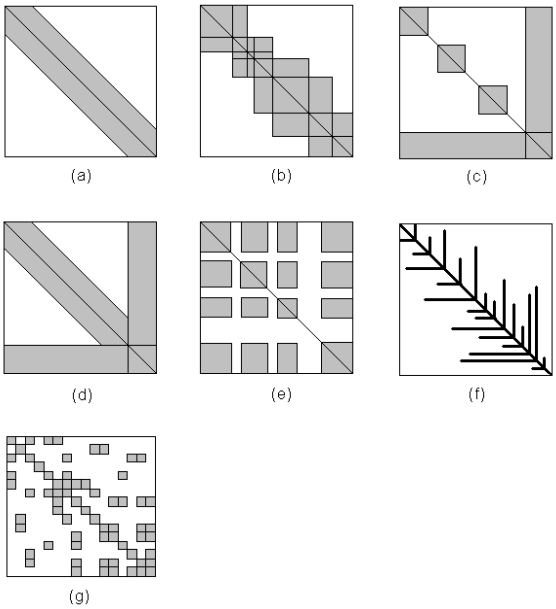

Figure 1. Some patterns of sparse symmetric matrices

2. THE CUTHILL-MCKEE ALGORITHM

The Cuthill- Mckee algorithm reorders the coefficients of the system matrix using some permutation methods. The problem of re- arranging the elements leads to the construction of a P permutation matrix such as the symmetric P K PT matrix obtained from the K stiffness matrix to have nonzero elements very closed to the main diagonal. Jennings advocated a storage scheme for K such as P K PT minimize a functional with the following expression:

$$\frac{1}{N}\sum_{i=1}^{N}\theta_i \qquad (1),$$

where θi is the difference between the column index for the diagonal coefficient from "i" column and the first nonzero coefficient from the "i" row and N is the order of K.

For the diagonal band storage pattern this leads to the bandwidth minimization, thus it is computed:

$$\min\left\{\max_i \theta_i\right\} \qquad (2).$$

Let us consider the linear system of equations K X = F where K is a sparse symmetric matrix, positive definite of N order. Elements of K are denominated by kij where "i" is the line index and "j" is the column index. The maximum value of |i-j| for kij nonzero is used as a measure of K bandwidth.

For the G(K) graph corresponding to K we have N joints denominated with i = 1, 2, ..., N. For each nonzero element kij with i < j it will exist an edge that connects the nodes i and j. From the graph of K we can determinate the positions of all nonzero elements sited outside the main diagonal.

Generally, for a given graph one can construct the associated connectivity matrix. For a stiffness matrix K at least theoretically the graph G(K) can be constructed. The renumbering algorithms are subjected to the Harwell-Boeing WEST0479 [18] matrix workbench (denominated by S) that represents the connectivity matrix of a distillation column in eight steps, defined de Westerberg.

The matrix is of order N = 479 and has 7551 nonzero terms. In the figure no. 2 it is depicted the connectivity matrix and in the figure no. 3 one can notice the associated tree G(S).

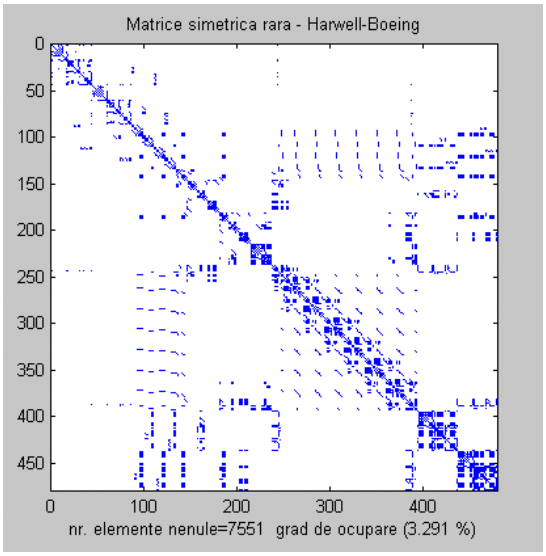

Figure No. 2. The connectivity matrix

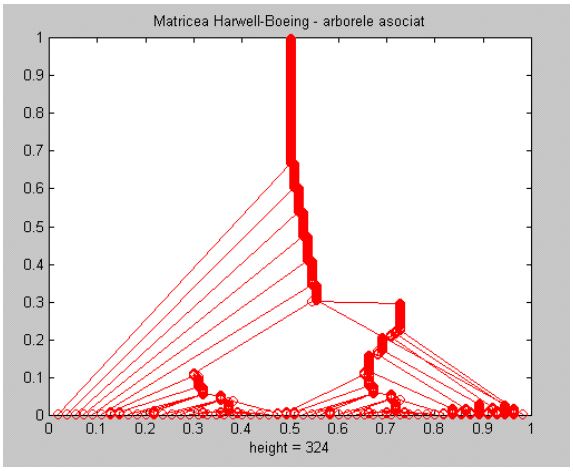

Figure No. 3. The G(S) tree

The first version of the Cuthill-Mckee algorithm (CM) contains the following steps:

- A start joint is selected (this can be one with a minimum degree). This is renumbered with 1.
- The adjacent joints to this first one are numbered in ascending order, starting with 2, in the order of the increase of the degree. These joints are

of a distance equal to 1 to the joint number 1. It is said that these joints are part of a level or renumbering plane, called level 1.

- Apply the previous step for each node from level 1, in ascending order of the degree and construct level number 2.
- The loop continues with the renumbering of all planes until all the joints of the structure (graph) are renumbered.

3. THE REVERSED CUTHILL-MCKEE ALGORITHM

This is an improved version of the classic CM algorithm. In step 1 the Cuthill-Mckee algorithm computes the nodal valences i.e. number of connections with neighbor joints. The starting node for renumbering is selected the one with the minimum valence.

In step no.2 we build connectivity planes, based on the information provided the graph edges. These planes will be recorded in a temporary matrix.

In step 3 it is performed the first renumbering, of the plane 2. The new node numbers will be recorded in a correspondence matrix with 2 columns. In a certain plane the renumbering joint order is ascending with respect to valence orders.

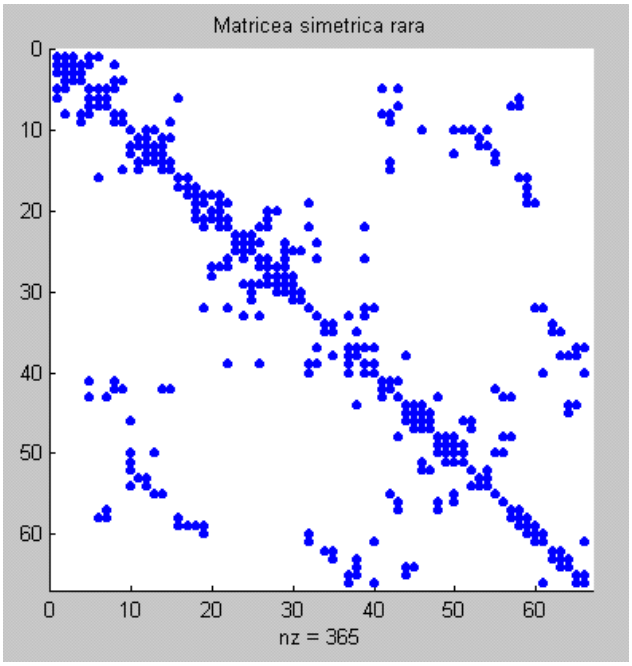

Figure No. 4. The G(S) tree

The step number 3 is repeated until no node remains to be processed. By implementing the Cuthill-McKee algorithm it is not absolutely necessary to storage of all planes. It is enough to use 2 vectors of N length (order of stiffness matrix) in which one stores the “I” plane and the next plane “I+1” immediately after plane ”I” is ready for processing. A supplementary buffering vector of N dimension is used as marking field. In this vector there are stored the instant processed nodes and the new ones to be analyzed.

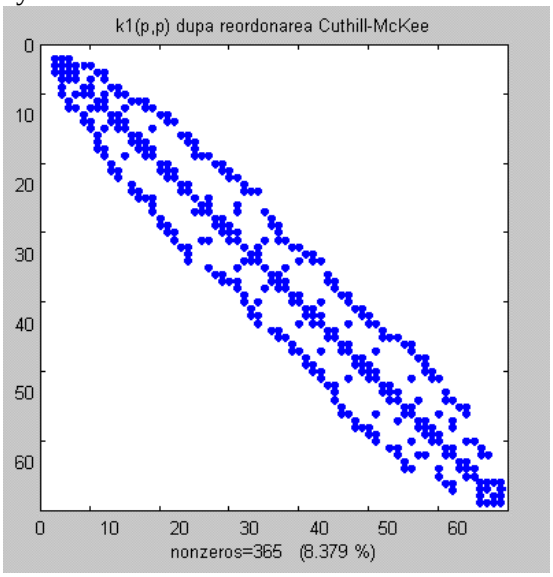

Figure No. 5. The conenctivity matrix after the CM renumbering process

A comparison based on the previous case study shows that in the case of RCM algorithm a faster convergeance is achieved and the average bandwidth is 5,0. In the figure no. 4 it is depicted the original connectivity matrix associated with the graph G(K). In the figure No. 5 it is depicted the conenctivity matrix of GCM(P K PT) after the classic CM renumbering process.

In the figure no. 6 it is presented the connectivity matrix of GRCM(P K PT), after the reverse Cuthill-Mckee process.

After analyzing the figures no. 5 and 6 one cannot notify a significat difference in between the RC and RCM algorithms. If one uses alternatively quadratic form functions for the same structure, a linear system with 173 equations is obtained; the RM algorithm induces an average bandwidth of 17,11 and the RCM algoritm produces an average 11,09 bandwidth. This difference increases in the case of 3D structures. The Gauss ellimination technique apllied on a 3000 eqs. system leaded to a time reduction of 45%.

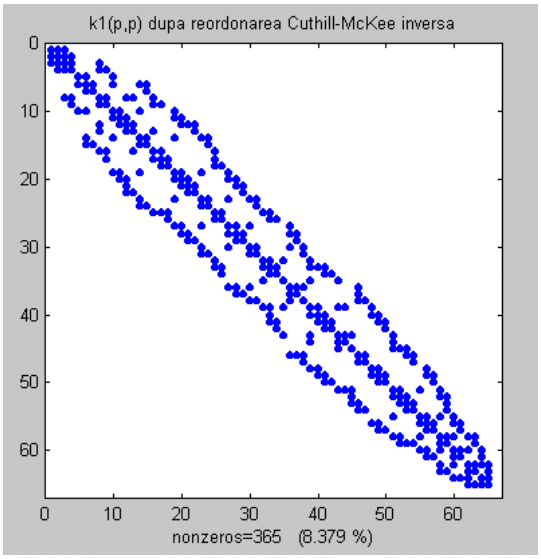

Figure No. 6. The conenctivity matrix after the RCM renumbering process

4. THE AKHRASH-DHATT ALGORITHM

This algorithm is very compact. It takes a node sequence and processes it in a „greedy" way to obtain a minimum bandwidth. Durin the last decades this method demonstrated the effectiveness, especially in the case of 3D structures. The algorithm is suitable for symmetric matrices stored in band format.

The Akhrash-Dhatt method (AD) is based on several criteria that establish the renumbering order, euristically deduced, after many observations were performed on the optimized numbered systems. Let us consider the next scheme consisting of quadrilateral elements that has the connectivity matrix with optimized bandwith of 4. The joint connectivity of the net is defined in the second column of the table no.2.

The connectivity matrix of this structure has the following properties:

Sum: the rows that possess the same number of elements are grouped together. Inside a group the sum of terms from each row is sorted in ascending order, as it is presented in the 3rd column of the table no. 2. For instance the rows 1, 3, 10 and 12 have 4 terms and their sum is 12, 16, 36 and 40 and the sums are sorted ascending.

Average: The 4th column of table no. 2 contains a weighted vector obtained after the division of the sum from column no.3 to the number of elements from the corresponding row. One can notice the ascending order.

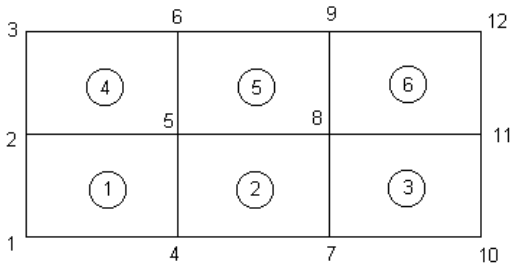

Figure No. 7. The quadrilateral element net

Span: in the last column the are presented the spans of the half bandwidths, sorted in ascending order.

Table No. 2

Node	The connectivity matrix	Sum	Average	Span
1	1 2 4 5	12	3	7
2	2 1 3 4 5 6	21	3.5	7
3	3 2 5 6	116	4	8
4	4 1 7 2 5 8	27	4.5	9
5	5 1 2 3 4 6 7 8 9	45	5	10
6	6 2 3 5 8 9	33	5.5	11
7	7 4 5 8 10 11	45	7.5	15
8	8 4 5 6 7 9 10 11 12	72	8	16
9	9 5 6 8 11 12	51	8.5	17
10	10 7 8 11	36	9	18
11	11 7 8 9 10 12	57	9.5	19
12	12 8 9 11	40	10	20

Each of the above criteria cannot be selected as keystone for inducing the minimum bandwidth. An hypothesis is advocated, i.e. all the threee criteria are satisfied, then a minimum bandwith is obtained. Till now a demonstration of the convergeance is not provided yet. In practice, the assumption provided correctly in almost all cases.

5. CONCLUSIONS

In this paper there are presented several algorithms that are widely used to decrease de bandwidth or the front width of the equation system. There are presented in comparison the performances of these and the domain for use.

In now days the FEM software contains algorithms to reorganize the structural topology (node renumbering/ element renumbering). The implementation of these routines leads to very important decrease of memory used and computational effort.

References

1. E. Cuthill, J. McKee, "Reducing the Bandwidth of Sparse Symmetric Matrices", NSRDC, Washington DC, 1969.
2. R. Rosen, "Matrix Bandwidth Minimization", Proc. of 23 rd. National Conference, ACM, ACM Publ. P-68, Brandon/Systems Press, Princeton, NJ, pp. 585-595, 1968.
3. K. J. Bathe, Edward L. Wilson, Numerical Methods in Finite Element Analysis, Prentice-Hall Inc., Englewood Cliffs, New Jersey, 1976.
4. R. S. Varga, "Matrix Iterative Analysis", Prentice Hall, Inc., NY, 1962.
5. B. A. Carré, "The Partitioning of Network Problems for Block Iteration", Comp. Jrnl., pp. 84-97, 1966.
6. S. Parter, "The Use of Linear Graphs in Gauss Elimination", SIAM Review, 3, 1961, pp. 119-130.
7. F. Harary, "A Graph Theoretic Approach to Matrix Invertion by Partitioning", Numerische, Mathematik, 4, 1962, pp. 128-135.
8. S. W. Sloan, W. S. Ng, "Direct Comparison of Three Algorithms for Reducing Profile and Wavefront", Computers & Structures, 33, 1989, pp. 411-419.
9. W. R. Spillers, "Techniques for Analysis of Large Structures", J. Struct. Div., ASCE, 94, No. ST11, 1968, pp. 2521-2534.
10. I. P. King, "An Automatic Reordering Scheme for Simultaneous Equations Derived from Network Systems", Int. J. Num. Meth. Engng., 2, 1970, pp. 523-533.
11. J. Barlow, C. G. Marples, "Comment on an Automatic Node – Relabelling Scheme for Bandwidth Minimization of Stiffness matrices", J. AIAA, 7, 1969, pp. 380-381.
12. H. R. Grooms, "Agorithm for Matrix Bandwidth Reduction", J. Struct. Div., ASCE, 98, No. ST1, 1972, pp. 203-214.
13. G. Akrash et al., "A Finite Element Software for the Analysis of Two Dimensional Continua", Second Symposium Applications of Solid Mechanics, McMaster University, Hamilton, Ontario, 1974.
14. A. George, J. W. H. Liu, "Computer Solution of Large Sparse Positive Definite Systems", Englewood Cliffs, NJ, Prentice-Hall, 1981.
15. NAG FORTRAN Library, Numerical Algorithms Group, 256, Banbury Road, Oxford.
16. Octavian V. Roşca, Ioan P. Ciongradi, "Metode numerice utilizate în programele de calcul automat al structurilor" Ed. Acad. Society "Matei-Teiu Botez", Iaşi, 2003.
17. J. R. Gilbert, C. Lewis, R. Schreiber, "Sparse matrices in MATLAB: Design and Implementation", Tech. Report CSL 91-4, XEROX Palo Alto Research Center, 1991.
18. United Kingdom Atomic Energy Authority, Harwell Subroutine Library: A catalogue of Subroutines, Tech. report AERE R 9185, Harwell Laboratory, Oxfordshire OX11 0RA, GB, 1988.

Probabilistic seismic risk assessment of the building stock in Medellín, Colombia

Mario A. Salgado[1], Daniela Zuloaga[2], Gabriel A. Bernal[1], Miguel G. Mora[1], Omar D. Cardona[3]

[1]*CIMNE, Universitat Politècnica de Catalunya, Barcelona, Spain*
[2]*Illinois Institute of Technology, Chicago, United States of America*
[4]*Universidad Nacional de Colombia, Manizales,Colombia*

Summary

A probabilistic seismic risk assessment using the CAPRA Platform is conducted for the urban area of Medellin, which is the second largest city in Colombia using a building by building database constructed and complemented using aerial images taking into account issues such as usage categories and socio-economical levels and replacement values. The seismic hazard used for the analysis corresponds to the most updated study available in the country and that is mandatory for use in the national building code. Given that the city has a seismic microzonation study, for each of the zones is determined a spectral transference function in order to take into account the dynamic soil response and amplification effects in the analysis. Several structural classes are defined for the city and for each of them a vulnerability function is assigned. Risk results are presented in the state of the art metrics such as the loss exceedance curves, probable maximum losses for different return periods and average annual losses as well as risk maps.

KEYWORDS: Seismic risk, probabilistic risk analysis, local site effects.

1. INTRODUCTION

Several tools have been developed in order assess natural risks since its importance has been understood at different decision-maker levels and then it is clear that now has been incorporated at government levels as a development issue. The CAPRA[1] initiative is one of the available tools for this purpose and the one that has been used in this study because it's open architecture and open source characteristics. The results that are presented here are part of a full probabilistic seismic risk assessment for the building

[1] Comprenhensive Approach for Probabilistic Risk Assessment (www.ecapra.org)

ISSN 2285-2735, Pages 120 - 135

portfolio using the most updated seismic hazard information for the country (in terms of seismic hazard at rock level) and for the city (using the seismic microzonation) as well as a building by building resolution exposure database where every element is identified and characterized with its most relevant parameters in terms of structural class, number of stories and age in order to assign a proper vulnerability function as well as the main usage and replacement value, required to obtain the risk results in categories and monetary units.

Medellin is located on an intermediate seismic hazard zone according to the national building code and important seismic sources (in shallow and subduction zones) can generate high intensities in the area of interest.

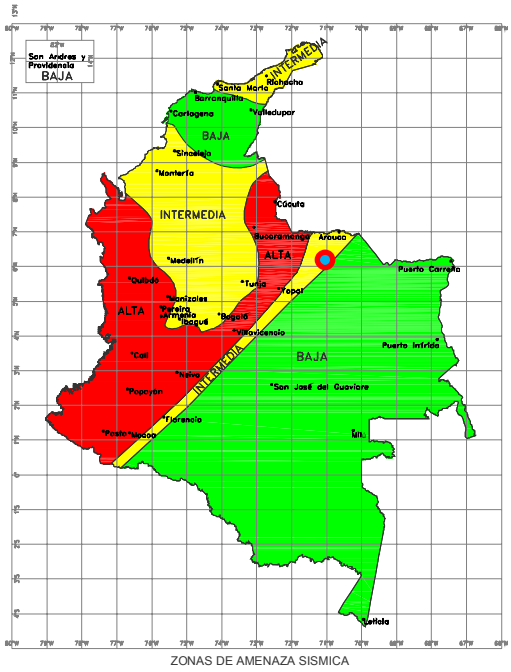

ZONAS DE AMENAZA SISMICA

Figure 1. Seismic hazard zonation map of Colombia

2. METHODOLOGY

Colombia as a country has several seismic hazard assessment studies and in the framework of the latest building code update in 2010 (AIS, 2010a) a complete national level study was conducted by local specialists (AIS,

2010b). That information, using the very same source's geometry, parameters and attenuation relationships was used in order to create a set of stochastic scenarios. The approach of scenarios allows to compute the risk in terms of a loss exceedance curve (LEC) having then information such as the average annual loss (AAL) and probable maximum losses (PML) for several return periods.

A building by building resolution exposure database was used for Medellin, the second largest city in Colombia from the official information of the local cadastral office (Alcaldía de Medellín, 2010) and complemented using aerial images. For the whole city a set of structural classes was identified in order to define a set of vulnerability functions that relate the intensities (spectral acceleration) with the expected loss in each element.

All input information for the risk assessment process was generated using the CAPRA modules such as CRISIS2007 (Ordaz et al., 2007) for the seismic hazard assessment, SiteEffects (ERN-AL, 2011) to use the spectral transfer functions and ERN-Vulnerability (ERN-AL, 2009a) to define and select the vulnerability functions. The risk assessment was done in the CAPRA-GIS platform (ERN-AL, 2009b) that constitutes the risk calculator of the initiative. Figure 2 presents a flowchart of the process.

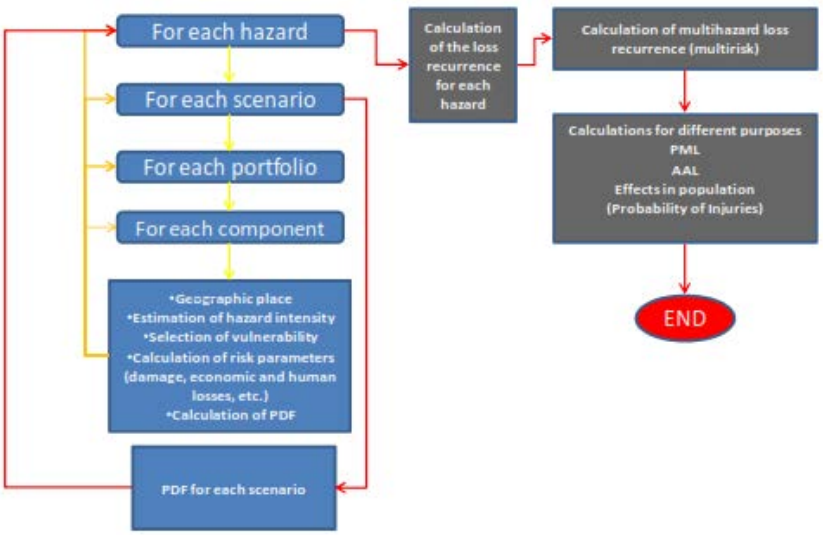

Figure 2. Probabilistic risk assessment flowchart

3. SEISMIC HAZARD

Using the very same information regarding the source's geometry and parameters as well as the assigned attenuation relationships to them a set of stochastic events was constructed for the country. All those events are characterized by several spectral ordinates and have a probabilistic representation by two statistical moments. Figure 3 presents the uniform hazard spectrums (UHS) in Medellin for different return periods (left) and the source's participation in the integrated hazard for 475 years return period.

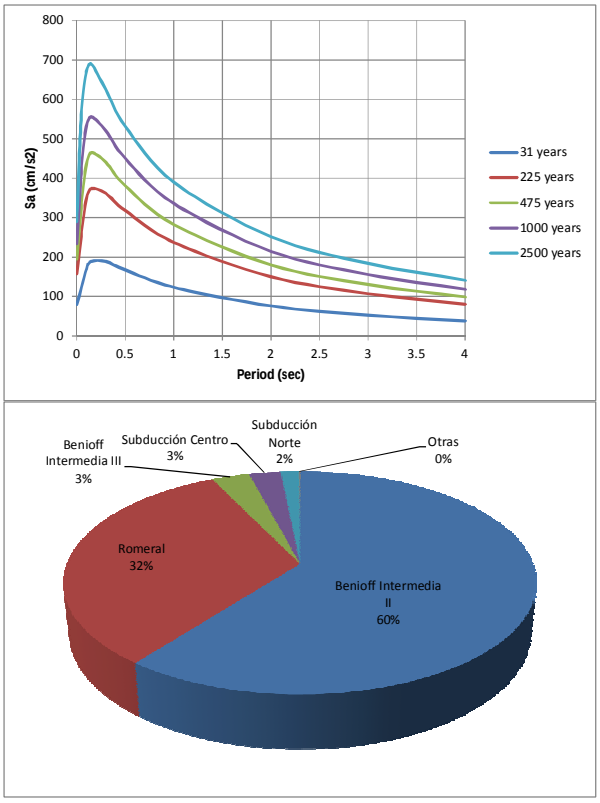

Figure 3. Uniform hazard spectrums for Medellin

The city has a seismic microzonation study (SIMPAD et al., 1999) that identifies 15 soil zones as presented in Figure 4. For each of those zones a spectral transfer function is defined in order to take into account in the risk assessment process the local site effects. The consideration of the local site-effects in Medellin is of important relevance due to the characteristics of

some soft soil and clay deposits that may give some important amplification values for the fundamental periods.

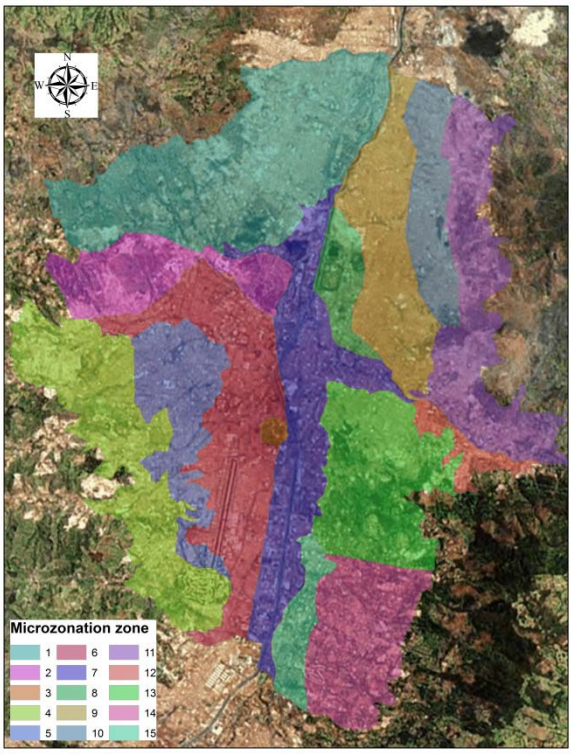

Figure 4. Seismic microzonation zones

4. EXPOSED ASSETS DATABASE

As stated above, a building by building resolution database was organized for the city using the official cadastral office information and complemented using aerial images for some zones in the city. The total number of identified buildings is 241,876 comprising only the metropolitan area and not including neighbor municipalities. After the identification process was completed a characterization phase was needed in order to assign to each of the elements the required information for the risk assessment. First of all a set of parameters related with the structural characteristics was defined such as the structural system, number of stories and building's age and finally a

classification by usage and socio-economical level was done in order to assign a replacement value.

4.1. Building stock appraisement

Given that no official cadastral values are published by the official entities given the confidential characteristics of that information, a set of indexes for replacement values was defined for each county (*comuna*) of the city. This information takes into account the building’s usage, structural system and the socio-economical level distribution in each of them to then assign the replacement value as a figure relative to the total constructed area. Figure 5 present the socio-economical level (left) and main usage (right) distribution.

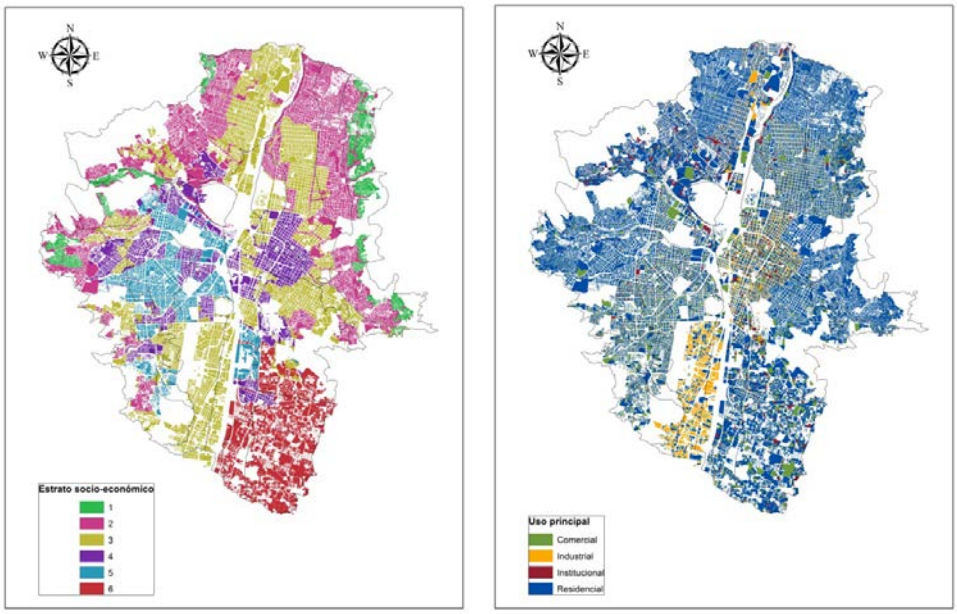

Figure 5. Socio-economical and main usage distribution

Figure 6 present the geographical distribution of the replacement values per square meter (left) and the total replacement value for each element in the database (right).

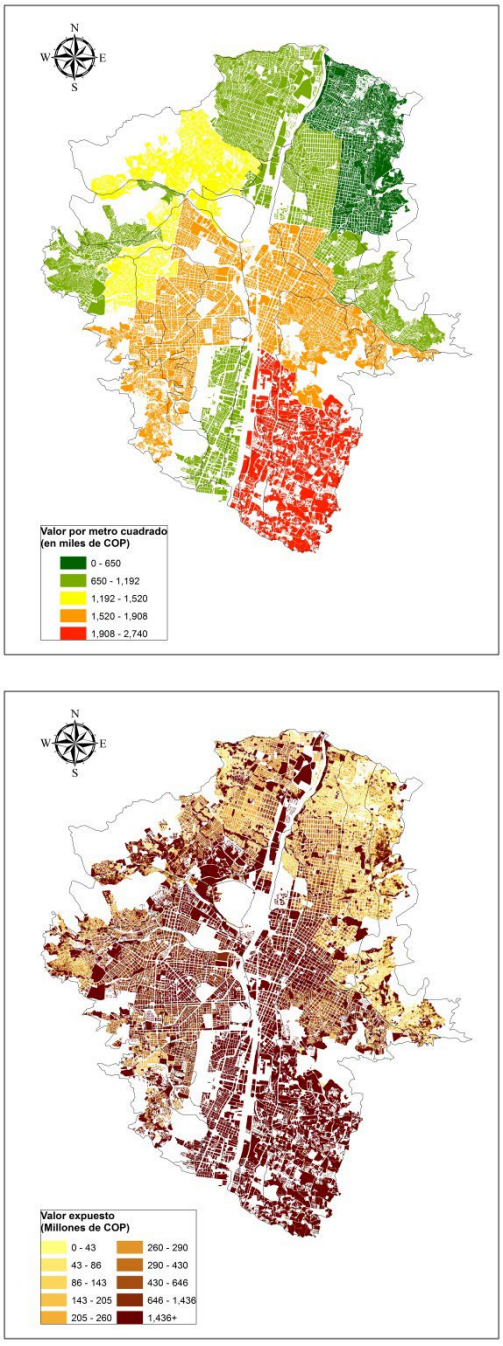

Figure 6. Building's replacement values

4.2. Definition of building classes

For the whole city, a set of structural classes that comprise the relevant parameters identified above is defined. 41 structural classes were identified as presented in Table 1. It is clear from those figures that the majority of the city has masonry buildings and that those are evenly spread across the urban area.

Table 1. Building classes and replacement values

Construction material	Structural class	Distribution		Exposed value	
		Number of elements	%	(COP) Millions	%
Steel frames	AC_1	88	0.04%	$ 461,579	0.17%
	AC_2	101	0.04%	$ 1,063,052	0.40%
Confined masonry	MC_1	13,088	5.41%	$ 2,155,513	0.82%
	MC_2	24,363	10.07%	$ 13,588,164	5.15%
	MC_3	11,634	4.81%	$ 12,906,820	4.89%
	MC_4	4,489	1.86%	$ 18,390,365	6.97%
	MC_5	69	0.03%	$ 153,709	0.06%
	MC_7	2	0.00%	$ 9,611	0.00%
Reinforced masonry	MR_1	2,244	0.93%	$ 353,434	0.13%
	MR_2	2,570	1.06%	$ 979,426	0.37%
	MR_3	1,192	0.49%	$ 788,076	0.30%
	MR_4	273	0.11%	$ 426,292	0.16%
	MR_5	20	0.01%	$ 46,299	0.02%
Unreinforced masonry	MS_1	21,080	8.72%	$ 3,452,790	1.31%
	MS_2	67,452	27.89%	$ 30,866,509	11.70%
	MS_3	24,619	10.18%	$ 17,382,759	6.59%
	MS_4	1,191	0.49%	$ 1,605,870	0.61%
Steel moment-resistent frames	PAA_10	25	0.01%	$ 179,501	0.07%
	PAA_2	287	0.12%	$ 1,106,335	0.42%
	PAA_3	1,063	0.44%	$ 2,163,888	0.82%
	PAA_4	772	0.32%	$ 2,888,599	1.09%
	PAA_5	557	0.23%	$ 6,135,853	2.33%
	PAA_6	115	0.05%	$ 751,952	0.28%
	PAA_7	225	0.09%	$ 4,101,376	1.55%
Dual system (concrete frame and shear wall)	PCM_10	175	0.07%	$ 3,190,403	1.21%
	PCM_5	753	0.31%	$ 15,233,236	5.77%
	PCM_6	255	0.11%	$ 2,870,541	1.09%
	PCM_7	945	0.39%	$ 16,428,899	6.23%
Reinforced concrete frames	PCR_1	2,830	1.17%	$ 762,229	0.29%
	PCR_10	74	0.03%	$ 1,080,865	0.41%
	PCR_2	15,271	6.31%	$ 10,023,478	3.80%
	PCR_3	8,985	3.71%	$ 12,124,639	4.59%
	PCR_4	6,804	2.81%	$ 16,098,505	6.10%
	PCR_5	5,340	2.21%	$ 35,036,015	13.28%
	PCR_6	1,171	0.48%	$ 6,578,138	2.49%
	PCR_7	959	0.40%	$ 18,301,547	6.94%
Non-technified	RI_1	1,977	0.82%	$ 120,898	0.05%
	RI_2	3,550	1.47%	$ 314,208	0.12%
Wood	W_1	3,056	1.26%	$ 267,943	0.10%
	W_2	11,131	4.60%	$ 2,853,850	1.08%
	W_3	1,081	0.45%	$ 651,956	0.25%
TOTAL		**241,876**	**100.00%**	**$ 263,895,125**	**100.00%**

Figure 7 presents the geographical distribution of the structural classes along the city (left) and number of stories (right).

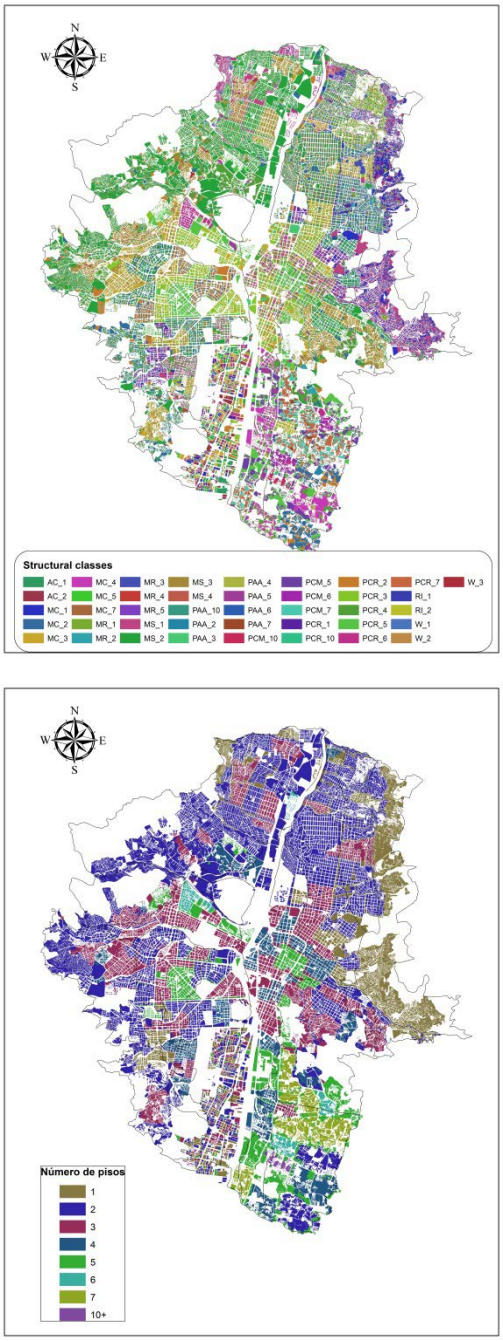

Figure 7. Building classes and number of stories geographical distribution

5. SEISMIC VULNERABILITY OF THE EXPOSED ASSETS

For each of the identified structural classes a vulnerability function is defined. The vulnerability functions relate the expected loss with the local intensities at ground level, in this case the spectral acceleration in the range of PGA to 4.0 seconds; this approach allows a probabilistic representation because also, for each function a standard deviation value is assigned for each point. A total number of 35 vulnerability functions are used for the analysis as presented in Table 2. Figure 8 shows a comparison of the different functions where it is evident that some of the identified classes are more vulnerable than another by having higher expected losses for the same intensity at ground level.

Table 2. Vulnerability function assignment

Structural class	Vulnerability function	Structural class	Vulnerability function
MC_1	MC_1p	PAA_6	PA+DIAG_6p
MC_2	MC_2p	PAA_7	PA+DIAG_7p
MC_3	MC_3p	PCM_10	PCR+MCR_10p
MC_4	MC_4p	PCM_5	PCR+MCR_5p
MC_5	MC_5p	PCM_6	PCR+MCR_6p
MC_6	MC_6p	PCM_7	PCR+MCR_7p
MC_7	MC_7p	PCR_1	PCR_1p
MR_1	MR_1p	PCR_10	PCR_10p
MR_2	MR_2p	PCR_2	PCR_2p
MR_3	MR_3p	PCR_3	PCR_3p
MR_4	MR_4p	PCR_4	PCR_4p
MR_5	MR_5p	PCR_5	PCR_5p
MS_1	MS	PCR_6	PCR_6p
MS_2	MC_2p	PCR_7	PCR_7p
MS_3	MC_3p	RI_1	W1
MS_4	MC_4p	RI_2	W1
PAA_1	PA+DIAG_1p	W_1	W1
PAA_10	PA+DIAG_10p	W_2	W1
PAA_2	PA+DIAG_2p	W_3	W1
PAA_3	PA+DIAG_4p	AC_1	PA_1p
PAA_4	PA+DIAG_4p	AC_2	PA_2p
PAA_5	PA+DIAG_5p		

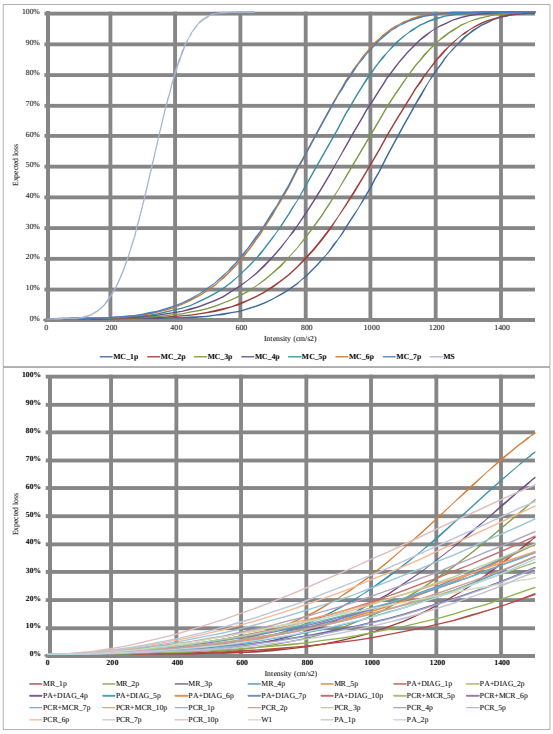

Figure 8. Vulnerability functions used in the analysis, masonry (left), frames and dual systems (right)

6. RISK ANALYSIS

After the convolution process between the hazard and vulnerability input information the expected losses information are obtained for the whole portfolio. Those results include the consideration of the complete set of stochastic scenarios and then the representation of small, moderate and big events, amplified by the soil conditions represented trough the transfer functions and the expected losses in each element according to the assigned vulnerability function. The results are expressed in terms of the loss exceedance curve and from it the average annual loss and probable maximum losses for different return periods can be derived. Figure 9 present the loss exceedance curve for Medellin. Figure 10 presents the probable maximum losses plot (left) and the loss exceedance probability for different exposure timeframes (right). Table 3 summarizes the obtained results.

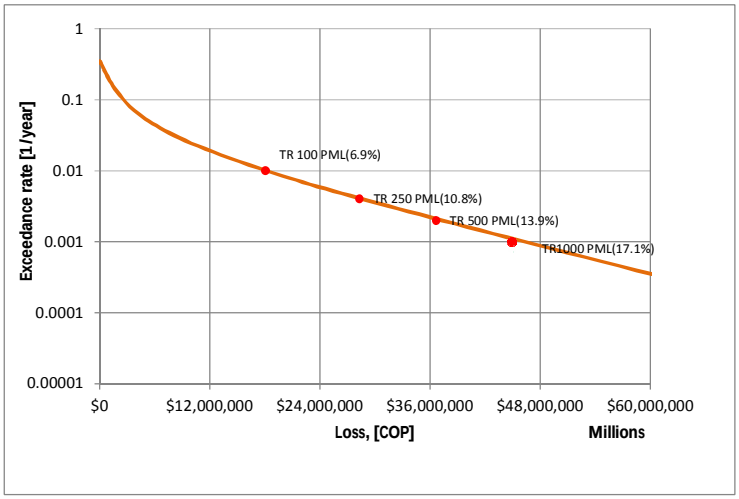

Figure 9. Loss exceedance curve

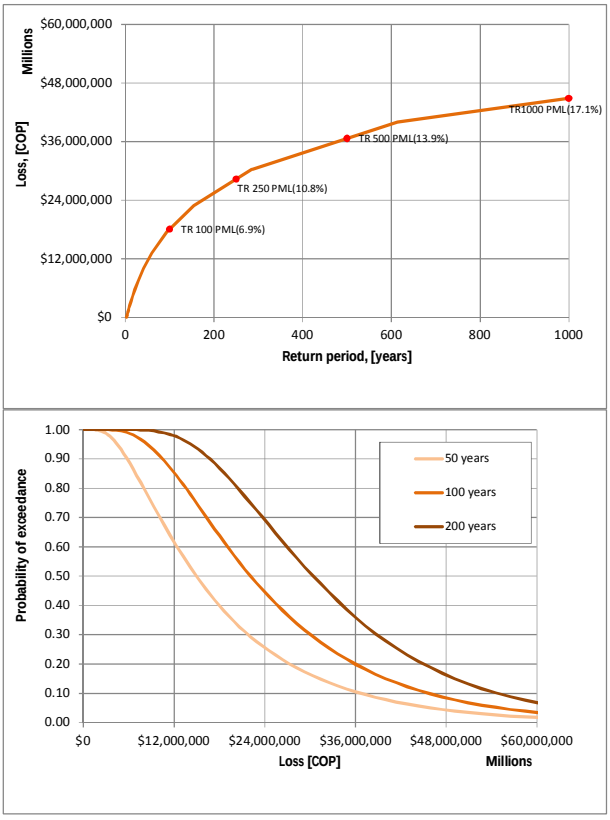

Figure 10. PML plot and loss exceedance probabilities for different timeframes

Table 3. Summary of the results

Results		
Exposed value	COP$ x10^6	263,895,000
Average annual loss	COP$ x10^6	1,088,355
	‰	4.124
PML		
Return period	Loss	
years	COP$ x10^6	%
100	$18,060,000	6.84
250	$28,288,591	10.72
500	$36,641,310	13.88
1000	$44,873,265	17.00

Another common way to express the risk results is through maps where the spatial distribution of the expected losses can be visualized. Figure 11 presents the average annual losses for each of the elements comprised in the exposed assets database in terms of their monetary (left) and relative (to its replacement cost) values (right). Relative losses distribution is important because it is this parameter that allows the comparison between risk levels across the analysis area.

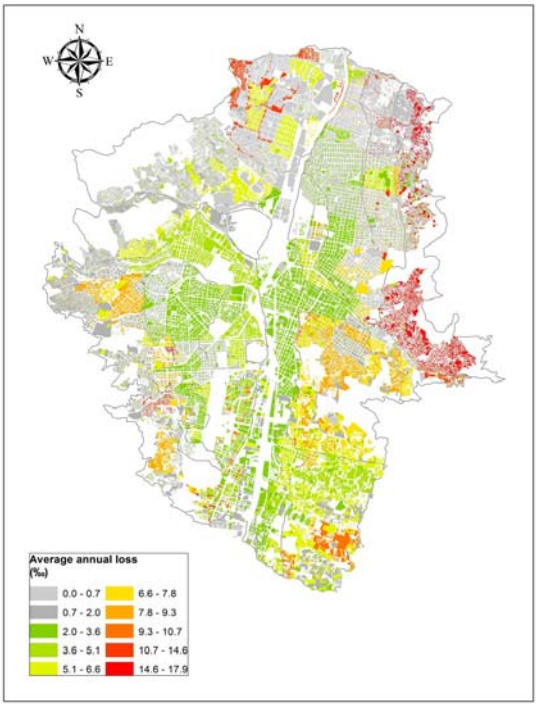

County	AAL (‰)	County	AAL (‰)
Comuna 1	2.7	Comuna 9	5.8
Comuna 2	1.6	Comuna 10	3.6
Comuna 3	2.7	Comuna 11	3.6
Comuna 4	1.5	Comuna 12	4.6
Comuna 5	2.8	Comuna 13	3.0
Comuna 6	3.4	Comuna 14	4.9
Comuna 7	2.2	Comuna 15	3.4
Comuna 8	5.9	Comuna 16	3.4

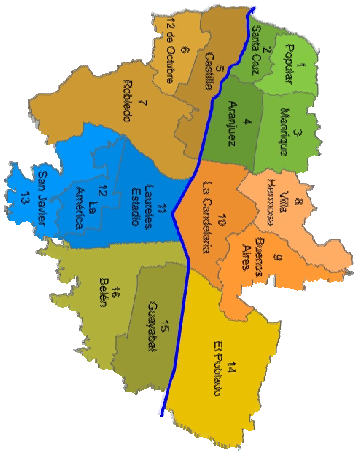

Figure 11. Risk map in terms of average annual loss for Medellín

Damage distribution is located mainly on the northwestern area of the city as well as in the east zone. This zone has clearly important amplification levels due to geotechnical and topographical effects that seriously modify the expected intensities in the ground when compared with the ones at the rock basement.

6.1. Risk results by structural class

Due to the characterization process in the exposure database construction it is possible to disaggregate the risk results in several categories. Table 4 summarizes those results in a structural class basis where it is evident that the structural class that has the highest risk values is unreinforced masonry and high-rise confined masonry.

Table 4. Summary of the risk results by structural class

Construction material	Structural class	Exposed value		Average annual loss	
		(COP) Millions	%	(COP) Millions	‰
Steel frames	AC_1	$ 461,579	0.17%	$ 761	1.6
	AC_2	$ 1,063,052	0.40%	$ 2,780	2.6
Confined masonry	MC_1	$ 2,155,513	0.82%	$ 980	0.5
	MC_2	$ 13,588,164	5.15%	$ 8,863	0.7
	MC_3	$ 12,906,820	4.89%	$ 69,660	5.4
	MC_4	$ 18,390,365	6.97%	$ 123,390	6.7
	MC_5	$ 153,709	0.06%	$ 1,870	12.2
	MC_7	$ 9,611	0.00%	$ 133	13.8
Reinforced masonry	MR_1	$ 353,434	0.13%	$ 54	0.2
	MR_2	$ 979,426	0.37%	$ 277	0.3
	MR_3	$ 788,076	0.30%	$ 2,333	3.0
	MR_4	$ 426,292	0.16%	$ 1,156	2.7
	MR_5	$ 46,299	0.02%	$ 272	5.9
Unreinforced masonry	MS_1	$ 3,452,790	1.31%	$ 44,194	12.8
	MS_2	$ 30,866,509	11.70%	$ 19,846	0.7
	MS_3	$ 17,382,759	6.59%	$ 111,749	5.4
	MS_4	$ 1,605,870	0.61%	$ 6,963	6.7
Steel moment-resistent frames	PAA_10	$ 179,501	0.07%	$ 348	1.9
	PAA_2	$ 1,106,335	0.42%	$ 2,122	1.9
	PAA_3	$ 2,163,888	0.82%	$ 2,889	1.3
	PAA_4	$ 2,888,599	1.09%	$ 3,539	1.2
	PAA_5	$ 6,135,853	2.33%	$ 11,126	1.8
	PAA_6	$ 751,952	0.28%	$ 2,014	2.7
	PAA_7	$ 4,101,376	1.55%	$ 12,415	3.0
Dual system (concrete frame and shear wall)	PCM_10	$ 3,190,403	1.21%	$ 10,644	3.3
	PCM_5	$ 15,233,236	5.77%	$ 67,420	4.4
	PCM_6	$ 2,870,541	1.09%	$ 15,416	5.4
	PCM_7	$ 16,428,899	6.23%	$ 66,495	4.0
Reinforced concrete frames	PCR_1	$ 762,229	0.29%	$ 2,166	2.8
	PCR_10	$ 1,080,865	0.41%	$ 4,923	4.6
	PCR_2	$ 10,023,478	3.80%	$ 41,234	4.1
	PCR_3	$ 12,124,639	4.59%	$ 49,054	4.0
	PCR_4	$ 16,098,505	6.10%	$ 77,901	4.8
	PCR_5	$ 35,036,015	13.28%	$ 178,421	5.1
	PCR_6	$ 6,578,138	2.49%	$ 34,075	5.2
	PCR_7	$ 18,301,547	6.94%	$ 106,412	5.8
Non-technified	RI_1	$ 120,898	0.05%	$ 137	1.1
	RI_2	$ 314,208	0.12%	$ 312	1.0
Wood	W_1	$ 267,943	0.10%	$ 255	1.0
	W_2	$ 2,853,850	1.08%	$ 3,045	1.1
	W_3	$ 651,956	0.25%	$ 710	1.1
TOTAL		**$ 263,895,125**	**100.00%**	**$ 1,088,355**	**4.1**

6.2. Risk results by county (comuna)

Table 5 presents the risk results classified by the different counties across the city; this information is useful at this resolution level because it allows local municipalities to identify its risk values and use them for retrofitting, financial protection and emergency plans schemes.

Table 5. Summary of the risk results by counties

County	Exposed value		Average annual loss	
	(COP) Millions	%	(COP) Millions	‰
Comuna 1	$ 1,299,282	0.5%	$ 3,457	2.7
Comuna 2	$ 1,464,410	0.6%	$ 2,297	1.6
Comuna 3	$ 3,493,632	1.3%	$ 9,515	2.7
Comuna 4	$ 5,884,772	2.2%	$ 8,911	1.5
Comuna 5	$ 7,437,272	2.8%	$ 20,736	2.8
Comuna 6	$ 4,986,059	1.9%	$ 16,889	3.4
Comuna 7	$ 15,606,046	5.9%	$ 34,062	2.2
Comuna 8	$ 3,386,916	1.3%	$ 20,083	5.9
Comuna 9	$ 14,081,971	5.3%	$ 81,146	5.8
Comuna 10	$ 23,020,074	8.7%	$ 82,611	3.6
Comuna 11	$ 24,182,883	9.2%	$ 86,449	3.6
Comuna 12	$ 9,874,359	3.7%	$ 45,804	4.6
Comuna 13	$ 8,543,876	3.2%	$ 25,309	3.0
Comuna 14	$ 115,453,088	43.7%	$ 564,757	4.9
Comuna 15	$ 6,675,783	2.5%	$ 22,840	3.4
Comuna 16	$ 18,504,701	7.0%	$ 63,485	3.4
TOTAL	**$ 263,895,125**	**100.0%**	**$ 1,088,355**	**4.1**

7. CONCLUSIONS

- Medellin has a state of the art seismic risk assessment that allows quantifying in several metrics the future catastrophic losses for the building's portfolio.
- The results obtained from this paper can be used to organize the risk results in terms of structural systems, main usage and number of stories.
- The county that has highest risk in relative terms in number 8 which is located in the eastern zone of the city and has a large participation of unreinforced masonry structural systems.
- The county that has highest average annual loss values in monetary units is number 14, the one with highest socio-economical level and where most of the high-rise buildings are located.

- The structural system that concentrates the highest risk is the unreinforced masonry which is a common in the poorest counties of the city; some essential buildings such as schools and hospitals located on those areas have this structural system and then, a retrofitting scheme can be planned for them.
- The results allow to generate risk maps with a building by building resolution that allow a visualization of the geographical distribution of the future losses; anyhow, it must be clear that risk should be preferable expressed in terms of loss exceedance rates and probabilities of exceedance.
- With this same information but using a single scenario approach, studies such as emergency plans can be developed for the city.
- These assessments should be updated every time new information related to the hazard, microzonation zones and exposed assets database is available.

Acknowledgements

The authors would like to thank Spain's Ministry of Economy and Competitiveness in the framework of the researches formation program (FPI) and the project "Comprenhensive probabilistic approach for seismic risk evaluation in Spain" (CGL2011-29063).

References

1. Alcaldía de Medellín. (2010). Geonetwork. http://poseidon.medellin.gov.co/geonetwork/srv/es/main.home
2. Asociación Colombiana de Ingeniería Sísmica-AIS, (2010ª). Reglamento Colombiano de Construcción Sismo Resistente, NSR-10. Comité AIS-100.
3. Asociación Colombiana de Ingeniería Sísmica-AIS, (2010b). Estudio General de Amenaza Sísmica de Colombia. Comité AIS-300.
4. Evaluación de Riesgos Naturales América Latina-ERN-AL, (2009ª). Informe Técnico ERN-CAPRA-T1-5. Vulnerabilidad de edificaciones e infraestructura.
5. Evaluación de Riesgos Naturales América Latina-ERN-AL, (2009b). Informe Técnico ERN-CAPRA-T1-3. Metodología de análisis probabilista del riesgo.
6. Ordaz M, Aguilar A, Arboleda J, (2007). CRISIS, Program for computing seismic hazard. Instituto de Ingeniería. Universidad Nacional Autónoma de México.
7. SIMPAD, Universidad EAFIT, Integral, INGEOMINAS, Universidad Nacional de Colombia Sede Medellín, (1999). Instrumentación y microzonificación sísmica del área urbana de Medellín.

Numerical analysis of FRP reinforced masonry cross vaults

Jerzy Szołomicki, Piotr Berkowski, and Jacek Barański
Departmen of Civil Engineering, Wrocław University of Technology, Wrocław, 50-370, Poland

Summary

The paper focuses on numerical modeling and analysis of computational calculations of masonry cross vaults strengthened with FRP strips. Masonry vaults and arches often need repair and strengthening because of many factors such as: material degradation, imposed displacements, and increased service loads. For this purpose FRP composites applied to the surfaces of vaults are a proper solution. The application of FRPs for strengthening is mainly aimed at reinforcing masonry structures by increasing their ultimate capacity (strength and displacement) and often this is achieved by modification of mechanisms at damage, which can involve further resisting phenomena. Among different solutions used to masonry vaults, FRPs are usually proposed as application of near surface mounted externally bonded strips or laminates. The use of carbon and glass fibers is predominant in comparison with other types of materials, due to their higher accessibility and sufficiently high mechanical properties together with epoxy resins. The main problem of numerical analysis of these type of constructions are limited information about mechanical properties of the masonry material used. Analysis of masonry vaults assumes that masonry has very low tensile strength. Most of historical masonry vaults generally fail not due to lack of compressive strength, but due to instabilities caused by differential foundation settlements, earthquakes, or long-term deformations. Therefore, in analysis of damage mechanism of vaults the attention was taken on forcing of the supports.

KEYWORDS: brick masonry vaults, strengthening, FRP composite.

1. INTRODUCTION

The increasing interest in historic architectural heritage and the need for conservation of historical structures has led to the continuous development of many methods used in the structural analysis of masonry vaults. However, some type of vaults have not been thoroughly analysed, mainly because of the problem of applying simplified theories to their complicated shapes. The main simplification that is usually taken into consideration is based on the reduction of the vault to

series of adjacent arches, without transversal connection. Therefore, this model is not able to simulate properly the three-dimensional effects in the vaults. This limitation and the need for a flexible method to study the different types of vaults could be solved by using the conception of the three-dimensional FEM analysis.

Masonry cross vaults are very important structural elements in many historical heritage buildings. These vaults are vulnerable to cracking and dangerous failure mechanisms under certain loading conditions. The structural behaviour of masonry vaults and their collapse mechanisms depend on the properties of the structural material from which they are made. Presented approach is based on the assumption of large compressive strength for the blocks, no tension transmitted across the joints and finite friction.

Traditional reinforcement techniques may guarantee an adequate increment in strength, stiffness and ductility, but are often short lived and labour intensive. Composite materials are applied in the case of necessity of considerable raising load-bearing capacity of strengthened structure. The strengthening methods based on CFRP and GFRP composite materials have favourable effects on the structural response and load bearing capacity. FRP composites may bring an important load bearing contribution by compensating the lack of tensile capacity of brick masonry elements. Application of FRP strips over the inside and outside surfaces of the cross vaults can prevent the cracks opening and the formation of hinges prior to collapse. However, reinforcement cannot prevent masonry from cracking. So cracks may form also at a reinforced boundary, but cannot open because the reinforcement clenches the crack. From review of investigations carried out in the world [2, 3, 4, 6, 7, 9, 10, 11, 12, 13, 14, 15, 16, 17] it is possible to state that the problem of reinforcing cross vaults by means of composite strips is widely analyzed, but there are still some details that need examination.

The computer code LUSAS was used to perform the numerical analysis of the masonry cross vault. LUSAS is a suite of general-purpose, advanced finite element analysis (FEA) programs. The material library in LUSAS includes different models of inelastic behaviour of materials, such as metals, cast iron, soils, and concrete. Unfortunately, there is no specific model available for non-linear modelling of unreinforced masonry structures. However, the multi-crack concrete model available in LUSAS software can be used to model masonry structures.

The Authors conduct two types of analyses of masonry vaults. The non-linear analysis of unreinforced cross vault was carried out in the aim to accurate determining of crack zones. In such points a structure of vault was reinforced by FRP strips. Linear analysis of reinforced cross vaults was carried out with the purpose of determining the effectiveness of strengthening.

2. NUMERICAL ANALYSIS OF CROSS VAULTS

Multi-crack concrete model

The main emphasis was put on to the adoption of concrete multi-crack model for masonry vault. The model couples directional damage with plasticity and employs contact mechanics to simulate crack opening and closing and shear contact effects. The model uses damage planes. Stresses on these damage planes are governed by a local constitutive relationship.

The damage, or contact matrix, is generated from the planes of degradation each of which is formed when a damage criterion is satisfied. Friction hardening and softening is included in the model to account for pre- and post -peak non-linear behavior. Work hardening is used such that the total work required to reach the peak stress envelope is a function of the mean stress.

A dilatancy parameter which allows plastic flow to be associated or non-associated is also included in the model.

The global stress-strain relationship is given by:

$$\underline{\sigma} = \underline{\underline{D}}_e \left((\underline{\varepsilon} - \underline{\varepsilon}_p) - \Sigma_{j=1}^{n_p} \underline{\underline{N}}_j^T \left(\underline{\underline{I}} - \underline{\underline{M}}_{xj} \right) \underline{e}_j \right) \qquad (1)$$

in which $\underline{\underline{D}}_e$ - is the elastic tensor, $\underline{\sigma}$ - stress vector, $\underline{\varepsilon}$ - the strain vector, and - $\underline{\varepsilon}_p$ the plastic strain vector, n_p- the number of damage planes, $\underline{\underline{M}}_x$ - is a local damage-contact matrix, and $\underline{e}$ - the local effective strains.

As a crack opens the relative proportion of debonded material that can regain contact in shear reduces as crack opening increases. The damage evolution function employed here is designed to improve the numerical performance of the model, and for this purpose, a completely continuous exponential softening curve, which has a smooth transition from undamaged to damaged states and from the pre-peak to the post-peak region has been introduced. The model assumes that the material can soften, and eventually lose all strength in positive loading, in any one of the predefined cracking directions. The function in terms of the fracture stress f_s and the strain parameter ζ has - as control parameters - the stress at first damage f_{ti}, the associated strain ε_{ti}, the uniaxial strength f_t, the strain at peak stress ε_k and the strain at the effective end of the curve ε_0. The basic function for a damage plane is as follows:

$$f_s = f_{ti}\, func(\zeta) = \left(1 - \omega(\zeta)\right) E \zeta \qquad (2)$$

with

$$\omega = 1 - \frac{\varepsilon_{ti}}{\zeta} e^{-c_1 \eta} \left(a - b e^{c_2 m \eta} - c e^{-c_3 m p \eta} \right) \qquad (3)$$

Numerical examples

Numerical FEM analyses were performed using LUSAS code (release 14.7). The analysis was completed with data from literature which indicated the mechanical parameters of masonry vaults for linear and non-linear range [6].The semi-circular cross vaults on square plan (4 m x 4 m) were the subject of the analysis (Figure 1).

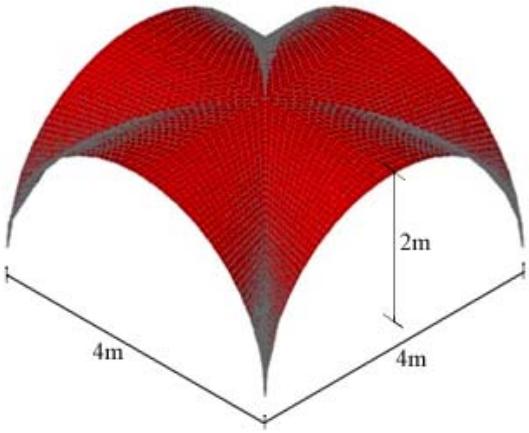

Figure 1. Geometry of analyzed cross vaults

In the first step there was carried out non-linear analysis of unreinforced cross vaults. The vaults were modeled by means of 3D solid Lusas elements (TH 10).

As the result of these analyses crack zones were determined. In these zones a structure of vault was reinforced by FRP strips. Next, linear analysis of cross vaults reinforced by using FRP strips was carried out. These vaults were modeled by means of shell Lusas elements TTS6 and QTS8. The purpose of this analysis was to determine the effectiveness of FRP strips strengthening.

In order to determine validity of the proposed technology, and up the ultimate conditions behaviour of analysed cross vaults, the following cases were investigated:

- vault without strengthening,

vault strengthened at the intrados and extrados by using CFRP (epoxy TB650+HS Carbon UD) and GFRP (TB650+E-Glass UD) strips (Table 1) [7, 17].

Table 1. Name of the table

Strips	Width (mm)	Thickness (mm)	Modulus E_x (N/m^2)	Modulus E_y (N/m^2)	Modulus G_{xy} (N/m^2)	Tensile strength (N/m^2)
CFRP	30	2	139,0E9	9,0E9	4,4E9	2200E6
GFRP	30	2	43,0E9	8,0E9	4,0E9	1900E6

Each model was studied considering two load cases (Fig. 2):
- forcing the horizontal displacement at the support,
- forcing the vertical displacement at the support.

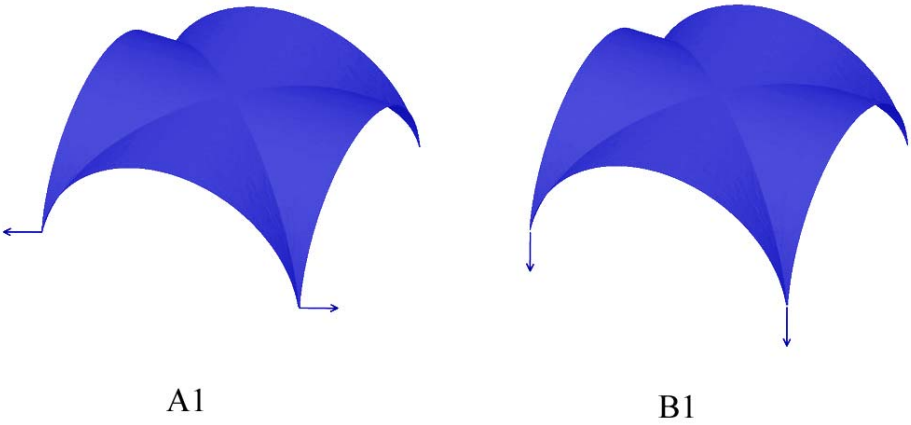

Figure 2. Different types of displacement loading of analyzed cross vault
A) forcing of horizontal displacement on the supports,
B) forcing of vertical displacement on the supports

Table 2. Parameters of non-linear masonry model [6]

f_c [N/mm^2]	$\varepsilon_{c,peak}$ [mm/m]	E [N/mm^2]	G_{fc} [N/mm]	f_t [N/mm^2]	$\varepsilon_{t,peak}$ [mm/m]	G_{ft} [N/mm]	*Poisson coefficient*
11,0	5	7500*	0,7	0,1	0,0185	0,002	0,18

* value proposed by Authors

It was very important to adopt multi-crack concrete model which generates a reliable pictures of cracks distribution able to predict the ultimate strength.

In the first step, using FE numerical non-linear analysis, there were determined limit values of tensile stress for different cases of horizontal displacement and settlement of supports of the considered type of vaults (Figs 3,7). Next, cross vault strengthened using CFRP and GFRP strips were calculated and the gained results

were compared with the maximum value of tensile stress for the selected cases under consideration (Tables 3 & 4).

Table 3. Principal tensile stresses S1 (bottom layer) for case of forcing of horizontal displacement on support u_x = 5 mm (case A1)

Node	Not strengthened vault S1 (MPa)	Vault strengthened by CFRP strips at the intrados S1 (MPa)	Vault strengthened by GFRP strips at the intrados S1 (MPa)
1455	0,509	0,2904	0,4036
5120	1,6973	0,7306	1,1617
7600	1,2965	0,7105	0,9655
8994	1,1999	0,2927	0,3128

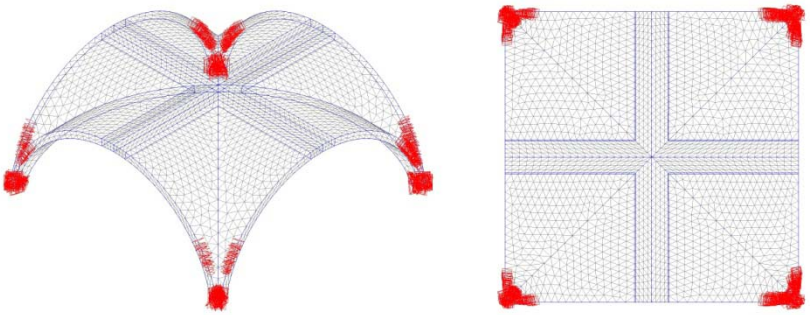

Figure 3. Damage planes in cross vault for case A1 (not reinforced cross vault)

In Figures 3 to 10 it is possible to see that CFRP strips transferred exceeded tensile stresses and significantly reduce it in cross vault. The analysis showed that the FRP strips limit distortion, reduce the tensile stress in masonry, reduce the width of the crack and increase fatigue resistance of vault. In the case of exceeding the tensile stress in the bottom or top layer of the vault, it must be reinforced at the intrados or extrados, respectively. If tensile stresses are exceeded on both sides the vault must be strengthened both at the intrados and extrados.

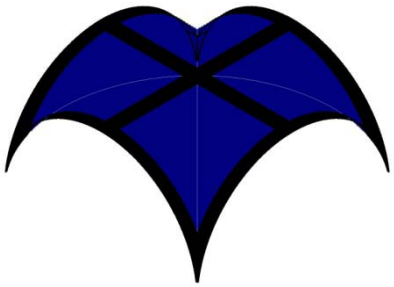

Figure 4. Proposed strengthening of cross vault by CFRP strips for case of forcing horizontal displacement on 2 supports u_x = 10 mm (case A1)

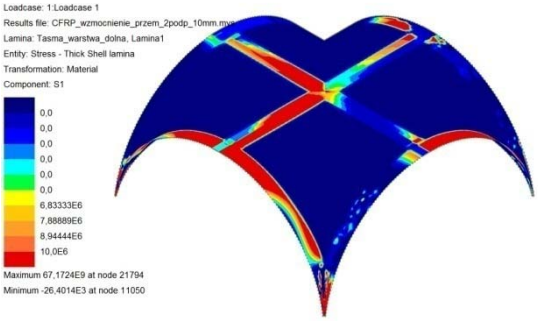

Figure 5. Distribution of tensile stress S1 in CFRP strips for case of forcing horizontal displacement on 2 supports for u_x= 10 mm (case A1)

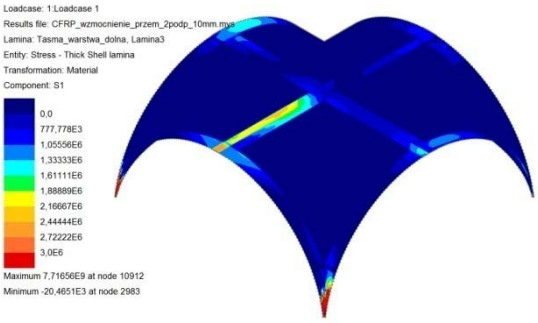

Figure 6. Distribution of tensile stress S1 (strengthened vault) in bottom layer of cross vault for case forcing horizontal displacement on 2 supports for u_x = 10 mm (case A1)

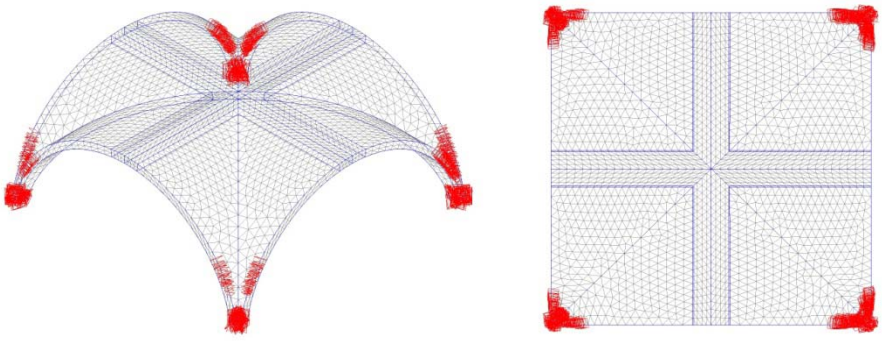

Figure 7. Damage planes in cross vault for case B1 (not reinforced cross vault)

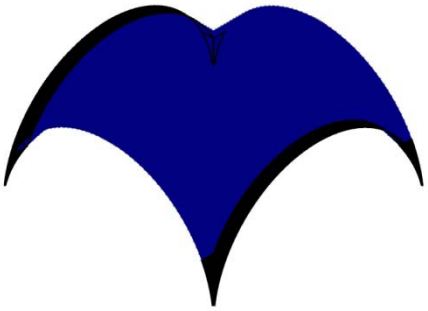

Figure 8. Proposed strengthening of cross vault by CFRP strips for case of forcing vertical displacement on 2 supports u_z = 10 mm (case B1)

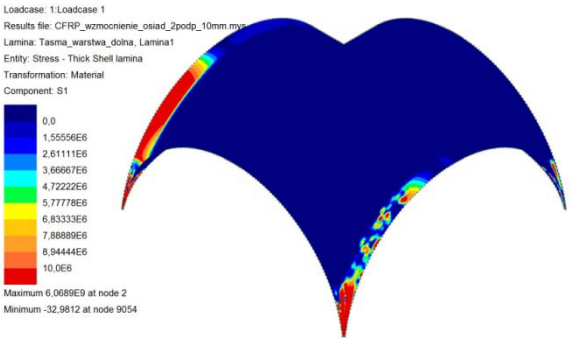

Figure 9. Distribution of tensile stress S1 in CFRP strips for case of forcing vertical displacement on 2 supports for u_z= 10 mm (case B1)

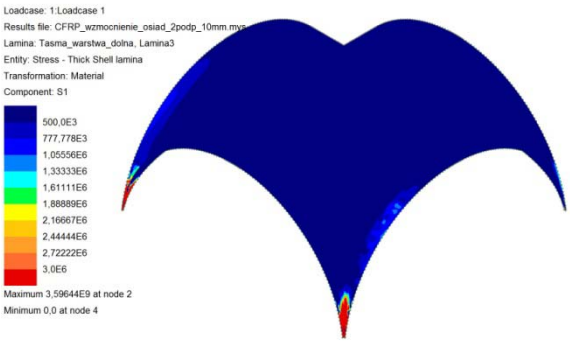

Figure 10. Distribution of tensile stress S1 (strengthened vault) in bottom layer of cross vault for case forcing vertical displacement on 2 supports for u_z = 10 mm (case B1)

Table 4. Principal tensile stresses S1 (bottom layer) for case of forcing of vertical displacement on supports u_z = 10 mm (case B1)

Node	Not strengthened vault S1 (MPa)	Vault strengthened by CFRP strips at the intrados S1 (MPa)	Vault strengthened by GFRP strips at the intrados S1 (MPa)
3016	1,4647	0,8075	0,8706
6965	1,4226	0,7445	0,8208
10691	2,5413	0,8895	1,1353
10713	2,0143	0,7331	0,9051

3. CONCLUSIONS

Behaviour of masonry cross vaults are significantly affected by the structural material low tensile strength. In the Author's opinion the adopted multicrack model is correct and it generates a reliable pictures of the distribution of cracks and possible damage mechanism. Therefore it is very useful at appointing crack zones requiring strengthening. In the case of the masonry cross vaults strengthened with CFRP or GFRP composite strips subjected to static loads there is significant reduction in tensile stress in masonry and minimization of displacements. These effects mainly depend on the arrangement of the FRP reinforcement. As a result of investigations the Authors concluded that the FRP strips should be applied with the following aims: limiting deformation, tensile stress reduction, reduction of the width of crack, and increased fatigue strength.

References

1. Aiello, M. A. , Pecce, M. , Experimental bond behavior between FRP sheets and concrete, Proceedings of the International Conference Structural Faults and Repair, London, UK [CD-ROM version] (2001).
2. Aiello, M. A., Sciolti, S. M., Bond analysis of masonry structures strengthened with CFRP sheets, Construction and Building Materials, 20 (1-2), 90–100 (2006).
3. Ceroni, F, Pecce, M, Manfredi, G., Marcari, A., Experimental bond behavior in masonry elements externally reinforced with FRP laminates, Proceedings of International Conference: Composites in Constructions – CCC 2003, Cosenza, Italy, Eds. D. Bruno, G. Spadea, N. Swamy, Editoriale Bios, 313–318 (2003).
4. Foraboshi, P., Strengthening of Masonry Arches with Fiber-Reinforced Polymer Strips, Journal of Composites for Construction, 191-202, 8 (3) (2004).
5. CNR DT 200/2004. Guide for the Design and Construction of Externally Bonded FRP Systems for Strengthening Existing Structures – Materials: RC and PC structures, masonry structures, Italy,(2004).
6. Domede, N, Sellier, A., Experimental and Numerical Analysis of Behaviour of Old Brick Masonries, Advanced Materials Research, vols. 133-134, pp 307-312 (2010).
7. Foster, P. , Gergely, J., Young, D. , McGinley, M., Strengthening masonry buildings with FRP composites, Proceedings of the 11th International Conference: Structural Faults & Repair, Edinburgh, UK, 183 (2006) [CD-ROM version].

8. Garbin, E., Valluzzi, M. R., Modena, C., Galati, N., Nanni, A., In-plane design for masonry walls strengthened by FRP materials, Proceedings of the 11th International Conference: Structural Faults & Repair, Edinburgh, UK, 184 (2006) [CD-ROM version].
9. Hamilton, H. R., Dolan, C. W., Flexural capacity of glass FRP strengthened concrete masonry walls, ASCE Journal of Composites for Construction, 5(3), 170-178 (2001).
10. Hanoush, S., McGinley, M., Mlakar, P., Scott, D., Murray, K., Out of plane strengthening of masonry walls, ASCE Journal of Composites for Construction, 5(3), 139-145 (2001).
11. Kiss, R. M., Kollar, L. P., Jai. J, Krawinkler, H., Masonry strengthened with FRP subjected to combined bending and compression, Part II: Test results and model predictions", Journal of Composite Materials, 36(9), 1049-1063 (2002).
12. Liu, Y., Dawe, J., McInerney, J., Behaviour of GFRP sheets bonded to masonry walls, Proceedings of the International Symposium on Bond Behaviour of FRP in Structures (BBFS 2005), Hong Kong, China, 473-480 (2005).
13. Mosallam, A. S., Out of plane flexular behaviour of unreinforced red bricks walls strengthened with FRP composites, Composites Part B: Engineering, 38 (5-6), 559-574 (2007).
14. Nanni, A., Tumialan, G., Fiber-reinforced composites for the strengthening of masonry structures, Structural Engineering International, 13(4), 271-278 (2003).
15. Panizza, M. , Garbin, E., Valluzzi, M. R., Modena, C., Bond behaviour of CFRP and GFRP laminates on brick masonry, Proceedings of the 6th International Conference on Structural Analysis of Historical Construction, Bath, UK, 763-770 (2008).
16. Valluzzi, M. R., Strengthening of masonry structures with Fibre Reinforced Plastics: From modern conception to historical building preservation, Proceedings of the 6th International Conference on Structural Analysis of Historical Construction, Bath, UK, 33-45 (2008).
17. Morbin, A., Strengthening of Masonry Elements with FRP Composites. University of Missouri-Rolla, pp. 192.
18. Theory Manual. LUSAS ver. 14.7.

FE modeling of a glass fiber reinforced mineral composite structure

George Taranu, Mihai Budescu, Raluca Plesu, and Ionut Ovidiu Toma
Department of Structural Mechanics, "Gheorghe Asachi" Technical University of Iasi, 700050, Romania

Summary

Finding new materials or improving the existing ones is a continuous concern of the researchers. If the alternative materials prove that can be considered for structural elements in building industry than, definitely these must be verified with adequate tools experimentally and theoretically. FEM is a powerful tool that can provide important results regarding the structural behavior.

This paper present some numerical results on a wall panel made of a glass fiber reinforced mineral composite based on ordinary Portland cement and recycled calcium sulfate. These results are compared and discussed with experimental tests performed on the same loading schema of the wall panel. Conclusions of the FE modeling shows that, the considered material and panel composition behave well in terms of stress and deformations for a maximum horizontal load action applied on top of the structure compared to an experimental test.

KEYWORDS: FE modeling, glass fiber reinforced mineral composite, structural model.

1. INTRODUCTION

Past decades showed that there is a considerable interest in the use of glass fiber reinforced plastics in the construction industry. In their present state of development, composite materials are flexible, expensive and flammable unless especially protections are added. So these materials are not very suitable as structural elements, e.g walls, floors, ceilings and partitions. For these building components, it would be desirable to replace the resin by a matrix or binder which does not suffer from these disadvantages. Ordinary Portland Cements (OPC) and calcium sulfate based binders obtained from recycled materials, can provide such inexpensive matrices which are required for structural elements. Cements and concrete are brittle materials, very weak in tension. This weakness is conventionally overcome by reinforcing concrete with steel. The thickness of

ISSN 2285-2735, Pages 146 - 154

concrete cover required protecting the steel from corrosion, and the strength of materials makes these elements relatively heavy. The result of using these materials is a structure whose weight is significant and the seismic force which is a part of total weight is considerable. The need to develop a lighter material and structural element based on inexpensive cements or combination of these and having high structural and impact strength has therefore grown in recent years both for engineering and architectural reasons. Extensive research carried out since the early 1964 in U.S.S.R has shown that a suitable composite material can be produced by reinforcing special cements such as gypsum-aluminous slag cement and high alumina cement with low alkali borosilicate glass fiber, commercially available all over the world (e.g. E glass). E glass fibers are not attacked by calcium sulfate binder and Portland cement combination matrix [1-4].

2. MATERIALS

2.1. Basic components and their source

According to recent studies in France it was observed that calcium sulfate in β anhydride III’ form can reduce the use of Portland cement in composition of building materials and obtaining good mechanical characteristics. A European private group exploits a new “State of the Art” technology which, once used on a large scale, will, on the one hand, help reduce massively the production of carbon dioxide and, on the other hand, provide commanding contribution to environmental preservation and societal developments [5, 6].

The technology consists in producing a new binder made exclusively from the processing of gypsum (CaSO4.2H2O). Gypsum is available both from the natural and the by-product of various chemical processes. In nature, gypsum exists with some deposits of anhydrite also. Among the by-product gypsum production, phosphogypsum, fluorogypsum and FGD gypsum are the waste products of phosphoric acid, hydrofluoric acid and the desulfurization of flue combustion gases of coal, foundary, oil refineries or power stations respectively. Gypsum products are known for their fire resistance, thermal insulation and acoustic properties. Gypsum has adequate strength but is not moisture resistant. The binder is entirely recyclable and can be used alone or in substitution of Ordinary Portland Cement (OPC) to produce various construction materials such as: building blocks, insulating panels using polystyrene or polyurethane as aggregates, self-leveling floor screeds.

The experimental tests carried out at the Faculty of Civil Engineering of Iasi, on the mineral matrix mixtures have provided tensile and compressive strengths and

also elastic modulus values. These were compared and lead to decision of using the optimum mix in structural elements fabrication. Flexural strengths obtained on 7 different mixtures have values between 4 and 8 MPa at 21 days. Compressive strengths have values between 14 and 24 MPa. These values are reasonable considering the components of mixtures. From all of the mixtures, NCK 60/30/10 has the minimum strengths both in tensile and compressive. In relation to the neutral mixture NCK 60/40/0 in which anhydrous calcium sulphate in the β-anhydrite iii' form is missing completely, the mechanical strengths in both flexure and compression are higher. The difference between this and others is a maximum of 30% and minimum of 15%. The elastic modulus has been calculated for two selected mixtures. The average values were obtained between 8840 MPa in case of unreinforced matrix NCK 50/25/25 and 8980 MPa in case of NCK 50/35/15. These results led to selection of NCK 50/35/15 as being the optimal mix for matrix. Next step of experimental program was the tests of the reinforced mixtures with three volume fraction. In this paper the numerical analysis used the properties for the selected binder mix NCK 50/35/15 and the mechanical properties obtained [7, 8].

2.2. Structural elements design

In the framework of a comprehensive research program, the main objective was developing of a new structural system using recyclable materials. In the first stage of the research, the materials were chosen by their accessibility on the market and their characteristics. The proposed building system is a modular structure made of panel units for walls and floor structural elements. In Fig. 1, there is presented the composition of the best three solutions for the wall elements as they evolved.

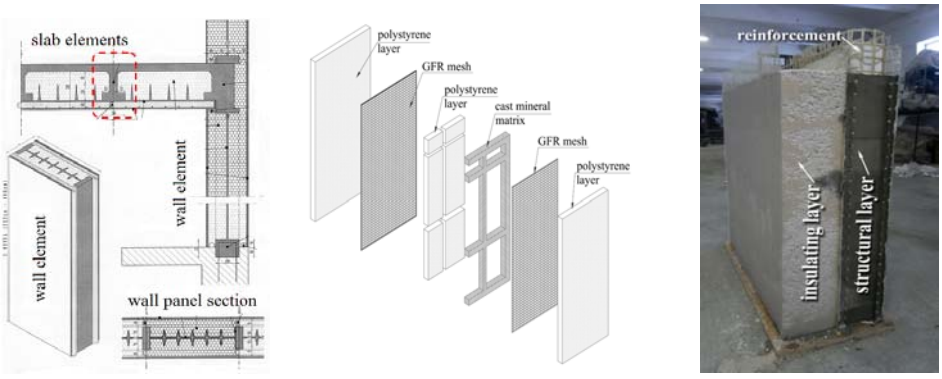

a b c

Figure 1. The composition of the wall panels units: a- first solution with 1 middle layer of composite material; b- second solution with 2 centered composite material layers; c- third solution with 2 composite material layers on interior side

The second stage of the research program consists in designing and building a structural system for experimental dynamic and static tests. One storey structural model was made by hybrid panels for a series of shaking table tests (Fig. 4). A perspective and a plan view of the structural model are presented in Fig. 2.

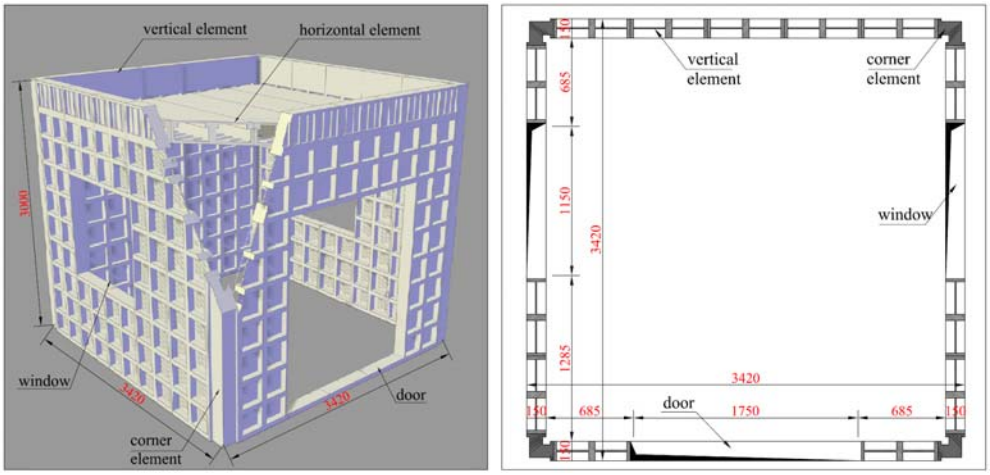

Figure 2. Perspective and plan view of the structural tested model

Fig. 3 shows the composition of the structural elements used and the construction process for the experimental model. For the mineral matrix used was chosen the mixture NCK 50/35/15 with 15% of calcium sulfate.

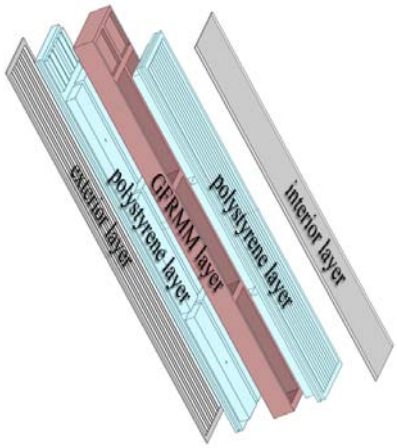

Figure 3. Structural elements: a- constitutive layers; b- mounting of the model structure on the shaking table; c- cast of the fluid mineral matrix over the reinforced polystyrene panels

3. NUMERICAL ANALYSIS

For preliminary evaluation and further comparison, some numerical studies were carried out with finite element method – FEM in some linear analyses [7], [8]. Finite element analyses were performed using AUTODESK ROBOT STRUCTURAL to simulate the general behavior of the structural model and includes general-purpose shell elements as well as elements that are valid for thick and thin shell problems. The three-dimensional model as shown in Figure's 4, is subjected to static loads, vertical and horizontally applied (Figure 5). Model structure characteristics are:

- gravity center coordinates:
- X =1.635 *(m)*
- Y =1.680 *(m)*
- Z =2.435 *(m)*
- central moments of inertia of the structure:
- Ix = 22072.048 *(kg* m2)*
- Iy = 22350.446 *(kg* m2)*
- Iz = 28201.214 *(kg* m2)*
- global mass = 10835.048 *(kg)*

The structural model was discretized in shell and bar finite elements. The mesh density and the discretization of the shell elements which consists in square and triangle elements is presented in figure 4:

- *Number of nodes: 4 3 9 4*
- *Number of bars: 3 3 1*
- *Bar finite elements: 173 3*
- *Planar finite elements: 4 3 58*
- *Volumetric finite elements: 0*
- *No of static degrees of freedom: 2 5752*

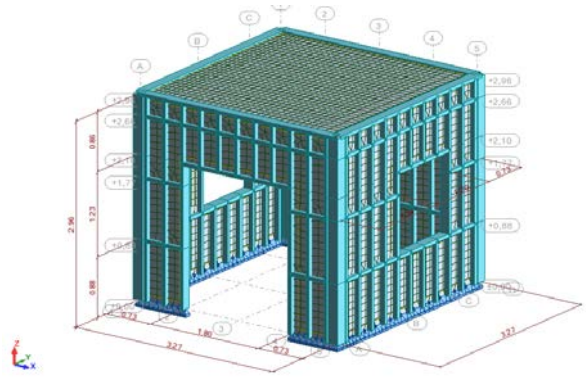

Figure 4. Mesh definition and the composition of the numerical model with shell and bar elements

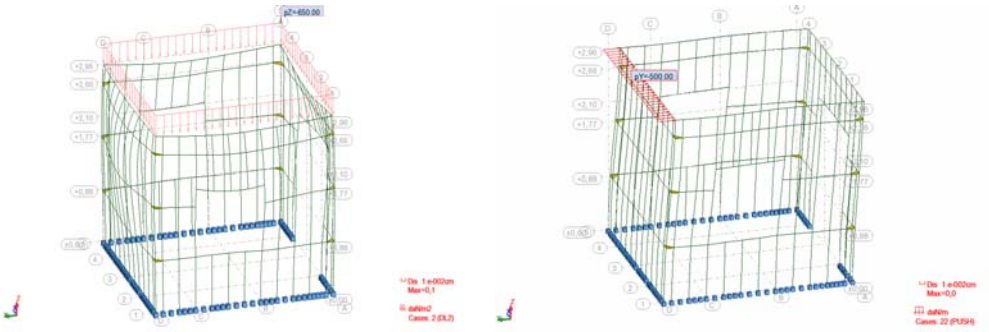

a b

Figure 5. Mesh definition and the composition of the numerical model with shell and bar elements a) vertical loads from additional masses; b) laterally applied load

The base of the model was considered fixed. In the first analysis beside the self weight of the structure was considered an additional mass of 2 tones uniformly distributed applied on top of the model. In the second analysis the load was laterally uniformly applied on the back side of the model, on Y global direction.

4. RESULTS AND DISCUSSION

Linear elastic analyses performed showed that in the case of the vertical load condition, the model has a stress distribution as presented in Figure 6, with local concentration on top of the openings for door and windows.

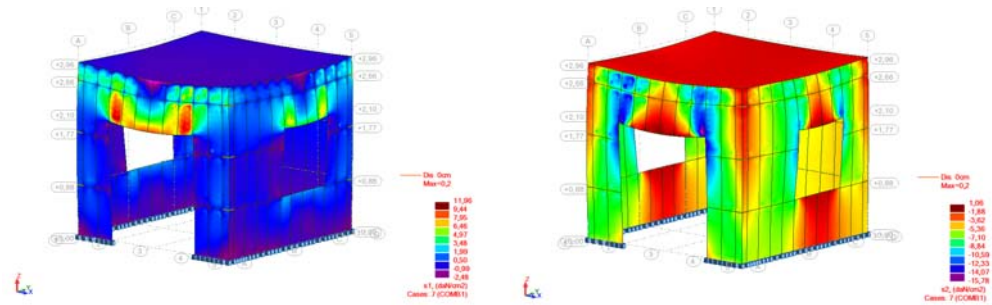

a b

Figure 6. Maps with principal stress distribution a) maximum stress; b) minimum stress

From the modal analysis the fundamental frequency in first mode of vibration is 9.38 Hz and 10.03Hz in the second mode. The modal deformations and

corresponding natural frequencies are presented in Figure 7. Both shapes of vibration show the translations on X and Y global directions.

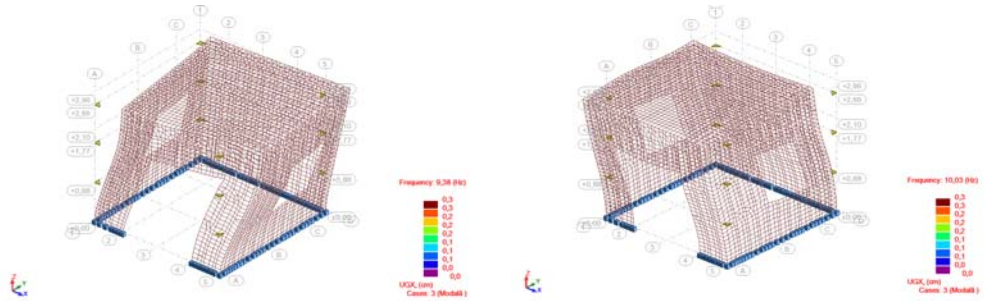

a b

Figure 7. Modes of vibration a) first mode of vibration, translation on Y global direction; b) second mode of vibration, translation on X global direction

The model analyzed with finite element method showed the distribution of stress around the windows. In the bottom area of the structure the presence of stress concentration means the possibility of cracks apparition in the experimental test.

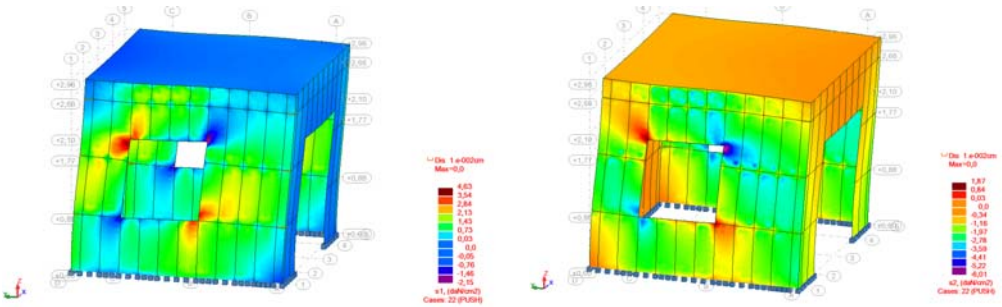

a b

Figure 8. Principal stress map in case of laterally load: a) maximum principal stress, b) minimum principal stress

The experimental test performed on the structural model consists in applying of a concentrated load, distributed at the top floor level. The load was applied in sinus cycles with a low frequency of 0.1 Hz …1.0 Hz. The maximum load applied was about 20 kN. The numerical model results were confirmed in the experimental stage, when the cracks occurrence was distributed in the same area around the window corners and the bottom side.

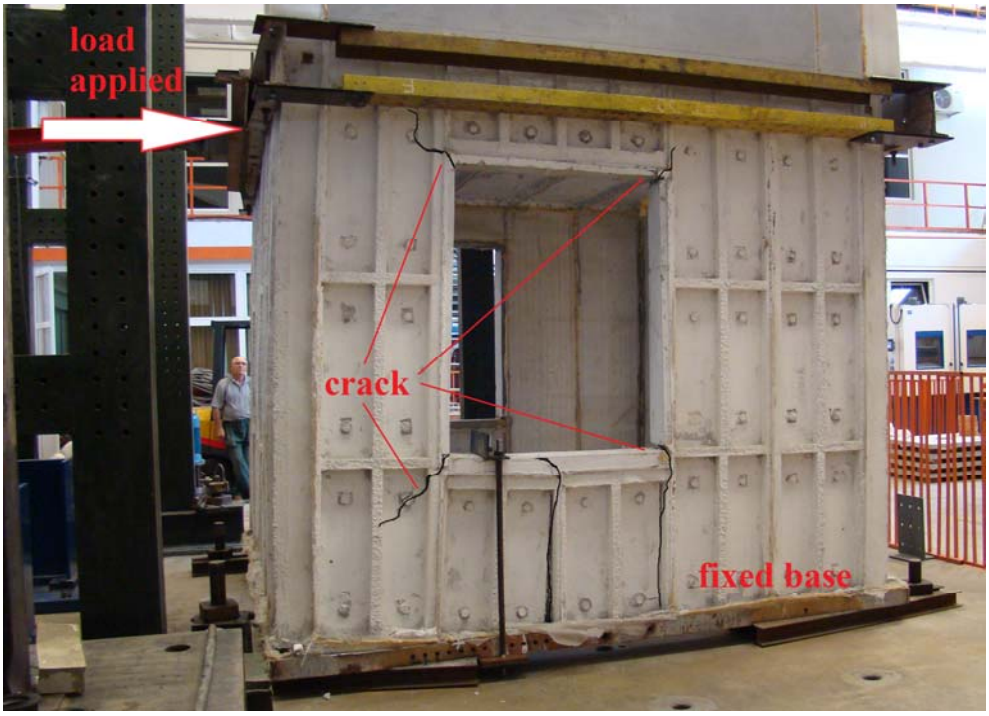

Figure 9. Image of the model after the experimental test

5. CONCLUSIONS

In this paper some numerical results performed with FEM on a structural model made of mineral reinforced composite were presented and discussed. Based on the numerical results the experimental test could be well organized and the anticipated behavior was confirmed. Also the numerical analyses provide an approximate value for the maximum stress and strain which can occur. These values are necessary for the structural design and the behavior evaluation.

After the experimental test the maximum value for laterally carrying load was 20 kN. At the same value in the numerical model the maximum principal stress was around 0.6 N/mm^2.

The types of composite structures represent an alternative to traditional materials for low cost houses or different types of shelters. The absence of the steel, the low weight and the high stiffness make this structure to have a good performance in accordance with different environment actions.

Acknowledgements

This paper was supported by the project "Develop and support multidisciplinary postdoctoral programs in primordial technical areas of national strategy of the research - development - innovation" 4D-POSTDOC, contract nr. POSDRU/89/1.5/S/52603, project co-funded from European Social Fund through Sectorial Operational Program Human Resources 2007-2013.

References

1. Majumdar, A.J., Glass fibre reinforced cement and gypsum products. Proceedings of the Royal Society (Series A) Composites, 1971. 319(3): p. 6.
2. Thomas, J.A.G., Fibre composites as construction materials. Composites, 1972. 3(2): p. 2.
3. Brandt, A.M., Present trends in the mechanics of cement based fibre reinforced composites. Construction and Building Materials, 1987. 1(1): p. 11.
4. Ando, T., T. Ikeda, H. Sakai, et al., Fibre reinforced cement mortar product, in Composites1992: Japan. p. 62.
5. Baux, C., Process for the industrial manufacture of compositions based on anhydrous calcium sulphate in the b-anhydrite iii' form, and corresponding compositions and binders, 2010, K and CO (16 route d'Avignon, Quartier du Grand Gres, Cavaillon, F-84300, FR); Baux, Christophe (17 route de Bonaban, LA Gousniere, F-35350, FR): France.
6. Aranda, B., O. Guillou, C. Lanos, et al. Synthese d'un liant vert capable de concurrencer le ciment Portland. in Journée des doctorants, Comunication orale. 2011. Université de Rennes, France.
7. Taranu, G., I.O. Toma, R. Plesu, et al., Evaluation of Mechanical Properties of Cement and Calcium Sulphate Mineral Matrix. Bulletin of the Polytechnic Institute of Iasi. Construction and Architecture Section, 2011. LVII (LXI)(2): p. 9.
8. Toma, I.O., G. Taranu, A.-M. Toma, et al., Influence of Cement and Sand Type on the Strength Characteristics of Mortars with Various Contents of Green Binder. Procedia Engineering, 2011. 21(0): p. 7.

Hybrid loss exceedance curve (HLEC) for risk assessment

César Velásquez[1], Omar Cardona[2], Luis Yamin[3], Miguel Mora[1], Liliana Carreño[1,4] and Alex H. Barbat[1,4]

[1]*Centro Internacional de Métodos Numéricos en Ingeniería, CIMNE, Barcelona, 08 03 4 , Spain*
[2]*IDEA, Universidad Nacional de Colombia, Manizales, 170004 , Colombia*
[3]*ICYA, Universidad de los Andes, Bogotá, 111711, Colombia*
[4]*Departamento RMEE, Universitat Politècnica de Catalunya, Barcelona, 08 03 4 , Spain*

Summary

Countries need to assess the expected risk due to natural hazards as a permanent activity in their financial plan; otherwise, they will experience a lack in the information required by the application of disaster risk reduction policies. In this article, a risk assessment methodology is proposed that uses, in one hand, empiric estimations of loss, based on information available in local disaster data bases, allowing to estimate losses due to small events; on the other hand, it uses probabilistic evaluations to estimate loss for greater or even catastrophic events for which information is not available due the lack of historical data. A "hybrid" loss exceedance curve, which represents the disaster risk in a proper and complete way, is thus determined. This curve merges two components: the corresponding to small and moderate losses, calculated by using an inductive and retrospective analysis, and the corresponding to extreme losses, calculated by using a deductive and prospective analysis. Applications of this new probabilistic risk assessment technique are given in this article for three countries.

KEYWORDS: risk, prospective analysis, retrospective analysis, loss exceedance curve, hybrid loss exceedance curve.

1. INTRODUCTION

The impact of natural hazards in terms of human and economic losses is continuously increasing all around the globe due to several factors like urban developing, population growth and migration, off-code constructions and climate change, among others. It has been infrequent, so far, for disaster risk management (DRM) to play a role in urban planning, even if many developing countries include in their budgets allocations for disaster mitigation.

But these go mostly for preparedness and response during the emergencies and only in some cases efforts are being made to direct resources towards planning activities related to risk mitigation. In order to understand risk, we need to define it along with its components. Hazard, H, is understood as the possible occurrence of a natural event which can affect a community, cause damage and human and economic losses. Exposure, E, refers to the assets (from houses to infrastructure) existent in the hazard prone area that can be impacted during a hazard event. Vulnerability, V, is the susceptibility of the exposed elements to suffer damage or to be affected due the hazard.

Finally, risk, R, is defined as the potential consequences over the community if the natural event materializes. Accordingly, UNDRO (1980) proposed the following definition of risk.

$$R = E \cdot H \cdot V \tag{1}$$

The probabilistic assessment of catastrophic risk requires specialized computational tools and we choose for this research the CAPRA platform (ERN-AL, 2010). This platform has been developed within an initiative sponsored by the WorldBank Group, the Inter-American Development Bank and UN-ISDR, among others, and allows evaluating the natural hazards, the exposure and the disaster risk at different scales (ERN-AL 2010; Cardona et al. 2010a, Cardona et al 2010b).

A new comprehensive methodology for risk assessment is proposed herein, in which the effect of minor and frequent past events, in terms of accumulated impact, is combined with that of expected future catastrophic events, allowing this methodology to achieve a closer insight within disaster risk (Marulanda et al. 2010; Cardona et al. 2008a).

The objective of this article is to develop a risk assessment approach that allows measuring the impact of multiple minor events which, when taken together, have a considerable cost and significant social and environmental effects. At the same time, this approach considers the potential occurrence of extreme events whose impact can have consequences affecting the fiscal sustainability and sovereignty of

a country. Thus, the proposed approach considers both, the extensive, repetitive, risk which must be mitigated with effective intervention strategies, as well as the intensive risk, for which are needed contingent liabilities that must be the object of strategies for financial protection and risk transfer.

The effect of insurance policies or risk transfer instruments has been not considered herein. Results obtained by using the proposed method are finally given for three countries: Colombia, Mexico and Nepal.

2 THE CAPRA PLATFORM

The CAPRA platform (ERN-AL, 2010) is a compendium of tools developed for the assessment of probabilistic hazard risk, as a main component for disaster risk reduction (DRR) policies. These tools consider the variability and, in the characteristics of the natural phenomena, in the definition and location of the exposed assets and in the vulnerability of the building and infrastructure types.

The occurrence of the natural hazard is assumed to follow a Poisson process; accordingly, all the possible events are independent from each other. When calculating risk with CAPRA, a special file is required, called AME file, in which all the possible occurrences of the considered natural phenomena have to be defined but in which one event has to be included only once. Each hazard scenario is defined as a raster map, where each location is defined as a statistical pair (by its mean value and standard deviation).

For the exposure, the CAPRA platform uses a geospatial database which has the format of a shape file. The different exposed assets are represented using geographic located points, lines or polygons and their main characteristics (e.g. building type, number of stories, economic value, and others) are linked. The CAPRA platform includes the necessary procedures to gather the information regarding the exposed elements based on the scale of analysis. Moreover, in certain cases the cadastral information of the city is available but, in others, this information has to be generated from remote sensing and in other cases, it has to be generated by using proxy models.

CAPRA evaluates the expected behavior of the different assets by means of vulnerability functions which correlate a certain characteristic of the natural phenomena (like gust speed, spectral acceleration, depth of flood, among others) with the mean damage ratio, MDR. The vulnerability functions are not available for each individual element but for a set of elements with similar characteristics, that is, for the building and infrastructure types included in the portfolio of the exposed assets.

As shown in Figure 1, a vulnerability function has to account for the dispersion and uncertainty of the expected damage. This dispersion has its origin in several factors, like the construction process, the quality of construction materials, the weather during construction phase, maintenance, etc., and also due to the uncertainties and the approximations made during the design phase.

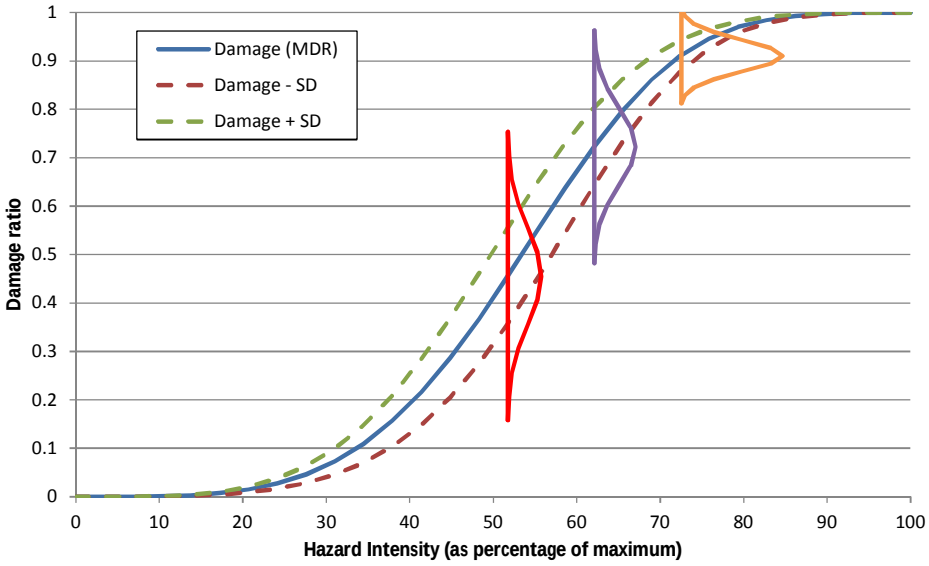

Figure 1. Probabilistic vulnerability function. It can be seen the expected mean damage ratio, MDR, and the dispersion characterized by the standard deviation, SD.

For risk calculations, CAPRA considers all the terms of equation 1 and accounts for all the uncertainties in its different components

$$v(p) = \sum_{i=1}^{Events} \Pr(P > p | Event_i) F_A(Event_i) \qquad (2)$$

In this equation, $v(p)$ is the exceedance rate of loss, p; $F_A(Event_i)$ is the annual frequency of occurrence of the $Event_i$; $\Pr(P > p | Event_i)$ is the probability of the loss to be greater than or equal to p, conditioned by the occurrence of the $Event_i$.

The loss exceedance curve, LEC, is a graphical representation of risk, usually made in logarithmic scales. It shows the relation between a given loss (usually economical) and the annual frequency of occurrence of that loss or of a larger one. Figure 2 shows a LEC and it can be seen that it correlates an expected loss represented in the horizontal axis with an estimated frequency represented in the

left vertical axis. As the frequency is the inverse of the return period, the loss can also be represented in function of the return period (the right vertical axis).

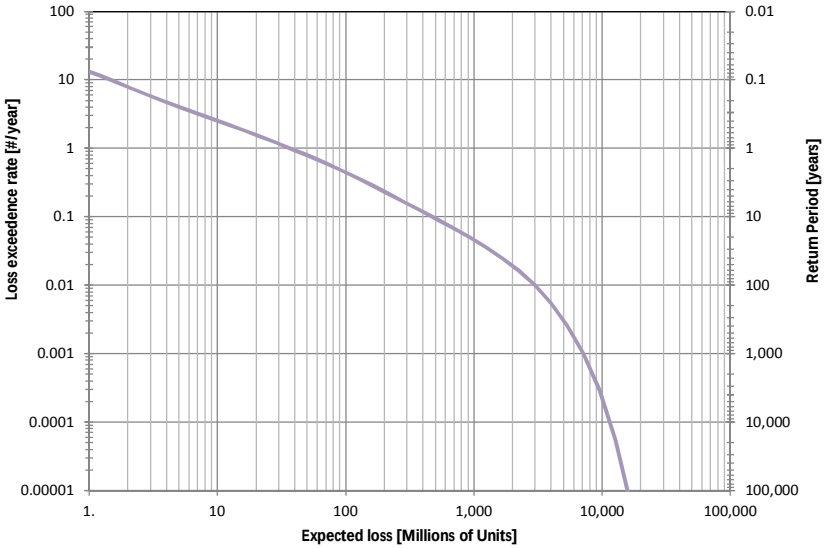

Figure 2. Loss exceedance curve. The vertical axis shows the frequency (left) and his inverse value, the return period (right); the horizontal axis displays the expected loss.

Other risk metrics that can be obtained with CAPRA are the annual average loss, AAL, and the probable maximum loss, PML. The AAL is the loss expectation, that is, the weighted average of all plausible loss values; in other words, it is the value expected to be saved every year in order to cope with all the future losses. The PML is the maximum foreseeable loss for the exposed portfolio.

3 PROSPECTIVE RISK ASSESSMENT WITH CAPRA

Considering the possibility that highly destructive events might occur in the future, risk estimation must focus on probabilistic models which make possible using the available information to calculate possible catastrophe scenarios in which high uncertainties are inherent. Accordingly, risk assessment must also follow a prospective approach, anticipating the events and the expected possible consequences that can occur in the future, considering uncertainties associated to the severity and frequency of the events.

Over the past decades, risk estimation models have been based on historical data, on consequences of past events and on insurance claims; these models were characterized by the lack of information regarding major, catastrophic, events. For this reason, different academic models were developed which considered the hazard intensity and frequency, the increasing portfolio of assets and its vulnerability into the probabilistic estimation of the hazard risk (Barbat et al. 2010).

In general, it should be recognized that the reliable historical information is limited, in most cases, to the last decades, and many catastrophic events are expected to occur in the future. For this reason, it is impossible to predict the consequences of extreme events based on the available information. In other words, the existing disaster databases (EM-DAT, DesInventar, and others) lack of sufficient records for low frequency and high consequences events, because the window covered by those databases is very narrow.

3.1 Hazard assessment

The identification and evaluation of the intensity and the annual recurrence of certain hazards that can affect a specific region, constitutes a step prior to risk analysis. The historical knowledge about the occurrence of events with high consequences and of their characteristics provides an initial idea of the destructive potential of the phenomena. This allows the description of the hazard in the region and makes possible to establish the approximate return periods of the most significant events.

3.2 Characterization of exposure

Exposure refers to assets like infrastructure or population existing in the hazard prone area, which are susceptible of being damaged by a specific event. In order to define the exposure, it is necessary to identify each of the different elements along with their characteristics including the geographical location, their vulnerability to the considered hazard event and their economical replacement value. The exposure values of goods at risk are normally estimated using secondary information sources, such as existing databases, or can be derived by using simplified procedures based on general social and macroeconomic information, such as population density, statistics of constructions and other parameters.

To completely include the exposure in the model, other physical assets of special importance, such as main infrastructure, have to be included. This requires several assumptions when aggregation is made from a local to a national scale. In general, the exposure model includes information about the following exposed components or elements:

- Buildings and houses;
- Industrial facilities;
- Roads and bridges;
- Electricity systems;
- Communications systems;
- Distribution systems;
- Relevant infrastructure (like airports, ports and others).

The level of detail of the exposure model has to be changed according to the availability of the information, going from the small scale of the individual buildings or blocks to the larger scale of the neighborhoods, cities, regions or countries. This variability in the disaggregation of the exposed elements is reflected in the level of resolution of the results and, thus, in the use of those; nevertheless, the expected overall results will have certain similarities.

3.3 Characterization of vulnerability

The physical vulnerability of an exposed element is characterized by functions that relate the parameter used to describe the hazard with the level of loss or damage suffered by that element. The functions of vulnerability have to be evaluated for each of the principal construction types existing in the studied area; such a function has to be assigned to each of the elements of the exposure database. They allow estimating consequences produced in each of the assets under the action of an event. In a probabilistic way, a vulnerability function defines for each value of the hazard intensity a mean damage ratio, MDR, and its standard deviation, SD.

As an example, the figures 3 and 4 show vulnerability functions for different building types and infrastructure elements. Due the number of the represented elements, only the MDR has been plotted.

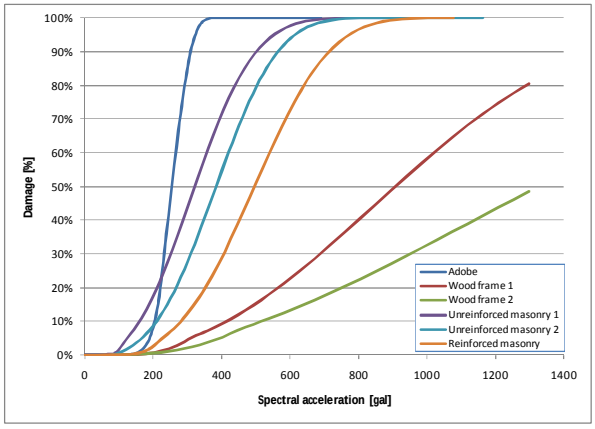

Figure 3. Seismic vulnerability functions for typical buildings

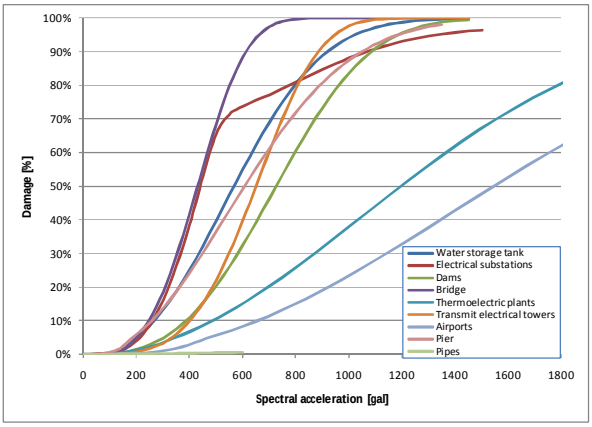

Figure 4. Seismic vulnerability functions for elements of infrastructure

Each vulnerability function corresponds to the expected statistical behavior of a typological group; this means that the results are valid only for the group of assets as a whole and not for each exposed element.

3.4 Results of the analysis

The results of the analysis can be presented for different portfolios or sectors, summarizing the annual average losses, AAL, and the probable maximum loss, PML, for the evaluated area. The PML values depend on the degree of dispersion of the evaluated assets. It should be kept in mind that the values obtained for different return periods correspond to the PML of the entire area and that these values, when evaluated for a part of this area, could significantly change because of the level of risk concentration.

For a given area the following portfolios could be considered:

- National: National infrastructure assets, private and also public buildings;
- Fiscal: Government assets, public health assets, public education assets and low income population assets;
- Public health: public assets used for medical and healthcare services;
- Public education: public assets used for educational and cultural services;
- Government: public assets used for administrative service;
- Private: assets of moderate and high income population sectors, industrial and commercial sectors.

The AAL, and the PML, for fiscal responsibility are obtained at country level. These correspond to the losses that the country would have to face due to potential damage in public and low income population assets, which would have to be covered by the government in the case of a major disaster.

The curve of Figure 5 is obtained analytically and only covers events such as strong earthquakes, hurricanes or other phenomena that can cause catastrophic consequences due to the correlation or simultaneousness of the effects on the exposed assets of the portfolio. It shows the fiscal LEC for an analyzed area following the previous methodology. This methodology can be resumed as follows:

- Construction of a hazard model. This model has to define all the possible scenarios in which the studied hazard can occur; for each one of those scenarios, the frequency, severity and expected deviation has to be included.
- Preparation of a geo-referenced database of exposed elements. It has to be built by using demographic and economic statistics.
- Assignation of vulnerability functions for each building and infrastructure type of the exposed elements. These functions are defined from the existing literature (HAZUS, Risk-UE) and by using computational models (Lagomarsino et al. 2006, Lantada et al. 2009, Vargas et al. 2012).

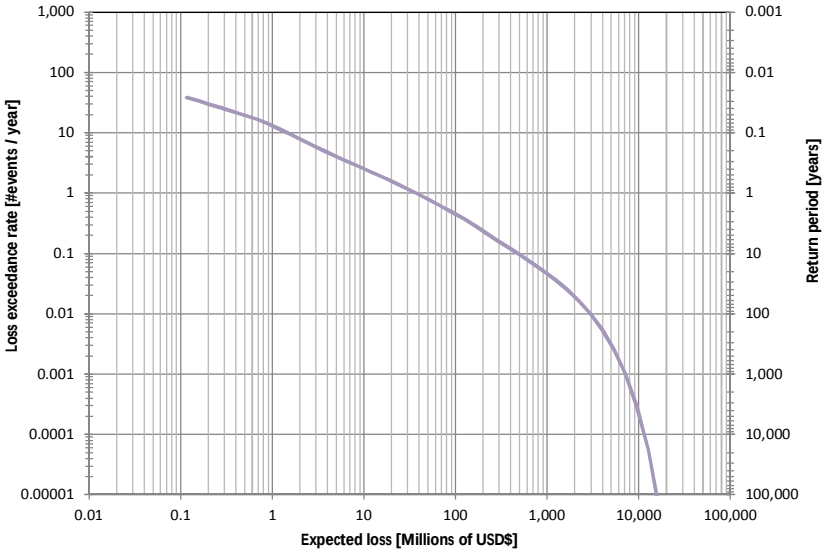

Figure 5. Prospective LEC. The vertical axis shows the frequency (left) and his inverse value, the return period (right); the horizontal axis displays the expected loss.

It should be noted in Figure 5 that there is a gap in the information related to small events with a high frequency, of more than 10 occurrences each year. The missing information in the LEC is because the prospective methodology considers only catastrophic hazards and dismisses the small and frequent hazards. Moreover, these small hazards require a large amount of data and a detailed analysis, beyond the normal capabilities of the existing risk evaluation models, including CAPRA. For example, the flooding hazard could be evaluated for a specific basin but not for all the basins of a large region at the same time; this is also true for landslides and

other hazardous events which, many times, are considered as “minor”. That is why we propose a retrospective analysis, with its limitations and restrictions, but which can provide the solution we are searching for those small and frequent events.

4 RETROSPECTIVE RISK ASSESSMENT USING THE DESINVENTAR DATABASE

The retrospective risk assessment consists in the empirical estimation of economic losses due to events contained in the historical information databases, in which the losses caused by minor but frequent events are considered. Therefore, the DesInventar disaster database (Desinventar.net; Desinventar.org) has been chosen in order to perform the retrospective risk assessment because it contains numerous reliable records of past events, reasonably described by means of variables like: type of event; date of occurrence, geographical location, as well as other credible variables which can be used in the analysis, like the number of damaged houses, the number of destroyed houses, crops area, cattle and others.

For the effects of this analysis, the DesInventar records have to be submitted first to a process of filtering, merging and economic valuation, in order to develop a database that include, in addition to the available information, an estimate of the economic impact of each event, considering only the direct effects. The information included in the DesInventar database is used to estimate the economic cost associated with each event. The model used to evaluate losses takes into account criteria from the Manual for Assessment of the Socio-economic and Environmental Impact of Disasters (ECLAC, 2003) which is a guide for estimating the economic impact of individual events. The effects upon social sectors, infrastructure and economic sectors are considered along with the impact upon the environment, the women, employment and income.

Considering the small severity and the regional dispersion of most of the events contained in the DesInventar database records, we can conclude that they affect the more vulnerable sectors of society, which require the help of the government for shelter, healthcare and reconstruction after each event.

4.1 Steps of risk assessment

In order to carry out a retrospective risk analysis and the empirical development of a loss exceedance curve using minor but frequent events, the following steps have to be carried out:

- Selection of the database. In this study, we decided to use the DesInventar database because it has some relevant advantages: the number of countries covered by this database is increasing. The database is periodically updated to

cover larger time periods and it contains a large set of fields which are useful in this study.

- Removing from the database the records corresponding to non-natural hazards. Due to the fact that we consider in the LEC only natural hazards, the records corresponding to other hazards, like biological technological, etc., have to be removed.
- General statistical analysis of the database. The selected database is analyzed for an adequate distribution of the number of records and of the consequences by year, for the distribution of the records over the studied area rather than their concentration at the main cities, etc. This statistical analysis permits the revision and check of the reliability of the database.
- Selection of the parameters for merging the records corresponding to the same events. In the specific case of DesInventar database, the consequences of a unique event can be stored over several records, each one corresponding to a different locality.
- Unification of the effects, by merging together records corresponding to the same hazardous event. Because the consequences of an event are stored in several records, it is necessary to sum those consequences in a unique record.
- Classification of the records by categories. The database includes several event types, allowing this a better understanding of the local risk. But this fact makes the database inadequate for regional or national analysis. The following hazards categories are considered in the DesInventar database: seismic (earthquakes and tsunamis), landslide, volcanic and hidro-meteorological (rainfall, flood, hail storm, and others).
- General statistical analysis of the record by categories. Statistics of the records are performed in order to establish the injured and dead people, the damaged or destroyed houses and several other aspects contained in the database by hazard category. This analysis allows a better understanding of the severity and spatial distribution of the events occurred in the studied region.
- Definition of the parameters necessary for the loss assessment by event. These parameters account for the affected assets over several sectors and have to be consistent with the variables existing in the database. For example, for evaluating the effects upon the house sector, the variables of the database corresponding to the number of damaged and destroyed houses can be used.
- Calculation of losses by event. The previously selected parameters are used in this step. Each record has to be processed for the estimation of economic value of the consequences.
- Statistical analysis of losses by hazard categories. The economic distribution of the losses for all an each one of the different hazards over the studied area and over the database time window is obtained in this step.
- Development of the LEC for each category of natural hazard. A loss exceedance curve is obtained for each natural hazard category considered in the analysis.

- Development of the multihazard LEC. A loss exceedance curve for all the events present in the database is obtained and will be used for the construction of the hybrid LEC.

4.2 Results of empirical risk assessment

Following the proposed methodology, the LEC for minor but frequent events is determined and it can be used for the assessment of the risk at regional level. Figure 6 shows which of the hazard categories have the highest economic effect for different return periods and over the time window covered by the database. It can be noted how the hydro-meteorological hazards have the most important annual impact and how the seismic hazard produces the most important losses in the long term.

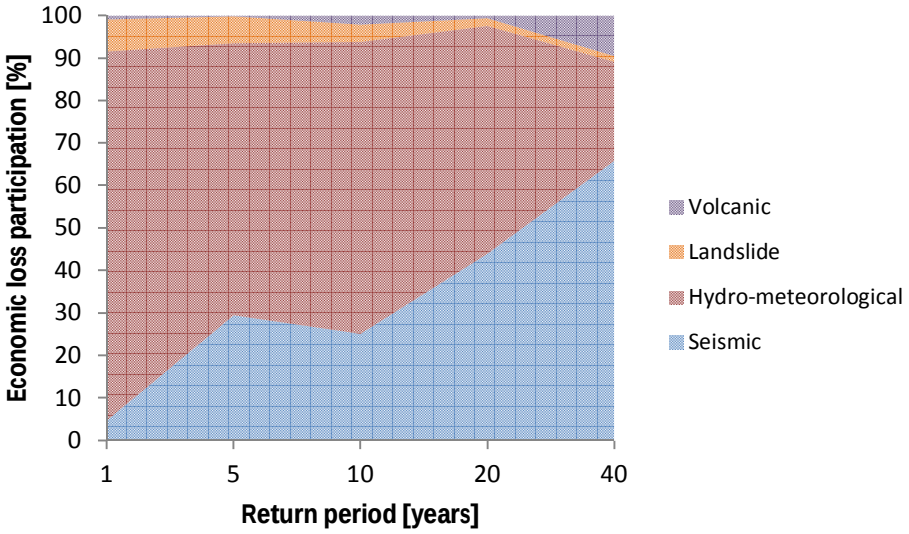

Figure 6. Economic losses by categories of hazards and return periods

Another result very useful for the awareness of political institutions is how the economic losses due to small but frequent events affect the communities over the years. Specifically, Figure 7 shows this effect for regular periods of 4 years which, for instance, can correspond to the government periods of a country; it shows how much of the budget is expected to be used by that government for risk response and recovering. In this case, using the purchase parity power (PPP) correction, it can be noted that the economic losses increase and are more frequent.

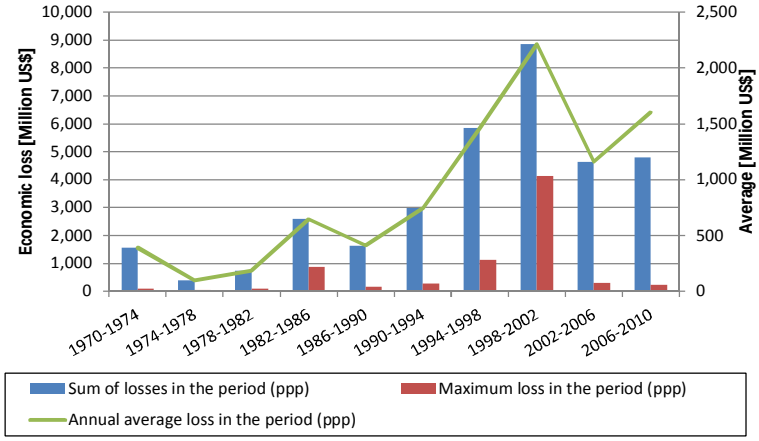

Figure 7. Economic losses (PPP) per presidential period.

Finally, the LEC can be obtained for each individual hazard category and also for all the events of the database, resulting in, a multihazard LEC, as it can be seen in Figure 8. The economic losses shown in this figure correspond to what a government or the society had to assume for a prompt community recovery, including replacing, repairing or compensating the suffered losses. In any case, the proposed procedure of assessment allows establishing the amount of resources that the government must spend every year to meet its fiscal responsibility, under the supposition that the affected private parties have been the most disadvantaged sectors of the society. In general terms, these losses are those which would be not covered by catastrophic risk insurance, if any is contracted by the government, because they correspond approximately to what the deductible would be. Those would be the losses that the governments should try to reduce by developing prevention-mitigation policies.

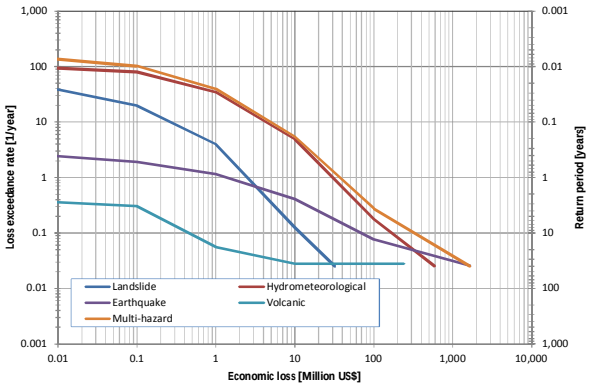

Figure 8. Economic LEC by hazard category and the multihazard LEC

5 THE HYBRID LOSS EXCEEDANCE CURVE (HLEC)

In the previous sections, two LEC where obtained, each one by using a different approach. The first one is the prospective LEC, shown in Figure 5, and it corresponds to large losses, with very low annual frequencies; the second one is the retrospective LEC, shown in Figure 8, which considers small but frequent losses. Now we represent both LEC in the same graphic as it can be seen in Figure 9, obtaining the whole picture of the risk in the study area.

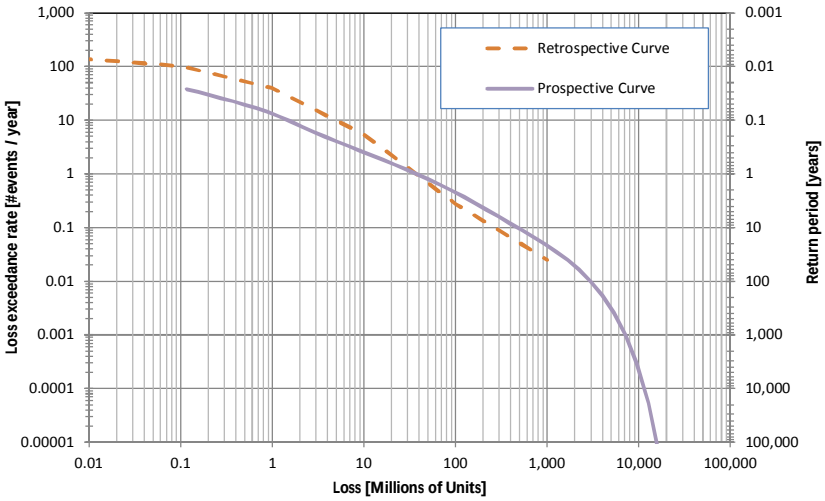

Figure 9. The retrospective and the prospective LEC represented in the same graphic

Using the previous obtained LEC's as input we build the new hybrid loss exceedance curve, HLEC, by using the envelope values of both curves and by overlapping the common part making use of interpolation. This new LEC is shown in Figure 10. In other words, the proposed technique for risk analysis is based on combining the first LEC, corresponding to all natural hazard events, with the second LEC obtained for hazards that have the potentiality of producing catastrophic risk.

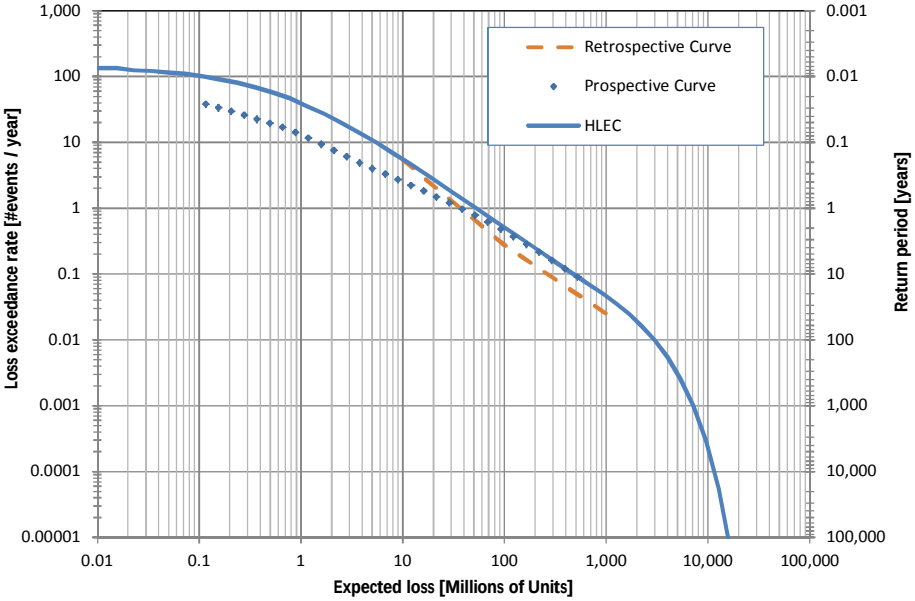

Figure 10. Hybrid Loss Exceedance Curve

In the insurance industry, an attachment point, or deductible, is defined for every insurance policy, as the value to be met by the policy holder and from which the insurance company starts his responsibility. In some cases, it can be understood as a discount from the total claimed value. This means that losses below the attachment point have to be completely covered by the policy holders. In this article, we present in the next section a few examples of LEC corresponding to three countries. In these cases, those countries have to assume the consequences caused by small intensity events from their own budget. The analytical, prospective, loss exceedance curves have been used so far by the insurance companies whose interest is not to evaluate losses below this deductible point, nor taking into account the accumulative effects and the implications of dealing repeatedly with small events that can lead to an administrative decline. In other words, “minor” and frequent events, which should be in the interest of the governments, are not of the interest of insurers.

6 APPLICATIONS OF THE PROPOSED HLEC

Three case studies were performed, considering the available information for the retrospective analysis and the necessary data for the prospective risk models. The selected developing countries are Colombia, Mexico and Nepal and the

corresponding HLEC are shown in figures 11 to 13. The prospective analysis for all the countries was made for the seismic hazard and, only in the case of Mexico, also for hurricane wind. The required information for the risk model was gathered with the help of several institutions; among the collected information was the population census, the building census, the construction prices, utilities sector coverage and prices, macroeconomic indicators, etc.

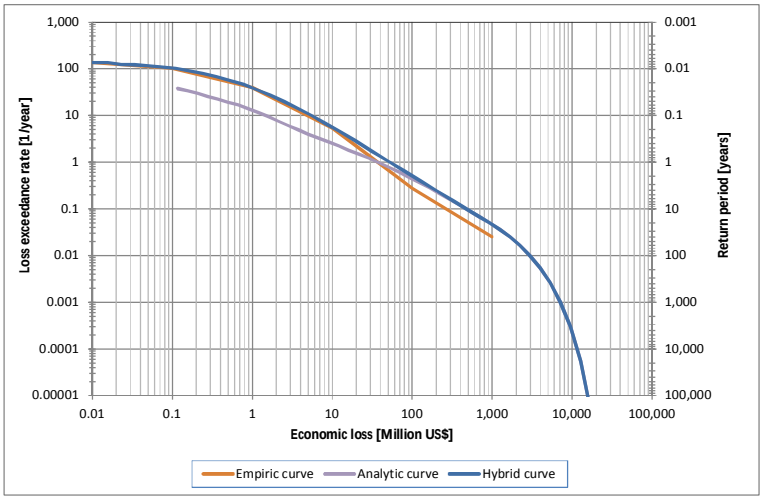

Figure 11. Hybrid loss exceedance curve for Colombia

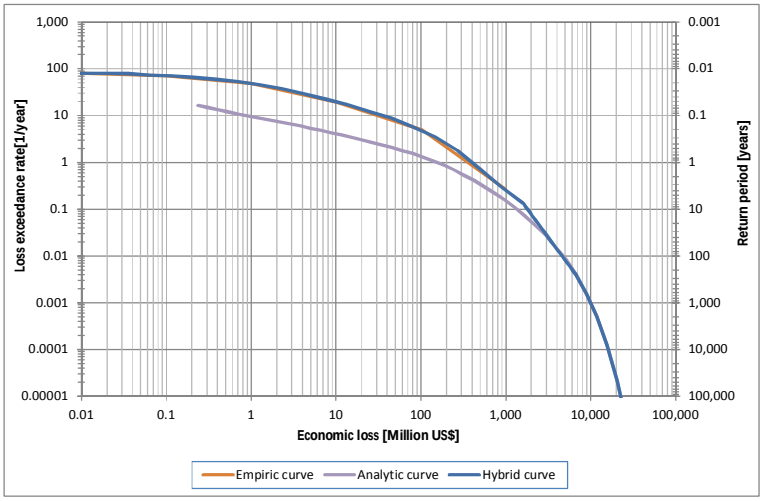

Figure 12. Hybrid LEC for Mexico

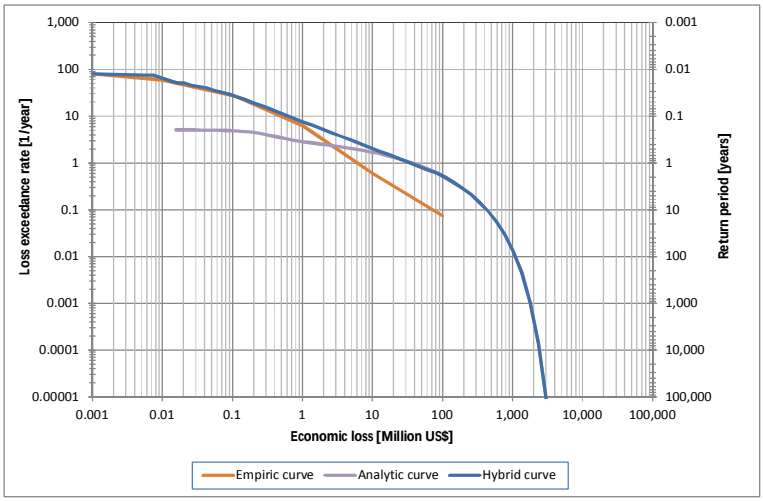

Figure 13. Hybrid LEC for Nepal

Table 1 illustrates the differences in the values of the AAL obtained by using the retrospective analysis, the prospective analysis of the fiscal responsibility of the Governments and the proposed HLEC.

Table 1. Comparison of expected AAL values

	Retrospective analysis	Prospective analysis – Fiscal Sector	Hybrid Curve
Colombia	360	316	490
Mexico	2,540	810	2,424
Nepal	52	207	235

It can be observed, in all the cases, an interesting situation: the AAL values obtained by using the hybrid loss exceedance curve are greater in the cases of Colombia and Nepal than the AAL values obtained by using the retrospective analysis. In the case of Mexico, this value is slightly lower than the one obtained by using the retrospective analysis but, even so, several times higher than the expected AAL value provided by the prospective analysis.

However, these AAL are the amount which the governments would have to pay annually in order to cover all the future disasters. In the case of insurance industry, a part of this value would have to be paid to the insurance and reinsurance companies; that part could well be the premium to cover the catastrophic risk. As seen before, the insurance companies cover losses only above a certain value, known as the attachment point or priority, and leave as deducible for each country the losses caused by small events. These events correspond to small losses, reason

for which governments must have an explicit strategy of disaster risk reduction and management, through effective mitigation and prevention policies; otherwise, the losses due to minor events would continue to have a very high economic and social impact upon the countries.

7 CONCLUSIONS

In this article, a new risk analysis methodology has been proposed based on a hybrid loss exceedance curve, which represents risk in a proper and complete way. This loss exceedance curve has two components. The first one corresponds to multiple minor events usually producing small and moderate, but repetitive, extensive, losses and is calculated by using an inductive and retrospective analysis; the second one considers the potential occurrence of extreme events which produce intensive, huge losses and is calculated by using a deductive and prospective analysis. The extensive risk has to be mitigated with efficient intervention strategies while for the intensive risk, strategies of financial protection and risk transfer are required.

The study performed at the country level shows that it is indispensable to measure risk retrospectively, with an empirical focus, and, at the same time, prospectively, with a probabilistic focus. The lack of procedures to evaluate losses due minor and repetitive events has prevented until now that governs be aware of the enormous losses due to such events. The proposed approach and the case studies performed in this article permit not only to illustrate but also to promote the interest of decision makers for an effective risk management based on the complete and multihazard risk assessments facilitated by the hybrid loss exceedance curve. The proposed hybrid curve allows capturing aspects which the prospective LEC is not able to consider, avoiding the underestimation of the consequences of minor and repetitive events. And, obviously, it is important to have the possibility of estimating expected losses that a country may face perhaps every year and of planning the economical mechanism needed to recover more promptly.

The proposed methodology has been used as a background paperwork in the GAR2011 (UNISDR, 2011a) and it brought a new interest of the UNISDR, WB Group and the InterAmerican Development Bank to be used in their DRR policies.

Acknowledgements

This work has been sponsored by UNISDR, and has been used as a background paper in the GAR2011 (UNISDR, 2011a). We want to thank the following local institutions for their help and collaboration: Colombia (ITEC S.A.S., INGENIAR), México (ERN Ingenieros Consultores) y Nepal (NSET). We also thank to the

Florida International University for their support in the PhD studies of one of the authors. This work has been also partially sponsored by the European Commission (project DESURBS-FP7-2011-261652). The authors are also grateful for the support of the Ministry of Education and Science of Spain, project “Enfoque integral y probabilista para la evaluación del riesgo sísmico en España”-CoPASRE (CGL2011-29063).

References

1. Barbat, A. H., Pujades, L. G., Lantada, N., & Moreno, R. (2008). Seismic damage evaluation in urban areas using the capacity spectrum method: Application to Barcelona. Soil Dynamics and Earthquake Engineering, 28(10-11), 851 - 865.
2. Barbat, A. H., Carreño, M. L., Pujades, L. G., Lantada, N., Cardona, O. D., & Marulanda, M. C. (2010). Seismic vulnerability and risk evaluation methods for urban areas. A review with application to a pilot area. Structure and Infrastructure Engineering, 6(1), 17-38.
3. Cardona, O. D., Ordaz, M. G., Yamin, L. E., Marulanda, M. C., & Barbat, A. H. (2008a). Earthquake Loss Assessment for Integrated Disaster Risk Management. Journal of Earthquake Engineering, 12, 48-59.
4. Cardona, O. D., Ordaz, M. G., Marulanda, M. C., & Barbat, A. H. (2008b). Estimation of Probabilistic Seismic Losses and the Public Economic Resilience—An Approach for a Macroeconomic Impact Evaluation. Journal of Earthquake Engineering, 12, 60-70.
5. Cardona, O. D., Ordaz, M. G., Marulanda, M. C., Carreño, M. L., & Barbat, A. H. (2010a). Disaster risk from a macroeconomic perspective: a metric for fiscal vulnerability evaluation. Disasters, 34(4), 1064-1083.
6. Cardona, O. D., Ordaz, M. G., Reinoso, E., Yamin, L. E., & Barbat, A. H. (2010b). Comprehensive Approach for Probabilistic Risk Assessment (CAPRA): International Initiative for Disaster Risk Management Effectiveness. Presented at the 14th European Conference on Earthquake Engineering, Ohrid, Macedonia.
7. Carreño, M. L., Cardona, O. D., & Barbat, A. H. (2007). A disaster risk management performance index. Natural Hazards, 41(1), 1-20.
8. Carreño, M. L., Cardona, O. D., & Barbat, A. H. (2006). Urban Seismic Risk Evaluation: A Holistic Approach. Natural Hazards, 40(1), 137-172.
9. CEPAL (2003). Manual para la estimación de los efectos socio-económicos de los desastres naturales (Report LC/MEX/G.5). México DF, México: CEPAL, Banco Mundial.
10. Desinventar.net - DesInventar Disaster Information Management System, Version 9.15 - June 2011. (n.d.). Geneva, Switzerland: UNISDR. Dirección web http://www.desinventar.net/index.html. Última visita 2 de febrero de 2012.
11. Desinventar.org - DesInventar Project. (n.d.). Cali, Colombia: Corporación OSSO. Dirección web http://desinventar.org/en/. Última visita 2 de febrero de 2012.
12. EM-DAT: The OFDA/CRED International Disaster Database – www.emdat.net. (n.d.). Brussels, Belgium: Université catholique de Louvain. Dirección web http://emdat.be/. Última visita 2 de febrero de 2012.
13. ERN-AL (2010). CAPRA, Compressive approach for probabilistic risk assessment. World Bank, InterAmerican Development Bank. Retrieve from ecapra.org.
14. ERN-AL (2011). Probabilistic Modeling of Disaster Risk at Global Level: Development of a methodology and implementation of case studies. Phase 1A: Colombia, México and Nepal. Background paper prepared for the 2011 Global Assessment Report on Disaster Risk Reduction. Geneva, Switzerland. UNISDR.
15. FEMA (2006). Multi-hazard loss estimation methodology, HAZUS-MH MR2 technical manual, prepared for the Federal Emergency Management Agency, Washington DC, United States, Federal Emergency Management Agency and National Institute of Building Sciences.

16. Lagomarsino S., Giovinazzi S. (2006) Macroseismic and mechanical models for the vulnerability and damage assessment of current buildings. Bulletin of Earthquake Engineering; 4(4): 415-443.
17. Lantada N., Pujades L. G., Barbat A. H. (2009) Vulnerability index and capacity spectrum based methods for urban seismic risk evaluation. A comparison. Natural Hazards; 51(3): 501-524.
18. Lantada, N., Irizarry, J., Barbat, A. H., Goula, X., Roca, A., Susagna, T., & Pujades, L. G. (2009). Seismic hazard and risk scenarios for Barcelona, Spain, using the Risk-UE vulnerability index method. Bulletin of Earthquake Engineering, 8(2), 201-229.
19. Marulanda, M. C., Cardona, O. D., & Barbat, A. H. (2010). Revealing the socioeconomic impact of small disasters in Colombia using the DesInventar database. Disasters, 34(2), 552-570.
20. RISK-UE (2001–2004) An advanced approach to earthquake risk scenarios, with applications to different European cities. Website http://www.risk-ue.net
21. UNDP (2004). Reducing Disaster Risk: A challenge for development. Geneva, Switzerland. United Nations Development Programme, Bureu for Crisis Prevention and Recovery.
22. UNDRO (1980). Natural disasters and vulnerability analysis, Report of experts group meeting, UNDRO, Geneva.
23. UNISDR (2009). Global Assessment Report on Disaster Risk Reduction: Risk and poverty in a changing climate. Geneva, Switzerland: United Nations International Strategy for Disaster Reduction.
24. UNISDR (2011a). GAR2011: Global Assessment Report on Disaster Risk Reduction: Revealing risk, redefining development. Geneva, Switzerland: United Nations International Strategy for Disaster Reduction.
25. UNISDR (2011b). Desinventar.net Database: Nepal disaster inventory. Geneva, Switzerland. United Nations International Strategy for Disaster Reduction.
26. Vargas Y. F., Pujades L. G., Barbat A. H., Hurtado J. E. (2012) Evaluación probabilista de la capacidad, fragilidad y daño sísmico en edificios de hormigón armado. Métodos numéricos para cálculo y diseño en ingeniería; (in press).
27. Velásquez, C. A., Cardona, O. D., Yamin, L. E., Mora, M. G., & Barbat, A. H. (2011). Curva de excedencia de pérdidas híbrida para la representación del riesgo. Presented at the Cuarto Congreso Nacional de Ingeniería Sísmica, Granada, España.

Comparative analysis of the bending theories for isotropic plates

Mihai Vrabie and Sergiu Baetu
Departament of Structural Mechanics, Technical University "Gheorghe Asachi", Iasi, Zip code 700050, Romania

Summary

This paper presents an overview of the governing equations for the bending study of the isotropic plates, with several known plate theories from the literature. For the higher-order theories (Mindlin and Reddy) which take in consideration the transverse shear strains are mentioned the differences compared to the classical plate theory (Kirchhoff). In the end are shown the relations which link the bending parameters from the higher-order theories with the corresponding parameters from the classical isotropic plate theory.

KEYWORDS: plate theories, governing equations, bending deflection.

1. INTRODUCTION

The plates are bidimensional structural elements which have the dimensions from the middle plane larger than the thickness. Depending of the ratio between the minimum dimension from plane (l_{min} = min(a,b)) and the thickness h (fig. 1), the plates can be classified for the calculation in two classes [1], [2], [3], [5], [7]:

- ✓ Thin plates, at which $l_{min} > 10h$;
- ✓ Thick plates, at which $l_{min} < 10h$.

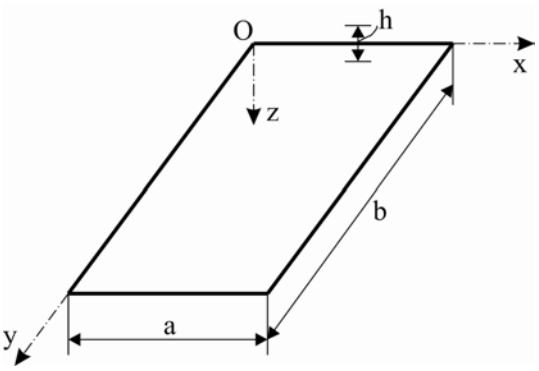

Figure 1. Geometric elements and the reference system

ISSN 2285-2735, Pages 175 - 188

Due to small thickness, for the thin plates can be used the most frequently 2D theories, while the thick plate model require the use of 3D elasticity theories [3], [4], [5]. Governing equations of the thin plates can be obtained using vectorial mechanics or variational and energetic principles.

In vectorial mechanics the internal forces and moments, which are disposed on a typical plate differential element, are summed with the purpose to obtain the equilibrium or motion equations. In the energetic methods in order to obtain the equations, various types of virtual work principles are used, such as the principles of minimum potential energy or the complementary potential energy [5], [6], [7].

The bidimensional plate theories can be classified in [2], [3], [5]:

1) Classical plate theory, in which the transverse shear deformation effects are neglected;
2) Shear deformation plate theories in which the shear strains are considered.

Further, an overview of these theories is done highlighting the differences and the connections that exist between the governing equations of the studied bending plate theories.

2. DISPLACEMENT FIELD

The plate theories developed into the literature are based on the adoption of a form of the displacement field like a linear combination of unknown functions and on coordinate on thickness direction

$$\varphi_i(x,y,z,t) = \sum_{j=0}^{n} (z)^j \varphi_i^j(x,y,z) \qquad (1)$$

where: is the "*i*" component of displacement, (*x*,*y*) are the coordinates from the middle plane of the plate, *z* is the thickness coordinate, *t* is the time and are functions which must be determinate.

The classical bending plate theory (Kirchhoff) is based on the following displacement field [1], [2], [8], [9], [10]:

$$u(x,y,z) = -z\frac{\partial w_0}{\partial x}, \qquad v(x,y,z) = -z\frac{\partial w_0}{\partial y}, \qquad w(x,y,z) = w_0(x,y) \qquad (2)$$

where: *(u,v,w)* are displacement components of a point on the coordinates axis directions *(x,y,z)*, and w_0 is the transversal displacement of a point from the middle plane, $z = 0$.

The adopted displacement field implies the fact that a normal rectilinear segment on the middle plane before deformation remains straight and normal on middle surface after the deformation of the plate (Kirchhoff hypothesis). This hypothesis permits neglecting the transversal shear effects ($\tau_{xz} = \tau_{yz} = 0$), but also of the normal ones ($\sigma_z = 0$). In other words the plate deformations are given entirely by bending and the axial forces (fig. 2a).

The simplest plate theory with shear deformation is the first-order one (Mindlin - Reissner), which is based on the following displacement field [4], [5], [7]:

$$u(x,y,z) = -z\phi_x(x,y), \qquad v(x,y,z) = -z\phi_y(x,y), \qquad w(x,y,z) = w_0(x,y) \quad (3)$$

where: ϕ_x and ϕ_y are the rotations reported at *x* and *y* axis (fig. 2b).

The Mindlin theory includes in the equations (3) a global transverse shear strain considered constant on the plate thickness. To correct the discrepancy between the real distribution of the transverse shear force and the one resulted from the utilization of the kinematic relations is introduced a shear correction factor. This factor depends on both the geometric parameters as the plate loading and restraints.

The second-order and the higher-order theories with shear deformations use higher order polynomial functions to extend displacement components in the *z* axis direction. The higher-order theories introduce additional unknowns which often is difficult to interpret them physically. An example is represented by the second-order theory with transverse inextensibility which is based on the following displacement field:

$$\begin{aligned} u(x,y,z) &= z\phi_x(x,y) + z^2\psi_x(x,y) \\ v(x,y,z) &= z\phi_y(x,y) + z^2\psi_y(x,y) \\ w(x,y,z) &= w_0(x,y) \end{aligned} \quad (4)$$

where: ψ_x and ψ_y are unknown functions without physically signification.

From the third-order theories, the most known is the one of Reddy [5], which proposed the following displacement field:

$$u(x,y,z) = z\phi_x(x,y) - \alpha z^3\left(\phi_x + \frac{\partial w_0}{\partial x}\right)$$

$$v(x,y,z) = z\phi_y(x,y) - \alpha z^3(\phi_y + \frac{\partial w_0}{\partial y}) \quad (5)$$

$$w(x,y,z) = w_0(x,y)$$

where: $\alpha = 4/3h^2$ (fig. 2c).

The displacement field lead to a quadratic variation of transverse shear strain (and of corresponding stresses) that are null on the superior and inferior faces of the plate. It must be noted that the third-order theory doesn't need a shear correction factor, and for $\alpha=0$ we obtain the displacement field from the first-order theory.

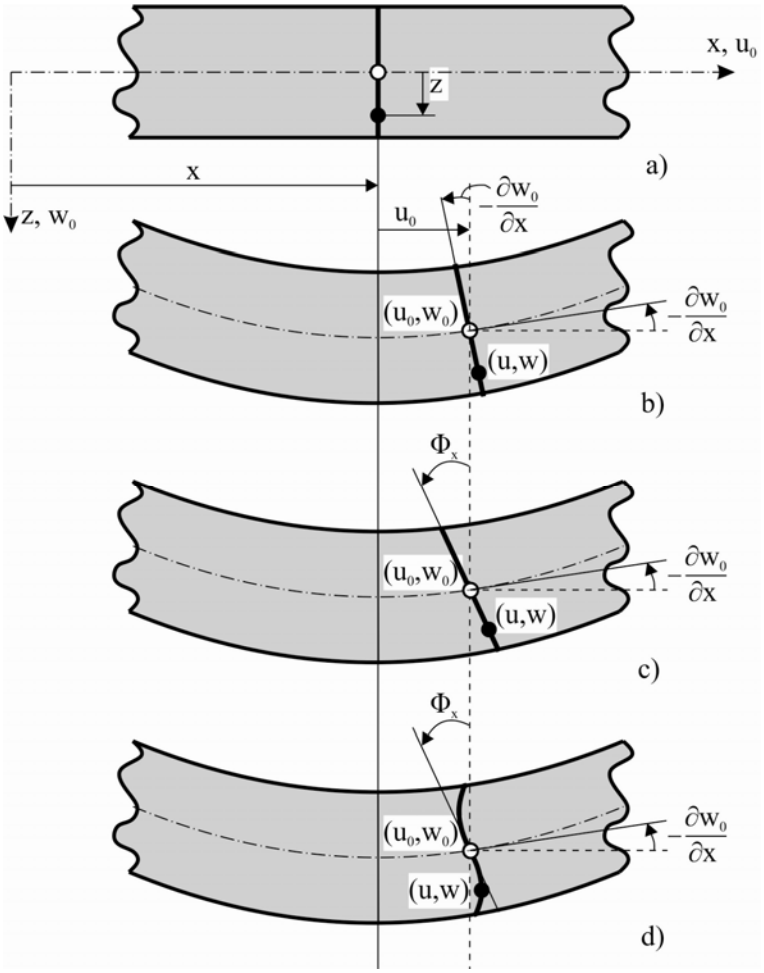

Figure 2. Undeformed and deformed geometries of an edge plate a) undeformed; b) Kirchhoff plate theory; c) Mindlin-Reissner plate theory; c) Reddy plate theory

3. GOVERNING EQUATIONS

3.1. General considerations

The plate theories mentioned before follow with great accuracy the description of the plate behavior under loading, determining the response parameters in various situations of loading and restraint. Any calculation theory is based on a physically model, established on the idealization and simplifying hypotheses adopted, as well as on a calculation mathematical model.

Basically, the formulation of a mathematical model for any structure or physically system, lies in determining a mathematical relation between input parameters (loads), the parameters of the system (geometry, physical-mechanical characteristics of the constitutive material, boundary conditions) and the output or response parameters of the system, which represents the unknowns of the problem (displacements, deformations, stresses or internal forces, temperatures, speeds, vibrations frequencies etc.). This relation between mentioned parameters named also an operational equation which is of the nature of a system equation of definition based on three types of conditions which the deformed structure must fulfill under exterior forces:

- ✓ equilibrium equations (static or/and dynamic);
- ✓ geometrical compatibility conditions;
- ✓ physically conditions (of behavior of the constitutive materials).

Corresponding to these conditions can be establish three groups of equations (of equilibrium, geometrical or of deformation and physically or constitutive).

The equations of definition together with the boundary conditions are the governing equations of the system that allow the determination of the response parameters selected as problem unknowns.

3.2. Classical plate theory (Kirchhoff)

Taking in account that the Kirchhoff plate theory is well known and used, in this paper are shown only some of the aspects which will be useful in the comparison with the others theories.

The equilibrium equations of the plate element can be reduced at:

$$\frac{\partial^2 M_x}{\partial x^2} + 2\frac{\partial^2 M_{xy}}{\partial x \partial y} + \frac{\partial^2 M_y}{\partial y^2} + q(x,y) = 0 \qquad (6)$$

where: M_x and M_y are the bending moments, $M_{xy}= M_{yx}$ is the torsion moment, $q(x,y)$ is the force intensity distributed normally on the plate surface.

In fig. 3 are shown all the internal forces including on a inclined section, having the normal $\bar{n}$ and the tangent $\bar{s}$.

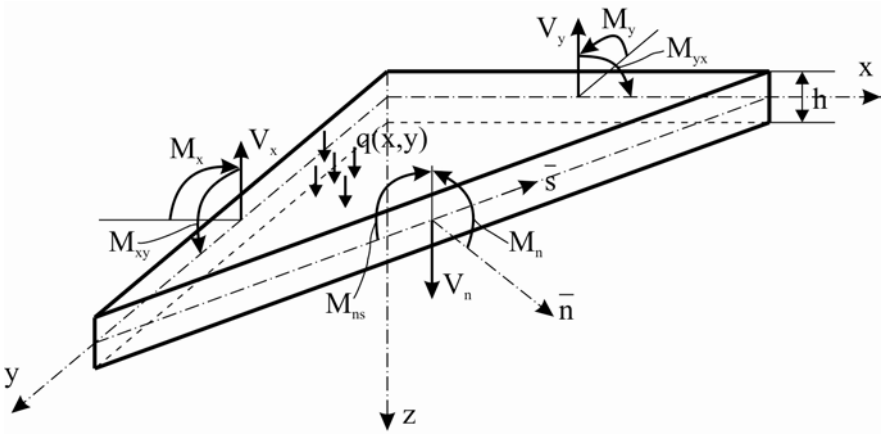

Figure 3. The internal forces and the loading on a plate element

The plane internal forces can be expressed in function of displacement $w(x,y)$ with the following relations:

$$M_x = -D\left(\frac{\partial^2 w}{\partial x^2} + \nu\frac{\partial^2 w}{\partial y^2}\right), \qquad M_y = -D\left(\frac{\partial^2 w}{\partial y^2} + \nu\frac{\partial^2 w}{\partial x^2}\right)$$

$$M_{xy} = M_{yx} = -D(1-\nu)\frac{\partial^2 w}{\partial x\,\partial y} \tag{7}$$

$$V_x = -D\frac{\partial}{\partial x}\nabla^2 w, \qquad V_y = -D\frac{\partial}{\partial y}\nabla^2 w$$

where: V_x and V_y are the shear forces; $D = \frac{Eh^3}{12(1-\nu^2)}$ is the bending plate stiffness;

ν is the Poisson coefficient; E is the Young modulus; $\nabla^2 = \Delta = \frac{\partial^2}{\partial x^2} + \frac{\partial^2}{\partial y^2}$ is the Laplace operator.

For the constant thickness plates, replacing the moment expressions from (7) into (6), it can be obtained the biharmonic equation of a deformed middle surface of the plates:

$$\frac{\partial^4 w}{\partial x^4} + 2\frac{\partial^4 w}{\partial x^2 \partial y^2} + \frac{\partial^4 w}{\partial y^4} = \frac{q(x,y)}{D} \tag{8}$$

or, into a compact form it can be written: $D\nabla^4 w(x,y) = q(x,y)$ (9)

For the determination of the constants which results from biharmonic equation integration, it can be used the boundary conditions. These consist in specification of some displacements or internal forces on the plate boundaries in function of their restraints:

- ✓ clamped edge $w = 0; \frac{\partial w}{\partial n} = 0$ (10)
- ✓ hinged edge (or simply supported edge) $w = 0; M_n = 0$ (11)
- ✓ free edge (without loads) $V_n^* = V_n + \frac{\partial M_{ns}}{\partial s} = 0; M_{nn} = 0$ (12)

where: V_n^* is named the generalized shear force.

In particular, on the simple supported edge can be applied a distributed bending moment and the free edge can be loaded with forces and/or specified moments. In this cases the conditions (11) and (12) will be adequately changed.

3.3. Mindlin plate theory

The displacement field (3), which defines the Mindlin plate theory, leads to a linear variation over the plate thickness of ε_x, ε_y and γ_{xy} strains, while the γ_{xz} and γ_{yz} are constants:

$$\varepsilon_x = z\frac{\partial \phi_x}{\partial x};\ \varepsilon_y = z\frac{\partial \phi_y}{\partial y};\ \gamma_{xy} = z\left(\frac{\partial \phi_x}{\partial y} + \frac{\partial \phi_y}{\partial x}\right)$$

$$\gamma_{xz} = \phi_x + \frac{\delta w}{\partial x};\ \gamma_{yz} = \phi_y + \frac{\partial w}{\partial y} \tag{13}$$

Because the shear strains γ_{xz} and γ_{yz} are represented as constant functions on the plate thickness, the transverse shear stresses τ_{xz} and τ_{yz} will be the same constants, which contradicts the well known parabolic distribution of these. Because this contradiction these cannot be corrected through cinematic plate limitation at displacement field level still the shear forces can be corrected through amplification of the integrals from the equivalence relations with a K_s parameter, named shear correction factor

$$V_x = K_s \int_{-h/2}^{h/2} \tau_{xz} dz, \quad V_y = K_s \int_{-h/2}^{h/2} \tau_{yz} dz \tag{14}$$

The shear correction factor K_s is calculated from the condition that the strain energy given by transverse shear stresses from Mindlin theory to be equal with strain energy from the transverse shear stresses from 3D elasticity theory.

Considering that the plate constitutive material is isotropic and follow the Hooke's law, the constitutive equations lead to the following expressions for the internal forces:

$$M_x = \int_{-h/2}^{h/2} \sigma_x z dz = D\left(\frac{\partial \phi_x}{\partial x} + \nu \frac{\partial \phi_y}{\partial y}\right)$$

$$M_y = \int_{-h/2}^{h/2} \sigma_y z dz = D\left(\frac{\partial \phi_y}{\partial y} + \nu \frac{\partial \phi_x}{\partial x}\right)$$

$$M_{xy} = \int_{-h/2}^{h/2} \tau_{xy} z dz = \frac{D(1-\nu)}{2}\left(\frac{\partial \phi_x}{\partial y} + \frac{\partial \phi_y}{\partial x}\right) \tag{15}$$

$$V_x = K_s \int_{-h/2}^{h/2} \tau_{xz} dz = \frac{K_s E h}{2(1+\nu)}\left(\phi_x + \frac{\partial w}{\partial x}\right)$$

$$V_y = K_s \int_{-h/2}^{h/2} \tau_{yz} dz = \frac{K_s E h}{2(1+\nu)}\left(\phi_y + \frac{\partial w}{\partial y}\right)$$

The classic equations of equilibrium are:

$$\frac{\partial V_x}{\partial x} + \frac{\partial V_y}{\partial y} = -q, \quad \frac{\partial M_x}{\partial x} + \frac{\partial M_{yx}}{\partial y} = V_x, \quad \frac{\partial M_{xy}}{\partial x} + \frac{\partial M_y}{\partial y} = V_y \tag{16}$$

After internal forces replacement from (15) and some processing, we can write:

$$\frac{K_s E h}{2(1+\nu)}\left(\frac{\partial^2 w}{\partial x^2} + \frac{\partial^2 w}{\partial y^2} + \frac{\partial \phi_x}{\partial x} + \frac{\partial \phi_y}{\partial y}\right) = -q(x,y)$$

$$\frac{D(1-\nu)}{2}\left(\frac{\partial^2 \phi_x}{\partial x^2} + \frac{\partial^2 \phi_x}{\partial y^2}\right) + \frac{D(1+\nu)}{2}\frac{\partial}{\partial x}\left(\frac{\partial \phi_x}{\partial x} + \frac{\partial \phi_y}{\partial y}\right) -$$

$$-\frac{K_s E h}{2(1+\nu)}\left(\frac{\partial w}{\partial x} + \phi_x\right) = 0$$

$$\frac{D(1-\nu)}{2}\left(\frac{\partial^2\phi_y}{\partial x^2}+\frac{\partial^2\phi_y}{\partial y^2}\right)+\frac{D(1+\nu)}{2}\frac{\partial}{\partial y}\left(\frac{\partial\phi_x}{\partial x}+\frac{\partial\phi_y}{\partial y}\right)-$$

$$-\frac{K_sEh}{2(1+\nu)}\left(\frac{\partial w}{\partial y}+\phi_y\right)=0 \qquad (17)$$

If the moment sum is introduced

$$M=\frac{M_x+M_y}{1+\nu}=D\left(\frac{\partial\phi_x}{\partial x}+\frac{\partial\phi_y}{\partial y}\right) \qquad (18)$$

and is used the Laplace operator, the Eqs. (17) became:

$$\frac{K_sEh}{2(1+\nu)}\left(\nabla^2 w+\frac{M}{D}\right)=-q(x,y)$$

$$D(1-\nu)\nabla^2\phi_x+(1+\nu)\frac{\partial M}{\partial x}-\frac{K_sEh}{1+\nu}\left(\frac{\partial w}{\partial x}+\phi_x\right)=0 \qquad (19)$$

$$D(1-\nu)\nabla^2\phi_y+(1+\nu)\frac{\partial M}{\partial y}-\frac{K_sEh}{1+\nu}\left(\frac{\partial w}{\partial y}+\phi_y\right)=0$$

The boundary conditions are given by:

- ✓ clamped edge $w=0;\ \phi_n=0;\ \phi_s=0$ (20)
- ✓ soft simply supported edge $w=0;\ M_n=0;\ M_{ns}=0$ (21)
- ✓ hard simply supported edge $w=0;\ M_n=0;\ \phi_s=0$ (22)
- ✓ free edge

$$V_n=K_sGh\left(\phi_n+\frac{\partial w}{\partial n}\right)=0$$

$$M_n=D\left(\frac{\partial\phi_n}{\partial n}+\nu\frac{\partial\phi_s}{\partial s}\right)=0 \qquad (23)$$

$$M_{ns}=\frac{D(1-\nu)}{2}\left(\frac{\partial\phi_n}{\partial s}+\frac{\partial\phi_s}{\partial n}\right)=0$$

3.4. Reddy plate theory

The displacement field (5), proposed by Reddy in the third-order shear deformation plate theory, lead to the following strains:

$$\varepsilon_x = z\frac{\partial \phi_x}{\partial x} - \alpha z^3\left(\frac{\partial \phi_x}{\partial x} + \frac{\partial^2 w}{\partial x^2}\right), \qquad \varepsilon_y = z\frac{\partial \phi_y}{\partial y} - \alpha z^3\left(\frac{\partial \phi_y}{\partial y} + \frac{\partial^2 w}{\partial y^2}\right)$$

$$\gamma_{xy} = z\left(\frac{\partial \phi_x}{\partial y} + \frac{\partial \phi_y}{\partial x}\right) - \alpha z^3\left(\frac{\partial \phi_x}{\partial y} + \frac{\partial \phi_y}{\partial x} + 2\frac{\partial^2 w}{\partial x \partial y}\right) \tag{24}$$

$$\gamma_{xz} = (1 - \beta z^2)\left(\phi_x + \frac{\partial w}{\partial x}\right), \qquad \gamma_{yz} = (1 - \beta z^2)\left(\phi_y + \frac{\partial w}{\partial y}\right)$$

where $\alpha = 4/3h^2$ and $\beta = 4/h^2$ [5].

In the equilibrium equations, once with the classical internal forces represented by moments (M_x, M_y, M_{xy}) and by the shear forces (V_x and V_y), appear supplementary the higher-order resultants of the stresses (P_x, P_y, P_{xy}) and (R_x and R_y), defined with the following relations:

$$\begin{Bmatrix} P_x \\ P_y \\ P_{xy} \end{Bmatrix} = \int_{-h/2}^{h/2} \begin{Bmatrix} \sigma_x \\ \sigma_y \\ \tau_{xy} \end{Bmatrix} z^3 dz, \qquad \begin{Bmatrix} R_x \\ R_y \end{Bmatrix} = \int_{-h/2}^{h/2} \begin{Bmatrix} \tau_{xz} \\ \tau_{yz} \end{Bmatrix} z^2 dz \tag{25}$$

Following the same pattern as in Mindlin plate theory, it can be obtained the constitutive plate equation like an internal forces-displacements relations form:

$$M_x = \frac{4D}{5}\left(\frac{\partial \phi_x}{\partial x} + \nu\frac{\partial \phi_y}{\partial y}\right) - \frac{D}{5}\left(\frac{\partial^2 w}{\partial x^2} + \nu\frac{\partial^2 w}{\partial y^2}\right)$$

$$P_x = \frac{4h^2 D}{35}\left(\frac{\partial \phi_x}{\partial x} + \nu\frac{\partial \phi_y}{\partial y}\right) - \frac{h^2 D}{28}\left(\frac{\partial^2 w}{\partial x^2} + \nu\frac{\partial^2 w}{\partial y^2}\right)$$

$$M_y = \frac{4D}{5}\left(\frac{\partial \phi_y}{\partial y} + \nu\frac{\partial \phi_x}{\partial x}\right) - \frac{D}{5}\left(\frac{\partial^2 w}{\partial y^2} + \nu\frac{\partial^2 w}{\partial x^2}\right)$$

$$P_y = \frac{4h^2 D}{35}\left(\frac{\partial \phi_y}{\partial y} + \nu\frac{\partial \phi_x}{\partial x}\right) - \frac{h^2 D}{28}\left(\frac{\partial^2 w}{\partial y^2} + \nu\frac{\partial^2 w}{\partial x^2}\right)$$

$$M_{xy} = \left(\frac{1-\nu}{2}\right)\left[\frac{4D}{5}\left(\frac{\partial \phi_x}{\partial y} + \frac{\partial \phi_y}{\partial x}\right) - \frac{D}{5}\left(2\frac{\partial^2 w}{\partial x \partial y}\right)\right] \tag{26}$$

$$P_{xy} = \left(\frac{1-\nu}{2}\right)\left[\frac{4h^2D}{35}\left(\frac{\partial\phi_x}{\partial y}+\frac{\partial\phi_y}{\partial x}\right)-\frac{h^2D}{28}\left(2\frac{\partial^2 w}{\partial x\,\partial y}\right)\right]$$

$$V_x = \frac{2hG}{3}\left(\phi_x+\frac{\partial w}{\partial x}\right), \qquad V_y = \frac{2hG}{3}\left(\phi_y+\frac{\partial w}{\partial y}\right)$$

$$R_x = \frac{h^3G}{30}\left(\phi_x+\frac{\partial w}{\partial x}\right), \qquad R_y = \frac{h^3G}{30}\left(\phi_y+\frac{\partial w}{\partial y}\right)$$

where $G=E/2(1+\nu)$ is the shear modulus of the material.

4. COMPARISONS AND BENDING LINKING RELATIONSHIPS BETWEEN KIRCHHOFF AND MINDLIN THEORIES

In order to avoid the confusions between various response parameters in these plate theories, the parameters will be indexed above with "*K*" in the classical theory (Kirchhoff) and with "*M*" in the first-order shear deformation plate theory (Mindlin).

Using the mentioned notations, the biharmonic Eq. (9), governing the plate bending according to the Kirchhoff theory, can be expressed as a pair of Poisson equations:

$$\nabla^2 M^K = -q \qquad a); \qquad \nabla^2 w^K = -\frac{M^K}{D} \qquad b) \tag{27}$$

where M^K is the moment sum (or Marcus moment)

$$M^K = \frac{M_x^K + M_y^K}{1+\nu} = -D\left(\frac{\partial^2 w^k}{\partial x^2}+\frac{\partial^2 w^k}{\partial y^2}\right) = -D\nabla^2 w^K \tag{28}$$

Similarly, the governing equations of static equilibrium of plates according to the Mindlin plate theory (19), can be expressed in terms of the deflection w^M and the moment sum M^M:

$$\nabla^2 M^M = -q \qquad a); \qquad \nabla^2\left(w^M - \frac{M^M}{K_s G h}\right) = -\frac{M^M}{D} \qquad b) \tag{29}$$

where M^M is given by Eq. (18).

After some processing we obtain a more compact form:

$$D\nabla^4 w = \left(1 - \frac{D}{K_s Gh}\nabla^2\right) q \tag{30}$$

Comparing the relations (27a) and (29a) and considering the moment sum expressions M^M and M^K, between them it can be written the following linking relationship:

$$M^M = M^K + D\nabla^2\Phi \tag{31}$$

where Φ is a biharmonic function (such as w^K, which is in the equation of M^K), so satisfies the condition $\nabla^2\nabla^2\Phi = 0$.

Similarly, comparing the Eqs. (27b) and (29b), and considering the Eq. (31), after some processing it can be obtained:

$$w^M = w^K + \frac{M^K}{K_s Gh} + \frac{D}{K_s Gh}\nabla^2\Phi - \Phi = w^K + \frac{M^K}{K_s Gh} + \Psi - \Phi \tag{32}$$

where $\Psi = \frac{D}{K_s Gh}\nabla^2\Phi$ is a harmonic function ($\nabla^2\Psi = 0$).

If we replace M^K from (27b) and will write *D* and *G* in terms of *E* and *ν*, the relation (32) can be written:

$$w^M = w^K - \frac{h^2}{6K_s(1-\nu)}\nabla^2 w^K + \Psi - \Phi \tag{33}$$

The relation (32) (respectively (33)) is valid for plates with arbitrary loading and restraints. The functions Φ and Ψ can be determined from the restraint conditions on the plate boundary. Limiting the analysis to the case in which $w^M = w^K = 0$ on the border, and M^K is either zero or a constant value M_c^K, the difference $\Psi - \Phi$ is equal to $-\frac{M_c^K}{K_s Gh}$ and the relation (32) can be written:

$$w^M = w^K + \frac{M^K - M_c^K}{K_s Gh} \tag{34}$$

Starting from this linking relation between the displacements in the two plate theories, the other response parameters can be express similarly:

$$\frac{\partial w^M}{\partial x} = \frac{\partial w^K}{\partial x} + \frac{V_x^K}{K_s Gh}; \quad \frac{\partial w^M}{\partial y} = \frac{\partial w^K}{\partial y} + \frac{V_y^K}{K_s Gh}$$

$$M_x^M = M_x^K + \frac{D(1-\nu)}{K_s Gh}\frac{\partial}{\partial x}\left(V_x^M - V_x^K\right)$$

$$M_y^M = M_y^K + \frac{D(1-\nu)}{K_s Gh}\frac{\partial}{\partial y}\left(V_y^M - V_y^K\right)$$

$$M_{xy}^M = M_{xy}^K + \frac{D(1-\nu)}{2K_s Gh}\left[\frac{\partial}{\partial y}\left(V_x^M - V_x^K\right) - \frac{\partial}{\partial x}\left(V_y^M - V_y^K\right)\right] \quad (35)$$

$$V_x^M = V_x^K + \frac{D(1-\nu)}{2K_s Gh}\nabla^2\left(V_x^M - V_x^K\right)$$

$$V_y^M = V_y^K + \frac{D(1-\nu)}{2K_s Gh}\nabla^2\left(V_y^M - V_y^K\right)$$

In the case of simply supported polygonal plates (with straight borders), in the Kirchhoff plate theory, the boundary conditions are:

$$w^K = M^K = 0 \quad (36)$$

In the Mindlin plate theory, the simply support of the border can considered to be "soft" or "hard". In the last case we can obtain similar conditions with the classical theory:

$$w^M = M^M = 0 \quad (37)$$

Because on these borders we have $M^M = 0$, results also $M_s^M = 0$, from these the relation (34), which give the displacement becomes:

$$w^M = w^K + \frac{M^K}{K_s Gh} \quad (38)$$

The relation (38) link the bending deflection of the plate in Mindlin theory by the w^K and M^K of the plates from the classical theory.

5. CONCLUSIONS

The calculation of the plate bending response parameters is done often using the classical theory. The simplicity of this theory is based on the normal rectilinear and inextensible segment hypothesis (Kirchhoff hypothesis). This hypothesis neglects the transverse shear effects (strains, stresses). As a result the bending deflection

calculated in classical theory is underestimated. The higher-order theories take in consideration the transverse shear effects through kinematic field relaxation, this being reflected in the selection of the displacement field.

The first-order shear deformation plate theory (Mindlin-Reissner) relaxes the normal segment hypothesis and takes into consideration a constant shear strain on the plate thickness. In order to correct the discrepancy between this constant distribution and the real parabolic distribution a shear correction factor K_s was introduced.

The third-order shear deformation plate theory (Reddy) relaxes more the cinematic hypotheses by adopting a displacement field with a cubic variation on the thickness plate for both *u* and *v* displacements. This higher-order plate theory can be avoided because the complexity of calculation is high and the surplus of precision can be neglected. The researchers' unanimous conclusion is that Mindlin theory is sufficient for the required engineering accuracy.

However, the Mindlin theory has also enough complications compared to the classical theory. That why, through the analysis and comparison between the governing equations of the two theories, it were establish some relations which link the plate response parameters from the Mindlin theory with the ones from the classical theory. In this way, for plates with polygonal shape, as for the axisymmetric circular plates, simply supported on boundary, it was establish the relation (38), which permit the calculation of the Mindlin plate deflection with the bending deflection and the moment sum from the Kirchhoff theory. The bending response parameters w^k and M^k are easier to calculate and, often, can be found in the literature, avoiding in this way the plate bending analyses with shear strain.

References

1. Timoshenko, S., Woinowski-Krieger, S., *Teoria plăcilor plane şi curbe*, Ed. Tehnică, Bucureşti, 1968 (in Romanian).
2. Pank, Vl., *Theories of elastic plates*, Noordhoff International Publishing, Leyden, 1975.
3. Rehfield, L.W., Valisettz, R.R., *A simple, refined theory for bending and stretching of homogeneous plates*, AIAA Journal, Vol. 22, No. 1, pp. 90-95, 1984.
4. Reissner, E., *Reflections on the theory of elastic plates*, Appl. Mech. Rev., Vol. 38, No. 11, pp. 1453-1464, 1985.
5. Wang, C.M., Reddy, J.N., Lee, K.H., *Shear deformable beams and plates*, Elsevier Science Ltd., 2000.
6. Atanackovic, T.M., Guran, A., *Theory of elasticity for scientists and engineers*, Birkhauser Boston, 2000.
7. Qatu, M., *Vibration of laminated shells and plates*, Academic Press, 2004.
8. Vrabie, M., Ungureanu, N., *Calculul plăcilor – teorie şi aplicaţii*, Ed. Soc. Academice "Matei – Teiu Botez", Iaşi, 2012 (in Romanian).
9. Steel C., Balch, C., *Introduction to the theory of plates*, http://www.stanford.edu/ chasst/course%20Notes/PlatesBook

Considerations regarding the bending of sandwich plates

Mihai Vrabie, Vasile-Mircea Venghiac
Department of Structural Mechanics, "Gheorghe Asachi" Technical University, Iasi, 700050, România

Summary

The construction of sandwich plates leads to thickness/in-plane dimensions ratios, which no longer satisfy the conditions for thin plates. Therefore, the analysis of the response of these plates to normal actions on the middle plane is usually done in the first-order shear deformation theory (Mindlin theory). This paper presents the governing equations for sandwich plates in Mindlin theory and compared with the classical theory of plates (Kirchhoff), establishing relationships linking them. It also presents relationships between the deflection of a sandwich plate and the deflection of a homogeneous plate (single layer) in Kirchhoff theory and Mindlin theory.

KEYWORDS: sandwich plates, classical plate theory (Kirchhoff), first-order plate theory (Mindlin), bending deflection.

1. INTRODUCTION

Sandwich plates are made of three layers: a core or central nucleus, generally thicker but with low density and strength, and two thin layers or faces, made of a high strength material. If the faces are, generally, made of steel, the core can be made of a polyurethane foam or it can have a discontinuous structure (corrugated or folded steel sheets, [or Z thin sections stiffeners, honeycomb structure etc.) [1], [2], [3], [4].

Using the classical theory of plates (Kirchhoff) leads to underestimated values of the maximum bending deflection, because it does not capture the effect of the transverse shear deflection [5], [6]. In fact, the external layers take over tensile-compressive and bending stresses, and the core of a bigger thickness takes over the transverse shear stresses. Considering these "functions" of the layers for the global response under bending (the maximum deflection), and to determine other aspects of the response, such as the critical buckling force or the vibration frequencies, it is more indicated to use the first order shear deformation theory [3], [5], [7], [8], [9].

ISSN 2285-2735, Pages 189 - 198

Knowing the plate deflection in the classical bending theory (Kirchhoff) the deflection in the first order shear deformation theory (Mindlin) can be expressed, both for the homogeneous plate (single layer) and for the sandwich plate.

2. GOVERNING EQUATIONS FOR ISOTROPIC PLATES BENDING IN CLASSICAL THEORY (KIRCHHOFF)

The governing equations of a phenomenon are given by the definition equation/equations, plus a set of boundary conditions.

The response parameter of isotropic plates in bending is the deflection, *w*, which in the classical theory is obtained from the biharmonic equation [2], [5], [10]:

$$\nabla^2\nabla^2 w = \frac{q}{D} \tag{1}$$

where:

D is the flexural rigidity of the plate,

q – transverse load,

∇^2 – Laplace operator.

The flexural rigidity of the plate can be written as:

$$D = \frac{Eh^3}{12(1-\upsilon^2)} \tag{2}$$

where:

E is the Young modulus of the material,

υ – Poisson's ratio,

h – thickness of the plate.

Equation (1) can be written in terms of the rectangular coordinates (x, y) for polygonal plates, or in terms of the polar coordinates (r, θ) for circular and annular plates. In these cases the Laplace operator is written as:

$$\nabla^2 = \frac{\partial^2}{\partial x^2} + \frac{\partial^2}{\partial y^2} \tag{3}$$

$$\nabla^2 = \frac{\partial^2}{\partial r^2} + \frac{1}{r}\frac{\partial}{\partial r} + \frac{1}{r^2}\frac{\partial^2}{\partial \theta^2} \tag{4}$$

For axisymmetric circular and annular plates, the Laplace operator becomes:

$$\nabla^2 = \frac{d^2}{dr^2} + \frac{1}{r}\frac{d}{dr} \tag{5}$$

It should be noted that the deflection in any point of the plate is equal to the deflection of the middle plane, as a consequence of the hypothesis of the normal, linear and inextensible segment (Kirchhoff), therefore:

$$w(x, y, z) = w_0(x, y) \quad \text{a}); \qquad w(r, \theta, z) = w_0(r, \theta) \quad \text{b}); \tag{6}$$

The well known equation for isotropic Kirchhoff plate bending problem (1) can be written as a pair of Poisson equations [5], [10]:

$$\nabla^2 M = -q \quad \text{a}); \qquad \nabla^2 w = -\frac{M}{D} \quad \text{b}); \tag{7}$$

where M is the moment sum (Marcus moment)

$$M = \frac{M_x + M_y}{1+\upsilon} = \frac{M_r + M_\theta}{1+\upsilon} \tag{8}$$

In Equation (8) M_x, M_y and M_r, M_θ are the bending moments in rectangular coordinates and in polar coordinates, respectively.

In the case of polygonal Kirchhoff plates with straight simply supported edges, the boundary conditions associated with Eqs. (7a) and (7b) are given by:

$$w = 0; \quad M = 0 \tag{9}$$

On a fixed (or clamped) edge the boundary conditions are given by:

$$w = 0; \quad \frac{\partial w}{\partial n} = 0 \tag{10}$$

and for an unloaded free edge:

$$V_n^* = V_n + \frac{\partial M_{ns}}{\partial s} = 0; \quad M_n = 0 \tag{11}$$

In conditions (10) and (11), for generality, the direction of the normal to the edge was denoted with "n", "s" is the parallel direction to the edge, V_n^* is the generalized shear force, V_n, M_n, M_{ns} are the shear force, bending moment and the torsion moment, respectively, on the edge with the "n" normal.

For axisymmetric circular plates of radius R, on the $r=R$ edge the boundary conditions can be written as follows:

- clamped edge

$$w = 0; \quad \frac{dw}{dr} = 0 \Rightarrow M = -D\frac{d^2 w}{dr^2} \tag{12}$$

- simply supported edge

$$w = 0; \quad M_r = 0 \Rightarrow M = -D(1-\upsilon)\frac{1}{r}\frac{dw}{dr} = D\frac{1-\upsilon}{\upsilon}\frac{d^2 w}{dr^2} \tag{13}$$

It is noted that for an axisymmetric circular plate subjected to bending, the sum moment M is constant on the boundary.

3. GOVERNING EQUATIONS FOR SANDWICH PLATES IN THE FIRST ORDER SHEAR DEFORMATION THEORY (MINDLIN)

Consider a general polygonal shaped (fig. 1a) or circular shaped (fig. 1b) sandwich plate. The facings of thickness h_f and the core of thickness h_c (fig. 1c) are made of isotropic materials, having the following elastic constants: E – the Young's modulus of elasticity, ν – Poisson's ratio, and shear modulus, G, identified by the subscript index "f" for the facings and "c" for the core.

In the first order shear deformation plate theory (Mindlin), the transversal shear deformation is considered to be continuous and constant on the thickness. As a result a linear and normal segment on the middle plane remains linear and inextensible after deformation, but it will rotate after deformation with the angles φ_x and φ_y from the initial position. Considering the relative small thickness of the two facings, the hypothesis of equal rotation of the core and of the facings is accepted. Under these conditions, for the polygonal shaped sandwich plates the moment-displacement relations are given by [5]:

$$\begin{aligned}
M_x &= (D_c + D_f)\frac{\partial \phi_x}{\partial x} + (\upsilon_c D_c + \upsilon_f D_f)\frac{\partial \phi_y}{\partial y} \\
M_y &= (D_c + D_f)\frac{\partial \phi_y}{\partial y} + (\upsilon_c D_c + \upsilon_f D_f)\frac{\partial \phi_x}{\partial x} \\
M_{xy} &= \frac{1}{2}\left[(1-\upsilon_c)D_c + (1-\upsilon_f)D_f\right]\left(\frac{\partial \phi_x}{\partial y} + \frac{\partial \phi_y}{\partial x}\right) \\
V_x &= K_s\left(G_c h_c + 2G_f h_f\right)\left(\phi_x + \frac{\partial w}{\partial x}\right)
\end{aligned} \tag{13}$$

$$V_y = K_s\left(G_c h_c + 2G_f h_f\right)\left(\phi_y + \frac{\partial w}{\partial y}\right) \tag{13}$$

where the flexural rigidities of the core, D_c, and of the facings, D_f, are:

$$D_c = \frac{E_c h_c^3}{12(1-\upsilon_c^2)};\quad D_f = \frac{2E_f h_f\left(\frac{3h_c^2}{4} + \frac{3h_c h_f}{2} + h_f^2\right)}{3(1-\upsilon_f^2)} \tag{14}$$

K_s is the shear correction coefficient, typically taken at 5/6 [2], [5], [6].

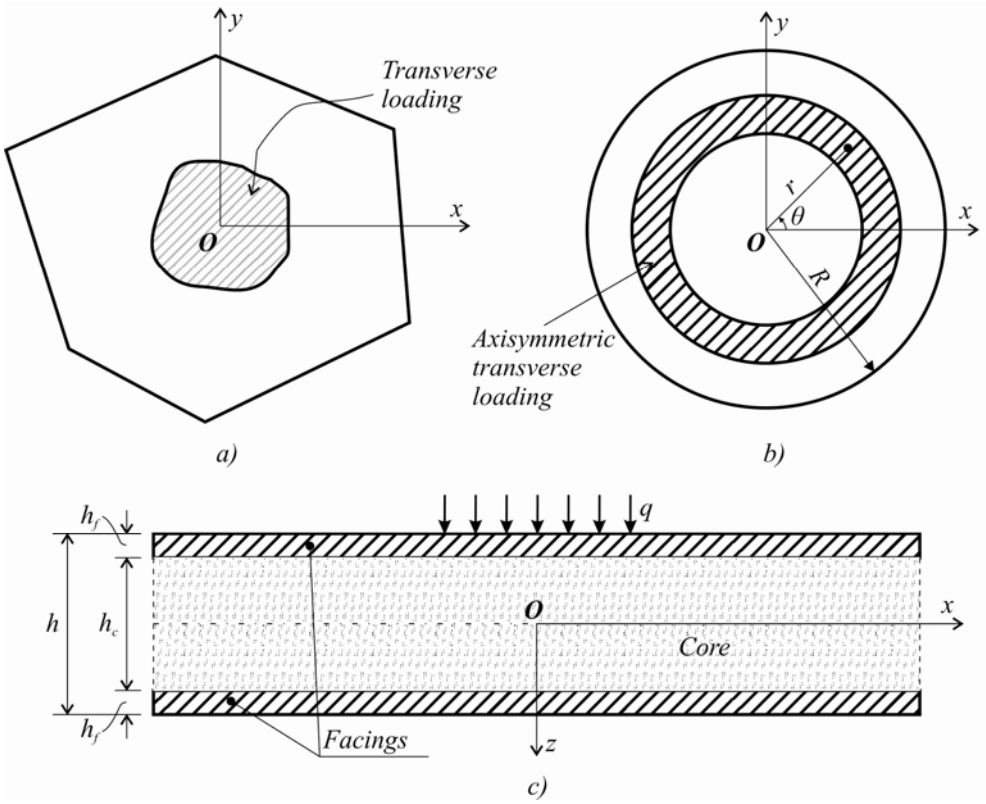

Figure 1. Geometry and loading of a sandwich plate: a) general polygonal shape; b) circular shape; c) plate cross-section.

The moment sum of the Mindlin plate theory from Eq. (8) becomes:

$$M = \frac{M_x + M_y}{(1+\upsilon_c)D_c + (1+\upsilon_f)D_f} = \frac{\partial \phi_x}{\partial x} + \frac{\partial \phi_y}{\partial y} \tag{15}$$

The equilibrium equations of a sandwich plate with the Mindlin plate theory are the same as those with the classical plate theory [2], [5], [10]:

$$\frac{\partial V_x}{\partial x}+\frac{\partial V_y}{\partial y}=-q \qquad \text{a)}$$

$$\frac{\partial M_x}{\partial x}+\frac{\partial M_{xy}}{\partial y}-V_x=0 \qquad \text{b)} \tag{16}$$

$$\frac{\partial M_{xy}}{\partial x}+\frac{\partial M_y}{\partial y}-V_y=0 \qquad \text{c)}$$

By substituting into Eqs. (16) the moments and shear forces from Eqs. (13), using the moment sum from Eq. (15), and after some processing, the following relationships are obtained:

$$K_s\left(G_c h_c+2G_f h_f\right)\left(\phi_x+\frac{\partial w}{\partial x}\right)=\left(D_c+D_f\right)\frac{\partial^2\phi_x}{\partial x^2}+$$

$$+\left(\upsilon_c D_c+\upsilon_f D_f\right)\frac{\partial^2\phi_y}{\partial x\partial y}+\frac{1}{2}\left[\left(1-\upsilon_c\right)D_c+\left(1-\upsilon_f\right)D_f\right]\left(\frac{\partial^2\phi_x}{\partial y^2}+\frac{\partial^2\phi_y}{\partial x\partial y}\right) \qquad \text{a)}$$

$$K_s\left(G_c h_c+2G_f h_f\right)\left(\phi_y+\frac{\partial w}{\partial y}\right)=\left(D_c+D_f\right)\frac{\partial^2\phi_y}{\partial y^2}+ \tag{17}$$

$$+\left(\upsilon_c D_c+\upsilon_f D_f\right)\frac{\partial^2\phi_x}{\partial x\partial y}+\frac{1}{2}\left[\left(1-\upsilon_c\right)D_c+\left(1-\upsilon_f\right)D_f\right]\left(\frac{\partial^2\phi_y}{\partial x^2}+\frac{\partial^2\phi_x}{\partial x\partial y}\right) \qquad \text{b)}$$

$$K_s\left(G_c h_c+2G_f h_f\right)\left(M+\nabla^2 w\right)=-q \qquad \text{c)}$$

If Eq. (16b) is derived by *x*, Eq. (16c) by *y* and then by summing them up considering Eq. (16a), the following equation is obtained:

$$\frac{\partial^2 M_x}{\partial x^2}+2\frac{\partial^2 M_{xy}}{\partial x\partial y}+\frac{\partial^2 M_y}{\partial y^2}=-q \tag{18}$$

The moments M_x, M_y and M_{xy} from Eqs. (13) are replaced in Eq. (18) and after a some convenient processing, considering Eq. (15), an extremely compact form of Eq. (18) is obtained:

$$\nabla^2 M=-\frac{q}{D_c+D_f} \tag{19}$$

The moment sum from Eq. (17c), *M*, can be expressed as:

$$M = -\nabla^2 w - \frac{q}{K_s\left(G_c h_c + 2G_f h_f\right)} \tag{20}$$

consequently Eq. (19) can also be written:

$$\nabla^2 M = \nabla^2\left[-\nabla^2 w - \frac{q}{K_s\left(G_c h_c + 2G_f h_f\right)}\right] = -\frac{q}{D_c + D_f} \tag{21}$$

On a straight simply supported edge (with the normal, "*n*", and the tangential direction "*s*") of a polygonal plate, in *xy* plane, the following boundary conditions can be written:

$$w = 0; \quad M_n = 0; \quad \phi_s = \phi_x l + \phi_y m = 0 \tag{22}$$

where *l*, *m* are the guiding cosines of the normal to the contour. Due to the last two conditions (M_n=φ_s=0), on the simply supported edge the following condition is also satisfied:

$$M = 0 \tag{23}$$

For axisymmetric circular plates subjected to bending Eq. (21) is valid provided that the Laplace operator, ∇^2, is expressed in polar coordinates. On the simply supported or clamped edge (*r*=*R*) of such plates the following conditions are written:

$$w = 0; \quad M = \frac{d\phi_r}{dr} + \frac{1}{r}\phi_r = C\,(\text{constant}) \tag{24}$$

where φ_r is the rotation of the normal to the middle plane in radial direction.

4. COMPARISONS AND RELATIONSHIPS BETWEEN THE KIRCHHOFF AND MINDLIN THEORIES

In order to avoid the confusion between response parameters from the two plate theories, the following superscript indexes are considered: "*K*" for the classical theory (Kirchhoff) and "*M*" for the first order shear deformation plate theory (Mindlin).

A first connection between the response parameters from the two plate theories is obtained by comparing Eq. (7a) with Eq. (21).

By using the notation with superscript indexes previously described and by replacing q from Eq. (7a) into Eq. (21), Eq. (25) is obtained:

$$\nabla^2 M^M = \nabla^2\left[\nabla^2\left(-w^M + \frac{M^K}{K_s\left(G_c h_c + 2G_f h_f\right)}\right)\right] = -\frac{q}{D_c + D_f} \tag{25}$$

On the boundary of a simply supported polygonal plate, the synthesis of the governing equations (Eqs. (7) and boundary conditions (9)) in the Kirchhoff plate theory leads to the following conditions:

$$w^K = M^K = \nabla^2 w^K = 0 \tag{26}$$

In the Mindlin plate theory, the same plate will satisfy the following boundary conditions, resulted from Eqs. (22), (23) and (25):

$$w^M = M^M = \nabla^2\left(-w^M + \frac{M^K}{K_s\left(G_c h_c + 2G_f h_f\right)}\right) = 0 \tag{27}$$

Conditions (26) and (27) enable the establishment of connections on the boundary of the simply supported polygonal plate, between parameters w and M from the two plate theories.

Finally, the comparison between Eqs. (1) and (25) leads to a relationship which links the deflection of the sandwich plate, w^M, to the parameters, w^K and M^K, computed for the equivalent homogeneous plate in the classical theory.

$$w^M = \frac{D}{D_c + D_f} w^K + \frac{M^K}{K_s\left(G_c h_c + 2G_f h_f\right)} \tag{28}$$

Since the moment sum, M, at the circular plate is constant on the boundary (different from zero), Eq. (28) must be corrected by introducing a constant C in the second member of the equation. From the boundary conditions on the edge (r=R) the following results:

$$w^K = w^M = 0 \quad \Rightarrow \quad C = M^K(R) \tag{29}$$

and the deflection of the circular sandwich plate is:

$$w^M = \frac{D}{D_c + D_f} w^K + \frac{M^K - M^K(R)}{K_s\left(G_c h_c + 2G_f h_f\right)} \tag{30}$$

where $M^K(R)$ is given by Eq. (12) and (13) for a clamped edge and for a simply supported edge, respectively.

The moment sum for an axisymmetric circular plate can be obtained by integrating Eq. (7a):

$$M = -\int \left[\frac{1}{r} \int q(r) r dr \right] dr \tag{31}$$

If the face thickness of the sandwich plate is h_f=0, and the core thickness is h_c=h, which in terms of rigidities can be expressed as D_f=0 and D_c=D, an equivalent single layer isotropic plate is obtained, having the thickness h, Poisson's ratio v and Young's modulus E. The bending deflection of this Mindlin plate, w^M, can be written by adapting Eqs. (28) and (29), respectively, as follows:

- for simply supported polygonal plates

$$w^M = w^K + \frac{M^K}{K_s G h} \tag{32}$$

- for circular plates

$$w^M = w^K + \frac{M^K - M^K(R)}{K_s G h} \tag{33}$$

If the moment sum is isolated from Eq. (32):

$$M^K = \left(w^M - w^K \right) K_s G h \tag{34}$$

and is replaced in Eq. (28), after some processing, it results:

$$\left(w^M - \frac{D}{D_c + D_f} w^K \right) \left(G_c h_c + 2 G_f h_f \right) = \left(w^M - w^K \right) G h \tag{35}$$

Eq. (35) allows the sandwich plate deflection calculation using only the deflections of the equivalent single layer plate, deducted from the two plate theories (Kirchhoff – w^K and Mindlin – w^M).

5. CONCLUSIONS

This paper presents, in synthesis, the governing equations for the bending of homogeneous and isotropic plates in the classical theory (Kirchhoff) and, more detailed, the same equations for sandwich plates in the first order shear deformation plate theory (Mindlin).

The analysis and comparison of the two groups of equations allow the establishment of specific differences, but also of useful connections between the

response parameters of the plate in the two theories. The analysis was limited to simply supported polygonal plates and for simply supported and clamped axisymmetric circular plates.

The fundamental bending response parameter, w^M, of sandwich plates can be deducted from Eqs. (28) and (30), depending on the deflection w^K and the moment sum, M^K, deducted from the Kirchhoff plate theory for the equivalent single layer, homogeneous and isotropic plate. Thus, a laborious calculation in the Mindlin theory is avoided, the parameters w^K and w^M being much easier computed (these parameters are often found in the technical literature).

The second term in the second member of Eq. (30) has the same value whether the circular plate is clamped or is simply supported. This is due to the fact that the difference between the deflection of a simply supported circular plate and the deflection of a clamped circular plate is equal to the deflection produced by a uniformly distributed moment on the boundary of a clamped plate.

Another useful connection is given by Eq. (35), and it allows the deduction of a sandwich plate deflection, based on the deflections w^K and w^M calculated from the two theories for an equivalent single layer, homogeneous and isotropic plate. In this case the assessment of the moment sum M^K is no longer necessary.

References

1. Plantema, F.J., *Sandwich constructions: the bending and buckling of sandwich beams, plates, and shells*, Willey, 1966.
2. Timoshenko, St., Woinowski-Krieger, S., *Teoria plăcilor plane şi curbe*, Ed. Tehnică, Bucureşti, 1968. (in Romanian)
3. Pandya, B.N., Kant, T., *Higher-order shear deformable theories for flexure of sandwich plates – Finite element evaluations*, Int. J. of Solids and Structures, Vol. 24, No. 12, pp. 1267-1286, 1988.
4. Zlatibor, V., *Application on a More Accurate Bending Theory of a Sandwich Plate with a Light Core*, Facta Universitatis, Series: Mechanics, Automatic Control and Robotics, Vol. 2, No. 9, pp. 929-938, University of Nis, 1999.
5. Wang, C.M., Reddy, J.N., Lee, K.H., *Shear Deformable Beams and Plates*, Elsevier Science Ltd., 2000.
6. Qatu, M., *Vibration of Laminated Shells and Plates*, Academic Press, 2004.
7. Vrabie, M., *Plăci curbe ortotrope cu aplicaţii la rezervoare – teorie şi calcul*, Ed. Soc. Academice "Matei-Teiu Botez", Iaşi, 2004. (in Romanian)
8. Cetković, M., Vuksanović, Dj., *Bending, free vibration and buckling of laminated composite and sandwich plate using a layerwise displacement model*, Composite Structures, Vol. 88, pp. 219-227, 2009.
9. Liu, J., Cheng, Y.S., Li, R.F., Au, F.T.K., *A Semi-Analytical Method for Bending, Buckling and Free Vibration Analyses of Sandwich Panels with Square-Honeycomb Cores*, Int. J. of Structural Stability and Dynamics, Vol. 10, No. 01, pp. 127-151, March 2010.
10. Vrabie, M., Ungureanu, N., *Calculul plăcilor – teorie şi aplicaţii*, Ed. Soc. Academice "Matei-Teiu Botez", Iaşi, 2012. (in Romanian).